ISSN 0257 - 3660

ACTA MINERALOGICA PAKISTANICA

Volume 4

1988

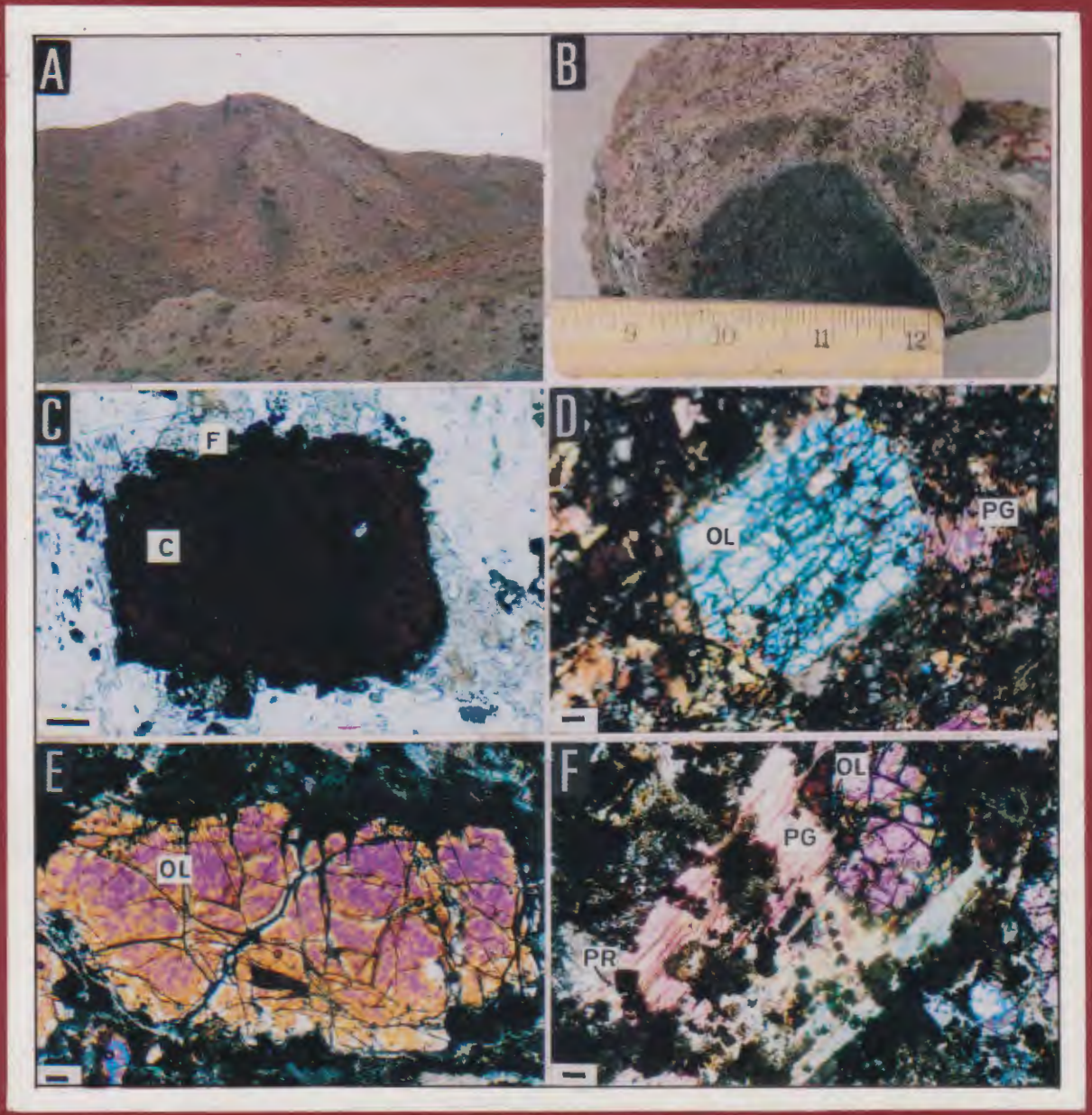

NATIONAL CENTRE OF EXCELLENCE IN MINERALOGY
(UNIVERSITY OF BALOCHISTAN), QUETTA, PAKISTAN

ACTA MINERALOGICA PAKISTANICA

VOLUME 4, 1988

ISSN 0257 – 3660

PRICE

PAKISTANI RUPEES 80.00 OR U.S. $ 11.00

OR U.K. £ 7.00 (Includes postage and handling charges)

Published in December each year.
Printed at KASHMIR OFFSET PRESS, QUETTA, PAKISTAN.

ACTA MINERALOGICA PAKISTANICA VOLUME 4, 1988

CONTENTS

ON THE COVER

VIEWS EXHIBITED IN THE TITLE PHOTOGRAPHS ARE THE FIRST-EVER REPORT ON THE PRESENCE OF ALKALINE ULTRAMAFIC MINOR IGNEOUS BODIES FROM THE BALOCHISTAN PROVINCE REVEALED BY THE RECENT WORK OF ZULFIQAR AHMED & GEORGE R. McCORMICK (IN PRESS). PHOTOGRAPH 'A' SHOWS FIELD OCCURRENCE AS DYKELETS AND LENSES OF DARK COLOUR PROTRUDING ABOVE THE HOST LOWER JURASSIC LIMESTONE. 'B' IS A HANDSPECIMEN OF THE ULTRAMAFIC ROCK WITH STICKING BRECCIATED PART. 'C' TO 'F' ARE PHOTOMICROGRAPHS SHOWING PORPHYRITIC TEXTURE WITH COARSE CRYSTALS OF OLIVINE (OL); CHROMIAN SPINEL (C) SURROUNDED BY A "FERRITCHROMIT" RIND (F); PHLOGOPITE (PG) AND TINY DARK EUHEDRA OF PEROVSKITE (PR). SCALE BARS ARE 0.1 mm LONG. 'C' WAS PHOTOGRAPHED UNDER PLANE POLARIZED LIGHT; 'D', 'E' & 'F' UNDER CROSSED NICOLS.

MAP OF PAKISTAN SHOWING LOCATIONS OF AREAS DEALTWITH IN THE PAPERS OF THIS ISSUE.

Roman numerals correspond to the serial number of each artical in the table of contents.

Major cities are shown by solid circles.

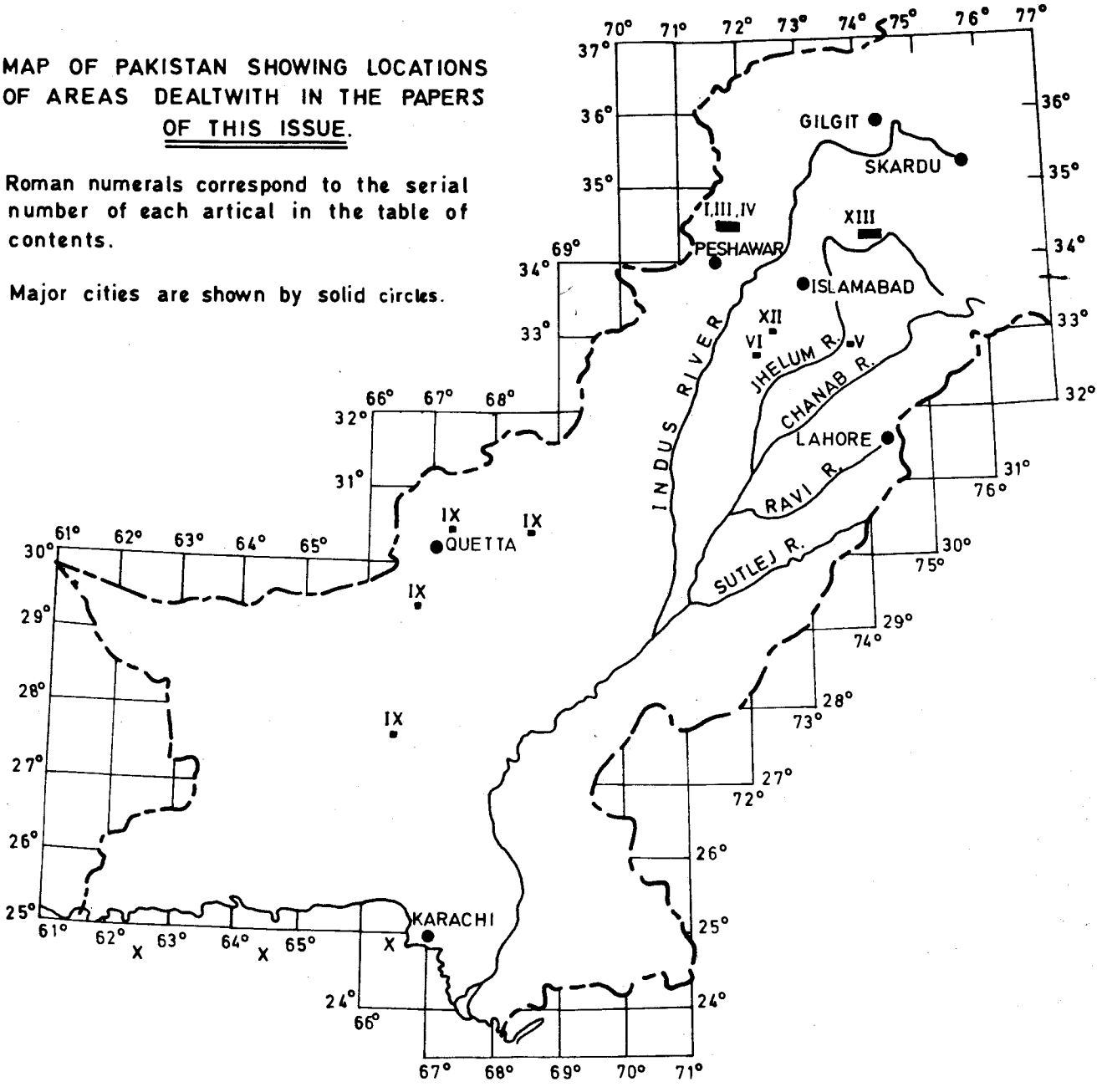

ACTA MINERALOGICA PAKISTANICA
VOLUME 4 (1988) pp. 4 - 29

BULK-ROCK CHEMISTRY AND PETROGRAPHY OF THE SAKHAKOT–QILA OPHIOLITE, PAKISTAN

ZULFIQAR AHMED
Centre of Excellence in Mineralogy, University of Balochistan, GPO Box 43, Quetta, Pakistan.

ABSTRACT: Petrographic observations on the Sakhakot-Qila ophiolitic rocks are supplemented by their characterization in terms of bulk-rock contents of major, trace and rare-earth elements. The thick, mantle-rock sequence exhibits Mg-rich compositions with very small variations. Strong magmatic differentiation is shown by non-cumulate dyke rocks. REE abundance levels progressively increase during the magmatic evolution, maintaining LREE-depleted patterns. The criteria used by Ishiwatari (1985) indicate derivation of this ophiolite after a moderate degree of partial melting of a lherzolitic mantle.

INTRODUCTION

The Sakhakot-Qila ophiolite (abbreviated SQO), located in southern Malakand Agency, Pakistan (Ahmed, 1982; Ahmed & Hall, 1983) is highly dismembered in its crustal sequence but has a relatively thick mantle sequence with abundant Mg-rich ultramafic rocks. Its dominant rock-types include harzburgite, clinopyroxene-bearing harzburgite, dunite, clinopyroxene-bearing dunite and wehrlite. In general, these rocks are weakly serpentinized, but intense serpentinite formation has effected certain locations. The rocks host chromite deposits at locations described earlier by Ahmed (1984). The rocks are cross cut by dykes of clinopyroxenite, orthopyroxenite, websterite, Fe-websterite, metadolerite, metasomatized metadolerite, and rodingites. Gabbroic rocks overlie the above rocks and exhibit differentiation and metamorphic effects and are topped by small lenses of plagiogranite.

This paper attempts to narrate the bulk-chemical and petrographic features of all the aforementioned rock-types, and discusses their petrogenetic implications.

ANALYTICAL METHODS

The unweathered bulk rock samples were pulverized in a jaw crusher and an agate mill. The samples were prepared and analyzed using the techniques and procedures described by Walsh and Howie (1980) employing an ICP spectrometer at the University of London, UK. For major element analyses, samples were fused with $LiBO_2$. For trace element analyses, a procedure of separate $HClO_4$ dissolution of chromite (Ahmad, 1969) before the $HClO_4$–HF digestion (Walsh and Howie, 1980) was usefully employed. The analytical precision achieved is better than 3% and the values obtained are accurate within 5% of the quoted values of the standards used. The REE were analyzed by procedures of Walsh *et al.* (1981), and carry similar precision and accuracy. A cation exchange method was used to concentrate REE in solutions that were analyzed simultaneously for 13 REE and 7 other elements (Ba, Sr, Zr, Cu, Cr, Ca and Fe) to determine the amounts separated by the cation exchange procedure. Each sample was run many times frequently interspersed with runs of blank solution and the standard REE concentration solution. The

method used is not accurate enough at REE concentrations below the chondritic values. Rb was measured with the "UNICAM SP 1900" atomic absorption spectrophotometer. Ferrous iron was determined separately using the Wilson's (1955) method, and H_2O^+ by the Penfield method.

GENERAL FEATURES

The geological mapping of SQO (Ahmed, 1982) shows that it lacks the "unconformity" (as described e.g., in Ishiwatari, 1985) between the cumulates and the residual harzburgite and both members may have a cogenetic relationship.

HARZBURGITE

The most abundant rock of the SQO is harzburgite. It weathers to brown and greenish brown surfaces of rough appearance due to pyroxene crystals. "Hobnail" outcrops are common. Orthopyroxene is often concentrated into thin, cm-scale, layers which are usually lenticular. Pyroxenes are usually very coarse and are readily seen on broken surfaces of hand specimens or thin sections. The rock is commonly xenomorphic granular in texture, and shows very little serpentinization, often below 20%. Fifteen modal counts gave the following variation ranges, in percents, and their means: Highly magnesian olivine, 53 to 80 ($\bar{x}$ = 70), magnesian orthopyroxene, 8 to 22 ($\bar{x}$ = 14), clinopyroxene, 0 to 1 ($\bar{x}$ = 0.2), serpentine, 4 to 25, chromite, 1.4 to 2.5 ($\bar{x}$ = 1.8). Magnesite, talc and tremolite are rarely seen, but magnetite specks are often present. The rock may be strongly serpentinized and composed of a petrographic variety of serpentines. Orthopyroxenes and olivines exhibit kink banding. Amphibole lamellae may be present in orthopyroxenes, having been formed by alteration.

Chemically, the harzburgite compositions are restricted in variation. Some analyses reported in Table 1 (analyses 1 to 5) show solidification indices from 82.51 to 84.68 which, if calculated after converting Fe^{3+} to Fe^{2+}, to avoid the effects of serpentinization, varies from 83.68 to 84.87. It compares well with that of tectonized harzburgites of ophiolites (Coleman, 1977). Anal. 5 is from a strongly serpentinized rock that differs from unserpentinized ones in H_2O^+ and MgO contents and Fe^{3+}: Fe^{2+} ratio, although the Mg/(Mg + total Fe^{2+}) is not different. As serpentinization is often considered an isochemical process except for hydration (Barnes *et al.*, 1967; Coleman, 1977; Green, 1964; Loney *et al.*, 1971; Malpas, 1978), many rock samples were also analyzed after ignition to 940°C, so that they may be compared avoiding the effects of serpentinization. The strongly serpentinized harzburgite (sp. no. Z351) in Table 1 shows its Fe content mostly as Fe^{3+} with much less Fe^{2+} and is quite high in SiO_2 (calculated on anhydrous basis) and lower in solidification index than the fresher harzburgite samples.

CLINOPYROXENE HARZBURGITE:

Not uncommonly, the harzburgites contain fair amounts of clinopyroxene (2 to 10%) which is not abundant enough to classify the rocks as lherzolites. These are similar to the harzburgites in field relations and hand specimens, but clinopyroxene is observed in thin sections; and their chemical analyses (Table 1, anal. 6–11) show slightly higher Al_2O_3 and CaO contents than harzburgites. The analyses also show their lower Al_2O_3 values than the lherzolite subtype rocks (Jackson & Thayer, 1972) whose average Al_2O_3 is about 3.6% (Coleman, 1977). Anal. 6 to 11 in Table 1 show the solidification indices of 80.78 to 84.46 if all the Fe^{3+} is converted to Fe^{2+}. In Table 1, the samples collected from near the chromite deposits, i.e., Z105, Z222 and Z16, show higher Cr contents, usually more than 2500 ppm than those sampled away from the deposits with Cr 970–1830ppm. However, the Ni content is not consistently enriched nearer the chromite deposits and varies overall from 2080 to 2710ppm. Two of the samples, Z323 and Z324, represent clinopyroxene-harzburgite and harzburgite from adjacent spots on the same location. The harzburgite is more magnesian and Fe-poorer than the clinopyroxene-harzburgite.

Table 1. **Analyses of selected samples of harzburgite (1 to 5) and clinopyroxene-harzburgite (6 to 11). Dashes denote no analysis, or in the norms, nil value. H_2O^+ roughly shows the extent of serpentinization. For each rock type the analyses are arranged in order of increasing SiO_2 calculated to 100% anhydrous totals.**

Anal. No.	1	2	3	4	5	6	7	8	9	10	11
Sp. No.	Z105A	Z105B	Z105C	Z324	Z351	Z222A	Z222B	Z222C	Z323	Z326A	Z16
SiO_2	39.86	40.51	42.70	43.31	41.33	39.92	41.25	43.79	43.98	44.91	45.07
TiO_2	0.02	0.02	0.02	0.00	0.01	0.02	0.02	0.01	0.00	0.00	0.00
Al_2O_3	0.46	0.42	0.40	0.49	0.98	0.75	0.74	0.82	0.66	0.63	0.99
Fe_2O_3	2.83	2.19	2.39	1.86	6.42	1.81	1.62	1.93	2.07	2.12	2.76
FeO	6.49	6.34	6.43	6.07	1.45	6.94	6.87	6.87	6.51	7.38	5.21
MnO	0.14	0.13	0.13	0.12	0.13	0.14	0.13	0.13	0.13	0.15	0.12
MgO	46.58	46.83	45.03	43.98	37.22	45.36	46.13	41.79	42.45	40.02	39.71
CaO	0.79	0.64	0.65	0.55	0.06	1.22	1.16	1.16	0.75	1.11	1.07
Na_2O	0.01	0.00	0.00	0.00	0.00	0.00	0.00	0.00	0.00	0.00	0.00
K_2O	0.04	0.05	0.06	0.03	0.02	0.00	0.00	0.00	0.03	0.02	0.03
P_2O_5	0.01	0.00	0.00	0.00	0.00	0.00	0.00	0.00	0.00	0.00	0.00
H_2O^+	3.29	3.28	3.00	2.25	10.92	1.90	1.05	2.21	1.96	2.29	3.15
H_2O^-	0.59	0.50	–	0.42	0.47	0.04	0.15	0.42	0.31	0.16	0.56
Total	101.11	100.91	100.81	99.08	99.01	99.25	99.13	99.13	98.85	98.79	98.67
S.I.	83.253	84.515	83.528	84.675	82.509	83.783	84.456	82.605	83.138	80.783	83.232
Trace elements in p.p.m.:											
Ba	–	–	4	1	5	4	4	2	4	4	3
Rb	–	–	7	9	–	5	6	6	8	9	11
Sr	–	–	6	1	–	6	4	5	1	2	<1
Zr	–	–	3	–	–	5	5	5	4	–	–
Ag	–	–	2	–	–	2	2	–	–	–	–
Co	–	–	89	89	100	85	80	100	83	100	100
Cr	3777	3769	3673	1410	1830	2645	2676	1970	1420	970	3250
Cu	–	–	12	4	<1	16	15	16	10	9	12
Li	–	–	18	–	–	38	35	38	10	2	16
Mo	–	–	0	–	–	0	0	0	0	–	–
Nb	–	–	18	–	–	14	13	13	–	–	–
Ni	2529	2473	2080	2270	2690	2370	2376	2600	2450	2710	2500
Sc	–	–	7	–	–	9	8	9	–	–	–
V	–	–	67	–	77	47	72	70	78	80	93
Y	–	–	0.7	–	2	1	0.2	2	2	2	2
Zn	–	–	3	–	–	68	66	69	70	80	–
C.I.P.W. norms:											
or	0.236	0.296	0.355	0.167	0.111	0.118	–	0.390	–	0.118	0.167
ab	0.085	–	–	–	–	–	–	–	–	–	–
an	1.092	0.999	0.914	1.252	0.306	1.942	2.019	2.031	1.808	1.660	2.615
C	–	–	–	–	0.846	–	–	–	–	–	–
Ca	1.153	0.909	0.583	0.616	–	1.716	1.560	1.557	0.798	1.606	1.127
Mg	0.936	0.737	0.472	0.497	–	1.375	1.251	1.245	0.645	1.267	0.924
Fe	0.080	0.064	0.042	0.046	–	0.142	0.127	0.132	0.058	0.160	0.066
di	2.169	1.710	1.097	1.159	–	3.233	2.938	2.934	1.502	3.033	2.117
en	2.479	6.211	18.085	22.116	44.744	3.571	6.616	23.652	27.388	31.082	36.683
fs	0.212	0.539	1.620	2.058	–	0.370	0.673	2.639	2.483	3.919	2.837
hy	2.691	6.750	19.705	24.174	44.744	3.941	7.289	26.871	29.871	35.001	39.520
fo	78.880	76.840	65.564	60.909	33.599	75.678	74.974	55.485	54.441	47.158	42.956
fa	7.435	7.349	6.472	6.256	–	8.630	8.403	6.796	5.440	6.554	3.668
ol	86.315	84.189	72.037	67.165	33.599	84.308	83.377	62.281	59.881	53.712	46.624
mt	4.103	3.175	3.465	2.685	5.719	2.624	2.349	0.015	3.010	3.074	4.006
il	0.038	0.038	0.038	–	0.015	0.038	0.038	–	–	–	–
op	0.023	–	–	–	–	–	–	–	–	–	–
cm	0.774	0.811	0.790	0.313	0.403	0.607	0.576	0.425	1.428	0.209	0.694
hm	–	–	–	–	2.475	–	–	–	–	–	–

Table 2. **Analyses of selected samples of dunites.**

Anal. No.	12	13	14	15	16	17	18	19
Sp. No.	Z68A	Z68B	Z68C	Z396A	Z396B	Z396C	Z377A	Z14
SiO_2	39.65	39.40	39.23	36.15	35.08	36.88	40.35	40.83
TiO_2	0.02	0.02	0.02	0.02	0.02	0.02	0.01	0.00
Al_2O_3	0.48	0.48	0.47	0.85	0.78	0.82	0.34	0.19
Fe_2O_3	2.59	2.67	2.49	11.31	8.95	9.57	3.93	5.14
FeO	5.65	5.67	5.66	3.38	3.35	3.33	5.33	4.59
MnO	0.13	0.14	0.13	0.19	0.17	0.18	0.07	0.13
MgO	49.94	49.57	48.34	38.01	36.21	37.69	43.45	40.90
CaO	0.23	0.24	0.24	0.56	0.65	0.69	0.13	0.15
Na_2O	0.00	0.00	0.00	0.00	0.00	0.00	0.00	0.00
K_2O	0.00	0.01	0.00	0.03	0.03	0.04	0.05	0.06
P_2O_5	0.00	0.00	0.00	0.04	0.02	0.02	0.00	0.00
H_2O^+	3.26	2.81	3.22	10.90	14.87	11.06	4.51	5.99
H_2O^-	0.40	0.00	0.90	–	–	–	0.71	1.05
Total	101.35	101.01	100.70	101.44	100.13	100.30	98.88	99.03
S.I.	85.837	85.584	85.573	72.084	74.598	74.442	82.354	80.687
Trace elements in p.p.m:								
Ba	9	–	8	23	–	23	1	2
Rb	5	5	5	5	–	5	–	–
Sr	5	5	5	11	–	10	< 1	2
Zr	6	6	6	8	–	9	–	–
Ag	2	2	2	2	–	2	–	–
Co	84	87	86	105	–	103	100	100
Cr	5070	5003	4963	2229	2996	3187	4430	–
Cu	12	12	12	18	–	18	–	10
Li	3	3	3	3	–	3	–	1
Mo	0	0	0	0	–	0	–	–
Nb	15	14	16	13	–	12	–	–
Ni	3303	3206	3196	3153	2819	2903	2770	3250
Sc	5	5	5	13	–	13	–	–
V	37	38	37	69	–	68	72	66
Y	< 1	1	0.2	1	–	3	2	1
Zn	69	–	–	82	–	82	–	80
C.I.P.W. norms:								
or	–	–	–	0.177	0.236	0.177	0.278	0.356
an	1.141	1.191	1.191	2.231	2.119	2.040	0.334	0.340
kp	–	0.034	–	–	–	–	–	–
C	0.062	0.033	0.034	–	–	–	–	–
wo	–	–	–	0.119	0.490	0.440	–	–
en	–	–	–	0.103	0.423	0.381	–	–
fs	–	–	–	–	–	–	–	–
di	–	–	–	0.223	0.913	0.821	–	0.322
en	–	–	2.308	22.237	24.546	22.588	19.426	27.622
fs	–	–	3.033	–	–	–	1.227	1.199
hy	–	–	5.341	22.237	24.546	22.588	20.653	28.821
fo	87.135	86.489	82.726	50.664	48.264	47.084	62.218	51.922
fa	6.598	6.572	6.539	–	–	–	4.320	2.484
ol	93.733	93.061	89.265	50.664	48.264	47.084	66.538	54.406
mt	3.755	3.871	3.610	12.202	11.696	11.737	5.696	7.453
il	0.038	0.038	0.038	0.038	0.038	0.038	0.015	–
ap	–	–	–	0.093	0.046	0.046	–	–
cm	1.091	1.091	1.068	0.480	0.686	0.645	0.963	0.213
hm	–	–	–	2.894	1.503	0.855	–	

Table 3. **Analyses of selected samples of clinopyroxene-bearing dunites.**

Anal. No.	20	21	22	23	24	25	26	27	28
Sp.No.	Z216A	Z216B	Z216C	Z375A	Z375B	Z375C	Z378A	Z378B	Z378C
SiO_2	40.16	39.98	40.34	38.90	38.39	38.54	41.40	41.59	42.58
TiO_2	0.03	0.02	0.02	0.02	0.02	0.02	0.02	0.02	0.02
Al_2O_3	0.57	0.54	0.55	0.21	0.18	0.18	0.71	0.72	0.73
Fe_2O_3	2.67	2.41	2.52	3.51	3.35	3.39	2.91	2.60	2.74
FeO	7.01	7.01	7.02	5.76	5.74	5.71	6.94	6.92	6.92
MnO	0.15	0.15	0.15	0.14	0.14	0.14	0.16	0.16	0.16
MgO	49.31	49.01	49.50	49.25	48.62	48.84	43.00	43.09	43.57
CaO	0.80	0.80	0.82	0.33	0.27	0.26	1.37	1.30	1.31
Na_2O	0.01	0.00	0.00	0.01	0.00	0.00	0.00	0.00	0.00
K_2O	0.02	0.02	0.02	0.01	0.00	0.00	0.03	0.00	0.01
P_2O_5	0.01	0.00	0.00	0.00	0.00	0.00	0.01	0.00	0.00
H_2O^+	0.80	1.52	0.52	3.01	3.56	3.61	3.03	2.96	2.62
H_2O^-	n.d.	0.00	n.d.	n.d.	n.d.	n.d.	0.55	0.38	n.d.
Total	101.54	101.47	101.54	101.15	100.27	100.70	100.13	99.74	100.66
S.I.	83.548	83.835	83.818	84.131	84.249	84.280	81.316	81.905	81.837
Trace elements (in p.p.m.):									
Ba	–	4	3	–	–	0	–	–	13
Rb	–	5	5	–	–	5	–	–	5
Sr	–	6	6	–	–	7	–	–	6
Zr	–	7	8	–	–	5	–	–	5
Ag	–	2	2	–	–	2	–	–	2
Co	–	86	84	–	–	87	–	–	90
Cr	3503	3470	3579	3837	3497	3507	2753	2782	2787
Cu	–	18	19	–	–	10	–	–	40
Li	–	5	4	–	–	2		–	13
Nb	–	45	45	–	–	16	–	–	90
Ni	2400	2425	2469	2787	2801	2871	2391	2215	2192
Sc	–	6	6	–	–	5	–	–	15
V	–	45	45	–	–	30	–	–	69
Y	–	1	0.5	–	0.1	<1	–	–	1
Zn	–	66	67	–	–	61	–	–	73
C.I.P.W. norms:									
kp	0.067	0.067	0.067	0.034	–	0.034	–	–	–
or	–	–	–	–	–	–	0.177	–	0.059
ne	0.046	–	–	0.046	–	–	–	–	–
cs	0.773	0.791	0.822	0.352	0.525	0.256	–	–	
an	1.406	1.385	1.412	0.499	0.491	0.462	1.849	1.965	1.962
wo	–	–	–	–	–	–	2.066	1.872	1.894
en	–	–	–	–	–	–	1.658	1.523	1.521
fs	–	–	–	–	–	–	0.167	0.126	0.152
di	–	–	–	–	–	–	3.891	3.527	3.567
en	–	–	–	–	–	–	13.605	14.720	16.440
fs	–	–	–	–	–	–	1.371	1.213	1.644
hy	–	–	–	–	–	–	14.976	15.933	18.084
fo	86.036	85.512	86.367	85.931	84.832	85.216	64.330	64.868	63.434
fa	8.488	8.674	8.615	6.212	6.322	6.265	7.146	5.891	6.990
ol	94.524	94.186	94.982	92.143	91.154	91.481	71.476	70.759	70.424
mt	3.871	3.494	3.654	5.089	4.857	4.915	4.219	3.770	3.973
il	0.057	0.038	0.038	0.038	0.038	0.038	0.038	0.038	0.038
ap	0.023	–	–	–	–	–	0.023	–	
cm	0.754	0.747	0.770	0.826	0.753	0.755	0.593	0.599	0.599

Trace element data for harzburgites and clinopyroxene-harzburgites show depletion of incompatible elements and enrichment of Cr, Ni and Co, in common with most ophiolitic harzburgites.

Compared to the spinel lherzolite-based upper mantle composition given by Maalφe & Aoki (1977); or the primitive mantle composition given by Taylor & McLennan (1981), the SQO harzburgites and clinopyroxene-harzburgites (Table 1) show lower values for SiO_2, TiO_2, Al_2O_3, CaO, Na_2O and K_2O and higher MgO, with the exceptions of SiO_2 and FeO values for a few clinopyroxene-harzburgite samples.

DUNITE:

Bodies of dunite are easily recognizable in the field because of smooth surfaces devoid of pyroxenes and the buckskin brown weathering colour. Layer-like, lensoid and irregular minor dunite bodies of various shapes and sizes occur in both harzburgite and wehrlite. They are concordant as well as discordant to the harzburgite foliation. The contacts between the two are usually sharp. Dunite is the immediate host for most of the chromite concentrations. The deformation in dunites, where observed, is usually parallel to the regional deformation. Some minor dunite dykes and veins ranging from a few cm to about a metre in width, cut across chromitites or other ultramafic rocks.

The SQO dunite is composed mainly of magnesian olivine (Fo_{91} Fa_9). Minor amounts of chrysotile, antigorite, magnesite, magnetite, pyroxene and chromite are often present. Dunites often have a granular texture overprinted by numerous serpentine veinlets. Some dunites are very slightly serpentinized, and are unusually fresh, as if recrystallized. Most of the accessory pyroxene in dunites is clinopyroxene not observable in hand specimens and may be identified under microscope by a careful examination. Accessory chromite is always present, and is in greater abundance than in the harzburgites or wehrlites. Most chrome ore bodies have a dunite host.

Dunite analyses are reported in Table 2, and dunites with "accessory clinopyroxenes" are also reported separately in Table 3. However, there are no significant differences between the two types. The solidification indices for both overlap and vary from 80.69 to 85.84, except the lower anomalous values for one sample (Z396). The sample with the highest CaO (Z378) shows higher SiO_2 and lower MgO values than the rest of the dunitic samples; and has distinctly higher normative diopside and hypersthene. Cr is generally much higher in the dunites than in the harzburgites.

WEHRLITE

Wehrlite is next to harzburgite in abundance at SQO and often reveals its disseminated coarse clinopyroxenes as coarse white specks on weathered outcrops. This feature proved useful in field mapping operations of SQO. Rarely wehrlite may be present at immediate contacts of chromite deposits. Within the 16 thin sections studied, the range and mean values are: olivine, 10-62 ($\bar{x}$=32), clinopyroxene, 13–40 ($\bar{x}$=25), serpentine, 22–68 ($\bar{x}$=40), orthopyroxene, 0.0–0.7 ($\bar{x}$ = 0.4), chromite, 0.2–2.0 ($\bar{x}$ = 1.3), secondary magnetite, 0.5–5.0 ($\bar{x}$=1.2). Some chemical analyses of wehrlites are reported in Table 4. Solidification indices range from 82.44 to 87.78. Maximum CaO is 2.83%, and Al_2O_3, 1.02%. However, the samples mild serpentinization may be ascertained from their H_2O^+ contents. Their Cr contents show considerable range of variation from 640 to 3006 ppm.

SERPENTINITES

Chemical analyses of samples of more or less completely serpentinized rocks are presented in Table 5. The H_2O^+ content in them is generally above 10% except in tremolite-bearing (anal. no. 58, Table 5) and actinolite-bearing serpentinites (anal. no. 60, 61 in Table 5). Analyses of the material from joint filling veins in unaltered ultramafic rocks and asbestos veins are also included in Table 5.

Table 4. **Analyses of selected samples of wehrlites.**

Anal. No.	29	30	31	32	33	34	35	36	37	38
Sp.No.	Z139A	Z139B	Z139C	Z183A	Z183B	Z183C	Z265A	Z265B	Z265C	Z147A
SiO_2	38.97	39.27	38.94	39.47	39.83	40.29	39.14	39.04	39.55	39.76
TiO_2	0.02	0.02	0.02	0.02	0.02	0.02	0.02	0.02	0.02	0.02
Al_2O_3	0.55	0.56	0.54	0.74	0.74	0.74	0.59	0.60	0.58	0.52
Fe_2O_3	1.86	2.23	2.00	1.63	1.52	1.70	3.34	3.28	3.45	1.08
FeO	7.03	7.03	7.06	5.62	5.66	5.67	4.01	3.99	4.04	5.83
MnO	0.14	0.14	0.14	0.11	0.11	0.11	0.12	0.12	0.13	0.10
MgO	46.23	45.68	45.08	44.01	44.66	43.24	44.64	44.60	43.78	45.53
CaO	1.43	1.56	1.52	2.81	2.64	2.83	1.46	1.39	1.48	1.37
Na_2O	0.00	0.00	0.01	0.00	0.00	0.01	0.00	0.00	0.01	0.00
K_2O	0.00	0.00	0.00	0.00	0.00	0.02	0.00	0.02	0.04	0.02
P_2O_5	0.00	0.00	0.00	0.00	0.00	0.00	0.00	0.00	0.01	0.00
H_2O^+	4.55	4.03	4.40	5.58	5.28	5.30	6.91	6.98	7.20	5.90
H_2O^-	0.25	0.00	0.02	0.00	0.00	0.00	0.00	–	–	0.18
Total	101.03	100.53	99.91	100.03	100.42	99.93	100.23	100.24	100.29	100.31
S.I.	83.872	83.130	83.250	85.790	86.216	85.387	85.863	85.951	85.308	86.790
Trace elements (in p.p.m.):										
Ba	4	–	–	–	8	–	9	–	–	–
Rb	3	–	–	5	5	5	4	–	–	–
Sr	7	–	–	–	4	–	6	–	–	–
Zr	5	–	–	–	5	–	4	–	–	–
Ag	2	–	–	–	3	–	2	–	–	–
Co	93	–	–	–	61	–	77	–	–	–
Cr	2585	2656	2604	2919	2851	2730	2623	2561	2619	–
Cu	11	–	–	–	7	–	10	–	–	–
Li	3	–	–	–	4	–	4	–	–	–
Nb	13	–	–	–	10	–	13	–	–	–
Ni	2772	2310	2326	2206	2139	2023	2322	2191	2289	–
Sc	10	–	–	–	7	–	9	–	–	–
V	59	–	–	–	82	–	50	–	–	–
Y	<1	0.2	–	0.6	3	–	<1	–	–	0.2
Zn	57	–	–	–	50	–	61	–	–	–
C.I.P.W. norms:										
or	–	–	–	–	–	0.118	–	0.118	0.236	0.118
ab	–	–	0.085	–	–	0.085	–	–	0.085	–
an	1.501	1.499	1.429	2.019	2.019	1.915	1.610	1.578	0.604	1.360
lc	–	0.046	–	–	–	–	–	–	–	–
wo	1.127	2.470	2.552	4.661	4.527	4.109	2.352	2.220	2.786	2.270
en	0.912	1.982	2.043	3.785	3.676	0.350	1.966	1.855	2.327	1.839
fs	0.093	0.200	0.213	0.320	0.312	5.062	0.088	0.084	0.106	0.162
di	2.132	4.652	4.808	8.766	8.515	9.521	4.406	4.159	5.219	4.271
cs	0.896	0.101	–	0.234	0.073	–	–	–	–	–
en	–	–	0.070	–	–	3.406	7.196	7.074	10.237	3.551
fs	–	–	0.007	–	–	0.290	0.323	0.319	0.466	0.312
hy	–	–	0.077	–	–	3.696	7.519	7.393	10.703	3.863
fo	80.029	78.313	77.175	74.136	75.347	70.199	71.467	71.560	67.582	75.684
fa	9.036	8.707	8.884	6.912	7.041	6.593	3.531	0.018	0.017	7.330
ol	89.065	87.020	86.059	81.048	82.388	76.792	74.998	71.578	67.599	83.014
mt	2.697	3.233	2.900	2.363	2.204	2.465	4.843	4.755	5.002	1.566
il	0.038	0.038	0.038	0.038	0.038	0.038	0.038	0.038	0.038	0.038
cm	0.556	0.574	0.560	0.628	0.613	0.587	0.564	0.551	0.564	n.d.

Table 4 (Continued)

Anal. No.	39	40	41	42	43	44	45	46	47	48
Sp. No.	Z147B	Z147C	Z264A	Z264B	Z264C	Z202	Z271	Z294A	Z24	Z347
SiO_2	40.07	39.94	39.76	39.91	39.86	41.97	41.68	42.19	41.87	42.18
TiO_2	0.02	0.02	0.02	0.02	0.02	0.00	0.00	0.00	0.00	0.01
Al_2O_3	0.49	0.49	0.34	0.33	0.33	0.81	0.63	0.79	0.45	1.02
Fe_2O_3	0.66	0.88	5.77	5.73	5.97	1.74	2.35	2.35	2.75	4.41
FeO	5.74	5.76	2.79	2.76	2.83	5.77	5.38	5.96	5.36	3.18
MnO	0.10	0.10	0.09	0.09	0.09	0.11	0.12	0.12	0.12	0.10
MgO	46.12	45.47	41.87	41.82	41.37	40.58	40.44	39.75	39.73	36.22
CaO	1.21	1.33	0.28	0.27	0.30	1.54	1.06	0.76	0.84	2.22
Na_2O	0.00	0.00	0.00	0.00	0.00	0.00	0.00	0.00	0.00	0.00
K_2O	0.02	0.01	0.00	0.00	0.01	0.02	0.00	0.06	0.04	0.04
P_2O_5	0.00	0.00	0.00	0.00	0.00	0.00	0.00	0.00	0.00	0.00
H_2O^+	5.23	5.56	9.98	9.84	9.22	5.92	6.81	6.69	7.35	9.37
H_2O^-	0.00	0.30	0.00	0.00	0.61	0.19	0.20	0.37	0.48	0.28
Total	99.66	99.86	100.90	100.79	100.61	98.65	98.67	99.04	98.99	99.03
S.I.	87.781	87.241	83.026	83.125	82.443	84.348	83.953	82.606	82.978	82.600
Trace elements in p.p.m.:										
Ba	–	–	9	10	–	1	1	3	5	4
Rb	–	–	5	5	–	8	8	–	9	8
Sr	2	–	4	6	–	1	0	10	3	1
Zr	5	–	5	6	–	–	–	–	–	–
Ag	<1	–	2	2	–	–	–	–	–	–
Co	–	–	73	73	–	80	94	92	90	80
Cr	–	–	2874	2845	3006	640	1370	1700	840	1180
Cu	–	–	10	10	–	13	14	10	13	9
Li	–	–	2	2	–	3	2	4	1	3
Nb	–	–	12	12	–	–	–	–	–	–
Ni	–	–	1856	1864	1879	2570	2590	2510	3070	2480
Sc	–	–	9	9	–	–	–	10	–	–
V	50	–	50	45	–	75	75	67	70	86
Y	<1	–	1	0.2	<1	1	1	2	2	2
Zn	–	–	66	66	–	90	90	120	50	110
C.I.P.W. norms:										
or	0.118	0.059	–	–	0.059	–	–	0.334	0.612	0.223
an	1.278	1.307	0.928	0.900	0.871	2.198	1.725	1.989	0.918	2.671
wo	1.973	2.209	0.193	0.183	0.258	2.227	1.475	0.743	1.359	3.485
en	1.598	1.789	0.166	0.158	0.222	1.831	1.195	0.602	1.104	2.941
fs	0.141	0.158	0.001	0.001	0.001	0.185	0.106	0.053	0.092	0.092
di	3.712	4.156	0.360	0.342	0.481	4.293	2.775	1.398	2.555	6.518
en	3.847	4.567	26.268	26.994	27.725	21.052	24.164	27.186	27.246	34 464
fs	0.340	0.403	0.137	0.121	0.118	2.058	2.058	2.635	2.151	1 069
hy	4.187	4.970	26.405	27.116	27.843	23.110	26.222	29.821	29.396	35 533
fo	76.676	74.903	54.530	53.959	52.598	54.784	52.805	49.899	49.470	36.997
fa	7.465	7.291	0.313	0.267	0.247	5.895	4.952	5.319	4.290	1.263
ol	84.140	82.194	54.843	54.227	52.845	60.679	57.757	55.218	53.760	38.260
mt	0.957	1.276	8.366	8.307	8.656	2.524	3.404	3.408	3.983	6.391
il	0.038	0.038	0.038	0.038	0.038	–	–	–	–	–
cm	n.d.	n.d.	0.619	0.611	0.647	0.134	0.291	0.365	0.183	0.246

Table 5. Serpentinite analyses.

Anal. No.	49	50	51	52	53	54	55	56	57	58	59
Sp. No.	Z350	Z349A	Z349B	Z349C	Z266A	Z266B	Z266C	Z348	Z364	Z132	ZB75
SiO_2	34.50	39.38	39.21	39.01	39.71	39.32	39.30	41.76	40.13	50.16	36.26
TiO_2	0.04	0.02	0.02	0.02	0.02	0.02	0.02	0.00	0.00	0.02	0.04
Al_2O_3	0.94	0.82	0.81	0.80	0.50	0.50	0.49	0.89	0.55	1.64	12.46
Fe_2O_3	5.20	5.23	5.33	5.25	4.14	4.07	4.03	5.04	6.38	0.86	0.63
FeO	1.65	2.29	2.29	2.31	2.78	2.76	2.81	2.16	2.54	3.14	5.24
MnO	0.15	0.08	0.08	0.09	0.05	0.05	0.05	0.04	0.04	0.08	0.06
MgO	36.55	41.65	41.74	41.40	42.05	41.70	41.86	38.78	37.42	29.82	38.53
CaO	12.60	0.13	0.14	0.13	0.12	0.12	0.12	0.04	0.08	6.61	2.67
Na_2O	0.01	0.00	0.00	0.00	0.00	0.00	0.00	0.00	0.01	0.01	0.01
K_2O	0.02	0.00	0.02	0.01	0.00	0.00	0.01	0.00	0.00	0.00	0.00
P_2O_5	0.02	0.00	0.00	0.00	0.00	0.00	0.00	0.00	0.00	0.00	0.08
H_2O^+	8.30	11.00	11.27	11.32	11.75	11.67	11.84	10.43	11.23	5.94	4.43
H_2O^-	0.24	0.10	0.00	0.15	0.04	0.11	0.07	0.25	0.54	0.50	0.54
Total	100.25	100.68	100.91	100.49	101.16	100.32	100.60	99.39	98.92	98.78	100.95
Trace elements in p.p.m.:											
Ba	20	13	13	13	8			1	2	1	0
Rb	6	–	–	–	4			16	7	7	5
Sr	–	5	5	5	5			0	8	3	3
Zr	7	6	5		5						4
Ag	2	2			2						2
Co	80	70			64			80	100	30	95
Cr	6266	2804	2906	2844	860	850	891	3430	3850	4010	5516
Cu	13	10			19			0	0	0	10
Li	13	3			2			0	0	0	8
Mo	0	0			0			0	0		0
Nb	12	12			39			0			90
Ni	2111	1888	1898	1884	2029	2007	1964	1910	3300	1100	2264
Sc	5	10	–	–	5	–				–	5
V	60	57	80	82	50			68	85	79	55
Y	2	0.4	<1	2	<1	0	2	2	<1	0.1	3
Zn	177	61			43			70	40	30	90

Anal. No.	60	61	62	63	64	65	66	67	68
Sp. No.	Z384A	Z384B	Z326B	Z381	ZA379A	ZA379B	ZB379A	ZB379B	ZB379C
SiO_2	47.78	47.75	44.77	43.20	44.61	42.33	40.62	40.36	39.63
TiO_2	0.04	0.04	0.02	0.00	0.01	0.02	0.02	0.02	0.02
Al_2O_3	4.95	4.90	8.91	0.78	0.79	0.86	1.13	1.13	1.12
Fe_2O_3	1.70	1.72	1.41	0.97	0.22	0.27	2.51	2.44	2.86
FeO	5.24	5.24	3.84	1.40	2.41	2.46	1.94	1.97	1.98
MnO	0.21	0.22	0.06	0.02	0.03	0.03	0.03	0.03	0.03
MgO	24.95	24.87	26.36	40.12	42.55	43.72	41.91	41.97	41.23
CaO	10.70	10.79	6.61	0.00	0.12	0.14	0.13	0.12	0.13
Na_2O	0.05	0.05	0.00	0.00	0.02	0.03	0.01	0.01	0.00
K_2O	0.02	0.02	0.09	0.00	0.00	0.01	0.00	0.00	0.00
P_2O_5	0.02	0.02	0.01	0.00	0.00	0.00	0.00	0.00	0.00
H_2O^+	3.49	3.98	6.21	12.27	9.69	9.67	11.84	12.00	11.90
H_2O^-	0.10	0.07	0.43	0.84	0.00	0.13	0.83	0.70	0.75
Total	99.25	99.67	98.72	99.60	100.45	99.67	100.97	100.75	99.65
Trace elements in p.p.m.:									
Ba	50	53	3	1	14	13	12	11	12
Rb	4	4	–	5	3	4	4	4	4
Sr	17	16	0	5	5	6	9	5	8
Zr	6	7	–	–	3	5	4	4	5
Ag	2	2	–	–	1	2	1	2	1
Co	68	69	50	28	42	44	45	46	42
Cr	2157	2221	1730	178	837	918	3044	3000	2900
Cu	17	19	0	1	5	5	7	7	6
Li	38	42	–	0	37	32	2	2	3
Mo	9	8	–	0	0	0	0	0	0
Nb	12	80	–	–	12	13	13	13	12
Ni	2656	2607	1720	290	579	636	390	389	929
Sc	11	11	–	–	7	6	8	8	7
V	73	72	140	65	62	65	83	58	81
Y	3	2	3	3	0.1	<1	<1	2	2
Zn	69	78	–	30	69	73	40	35	43

– = not determined. Anal. = Analysis. Sp. = Sample. Anal. 49 = Carbonate bearing serpentinite with pseudomorphed pyroxenes; its H_2O^+ is the loss on ignition. Anal. No. 50-52 = Serpentinite near northern contact with the metamorphics. Anal. 53-55 = Serpentinite near southern contact with the metamorphics. Anal 56, 57 = Massive hard serpentinite at the contact with metamorphics, and enclosed in the schistose serpentinite. Anal. 58 = Tremolite-bearing serpentinite. Anal. 59 = Rodingitized serpentinite. Anal. No. 60, 61 = Actinolite serpentinite from northern contact with schists. Anal. No. 62 = Serpentinous filling of joints in harzburgite. Anal. No. 63-65 = Green asbestos. Anal. No. 66-68 = Serpentinite wall of the green asbestos.

Table 6. **Analyses of samples of clinopyroxenites (69–74) and Fe-websterite (75–78).**

Anal. No.	69	70	71	72	73	74	75	76	77	78
Sp.No.	Z123A	Z123B	Z54	Z54	Z54	Z377B	Z36	Z36	Z36	Z36
SiO_2	45.25	48.38	49.89	49.96	49.69	53.70	49.10	49.03	48.82	48.80
TiO_2	0.02	0.02	0.04	0.04	0.04	0.05	0.21	0.21	0.21	0.21
Al_2O_3	0.92	1.07	0.96	0.96	0.96	1.49	2.33	2.33	2.27	2.28
Fe_2O_3	0.29	0.59	0.48	0.49	0.51	0.67	0.61	0.80	0.60	0.42
FeO	2.79	2.74	3.07	3.04	3.00	2.80	10.00	9.92	9.89	9.91
MnO	0.06	0.05	0.08	0.08	0.08	0.10	0.22	0.22	0.22	0.21
MgO	36.23	32.51	32.90	33.07	32.75	19.43	24.31	23.88	23.73	23.88
CaO	7.18	6.90	8.39	8.18	8.23	19.35	11.45	11.21	11.43	11.18
Na_2O	0.05	0.08	0.02	0.02	0.02	0.00	0.32	0.34	0.31	0.32
K_2O	0.09	0.04	0.03	0.01	0.02	0.01	0.06	0.09	0.07	0.06
P_2O_5	0.00	0.00	0.00	0.00	0.00	0.00	0.02	0.03	0.03	0.02
H_2O^+	8.23	8.05	5.42	5.60	5.50	1.18	1.85	1.73	1.80	1.61
H_2O^-	0.00	0.00	0.11	0.00	0.10	0.28	0.00	0.00	0.00	0.00
Total	101.11	100.43	101.39	101.45	100.90	99.06	100.49	99.79	99.38	98.90
S.I.	91.838	90.406	90.137	90.281	90.220	84.810	68.867	68.170	68.584	69.037
Trace elements in p.p.m.:										
Ba	6	6	11	15	10	2	13	14	13	13
Rb	4	4	4	4	4	6	6	–	5	6
Sr	14	14	7	16	8	7	16	11	14	16
Zr	18	14	4	5	5	–	9	8	10	9
Ag	1	1	2	2	2	–	3	–	3	4
Co	29	28	39	36	36	28	68	–	66	68
Cr	3152	3138	3178	3209	3070	1160	1789	1684	1744	1742
Cu	10	10	8	6	7	20	94	–	88	85
Li	8	8	5	6	5	4	5	–	5	5
Mo	0	0	0	0	0	–	5	–	11	4
Nb	10	10	10	9	10	–	10	–	9	10
Ni	798	776	655	781	756	660	327	316	311	320
Sc	15	14	21	20	20	–	65	–	62	63
V	58	57	108	79	105	206	236	232	237	230
Y	1	0.4	2	2	0.5	2	7	7	8	5
Zn	18	14	31	31	31	20	82	–	79	82
C.I.P.W. norms:										
q	–	–	–	–	–	0.991	–	–	–	–
or	0.532	0.237	0.178	0.059	0.118	–	0.356	0.532	0.414	0.356
ab	0.423	0.677	0.169	0.169	0.169	–	2.708	2.877	2.622	2.708
an	2.020	2.442	2.441	2.500	2.471	4.062	4.743	4.566	4.596	4.607
wo	14.029	13.272	16.359	15.900	16.016	38.379	21.654	21.231	21.674	21.179
en	11.658	11.004	13.503	13.131	13.230	30.890	15.298	14.996	15.274	14.917
fs	0.613	0.613	0.835	0.110	0.803	2.995	4.490	4.407	4.544	4.452
di	26.300	24.889	30.698	29.141	30.049	72.264	41.442	40.634	41.492	40.548
en	15.355	35.762	32.677	33.846	33.443	17.500	16.374	22.574	17.057	17.558
fs	0.081	1.991	2.021	2.067	2.030	1.699	4.806	6.634	5.074	5.240
hy	16.162	37.753	34.698	35.913	35.473	19.199	21.180	29.209	22.131	22.798
fo	44.284	23.951	25.043	24.780	24.435	–	20.222	15.338	18.747	18.909
fa	2.566	1.469	1.707	1.668	1.635	–	6.416	4.968	6.146	6.219
ol	46.850	25.420	26.750	26.448	26.070	–	26.637	20.306	24.893	25.128
mt	0.421	0.855	0.696	0.710	0.739	0.973	0.884	1.160	0.870	0.609
il	0.038	0.038	0.076	0.076	0.076	0.091	0.399	0.399	0.399	0.399
ap	–	–	–	–	–	–	0.070	0.070	0.070	0.046
cm	0.678	0.462	0.684	0.690	0.661	0.246	0.385	0.363	0.375	0.375

PYROXENITES

The pyroxenites do not occur in a large continuous outcrop, but are found everywhere within the ultramafic outcrops as dykes and veins cutting across harzburgite, dunite, wehrlite and chromitites. They may displace chromitite layers, e.g., at grid reference 4210-7173 on toposheet 38 N/15 near Darwazagai Kandao. However, pyroxenites are older than rodingites, which cut across and displace pyroxenites at numerous places. The width of pyroxenite dykes ranges from a few cms to about 10m. They are discordant to the pyroxene-rich layers of harzburgite and this relation is often clearly seen in the field. Among pyroxenites, four rock-types can be distinguished. Clinopyroxenites are the most abundant of these, websterites are much less abundant, orthopyroxenites are rarely seen and Fe-websterites are scarce. The clinopyroxenite (Table 6; anal. no. 69 to 74) crystallized from more evolved liquids than the ultramafic cumulate and residual rocks; being richer in SiO_2, slightly richer in TiO_2, Na_2O and the incompatible elements (e.g. Ba, K, Rb, Sr, Zr). However, higher water contents indicate serpentinization effects, except in anal. 74, which is a quartz-normative rock. Four replicate analyses from an Fe-websterite dyke in Table 6 indicate it crystallized from a highly differentiated liquid, richer in Fe, Al, Na and K, although its SiO_2 content is not very high. Trace element data also show differences between Fe-websterite and the rest of the pyroxenites, the Fe-websterite, in general, has higher Ba, Rb, Sr, Ag, Co, Cu, Mo, Sc, V, Y, Zn, and lower Cr and Ni than the other pyroxenites.

GABBROIC ROCKS

The low grade metamorphosed gabbroic rocks overlying the ultramafic rocks may belong to three levels of the ophiolite section. The low-level metagabbro outcrops just south of the Heru Shah village and continues westwards for about 6 kms. It maximum width is 300m. It has a fault contact with the underlying ultramafic outcrop of wehrlite, serpentinite and rodingitized rocks. The rock contains primary

Table 7. **Analyses of gabbroic rocks from the lower-level (79), middle-level (80, 81) and upper-level (82, 83) metagabbro.**

Anal. No.	79	80	81	82	83
Sp. No.	Z233	Z394	Z394	Z368A	Z368A
SiO_2	40.27	47.52	47.27	49.24	47.81
TiO_2	0.04	0.04	0.08	0.15	0.23
Al_2O_3	26.40	24.35	23.95	17.75	16.39
Fe_2O_3	1.17	1.08	1.23	3.53	4.56
FeO	0.80	1.35	1.53	2.49	3.21
MnO	0.05	0.03	0.04	0.11	0.12
MgO	5.91	5.37	6.73	7.55	9.97
CaO	20.68	14.49	13.43	14.75	14.47
Na_2O	0.11	2.80	2.87	1.96	0.94
K_2O	0.00	0.00	0.07	0.01	0.10
P_2O_5	0.06	0.05	0.04	0.04	0.04
H_2O^+	4.10	2.09	2.15	1.23	1.30
H_2O^-	0.22	0.08	0.20	0.62	0.60
Total	99.81	99.25	99.59	99.43	99.74
Trace elements in p.p.m.:					
Ba	10	4	6	11	9
Rb	5	3	–	5	–
Sr	219	127	90	64	53
Zr	43	39	5	48	10
Co	20	16	–	23	–
Cr	460	147	250	300	360
Cu	22	39	–	60	–
Li	30	25	–	5	–
Ni	470	350	230	260	200
V	27	48	26	161	209
Y	2	2	4	6	8
Zn	72	88	–	123	–
C.I.P.W. norms:					
q	–	–	–	1.526	2.072
or	–	–	0.414	0.056	0.591
ab	–	19.038	19.312	16.572	7.953
an	71.984	53.866	52.259	39.616	40.206
ne	0.050	2.521	2.694	–	–
Ca	2.577	7.383	11.799	13.904	13.086
Mg	2.150	5.837	9.401	11.284	10.665
Fe	0.101	0.715	1.046	0.963	0.847
di	4.828	13.935	22.246	26.151	24.598
cs	7.454	–	–	–	–
en	–	–	–	7.519	14.159
fs	–	–	–	0.647	1.125
hy	–	–	–	8.166	15.284
fo	8.807	5.281	4.226	–	–
fa	0.456	0.713	0.518	–	–
ol	9.263	5.994	4.744	–	–
mt	1.702	1.560	1.560	5.117	6.612
il	0.076	0.076	0.152	0.288	0.437
ap	0.139	0.131	0.093	0.099	0.099
cm	0.099	0.032	0.054	0.064	0.074

Table 8. Analyses of selected samples of metadolerites.

Anal. No.	84	85	86	87	88	89	90	91	92
Sp. No.	Z371	Z371	Z371	Z370	Z370	Z369A	Z369B	Z372	ZB182
SiO_2	33.34	33.89	34.24	41.88	41.28	41.05	41.53	43.77	49.15
TiO_2	2.04	2.03	2.01	2.20	2.33	2.04	2.16	2.18	0.38
Al_2O_3	16.27	16.41	16.31	15.63	14.64	14.88	15.06	14.52	14.50
Fe_2O_3	2.31	2.28	2.23	2.13	2.49	1.53	1.54	1.32	2.96
FeO	12.35	12.33	12.31	14.11	14.25	13.63	13.77	13.89	5.86
MnO	0.27	0.26	0.26	0.26	0.28	0.24	0.25	0.24	0.17
MgO	11.65	11.72	11.73	6.87	6.24	6.35	6.52	6.29	6.88
CaO	16.20	15.95	15.86	11.54	11.63	12.14	12.32	11.52	14.68
Na_2O	1.25	1.29	1.28	3.82	3.59	3.60	3.59	4.55	2.55
K_2O	0.24	0.08	0.25	0.18	0.31	0.15	0.20	0.08	0.16
P_2O_5	0.33	0.36	0.35	0.27	0.22	0.20	0.16	0.16	0.06
H_2O^+	4.34	4.34	3.60	1.92	1.88	2.50	2.38	0.87	1.29
H_2O^-	–	0.08	0.09		0.93	0.50	0.52	0.07	0.54
Total	100.59	101.02	100.61	100.81	100.07	98.80	100.00	99.46	99.18
S.I.	41.907	42.311	42.194	25.341	23.214	25.139	25.449	24.072	37.371
Trace elements in p.p.m.:									
Ba	18	19	18	27	33	13	19	7	20
Rb	5	6	6	–	7	–	7	7	5
Sr	29	28	31	74	69	69	74	60	–
Zr	35	34	34	35	80	36	82	67	66
Ag	7	5	6	–	–	–	–	–	–
Co	52	55	54	–	64	–	59	60	32
Cr	175	222	178	130	100	120	78	49	250
Cu	703	700	783	–	190	–	82	155	34
Li	8	9	8	–	10	–	9	10	10
Mo	27	33	30	–	–	–	–	–	–
Nb	–	12	8	–	–	–	–	–	–
Ni	243	247	273	390	363	150	160	190	220
Sc	45	44	42	–	–	–	–	–	–
V	457	528	506	504	600	491	577	570	270
Y	27	34	33	37	32	36	29	30	12
Zn	87	94	95	–	146	–	140	146	119

Table 9. Analyses of rodingite dyke samples (93 to 96) and their chloritic walls (97 to 100).

Anal. No.	93	94	95	96	97	98	99	100
Sp. No.	Z399A	Z361A	Z361A	Z361A	Z399B	Z361B	Z361B	Z361B
SiO_2	36.83	40.03	39.55	39.56	31.37	34.94	34.14	33.86
TiO_2	0.02	0.12	0.12	0.12	0.01	0.04	0.04	0.04
Al_2O_3	18.49	13.66	13.52	14.11	18.53	11.67	11.30	11.64
Fe_2O_3	1.77	0.96	0.96	1.05	2.22	3.09	2.89	2.98
FeO	0.65	2.32	2.31	2.36	3.53	2.92	2.88	2.93
MnO	0.07	0.10	0.10	0.10	0.07	0.06	0.05	0.05
MgO	3.85	13.72	13.60	14.11	31.88	36.17	35.16	36.13
CaO	36.55	26.90	26.92	26.86	0.16	2.78	2.70	2.65
Na_2O	0.02	0.08	0.08	0.10	0.02	0.02	0.02	0.01
K_2O	0.02	0.02	0.01	0.02	0.02	0.04	0.04	0.02
P_2O_5	0.04	0.08	0.07	0.08	0.05	0.09	0.09	0.09
H_2O^+	0.90	2.82	2.72	2.74	10.62	8.83	10.60	10.77
H_2O^-	0.40	0.00	0.00	–	0.55	–	–	–
Total	99.59	100.98	100.14	101.25	99.03	100.65	99.91	101.17
Trace elements in p.p.m.:								
Ba	1	14	10	9	1	10	11	10
Rb	5	5	5	4	5	4	3	3
Sr	17	12	12	9	6	7	7	8
Zr	5	7	7	6	–	5	5	5
Ag	–	2	2	–	–	1	2	1
Co	11	34	33	–	70	56	58	58
Cr	280	2725	2747	2610	5920	6504	6320	6207
Cu	4	54	53	–	–	152	152	151
Li	4	5	5	–	0	3	2	4
Mo	0	11	9	–	–	5	5	6
Nb	–	11	11	–	–	13	14	12
Ni	210	504	435	552	1190	900	1108	1138
Sc	–	29	28	–	–	10	11	4
V	22	132	135	118	80	76	79	74
Y	2	3	6	4	3	2	1	3
Zn	65	31	34	30	80	66	69	73

magmatic clinopyroxene, later metasomatic clinopyroxene, chlorite, clinozoisite, rare albite, and neither quartz nor olivine. It is silica-deficient rock with olivine and dicalcium silicate in the norm. The middle-level gabbros outcrop about 1 km SW of Musa Mena village and continue further SW elongated about 2.5 km. Its maximum NW-SE width is 350m. The rock contains tremolite, actinolite, actinolitic hornblende albite, clinozoisite, zoisite, epidote, chlorite, quartz and rarely, sphene. The rock shows albite in its CIPW norm. Thee is no normative quartz. The upper-level gabbro outcrops as "amphibole-rich gabbro" towards the western extremity of the middle-level gabbro outcrop. The outcrop is too small to be mapable except on very large scale, and a considerable part lies under alluvium. It contains abundant actinolite and actinolitic hornblende in addition to clinozoisite, albite and chlorite.

Chemical analyses (nos. 82, 83, Table 7) show that it is the most differentiated of the gabbroic rocks. It is quartz normative.

The solidification index of metagabbroic rocks was found to decrease from over 70 to below 50, from lower towards higher levels; although its significance is uncertain because of considerable metamorphism suffered by the rocks.

METADOLERITES

In most ophiolites, diabase dykes form a sheeted dyke complex consisting of 100% dyke rocks without intervening country rocks, that lies above the gabbros (Coleman, 1977; Thayer, 1977). At SQO, instead of such a unit, metadolerite forms discrete dykes mapped at three places within the northern (upper) part of the ultramafic rock outcrops (Ahmed, 1982). Thus, the dykes apparently lie below the gabbroic rocks. Dykes from three of the locations are described under A, B and C below. The chilled margins of the dykes are not glassy. The chemical compositions and CIPW norms of metadolerite dykes are given in Table 8. The samples are listed in order of increasing SiO_2

(A) At grid reference 4478–8073 on topographic sheet 38N/15 occurs a tabular dyke of dolerite and a few lenses. The dyke trends N40°E to N60°E and dips 70° to the northwest. It is parallel to the local northern contact of serpentinite with lower-level metagabbro. The white rodingitic hydrogrossular veins are nto present in this locality. The ophitic texture of the rock is conspicuous in parts of the dyke. Some primary minerals are also present. The minerals in a sample (ZB 182) from this dyke are; albite, edinite, actinolite, actinolitic hornblende, magnesiohornblende, clinopyroxene and clinozoisite. The amphibole has TiO_2 content of 0.1 to 1.0%.

Out of all the metadolerites studied, the SiO_2 content of true dolerite is found only in sample ZB182, relatively low TiO_2 is, comparable to the TiO_2 content of the sheeted dykes from ophiolites (Coleman, 1977, Table 6). The sample has ophitic texture intact. Both quartz and olivine are absent, although normative olivine is about 5% (Norms are not listed in Tabel 8 because of uncertain metamorphic effects). The sample is hypersthene-normative, and plots in the tholeiitic basalt field of MacDonald & Katsura (1964). The sample may represent the compositon of basaltic liquid before the appearance of brown amphibole and ilmenite phases.

(B) A swarm of six subparallel, steeply dipping dykes and some lenses occur at grid reference 453-875 on topographic sheet 38 N/15 of the Survey of Pakistan. These lenses and dykes are hosted by harzburgite in which minor patchy bodies of dunite also occur. The biggest of the six dykes shows curvature in trend from N35°W to N55°W with an average of N45°W trend and 53°NE dip. Samples Z369, Z369A, Z370, and Z371 were collected from these dykes. A few metres away, at grid-reference 451-877 on the same topographic sheet, another dolerite dyke outcrops with strike N75°E and dip 50°NW, and measures 3m × 50m. It is quarried for use as dimension stone as it is very hard rock. Sample Z372 was collected from this dyke. Metamorphism has transformed the ori-

ginal doleritic mineral assemblage to the present one consisting of high-Ti brown amphibole, low-Ti green amphibole, clinopyroxene, albite, altered plagioclase, grossular, sphene, ilmenite and chlorite. The dykes are cross-cut by white rodingitic ladder veins consisting of grossular, hydrogrossular, uvarovite, chlorite, ilmenite and nearer the wall zones, native copper, nantokite, and grossular inclusions in native copper. A sea-water source for the fluids of these rodingites was suggested by Ahmed & Hall (1984). The Cu seems to have been brought to the sites of deposition by the sea-water from ocean-floor sediments, whereas the Ti of ilmenites was not greatly mobilized from its initial place in metadolerite dykes.

Analyses from samples Z369, Z369A, Z370 and Z372 show rather lower SiO_2 (41.1 to 43.8%) and CaO (11.5 to 12.3%) and higher TiO_2 (2.04 to 2.33%) and Na_2O (3.6 to 4.6%) compared to the sample ZB182 described under 'A' above. Their modes contain abundant brown amphibole with TiO_2 content from 1.8 to 2.5% (Ahmed, 1987b), sphene, ilmenite, clinozoisite and grossular in addition to the minerals of sample no. ZB182. The samples could represent a basaltic liquid composition more evolved than that represented by sample ZB182. However, their lower SiO_2, and CaO may be indicative of some metasomatic activity.

The mode of sample Z371 contains abundant, Ti-rich, brown amphibole, sphene and ilmenite. Grossular and hydrogrossular are abundant as discrete grains and as cross cutting white veins. This is also reflected in its very low SiO_2 and lower Na_2O values, (Table 8) although megascopically visible white veins were avoided in the sample analyzed. The relatively high copper content of this sample indicates that the native Cu and nantokite mineralization found in the wall zones of hydrogrossular veins may be due to metasomatically introduced Cu. Overall, the sample is affected by strong metasomatism although its basaltic liquid must reflect the latest differentiation of the SQO basaltic magma. The brown amphibole, abundant in many dykes, may be of primary origin. It is always Ti-rich and since Ti is typically an immobile element, the amphibole may not be of metasomatic origin. In other ophiolites, brown amphibole crystallizes towards the differentiated tops of cumulate sections (Coleman, 1977). However, most of the primary minerals of the dykes are now lost due to metamorphism and in some cases, metasomatism.

(C) At grid reference 4454–8159 on topographic sheet 38N/15, two small dykes, each less than a metre thick, occur. One of these is enclosed in harzburgite and trends N38°W (sample Z219). The other crosscuts a chromitite, its dunite envelope, and the surrounding harzburgite as well. Its attitude is N28°W/45°SW.

The sampel Z219 consists mainly of various amphiboles (named after Ahmed, 1987b, as ferroan pargasite, ferroedinitic hornblende, edenite, ferroedinite, brown high-Ti edenitic hornblende and ferroan-pargasitic hornblende), clinozoisite, sphene, ilmenite and chlorapatite.

LEUCOCRATIC DIFFERENTIATES

Small felsic bodies, a few metres in each dimension, and sometimes dyke shaped, occur at the northern outer contact of the complex at a locality between the two metagabbro outcrops shown on map by Ahmed & Hall (1984) and immediately above the upper-level metagabbro (sample Z368A). This metagabbro outcrops in a canyon and is topped by alluvium. The felsic bodies are in direct contact with the schistose country rocks. This may suggest their possible linkage to the metamorphic country rocks which have quartzite and siliceous schist interbeds and quartz-only lenses, sometimes *en echelon*. The felsic rocks may also be linked to possible hydrothermal solutions derived from younger continental granites outcropping a few miles away. However, their location at the top contact of SQO favours their ophiolitic affinity. Moreover, the mineral assemblage is different from that of the siliceous bands of the metamorphic country rocks.

The rock, in addition to abundant quartz, contains albite, epidote, apatite, chlorite, sphene and ilmenite. K-feldspar or muscovite were not

found. A low grade metamorphism is commonly found in the leucocratic differentiates of ophiolites (Coleman, 1977).

RODINGITES

Rodingites occur in the following four fashions: –

(1) Small rodingite lenses and veins: As small dykes, ovoids and lenses of greenish white material, bounded by dark green to greenish black chloritic wall rocks, the rodingites are abundantly developed in the serpentinites along the northern contact of ultrabasics. The rock is mined and sold locally as 'jade'. Commonly, the lenses are up to 3m long and 1m wide. There is also open cavity development of grossular crystals with well developed faces and a reddish brown colour in vugs.

(2) Discrete rodingite dykes: As bigger dykes a few metres across and tens of metres long, rodingites are scattered through the ultramafic outcrops. Such rodingites are massive, hard and compact rocks with little dynamic deformation and cut across all types of ultramafic rocks including pyroxenite dykes, with small displacements.

(3) White grossular veins: Cm-scale veins of pure white grossular and hydrogrossular (as described in the metadolerite section), are of rodingitic affinity. This material occurs east of Sidrijor village, in the eastern part of the SQO. In the western part, white veins are found SW of Ospan Kharre village, running through chromitites. These veins have thin linings of uneven, light green staining produced by release of Cr from chromite grains. Sometimes uvarovite also crystallized in these linings.

(4) Rodingitized chromitites: Metasomatic minerals have replaced the silicate matrix surrounding chromite grains disseminated in rodingitized chromitites, at certain localities nearer the northern contact of the ultramafics. The chromitite matrix may be replaced by clinopyroxene and white grossular veins that run through the rock have thin linings of slightly greenish colour due to Cr released from chromite grains.

Rodingitic minerals, grossular and hydrogrossular, are dominant in the central white parts of the dykes and are often coarser grained in dyke peripheries, where, for example, prismatic hydrogrossular crystals project outwards into interstitial chlorite. Some accessory 'ferritchromit' grains are present. The greenish to dark greyish walls of rodingites are made mostly of chlorite and some accessory 'ferritchromit' grains. Chloritic walls in rodingites are dominantly developed where the country rock is serpentinite, and are not predominant where the country rock is unserpentinized ultramafic rock (cf. Coleman, 1977).

The chemical compositions of rodingite minerals are presented elsewhere (Ahmed, 1987a,b; 1988). The rodingites often contain clintonite and corundum is seen as an accessory mineral. The enrichment of rodingites in Al is often not emphasized (Liou *et al.*, 1977) and the present study is probably the first report of such strongly Al-rich minerals from rodingites.

Chemical analyses of major elements in rodingites are given in Table 9. The rocks are undersaturated with respect to SiO_2, enriched in Ca, and are Mg-rich compared to most rodingites.

REE GEOCHEMISTRY

The whole-rock REE determinations were made on samples representing different lithologies and locations within the SQO (Table 10).

Generally the dunite, harzburgite, wehrlite and chromitite samples gave values below the chondritic abundance. Considering that the method used was not accurate enough at such low REE concentrations, the values are not used for petrogenetic interpretations. However, the samples from metadolerite dykes, some gabbros, Fe-websterite and a few pyroxenites with higher REE abundance are discussed here.

The chondrite normalized REE patterns are plotted in fig. 1. Most pyroxenite dykes show values below chondritic abundances as shown by th representative plot of sample no. Z377B. However, the Fe-websterite dyke, sample no.

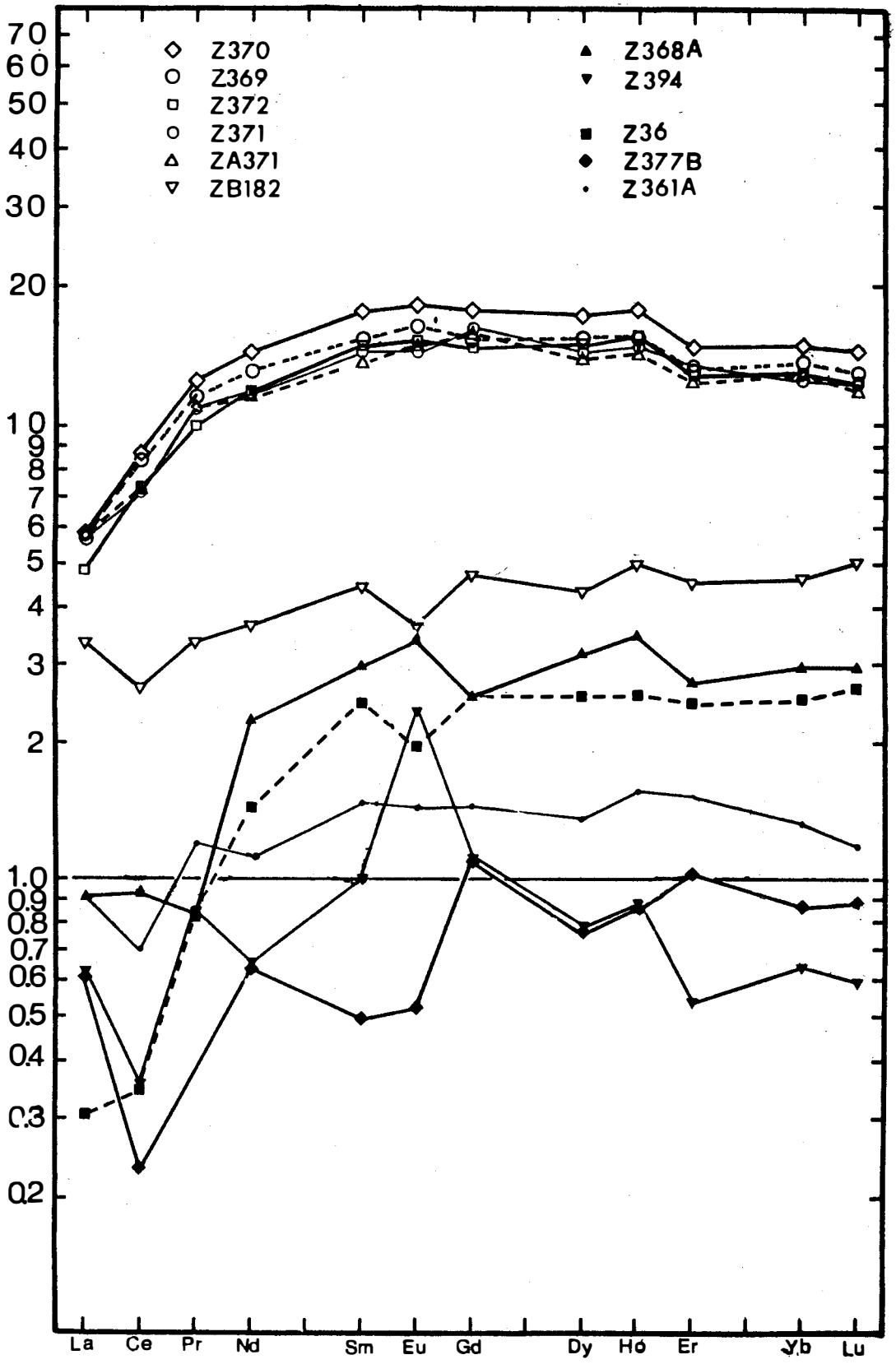

Fig. 1. Chondrite normalized REE plots, using the chondritic REE abundance values from Nakamura (1974), for the SQO rocks, using separate symbol for each sample. Values below horizontal line at chondritic abundance level, may have high error because of the limitations of the analytical method. The metadolerites (open symbols) display the highest REE enrichment from the SQO rocks and all the samples, except one, fall in a narrow band displaying strong LREE depletion.

Table 10. REE contents in p.p.m. for the SQO ophiolitic rocks.

Sp. No.	Z370	Z369	Z372	Z371	Z371	ZB182	Z368A	Z394	Z233
La	1.9	1.9	1.6	1.9	1.9	1.1	0.3	0.2	1.0
Ce	7.5	7.3	6.3	6.2	6.2	2.3	0.8	0.3	0.8
Pr	1.5	1.4	1.2	1.3	1.3	0.4	0.1	n.d.	0.1
Nd	9.1	8.2	7.5	7.4	7.2	2.3	1.4	0.4	0.7
Sm	3.6	3.1	3.0	2.9	2.8	0.9	0.6	0.2	0.2
Eu	1.39	1.26	1.18	1.11	1.14	0.28	0.26	0.18	0.28
Gd	4.9	4.2	4.1	4.5	4.3	1.3	0.7	n.d.	0.8
Dy	5.92	5.23	5.15	4.95	4.78	1.49	1.07	0.26	0.17
Ho	1.25	1.1	1.10	1.04	1.00	0.35	0.24	0.06	0.06
Er	3.33	2.93	2.91	2.96	2.80	1.03	0.61	0.12	0.33
Yb	3.28	3.01	2.85	2.74	2.78	1.02	0.65	0.14	0.15
Lu	0.49	0.44	0.42	0.42	0.40	0.17	0.10	0.02	0.03

Sp.No.	Z36	Z123	Z54	Z377B	Z399A	Z361A	Z361B	Z379A	Z381
La	0.1	0.6	0.3	0.2	0.2	0.3	0.3	0.1	n.d.
Ce	0.3	0.7	0.2	0.2	0.2	0.6	0.3	0.5	0.1
Pr	0.1	0.1	0.1	0.1	0.1	0.11	0.1	0.2	n.d.
Nd	0.9	0.5	0.3	0.4	0.3	0.7	0.2	0.3	0.1
Sm	0.5	0.2	n.d.	0.1	0.1	0.3	0.1	0.2	0.1
Eu	0.15	0.04	0.01	0.04	0.07	0.11	0.03	0.03	0.01
Gd	0.7	1.1	0.1	0.3	0.2	0.4	n.d.	0.2	0.1
Dy	0.86	0.09	0.06	0.26	0.05	0.47	0.13	0.04	0.11
Ho	0.18	0.04	0.01	0.06	0.01	0.11	0.03	0.15	0.02
Er	0.55	0.44	0.07	0.23	0.09	0.34	0.06	0.15	n.d.
Yb	0.55	0.09	0.08	0.19	0.02	0.29	0.09	0.04	n.d.
Lu	0.09	0.05	0.03	0.03	0.01	0.04	0.01	0.05	n.d.

Sp.No.	Z379B	Z384	Z132	Z350	Z349	Z266	Z364	Z265	Z264
La	0.4	0.7	0.6	1.2	0.8	0.8	0.1	2.7	0.3
Ce	0.4	0.8	0.3	2.2	0.9	0.6	0.2	1.7	0.5
Pr	0.1	0.1	0.1	0.2	0.1	0.1	0.1	0.3	0.2
Nd	0.1	0.4	0.3	1.2	0.4	0.3	0.2	1.1	0.4
Sm	0.3	0.1	0.2	0.3	0.4	0.3	0.1	0.8	0.1
Eu	0.19	0.03	0.03	0.06	0.19	0.12	0.01	0.17	0.02
Gd	0.08	0.04	0.09	0.3	1.0	1.4	0.04	5.6	0.5
Dy	0.02	0.22	0.02	0.16	0.08	0.01	0.03	0.03	0.04
Ho	0.23	0.05	0.01	0.05	0.07	0.05	0.01	0.06	0.02
Er	0.62	0.27	0.30	0.14	1.09	1.16	n.d.	1.65	0.19
Yb	0.06	0.17	0.04	0.07	0.08	0.04	0.02	0.08	0.03
Lu	0.19	0.02	0.02	0.01	0.31	0.29	0.01	0.22	0.01

Sp.No.	Z183	Z139	Z147	Z375	Z216	ZB275	Z68	Z105	Z222
La	0.1	0.1	0.1	0.1	0.19	1.0	0.1	0.5	0.1
Ce	0.3	0.1	0.3	0.3	0.4	1.3	0.3	0.7	0.3
Pr	0.1	0.1	0.1	0.1	0.1	0.02	0.1	0.2	0.1
Nd	0.3	0.1	0.3	0.1	0.3	0.3	0.3	0.3	0.2
Sm	0.1	0.1	0.1	0.1	0.4	0.1	0.1	0.1	0.1
Eu	0.03	0.01	0.01	0.01	0.01	0.28	0.01	0.05	0.03
Gd	0.2	0.1	0.2	0.1	0.1	0.8	0.1	0.2	0.2
Dy	0.11	0.02	0.03	0.02	0.09	0.02	0.03	0.07	0.04
Ho	0.02	0.01	0.01	0.01	0.04	0.08	0.04	0.02	0.12
Er	0.09	0.02	0.08	0.02	0.12	0.92	0.07	0.08	0.15
Yb	0.07	0.03	0.03	0.02	0.07	0.03	0.04	0.03	0.06
Lu	0.01	0.02	0.03	0.01	0.02	0.28	0.02	0.01	0.05

Z36, exhibits intermediate and heavy REE values of 2 to 3 times chondrtitic level, with a strong LREE depletion and a small negative Eu anomaly [Eu/Eu* = 0.779, where Eu* = (Sm + Gd)/2]. In gabbroic rocks the REE values may reach 3 times chondritic abundance. All metagabbro samples show positive Eu-anomalies. The upper level metagabbro sample no. Z368A is strongly depleted in LREE but this trend is not distinct in lower-level (sample no. Z394) or middle-level metagabbro samples (sp. no. Z233). The metadolerites show the highest REE contents within the igneous suite and most samples (Z369, Z370, Z371, ZA371 and Z372) cluster in a tight band giving a consistent strongly LREE-depleted trend without a distinct Eu anomaly. The intermediate REE, Sm to Ho, are slightly higher than even heavier REE, Er to Lu. One of the metadolerites sampled from just below the lower-level gabbro outcrop south of Heru Shah village (sample No. ZB182) has much lower REE content with a small negative Eu-anomaly, a negative Ce-anomaly, and an REE pattern which is only slightly LREE-depleted.

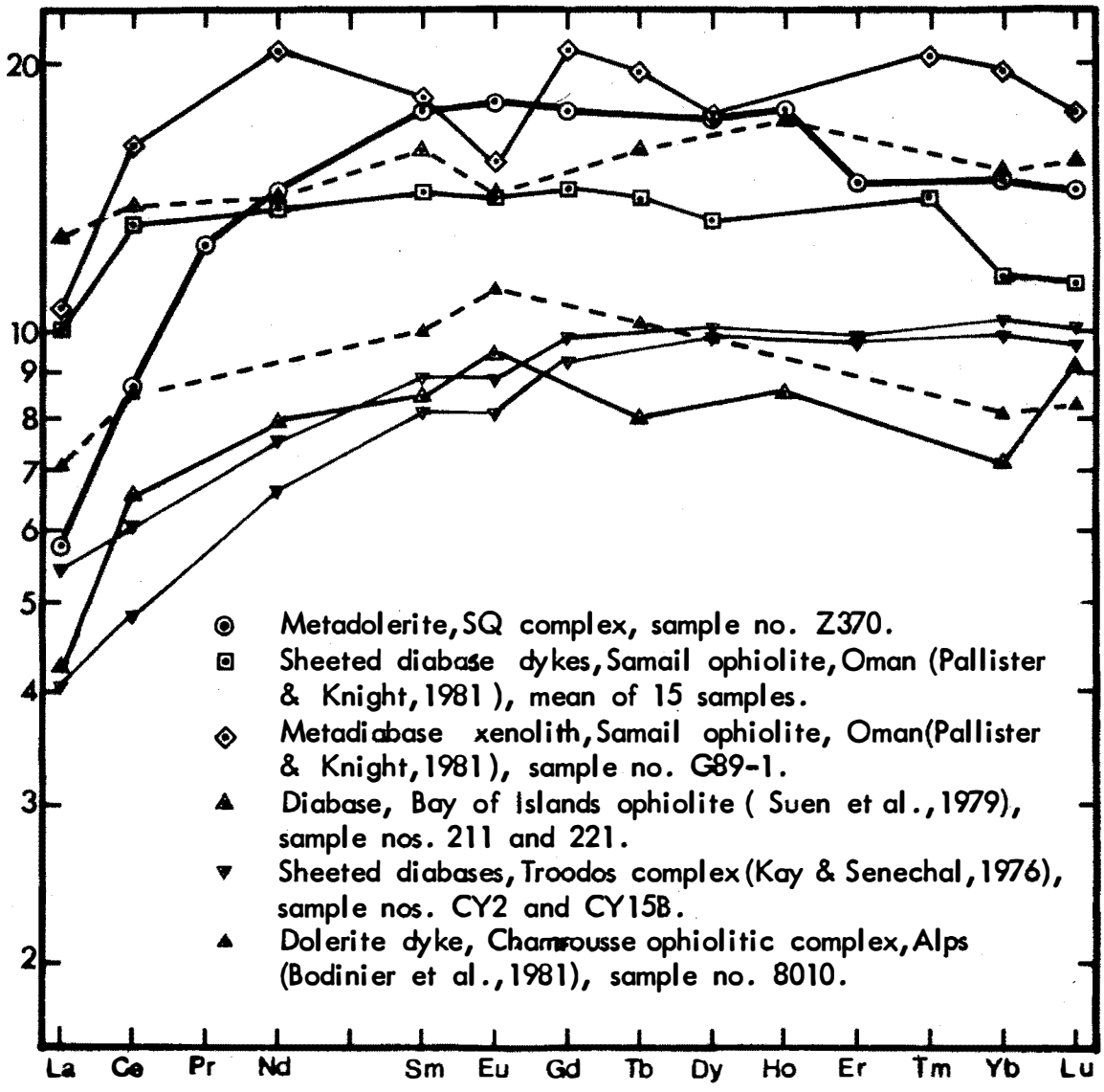

Fig. 2. The metadolerite sample Z370 from SQO (thick line) is compared with the chondrite - normalized REE plots of sheeted diabase and dolerite dykes from other ophiolites. All plots are based on chondritic values given by Nakamura (1974).

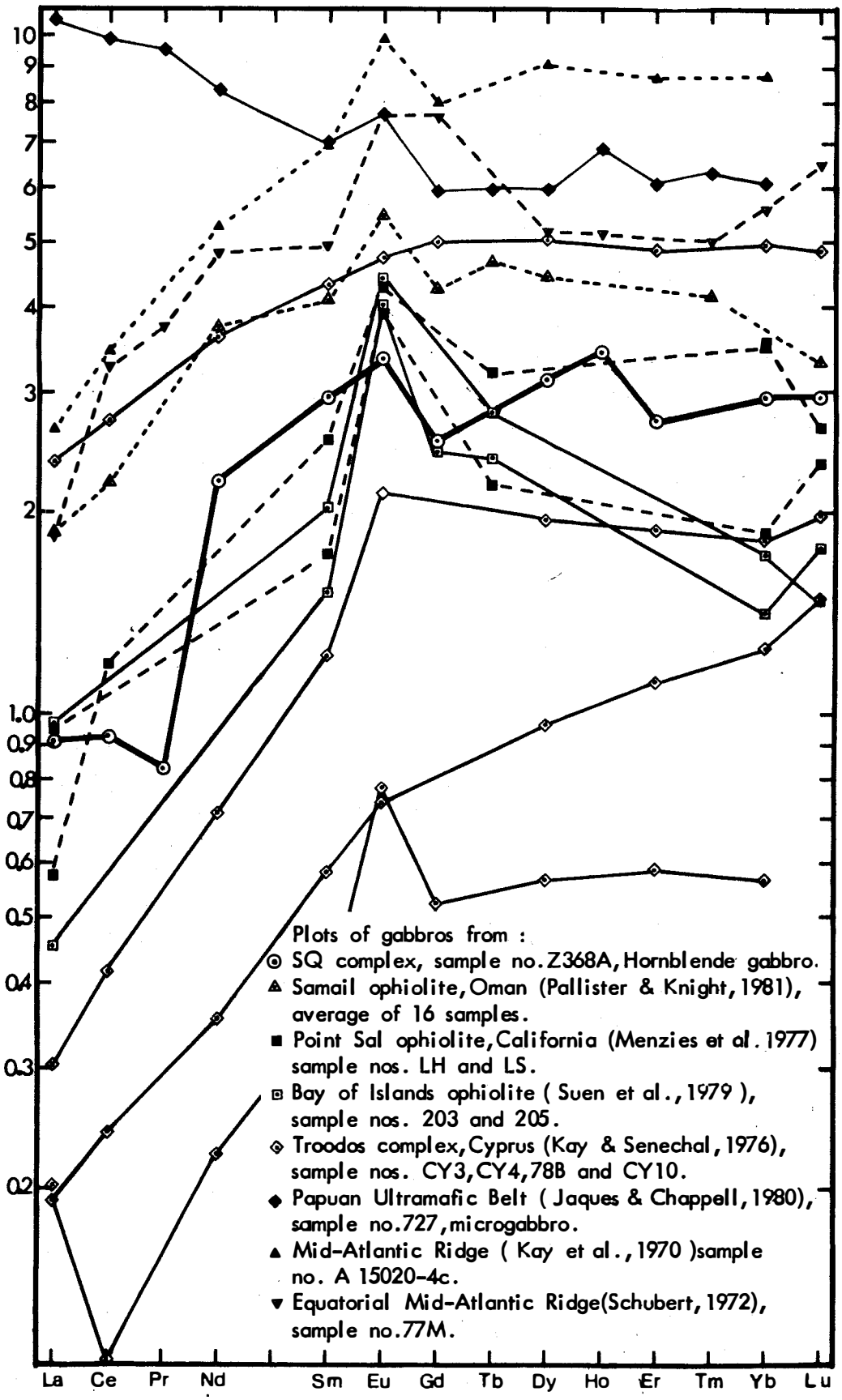

Fig. 3. Chondrite normalized plots using chondritic REE values from Nakamura (1974), for the gabbroic rocks from various ophiolites, in comparison to the SQO amphibole - gabbro (thick line).

Five out of six metadolerite samples in Fig. 1 plot in a narrow band and show LREE depletions stronger than those found in most diabase samples from other ophiolites and MORB. A comparison with diabase samples from Oman, Bay of Islands, Chamrousse and Troodos ophiolites is made in Fig. 2. Fig. 2 shows the higher REE contents in the SQO metadolerites (sp. No. Z370), except one sample from Oman. The two Troodos diabases show slight negative Eu anomalies. For the Bay of Islands ophiolite, the sample with lower REE values has a negative Eu anomaly. Most sheeted diabase samples from Ibra, Oman, show no Eu anomaly, but in some samples, a gradation from gabbros with lower REE and positive Eu anomalies to basaltic lavas with higher REE contents and negative Eu anomalies is observed (Pallister & Knight, 1981). The effects of later alteration or metamorphism on REE of basaltic rocks of ophiolites are generally considered either negligible or tending to increase the LREE content (Hellman *et al.*, 1977; Suen *et al.*, 1979). Therefore, the LREE depletion of metadolerites of SQO may reflect the primary distribution of REEs in the basaltic liquid produced during the formation of the SQO part of the Tethyan oceanic lithosphere. Although pillow lavas and basalts are not present at SQO the metadolerites show REE contents at the level of ophiolitic and oceanic basalts, and are better samples of primary magma chemistry than the volcanic rocks might have been (Pallister & Knight, 1981). The positive Eu anomalies, [Eu/Eu* = 1.23 to 2.26] and relative REE depletions found in the SQO metagabbros (Fig. 1) are in agreement with gabbro analyses from other ophiolites and Mid-Atlantic Ridge gabbros as plotted in Fig. 3. The Eu anomalies reflect the accumulation of plagioclase at low oxygen fugacity. The Eu anomalies at SQO are retained although the primary plagioclase is altered. The "eastern" part of metagabbro with modal quartz shows stronger Eu anomaly than either the lower olivine-normative, or the upper, amphibole-richer gabbro. The amphibole-rich metagabbro (sp. Z368A in Fig. 1) shows higher REE than the other two samples of metagabbro, and seems to represent a later fractionate.

Table 11. Variation ranges of trace elements, in p.p.m., for the SQO rock units.

	1	2	3	4	5	6	7	8	9	10	11	12
Ba	2-4	1-5	1-23	0-13	1-10	2-15	13-14	10	4-6	9-11	20	7-33
Rb	5-11	7-9	5	5	3-15	4-6	5-6	5	3	5	5	7
Sr	1-6	1-6	1-11	6-7	4-7	7-16	11-16	219	90-127	53-64	n.d.	60-74
Zr	4-5	3	6-9	5-8	4-6	4-18	8-10	43	5-39	10-48	66	35-82
Ag	2	2	2	2	1-3	1-2	3-4	n.d.	n.d.	n.d.	n.d.	n.d.
Co	80-100	81-100	84-105	84-90	61-90	28-38	66-68	20	16	23	32	59-64
Cr	970-3250	1410-3777	2229-5070	2753-3837	840-3006	1160-3209	1684-1789	460	147-250	300-360	250	49-130
Cu	9-16	1-12	10-18	10-40	7-14	6-20	85-94	22	39	60	34	82-155
Li	2-38	18	1-3	2-13	1-4	4-8	5	30	25	5	10	9-10
Mo	0	0	0	0	0	0	4-11	n.d.	n.d.	n.d.	n.d.	n.d.
Nb	13-14	18	12-16	16-90	10-13	9-10	9-10	n.d.	n.d.	n.d.	n.d.	n.d.
Ni	2370-2710	2080-2690	2770-3303	2192-2871	1856-3070	655-798	311-327	470	230-350	200-260	220-	150-390
Sc	8-9	7	5-13	5-15	7-10	14-21	62-65	n.d.	n.d.	n.d.	n.d.	n.d.
V	47-93	67-77	37-72	30-69	45-86	57-206	230-237	27	26-48	161-209	270	491-600
Y	0.2-2	0.7-2	0.2-3	0.1-1	0.2-3	0.4-2	5-8	2	2-4	6-8	9-12	29.37
Zn	66-80	3	69-82	61-73	50-120	14-31	79-82	72	88	123	119	140-146

1. Clinopyroxene-harzburgite. 2. Harzburgite. 3. Dunite. 4. Clinopyroxene-bearing dunite. 5. Wehrlite. 6. Clinopyroxenite. 7. Fe-websterite. 8. Lower level (quartz-free) metagabbro. 9. Middle-level (quartz-bearing) metagabbro. 10. Upper-level, amphibole-metagabbro. 11. Metadolerite. 12. Metasomatized metadolerite.

The relatively higher REE abundance and stronger LREE depletion observed in Fe-websterite (sp. no. Z36 in Fig. 1) compared to the rest of the pyroxenites indicates that Fe-websterite is more fractionated than other pyroxenites. This interpretation agrees with the results of major element chemistry as well as the mineral chemistry. A similar relation holds between the metadolerites and gabbro and other ultramafic rocks of SQO.

The consistently LREE depleted patterns of all the analyzed samples of SQO differ from certain ophiolites in which LREE enrichment has also been noticed. The Chamrousse ophiolite of Alps (Bodinier *et al.*, 1981), for instance, has been shown to have evolved in 3 stages with the earlier stages producing LREE-enriched rocks.

DISCUSSION

The rocks of the SQO have a very large ultramafic section dominated by harzburgite that has a relatively restricted range of chemical variation. The dunites and wehrlites that may have formed as cumulates, do not outcrop in a well defined separately mapable unit. Their chemical variations are small, although an Fe-enrichment trend is present. The lithological units with smaller volumes show correspondingly greater fractionation at SQO. Gabbro outcrops are of relatively much smaller volume but represent at least three levels. First olivine-normative 'western' gabbro is at a lower level than the middle-level gabbro with modal quartz (Table 7) and probably formed before the upper-level quartz-normative amphibole gabbro. Among ultramafic rocks, pyroxenites occupy the smallest bodies, i.e., dykes representing latest differentiates that generally are highly magnesian like all other ultramafic rocks. But the Fe–websterites represent strong Fe-enrichment. The metadolerites lie below the gabbro, but chemically belong to later stages, and within them, variation is indicated by the differences between sp. no. ZB182 and the others such as no. Z371.

The SQO ultramafic rocks are very low in TiO_2 (TiO_2 seldom exceeds 0.02 mass %); but the mafic rock units display enrichment in Ti and appearance of phases like ilmenite, Ti-rich brown amphibole and sphene. The ultramafic rocks lack modal anorthite, but the norms show ubiquitously small amounts of An. Alkalies are very low in ultramafic rocks and Na increases in preference to K in the mafic rocks (Coleman, 1977).

The variation ranges of trace element contents of various rock units (Table 11) may not be so significant as the individual analyses, but they do show the behaviour of certain elements with fractionation. Ba, Sr and Zr exhibit depletion in harzburgites, but increase towards later fractionates. The roughly constant amounts of Rb, around 5 ppm, may reflect the larger error of its separate analytical method (A.A.S.) at low concentrations, because at higher concentrations, e.g., in schists, Rb variation parallels that of Ba. Cr, Ni and Co are more concentrated in ultramafic rocks and decrease in later differentiates. Compared to the Cu contents in ophiolitic rocks (Coleman, 1977), the SQO ultramafic rocks are only slightly rich in Cu; but in metadolerites, Cu is rather high and in the dykes where hydrogrossular veins are abundant (e.g., sp. no. Z371), Cu values of upto 783 ppm may denote metasomatic introduction of Cu. This does not agree with the view that post-igneous hydrothermal alteration may remove Cu from ophiolites. Rather, the late hydrothermal activity seems to have concentrated Cu and caused its mineralization in the hydrogrossular veins. However, the increase of Cu in Fe-websterite (sp. no. Z36) over other pyroxenite dykes points towards increasing Cu content with differentiation because this websterite lacks field or petrographic evidence of metasomatism. Vanadium contents also increase steadily from residual and cumulate ultramafic rocks towards pyroxenites, hornblende gabbro and metadolerites. The trace element data also shows that Fe-websterite differs from the rest of the pyroxenites. Electron probe analyses of the Fe-websterite show the constituent minerals display

strong cryptic variation from the rest of the dykes. Thus, its mineral and whole-rock compositions tend to place it even after the gabbros. However, its SiO_2, Cr, Co and Ni contents show that it crystallized along with pyroxenites rather than the mafic differentiates. Probably the dyke represents a closed system evolution independent of the main magma chamber fractionation.

The REE abundance levels at the SQO, in parallelism with other ophiolites (e.g., Menzies *et al.*, 1977), follow the order: metadolerites–gabbros–ultramafic rocks. Moreover, all the rocks show LREE depletions. In the Ibra area, Samail ophiolite, Oman, Pallister & Knight (1981) related the REE abundance levels of various rock types to their stratigraphy. At the Bay of Islands ophiolite, the REE progressively increase from dunite/harzburgite to lherzolite, gabbro, dykes, and lavas (Malpas, 1978); and Suen *et al.*, (1979) found inverse correlation between REE content and mg* values of rocks (mg* = 100 X Mg/(Mg + total Fe as Fe^{2+})). At SQO, relatively higher REE contents of metadolerites show them to be later fractionates than the gabbros. Thus, the present locations of metadolerites within ultramafic outcrops below the gabbros may be caused by tectonic activity.

Earlier on, the rodingites were considered as:

(i) products of extreme magmatic differntiation (Bell *et al.*, 1911);

(ii) crystallization of basic magma after limestone digestion (Finalayson, 1909; Bilgrami, 1960);

(iii) metasomatism of gabbros, deriving lime from pyroxene in adjacent ultramafics (Grange, 1927; Miles, 1950);

(iv) garnetization of gabbros at high pressures by concentrated magmatic waters;

(v) action of CaO and CO_2 bearing hydrothermal solutions on gabbro (Bloxam, 1954);

(vi) granetization of dolerites by serpentinizing fluids taking Ca from pyroxenes of peridotite and Al from plagioclase of dolerite (Bilgrami & Howie, 1960).

In more recent literature, generally the rodingites are considered to have formed by serpentinization-related Ca-rich fluids acting metasomatically on a variety of rocks such as gabbro, diabase, dacite, granite, graywacke and shale. Moreover, rodingites may form during all the four types of ophiolite metamorphism, i.e., oceanic hydrothermal metamorphism, subduction metamorphism, obduction metamorphism and regional metamorphism of protolith peridotites (Coleman, 1977).

At SQO, most of the small rodingite lenses are contained in the northern serpentinite outcrop. Still, the rodingitization seems to be independent of serpentinization. The latter is usually a pervasive alteration, whereas the former occurs only along fractures and cracks in rocks. The accessory 'ferritchromit' in the chloritic walls and within the rodingite lenses probably didn't form by rodingitizing fluids because it is Al-depleted with respect to parent chromite grains, whereas the rodingitizing fluids are all Al-rich and have caused chlorite formation. 'Ferritchromit' might have formed earlier, during serpentinization. Al released by chromite alteration during serpentinization usually does not move great distances and may not have reached the rodingitizing fluids. Rather, the SQO rodingites seem to suggest formation by the action of sea water channelled through fractures and cracks in rocks during its spreading centre stage. The dispersed 'ferritchromit' crystals suggest rodingite formation in ultramafic environment or in fractures of such rocks, and does not necessarily require the prior occurrence of diabase or gabbro to be replaced. The brown grossular euhedra line the open cavities leaving vugs where they grow from low temperature solutions. The almost monomineralic white veins of hydrogrossular and grossular are most probably open cavity fillings, although they show some metasomatic activity localized to walls of veins, e.g., where the metadolerite dykes are touched (e.g., sp. no. Z371A), native Cu and nantokite are developed along with some nearby ilmenite which might be left over after replacement of metadolerite by the rodingitizing fluids.

The process of garnetization occurs after even the serpentinization. Thus, we see rodingite dykes enclosed even by only partly serpentinized ultramafic rocks and pyroxenites. The more frequent rodingite lenses in the northern serpentinite of the SQO are probably because of it being the upper (top) part where the sea waters would penetrate more as compared to the lower part of the ophiolite. The hydrogrossular is not related to the breakdown of original calcic plagioclase (cf. Coleman, 1977) because hydrogrossular veins traverse even the chromitites with no sign of earlier existence of plagioclase. Sea water origin for the rodingites of the Lizard complex, Great Britain, was suggested by Hall (1979). Evidence for the existence of hot circulating sea water within the upper few kms of newly formed oceanic crust at spreading centres is given by Coleman (1977). Francis (1981) has shown that the transform faults as well as 'gloria' faults penetrate into the mantle and provide a means of circulating large volumes of sea water through the oceanic mantle. Espinosa (1980) observed that serpentinization, and by-product rodingitization, in an ophiolite of Columbia occurred when the rock sequence was on the ocean floor. Kempe & Easton (1974) reported the occurrence of hydrogarnets in marine sediments in the Indian Ocean. Easton *et al.* (1977) noted the presence of hydrogarnet in the deep sea sediments formed at about 170°C from sea water hydrothermal solutions passing through altered basalts. Rodingites are reported from the present day ocean floors by Honnorez & Kirst (1975); and the metasomatism of rodingites is agreed upon by most workers to be a low temperature process (Dal Piaz *et al.*, 1980; Honnorez & Kirst, 1975).

Applying the criteria of Ishiwatari (1985), the SQO rocks represent products of moderate (15% to 30%) degree of partial melting in the lherzolitic source mantle.

SQO falls in-between the two end-member ophiolites (the Liguria-type and the Papua-type) as it contains high-alumina metadolerites, clinopyroxene-type cumulates with abundant wehrlite, and clinopyroxene-bearing harzburgite and dunite. The CaO and Al_2O_3 contents and incompatible elements of ultramafic rocks of SQO are slightly above and Mg/ (Mg + Fe) slightly below those of the typical clinopyroxene-free harzburgites such as Papua. The mineral chemistry such as the $Cr/(Cr+ Al+Fe^{3+})$ of chromite, Fo contents of olivine, and Al_2O_3 and TiO_2 contents of clinopyroxenes (Ahmed, 1987a, b) also support this relationship. Ophiolites may have an island- arc origin (Miyashiro, 1973). The absence of volcanic rocks shows that such an origin for SQO is not likely. Moreover, the harzburgite of SQO is not so strongly depleted as would be expected beneath the volcanic front of an arc (Tatsumi *et al.*, 1983).

CONCLUSIONS

The SQO is a dominantly ultramafic, highly dismembered ophiolite especially in its crustal sequence. It was emplaced tectonically just south of the suture zone between Indian and Eurasian plates. Tectonite harzburgite is the dominant rock type followed by wehrlite and dunite. The cumulate-tectonite contact is not clearly defined; although the harzburgite, dominant towards the southern part, is the refractory residual rock, and cumulate-wehrlite is concentrated upwards towards the north. Exceptions exist where wehrlites become dominant towards the southern contact. The harzburgite compositions compared to the average uppermost mantle compositions based on spinel lherzolites (Maalœ & Aoki, 1977) are depleted in Na_2O, K_2O, Al_2O_3, CaO and TiO_2 and enriched in MgO; and SiO_2 is lower in some samples.

The cumulate rocks do not contain orthopyroxene, although the non-cumulate pyroxenite dykes contain a limited amount of orthopyroxenes. The pyroxenites are highly magnesian, coarse-grained and rich in clinopyroxenes. At least one 'Fe-websterite' dyke has finer grain size than most pyroxenite dykes and exhibits an abnormally evolved Fe-rich chemistry. It may have fractionated independently of the fractionation in the main magma chamber. Serpentinization of the SQO is intense along a narrow belt adjacent to the northern (upper) contact of the ultramafic rocks; and is much weaker over the rest of the complex, except along some asbestos-bearing veins or shear zones. Rodingitization at SQO seems to

have been effected by the sea-water metasomatism contrary to the generally accepted view that sepentinization solutions are responsible for this process. The gabbroic rocks, now metamorphosed, show a limited development, but lower-level, middle-level and upper-level lithostratigraphic horizons are recognizable.

The basaltic liquid of the SQO is represented by the dolerites, now metamorphosed and metasomatized to varying degrees by the rodingitizing solutions. Their chondrite-normalized patterns of REE contents show characteristic and strong LREE depletions. The REE abundance levels progressively increase from ultramafic rocks to Fe-websterites, metagabbros and to metadolerites.

The rock assemblage of SQO could have been congenetically formed after moderate degree of partial melting in the lherzolitic source mantle. This concept is supported by the transitional relationship between the cumulates and residual peridotite of SQO, the high clinopyroxene content of cumulus wehrlite and dunite the presence of clinopyroxene-bearing harzburgite, the CaO, Al_2O_3 and Mg(Mg+Fe) contents of the bulk rocks and lithostratigraphic comparison with other ophiolites (e.g., Ishiwatari, 1985).

REFERENCES

AHMAD, S. (1969). An improved scheme for chromite analysis. Geol. Bull. Punjab Univ. 8; pp. 33-8.

AHMED, Z. (1982) Chromite deposits of the Sakhakot-Qila ultramafic complex, Pakistan. Ph.D. thesis, University of London King's College, UK, (Unpublished), 344 p.

———**(1984)** Stratigraphic and textural variations in the chromite composition of the Sakhakot-Qila complex, Pakistan. Econ. Geol. **79**, (6), pp. 1334-59.

———**(1987a)** Mineral chemistry of the Sakhakot-Qila ophiolite, Pakistan: Part 1, monosilicates. Acta Mineralogica Pakistanica **3**, pp. 26-41.

———**(1987b)** Mineral chemistry of the Sakhakot-Qila ophiolite, Pakistan: Part 2, polysilicates. Acta Mineralogica Pakistanica **3**, pp. 140-58.

———**(1988)** Mineral chemistry of the Sakhakot-Qila ophiolite, Pakistan: Part 4, disilicates, tectosilicates and non-silicates. This Volume.

——— **& HALL, A. (1981)** Alteration of chromite from the Sakhakot-Qila ultramafic complex, Pakistan. Chemic der Erde **40**, pp. 209-39.

——— & ——— **(1984)** Petrology and mineralization of the Sakhakot-Qila ophiolite, Pakistan. *In:* Gass, I.G., Lippard, S.J. & Shelton, A.W. (eds.) OPHIOLITES AND OCEANIC LITHOSPHERE. Geol. Soc. London Spec. Publ. **13**, pp. 241-52.

BARNES, I., LA MARCHE JR., V.C. & HIMMELBERG, G. (1967). Geochemical evidence of present-day serpentinization. Science **156**, pp. 830-2.

BELL, J.M., CLARKE, E. de C. & MARSHALL, P. (1911) The geology of the Dun Mountain Subdivision, Nelson. New Zealand Geol. Surv. Bull. **12**, pp. 1-71.

BUGRAMI, S.A. (1960) Serpentinite-limestone contact at Tleri Mohammad Jan, Zhob Valley, West Pakistan. Amer. Mineral. **45**, pp. 1008-19.

———, **& HOWIE, R.A. (1960)** The mineralogy and petrology of a rodingite dyke, Hindubagh, Pakistan. Amer. Mineral **45**, pp. 791-801.

BLOXAM, T.W. (1954) Rodingite from the Girvan-Ballantrae complex, Ayrshire. Min. Mag. **30**, pp. 525-28.

BODINIER, J.L., DUPUY, C., DOSTAL, J. & CARME, F. (1981) Geochemistry of ophiolites from the Chamrousse complex. (Belledonne Massif, Alps). Contrib. Mineral. Petrol. **78**, pp. 379-88.

COLEMAN, R.G. (1977) Ophiolites —— Ancient Oceanic Lithosphere? Springer-Verlag, Berlin, 229p.

DAL PIAZ, G.V., DI BATTISTANI, G., GOSSO, G. & VENTURELLI, G. (1980) Rodingitic gabbro dykes and rodingitic reaction zones in the upper Valtour nanche-Breuil area, Piemonte ophiolite nappe, Italian western Alps. Archives des Sciences **33** (2–3), pp. 161-79.

EASTON, A.J., HAMILTON, D., KEMPE, D.R.C. & SHEPPARD, S.M.F. (1977) Low temperature metasomatic garnets in marine sediments. Phil. Transac. Roy. Soc. London **A-286**, pp. 253-71.

ESPINOSA, A. (1980) Rodingites of the Los Azules ophiolitic sequence in the western Cordillera of the Colombian Andes. Archives des Sciences **33** (2-3), pp. 337-50.

FINALAYSON, A.N. (1909) The nephrite and magnesian rocks of the South Island of New Zealand. Quart. Jour. Geol. Soc. London **65**, pp. 351-81.

FRANCIS, T.J.G. (1981) Serpentinization faults and their role in the tectonics of slow spreading ridges. Jour. Geophys. Res. **86**, (B-12), pp. 11616-22.

GRANGE, L.I. (1927) On the 'rodingite' of Nelson. Transac. New Zealand Inst. **58**, pp. 160-6.

GREEN, D.H. (1964) The petrogenesis of the high-temperature peridotite intrusion in the Lizard area, Cornwall. Jour. Petrol. **5**, pp. 134-88.

HALL, A. (1979) Rodingites in the Lizard complex. Proceedings of the USSHER Society **4** (3), pp. 269-73.

HELLMAN, P.L., SMITH, R.E. & HENDERSON, P. (1979) The mobility of the rare earth elements: evidence and implications from selected terraines affected by burial metamorphism. Contrib. Mineral. Petrol. **71**, pp. 23-44.

HONNOREZ, J. & KIRST, P. (1975) Petrology of rodingites from the Equatorial and Mid-A lantic fracture zones and their geotectonic significance. Contrib. Mineral. Petrol.

HONNOREZ, J. & KIRST, P. (1975) Petrology of rodingites from the Equatorial and Mid-Atlantic fracture zones and their geotectonic significance. Contrib. Mineral. Petrol. **49**, pp. 233-57.

ISHIWATARI, A. (1985) Igneous petrogenesis of the Yakuno ophiolite (Japan) in the context of the diversity of ophiolites. Contrib. Mineral Petrol. **89**, pp. 155-67.

JACKSON, E.D. & THAYER, T.P. (1972). Some criteria for distinguishing between stratiform, concentric and alpine peridotite-gabbro complexes. 24th Internat. Geol. Congr. Montreal, Sec. 2, pp. 289-96.

JAQUES, A.L. & CHAPPELL, B.W. (1980) Petrology and trace element geochemistry of the Papuan ultramafic belt. Contrib. Mineral. Petrol. **75** (1), pp. 55-70.

KAY, R., HUBBARD, N.J. & GAST, P.W. (1970) Chemical characteristics and origin of oceanic ridge volcanic rocks. Jour. Geophys. Res. **75** (8), pp. 1585-613.

---- & SENECHAL, R.G. (1976) The rare-earth geochemistry of the Troodos ophiolite complex. Jour. Geophys. Res. **81**, pp. 964-70.

KEMPE, D.R.C. & EASTON, A.J. (1974) Metasomatic garnets in calcite (micarb) chalk at site 251, southwest Indian ocean. Initial Rep. Deep Sea Drill. Proj. **26**, pp. 593-601.

LIOU, J.G., LAN, C-Y., SUPPE, J. & ERNST, W.G. (1977). The East Taiwan Ophiolite: its occurrence, petrology, metamorphism and tectonic setting. Mining Res. Serv. Org., Indus. Tech. Res. Inst., Taiwan, Spec. Rep. **1**, 212p.

LONEY, R.A., HIMMELBERG, G.R. & COLEMAN, R.G. (1971) Structure and petrology of the alpine-type peridotite at Burro Mountain, California, U.S.A. Jour. Petrol. **12**, pp. 245-309.

MAALØE, S. & AOKI, K.I. (1977) The major element composition of the upper mantle estimated from the composition of lherzolites. Contrib. Mineral. Petrol. **63**, pp. 161-73.

Mac DONALD, G.A. & KATSURA, T. (1964) Chemical composition of Hawaiian lavas. Jour. Petrol. **5**, pp. 82-133.

MALPAS, J. (1978) Magma generation in the upper mantle, field evidence from ophiolite suites, and application to the generation of oceanic lithosphere. Phil. Trans. Royal Soc. London **A-288**, pp. 527-46.

MENZIES, M.A., BLANCHARD, D., BRANNON, J. & KOROTEV, R. (1977) Rare earth and trace element geochemistry of a fragment of Jurassic sea floor, Point Sal, California. Geochim. Cosmochim. Acta **41**, pp. 1419-30.

MILES, K.R. (1950) Garnetized gabbros from the Eulamina District, Mt. Margaret Goldfield. Geol. Surv. Western Australia Bull. **103** (2).

MIYASHIRO, A. (1973) The Troodos ophiolite complex was probably formed in an island arc. Earth Planet. Sci. Lett. **19**, pp. 218-24.

NAKAMURA, N. (1974) Determination of REE, Ba, Fe, Mg, Na and K in carbonaceous and ordinary chondrites. Geochim. Cosmochim. Acta **38**, pp. 757-75.

PALLISTER, J.S., & KNIGHT, R.J. (1981) Rare-earth element geochemistry of the Semail ophiolite near Ibra, Oman, Jour. Geophys. Res. **86**, pp. 2673-97.

SCHUBERT, C.E. (1972) Rare earth element distribution in Equatorial and Mid-Atlantic Ridge gabbros. Nature 237, pp. 26-8.

SUEN, J., FREY, F.A., & MALPAS, J. (1979) Bay of Islands ophiolite suite, Newfoundland: Petrolgic and geochemical characteristics with emphasis on rare earth element geochemistry. Earth Planet. Sci. Lett. **45**, pp. 337-48.

TATSUMI, Y., SAKUYAMA, M., FUKUYAMA, H. & KUSHIRO, I. (1983) Generation of are basalt magmas and thermal structure of the mantle wedge in subduction zones. Jour. Geophys. Res. **88**, pp. 5815-25.

TAYLOR, S.R. & McLENNAN, S.M. (1981). The composition and evolution of the continental crust: rare earth element evidence from sedimentary rocks. Phil. Transac. Roy. Soc. London **A-301**, pp. 381-99.

THAYER, T.P. (1977) Some implication of sheeted dyke swarms in ophiolitic complexes. Geotectonics (English translation) **11**, pp. 419-26.

WALSH, J.N. & HOWIE, R.A. (1980). An evaluation of the performance of an inductively coupled plasma source spedtrometer, dr the determination of the major and trace constituents of silicate rocks and minerals. Min. Mag. **43**, pp. 967-74.

WALSH, J.N., BUCKLEY, F. & BARKER, J. (1981) The simultaneous determination of the rare-earth elements in rocks using inductively coupled plasme source spectrometry. Chem. Geol. **33**, pp. 141-53.

WILSON, A.D. (1955) A method for the determination of iron in rocks. Bull. Geol, Surv. Great Britain **9**, pp. 56-8.

Manuscript received on 5.2.1988
Accepted for publication on 30.3.1988

ACTA MINERALOGICA PAKISTANICA
VOLUME 4 (1988) pp. 30 - 44.

MINERALOGY AND MINERAL CHEMISTRY OF SULPHIDE CHIMNEYS FROM ESCANABA TROUGH, GORDA RIDGE

KATHERINE J. HOWARD[1] & MARTIN R. FISK[2]
[1] Centre of Excellence in Mineralogy, University of Balochistan, Quetta, Pakistan.
[2] College of Oceanography, Oregon State University, Corvallis, Oregon, U.S.A.

ABSTRACT: Sulphide chimneys recovered from the Escanaba Trough, southern Gorda Ridge are dominantly lattices of boxwork pyrrhotite with interstitial minor sphalerite, chalcopyrite, isocubanite, galena and barite. Exceptions include one dominantly pyrite chimney fragment and one barite chimney. In pyrrhotite-rich samples, pyrrhotite laths are frequently rimmed by Cu-Fe sulphides and sphalerite, Zn-rich rims form around Cu-Fe sulphides and galena is included in sphalerite. Chimney weathering is similar to that observed in sulphide deposits recovered from the Guaymas Basin, Gulf of California. Initially, pyrrhotite oxidizes to marcasite. Final products of chimney weathering include elemental sulphur, amorphous Fe oxyhydroxides, goethite, lepidocrocite and possibly akaganeite and atacamite. Some Fe oxyhydroxides represent direct precipitation from cooler FeOOH saturated solutions rather than in situ alteration of sulphides. Clay minerals and detrital sediments are a significant fraction of weathered chimneys. Small amounts of minerals previously unidentified in mid-ocean ridge hydrothermal environments include bismuth telluride, cassiterite, a Ni-Cu-Zn sulphide and cinnabar. Cinnabar is a trace mineral in a barite chimney that contains fine-scale Sr zonation. Arsenopyrite identified in Escanaba Trough chimney samples is not commonly reported in mid-ocean ridge hydrothermal deposits. The presence of arsenopyrite, bismuth telluride and cassiterite are evidence for the interaction of hydrothermal fluids with terrigenous sediments filling the Escanaba Trough.

INTRODUCTION

Mid-ocean ridge massive sulphide deposits are formed by hydrothermal circulation of seawater in the oceanic crust. Seawater penetrates deep into the oceanic crust, becomes heated and exists at the seafloor chemically and isotopically changed by interaction with the crust. When the heated water mixes with cold, bottom water or pore fluids in sediments, several chemical compounds reach saturation and precipitate. The precipitation of minerals forms mounds and chimneys where hydrothermal fluids vent on the seafloor. Some of the more spectacular results are sulphide chimneys that grow into spires as high as five-story buildings.

Mid-ocean ridges are categorized by spreading rate and whether they are sediment-filled or sediment-starved. Sediment-filled ridges with slower spreading rates generally produce larger sulphide deposits (Rona, 1988). Also, sediment-covered ridges generally produce a greater diversity in the chemistry and mineralogy of hydrothermal deposits because of hydrothermal reactions in the sediments (perhaps associated with prolonged high temperature and slow water flow conditions) in addition to seawater-basalt interactions.

The Escanaba Trough is a slowly spreading, sediment-filled segment of oceanic ridge. Hence, it is a likely environment to find relatively large sulphide deposits. Preliminary evidence of active hydrothermal vents in this region was the discovery of anomalously high heat flow (> 1200 mW/m²) associated with sediment domes caused by underlying volcanic intrusions (Abbott, 1986). Subsequent dredging operations collected polymetallic sulphides in the sediments (Morton *et al.*, 1987). In 1986, the results of the above studies culminated in U.S. Navy sponsord SEACLIFF submersible dives around two of the larger volcanic edifices within the

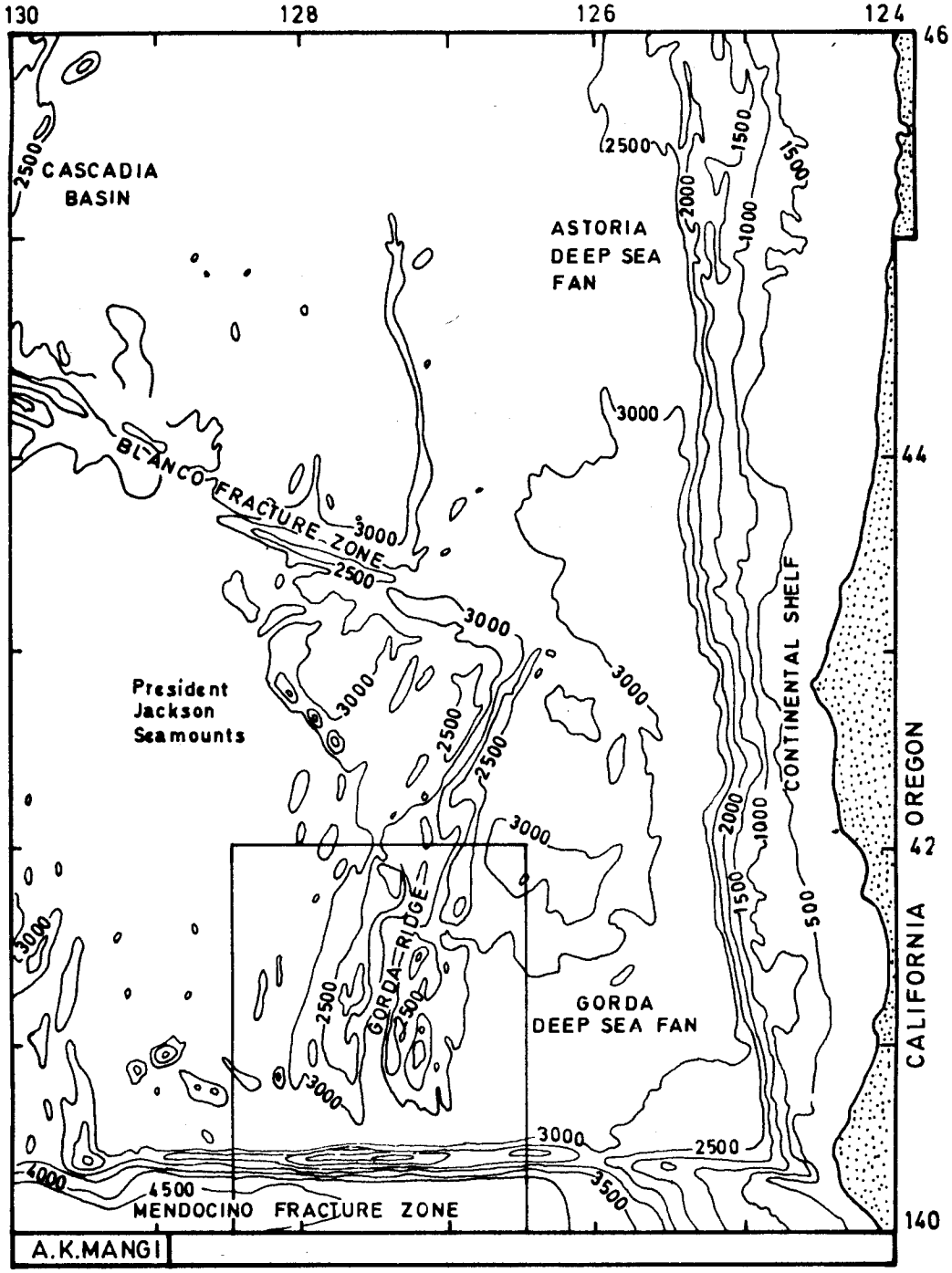

Fig. 1. Location of the Gorda Ridge off the coast of Oregon and California from Wilde *et al.*, (1978, 1979). Area outlined is shown enlarged in Fig. 2. Contour interval = 500m.

Escanaba Trough. Highly weathered, inactive chimneys were discovered and sampled at both volcanic domes visited.

This report summarizes the mineralogy and mineral chemistry of sulphide chimneys from the Escanaba Trough, southern Gorda Ridge collected by the submersible SEACLIFF in August, 1986. Studies of Escanaba Trough mineral deposits are of interest to researchers in Pakistan since the Murray Ridge, off the coast of Pakistan may be an analogous environment for substantial polymetallic sulphide formation (Farah & Lawrence, this issue).

TECTONIC SETTING

The Escanaba Trough is a slowly spreading (2.3 cm/yr full rate) segment of volcanic ocean ridge located within the U.S. Exclusive Economic Zone about 300 km off the coast of northern California (Fig. 1) (Atwater and Mudie, 1973, Riddihough, 1980). It is the southernmost of three segments that comprise the 300-km-long Gorda Ridge and unlike the northern two segments, it is filled with sediments. The northern limit of the Escanaba Trough is defined by a small right-lateral offset at 41° 30'N where the axial valley narrows to 3–5 km width (Riddihough, 1980). The Escanaba Trough is bounded to the south by the Mendocino Fracture Zone (40° 24'N), where the axial valley is up to 18 km wide. Within the Escanaba Trough, the water depth over the axial valley floor averages about 3,200 m and flanking ridges are 1,200 to 1,700 m high.

A gap between the end of the ridge and the Mendocino Fracture Zone creates a channel for turbidites originating from the North American continental margin (Moore, 1970). This terrigenous sediment, up to 500 m thick, fills the Escanaba Trough south of 41° 15'N where the axial valley shoals (Moore, 1970; Karlin & Lyle, 1989). The insulating blanket of sediment provides a mechanism for maintaining high temperatures in the hydrothermal system that enhance chemical exchange between the hydrothermal fluids and the sediments. Evidence of significant interaction between hydrothermal fluids and sediment at depth has been reported by Morton *et al.*, (1987) and deposition of sulphides and sulphates in the sediments has been documented by Karlin & Lyle (1989).

Sample Location

Six volcanic centres, located by seismic reflection profiles, are spaced at 15 to 20 km intervals along the axis of the Escanaba Trough and dome the otherwise flat-lying sediments up to 100 m high (Morton *et al.*, 1987). The two largest volcanic edifaces are located at 40° 45'N latitude and 41°N latitude (Fig. 2) and are designated Dome B and Dome D, respectively. The sites of SEACLIFF dives around Dome D are designated NESCA sites (for northern Escanaba Trough) and those around Dome B are designated SESCA sites (for southern Escanaba Trough). Fifteen chimney fragments were examined in this study. Ten samples are from NESCA Dome D (five from Dive 658 and five from Dive 659) and five samples are from SESCA Dome B (one from Dive 661, two from Dive 662 and two from Dive 663).

At NESCA, the neovolcanic centre is located on the eastern side of the axial valley. Dive 658 located a fault bounding Dome D to the north that contained the most extensive, best preserved, sulfide deposits at NESCA. A barite chimney, collected at the bottom of the slope at this site, is one of the fragments described in this report (sample 658-R2-B). Large outcrops of fresh, glassy pillow basalt are located on a nearby hill and in the basin surrounding the hill. Smaller chimneys growing through the sediments were discovered during Dive 659. At SESCA, the neovolcanic centre is located on the western side of the axial valley and has more extensive sediment cover than at NESCA. Dives 661, 662 and 663 are all located on faults bounding sediment domes.

METHODS

Subsampling

The fifteen chimney fragments were subdivided into samples based on (1) degree of

alteration, and (2) mineralogical variability. Generally, an outer surface that represents the weathered exterior exposed to more oxygenated seawater (designated "altered") was separated from the more protected, fresher chimney interior (designated "fresh"). One sample from the freshest portion of each chimney fragment was sampled for analysis and classified as "fresh" with the following exceptions. Samples 659-1 and 661-R1 were completely weathered throughout and subsamples of these were classified as "altered". Two additional samples from Dive 659 (samples 659-3 and 659-R1-F) and one additional sample from Dive 662 (662-3-2) were separated for analysis because each appeared mineralogically different. In "altered" samples, discernible differences in either hydrothermal precipitate mineralogy or alteration products from weathering, enabled further subdivision. Splits of all samples were subjected to X-ray diffraction to determine sample mineralogy and atomic absorption to determine bulk chemistry. Mineralogical results are presented here.

X-ray Diffraction

Samples were ground in a mortar and pestle and random, air-dried powder mounts were prepared on glass disks. Samples were initially analyzed from 2° to 100° 2θ at 1° 2θ/min on a SCINTAG X-ray diffractometer using Cu-Kα radiation. Sample diffractograms that indicated poorly crystalline material (low signal/background ratio) were rerun by a time averaging option using 6° 2θ/min and 20 consecutive scans over the same 2θ range. Peaks selected by computer were edited by hand and compared with the JCPDS files for inorganic minerals.

Electron Microprobe and Scanning Electron Microscope (SEM)

Polished sections of seven of the freshest chimney samples were prepared for microprobe analysis and scanning electron microscopy to examine primary and replacement mineralogy and the effects of alteration on sulphides. Six samples were chosen from Dome D and one from Dome B. Microprobe analyses were performed on the University of Oregon ARL/EMX microprobe using 15kV accelerating voltage and 0.15μA sample current. Each analysis was corrected using the standard Albee and Ray (1970) corrections. Scanning electron microscopy (SEM/EDS) was performed at the U.S.G.S., Menlo Park, California.

RESULTS

Mineralogy

The mineralogy of sulphide chimneys from the Escanaba Trough, divided between fresher interiors and weathered exteriors in direct contact with seawater, is summarized in Table 1. A more complete description of each subsample and selected X-ray diffractograms with mineral identifications are provided in Howard (1989). Complete separation of interior fresh sulphide from weathered exteriors was not attempted for mineralogical analysis, but major differences between the two subdivisions are apparent.

(a) Chimney interiors

Pyrrhotite dominates the fresher chimney interiors with the following exceptions: Sample 662 was dominantly pyrite, the interior of sample 662-R1 was dominantly lepidocrocite, four samples (658, 659-1, 661-R1, 663-R2) were primarily clays and in sample 663-R1, marcasite was the dominant iron sulphide. Sample 658-R2-B, the barite chimney, is essentially pure barite. Only hexagonal pyrrhotite was observed in X-ray diffractograms as in Guaymas Basin chimney samples studied by Koski *et al.* (1985).

Sphalerite, chalcopyrite/isocubanite and barite are secondary in abundance in sample interiors. Sphalerite is second in abundance in all samples from NESCA Dive 659, in one sample from NESCA Dive 658 (658-R1-1A) and in sample 662. Minor galena was found mainly by NESCA Dive 659 and SESCA Dive 662. Arsenopyrite was identified by XRD only in sample 659-R1-F. Otherwise, trace minerals were identified by SEM.

Four samples contain clays and three of these also contain quartz and plagioclase and/or phillipsite. These findings support the assertion of Vallier-Silver *et al.* (1987) that sediments are entrained in chimneys during ascent of hydrothermal fluids. In addition, the chimney deposits (samples 659-R1-F and 662-R1 from this study) have a petroliferous odour associated with asphaltic petroleum incorporated into the deposits by circulating hydrothermal fluids (Kvenholden, 1986; Morton *et al.*, 1987).

(b) Chimney exteriors

In contrast to fresher sulphide-rich chimney interiors, weathered exteriors have the following characteristics. First, clays, amorphous Fe-oxyhydroxides, goethite, lepidocrosite and akaganeite are in greater abundance in the exterior portions of the chimney. Second, sphalerite and barite are more abundant in sample exteriors, consistent with decreasing temperature and increasing oxidation, respectively, outward through the chimney walls (Haymon, 1983). Third, amorphous silica, elemental sulphur, gypsum and talc are identified primarily in sample exteriors.

Petrography

Samples chosen for petrographic examination are indicated in Table 1. Despite the effects of weathering, the freshest samples chosen for thin section preparation showed preservation of original textures and primary mineralogy. Open boxworks of pyrrhotite characterize all samples studied petrographically except sample 662 that contained primarily colloform pyrite. Larger pyrrhotite crystals, representing the main chimney flow channels, are surrounded by smaller, skeletal interlocking pyrrhotite crystals with an abrupt change in crystal size. Interstices in the pyrrhotite framework are partially filled with barite and secondary Fe-oxyhydroxides, implying later precipitation from cooling fluids. Minor replacement of pyrrhotite by sphalerite and chalcopyrite is observed in most samples. Sphalerite with inclusions of galena confirms the earlier crystallization of the latter.

Scanning Electron Microscopy (SEM)

Minerals in low abundance (≤5%) cannot usually be identified with certainty by XRD, and may not be distinguished by petrographic techniques employed in this study. However, minor minerals may be important in determining the distribution of trace elements and their contribution to ocean chemistry. To enable identification of minor mineralogy, as well as examine sulphide weathering in more detail, SEM was used on polished thin sections. One sample from Dome B and six samples from Dome D were examined by SEM to determine minor minerals, replacement textures and alteration affects (Table 1). The major SEM results are summarized below. Details of the observations are provided in Howard (1989).

(a) Trace Minerals

A Sn-rich mineral included in Fe-sulphide crystallized in samples from both Dome B (Dive 662) and Dome D (Dive 659). Although identification is not certain, low Fe and S concentrations recorded by the SEM probably represent contributions from the surrounding Fe-sulphide (pyrite at Dive 662 and pyrrhotite at Dive 659) and strongly suggest the Sn is incorporated in cassiterite (SnO_2). Another sample from Dive 659 contained as As-rich mineral intergrown with isocubanite. A significant sulphur concentration indicates the presence of arsenopyrite ($FeAs_2S$) although loellingite ($FeAs_2$) has also been reported in Escanaba Trough sulphide chimneys (Zierenberg *et al.*, 1986; Koski *et al.*, 1988). Bismuith telluride in pyrrhotite was identified in sample 658-R3-A and cinnabar was preserved in a portion of the barite chimney (658-R2-B). This is the first documentation of both minerals in mid-ocean ridge hydrothermal deposits studied to date.

(b) Replacement Minerals

Observations of replacement mineralogy by SEM confirm those obtained by microscopy. Pyrrhotite, chalcopyrite and isocubanite often have Zn-rich rims and are replaced primarily

by sphalerite. Both of the above observations are consistent with crystallization of sphalerite during later stage decrease in fluid temperature. In sample 658-R3-A, pyrrhotite is rimmed by Ni-Cu-Zn sulphide. Incorporation of Ni in a secondary replacement sulphide is unusual considering its immobility in seawater-basalt interaction experiments (Mottl, 1983; Seyfried & Janecky, 1985) and studies of natural metabasalts (Humphries & Thompson, 1978). However, some evidence for Ni mobility during alteration of basalt is observed on the northern Gorda Ridge (Howard & Fisk, 1986, 1988). From the above observations, the following paragenetic sequence is proposed:
pyrrhotite → Cu-Fe sulphides + galena → sphalerite → barite

(c) Alteration Minerals

The primary type of alteration observed in the chimney fragments is the oxidation of pyrrhotite ($Fe^{+2}S^{-2}$) to marcasite ($Fe^{+2}S_2^{-1}$) (Ramdohr, 1969). A decrease in the Fe/S ratio near the borders of corroding pyrrhotite cyrstals is evidence of this oxidation effect. A distinct separation between pyrrhotite crystals and Fe oxyhydroxides suggest that the latter in part precipitated from solution onto pyrrhotite crystals rather than formed entirely from in situ alteration of pyrrhotite grains. This hypothesis is consistent with the interpretation based on similar observations of altered chimney samples from the Guaymas Basin (Koski *et al.*, 1985).

No sulphate minerals were observed as an intermediate stage of alteration of pyrrhotite to Fe oxyhydroxides, but elemental sulphur is a common alteration product recorded by X-ray diffraction. Atacamite, tentatively identified in sample 659-R1, is formed from the weathering of Cu-Fe sulphides (Haymon & Kastner, 1983)

Mineral Chemistry

Tables 2 to 5 contain electron microprobe analyses of iron sulphides, isocubanite, sphalerite and barite. The Fe content of pyrrhotite determined by electron microprobe (Table 2) is consistent with precipitation of hexagonal pyrrhotite observed both megascopically and in X-ray diffractograms and implies temperatures of formation > 250°C (Krissen & Scott, 1982). All Fe sulphides are relatively free of impurities in contrast to pyrite from 21°N, East Pacific Rise (EPR) that crystallized with high Zn contents (up to 4.2 wt%) attributable to minute ZnS inclusions (Zierenberg *et al.*, 1984).

Microprobe analyses of Escanaba Trough sphalerites all have low totals (Table 3). This may reflect the absence of silica in the analyses as is the case for southern Juan de Fuca Ridge and 21°N, EPR in which precipitation of amorphous silica accompanied the crystallization of zinc sulphides (Koski *et al.*, 1984; Zierenberg *et al.*, 1984). Sphalerites are enriched in both FeS and CuS. CuS enrichment may signify minor Cu-Fe sulphide inclusions. In sample 659-3, FeS in sphalerite ranges from 30 to 36 mole%, similar to Guaymas Basin sphalerites also associated with pyrrhotite. Sphalerites from both Escanaba Trough and Guaymas Basin are richer in FeS than sphalerites from the southern Juan de Fuca Ridge (Fig. 3) reflecting the latter's association with pyrite. Sphalerite in sample 662-1 is associated with pyrite and its FeS content is hence, less (14 mole%).

Cu-Fe sulphides are similar in chemistry to cubanite ($CuFe_2S_3$) (Table 4) and are slightly higher in sulphur and lower in Cu than cubanites from the Juan de Fuca Ridge (Fig. 4). Zierenberg (pers. comm.) suggested this phase is actually cubic cubanite (or isocubanite) which could have precipitated in equilibrium with pyrrhotite (Craig & Scott, 1974; Haymon, 1983; Zierenberg *et al.*, 1984). X-ray diffraction analysis of this sample yielded only chalcopyrite. If this was an Fe-rich chalcopyrite of high temperature origin, cooling could result in exsolution of cubanite (Deer *et al.*, 1966) which was the mineral analyzed by microprobe. Hekinian *et al.*, (1980) report an X-ray diffraction pattern for high temperature cubanite with two major peaks indistinguishable from a-form chalcopyrite. Microprobe analyses are required to resolve the uncertainty in Cu-Fe sulphide mineralogy.

Table 1. **Mineralogy of weathered sulphide chimneys from NESCA and SESCA sites, Escanaba Trough, Gorda Ridge.**

NESCA

Sample	Mineralogy[a] Interior	Exterior
Dive 658		
(1) 658	clay, qz, pl	clay, qz, pl, gp?
(2) 658-R1-1A*	po, sp, cp, ba	ba, po, sp, cp, si
(3) 658-R2-B*	ba, cn[s]	amorph. Mn & Fe oxyhydroxide, ba, si[c]
(4) 658-R3-A*	po, mc, cp, iss, sp, ba gn, Ni-Cu-Zn sulphide[s] bismuth telluride[s]	sp, ba, hm, gt, sl, si?[m]
(5) 658-R4-1A*	po, cp, lp, sl, gt, mc[s]	
Dive 659		
659 – 1	clay(s), si[c]	
(6) 659-2*	po, sp, gn, cp, mc[s], ca[s]	ba, po, sp, cp, gn
(7) 659-3*	po, sp, cp, gn[s], as[s]	sl, po, sp, cp
(8) 659-R1	po, sp	gt, ak, clay, si[c], at?
(9) 659-R1-F$_{(p)}$	po, sp, cp, sl	gt, lp, sp, cp, iss, po, as, sl, ak, clays, mc?

SESCA

Dive 661		
661 – R1	clay, gt, ak, qz, pl/z	
Dive 662		
(10) 662*	py, sp, ba, gn, ca[s]	ba, gt, py, sp, clay, si[m]
(11) 662-R1$_{(p)}$	lp, po, cp, sl	sp, cp, lp, po, ba, sl
Dive 663		
(12) 663-R1	mc, cp, at, mica?	gp, gt, qz, ak?, ba, sp, pl/z? clay
(13) 663-R2	Fe-clay, ak, lp, gt	clay, gt, py, qz, pl, talc, si[m]

ak: akaganeite
as: arsenopyrite
at: atacamite
ba: barite
ca: cassiterite
cn: cinnabar
cp: chalcopyrite
gn: galena
gp: gypsum
gt: goethite
hm: hematite
iss: cubanite
lp: lepidocrosite
mc: marcasite
pl: plagioclase
po: pyrrhotite
py: pyrite
qz: quartz
si: amorphous silica
sl: sulphur
sp: sphalerite
z: zeolite (phillipsite)

[a] identified by XRD unless otherwise noted and listed in approximate order of decreasing abundance. [s] identified by SEM. [m] megascopic identification. [c] presence of amorphous silica predicted by Si/Al>> 3.
? tentative identification. $_{(p)}$ petroliferous odour.
* samples chosen for petrographic and SEM examination.

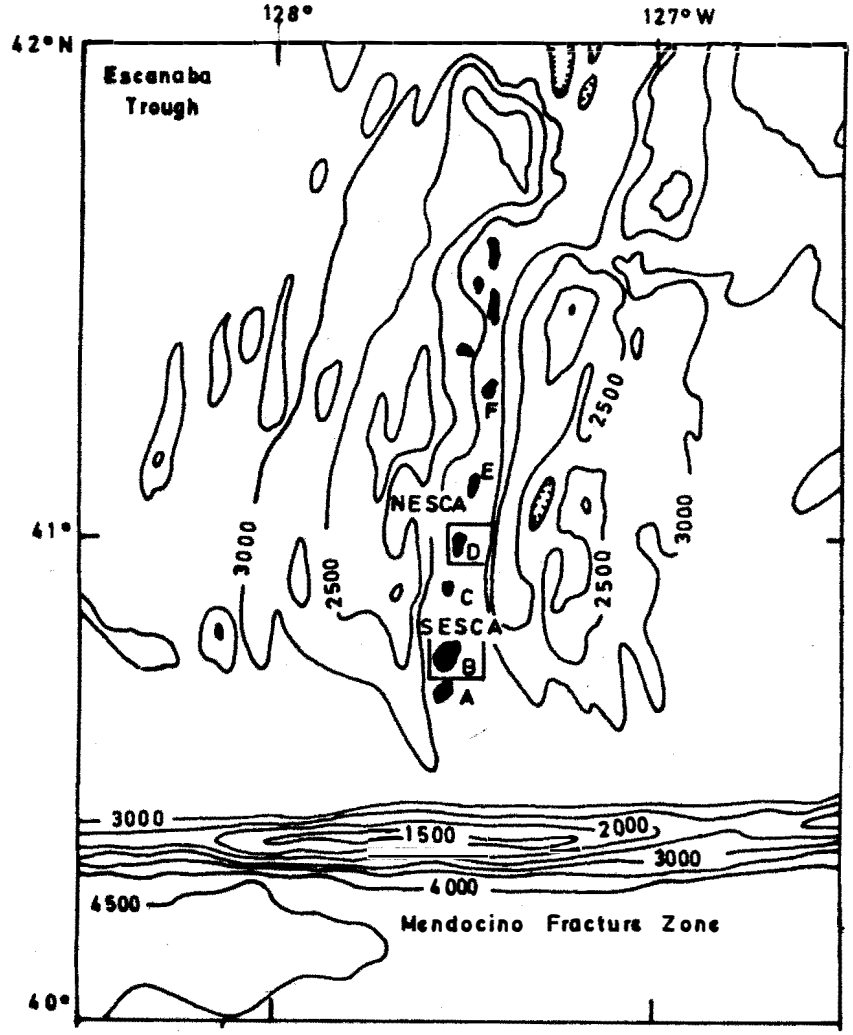

Fig. 2. Bathymetric map of the Escanaba Trough after Wilde et al., (1979) showing the locations of six major volcanic edifices (A through F shown in solid pattern) along the axis of the Gorda Ridge from Abbott et al., (1986).

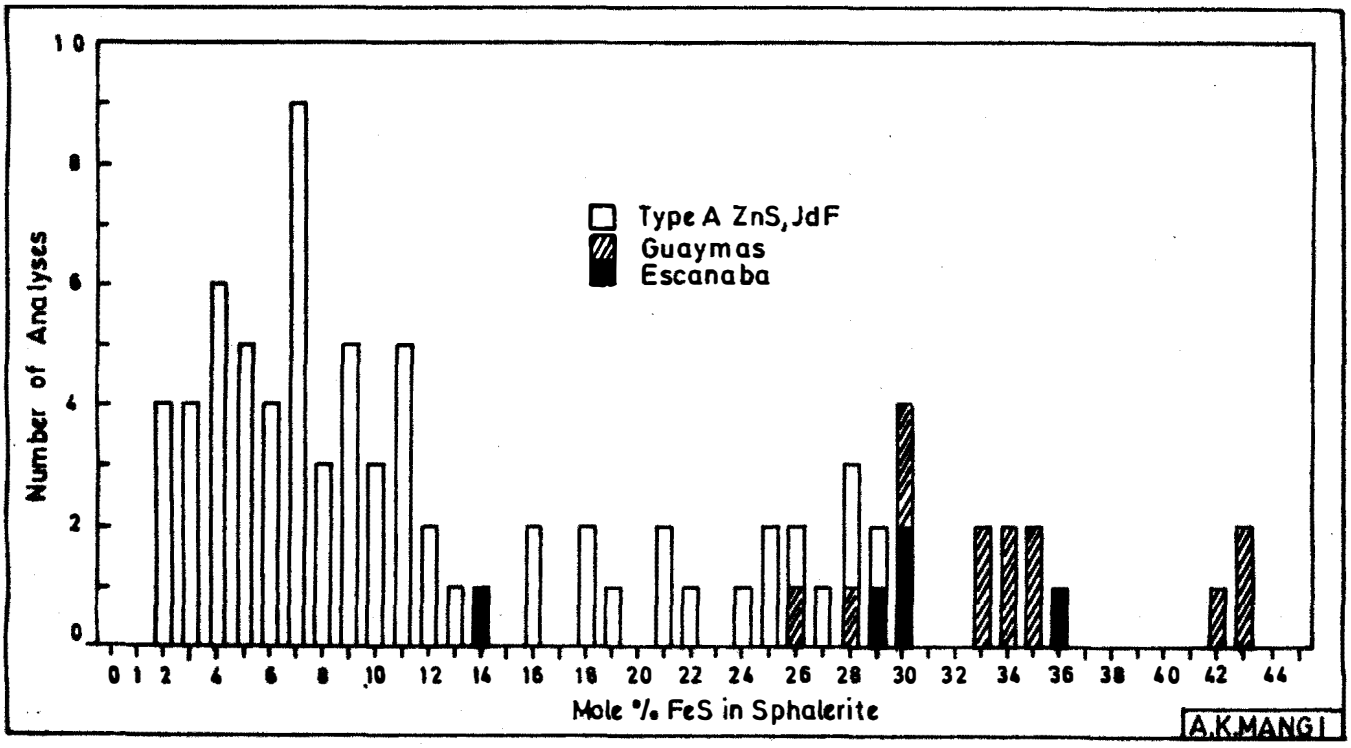

Fig. 3. Histogram of mole % FeS in sphalerite from the Escanaba Trough compared to Guyamas Basin (Koski *et al.*, 1985) and Type A sphalerite from the southern Juan de Fuca Ridge (Koski *et al.*, 1984).

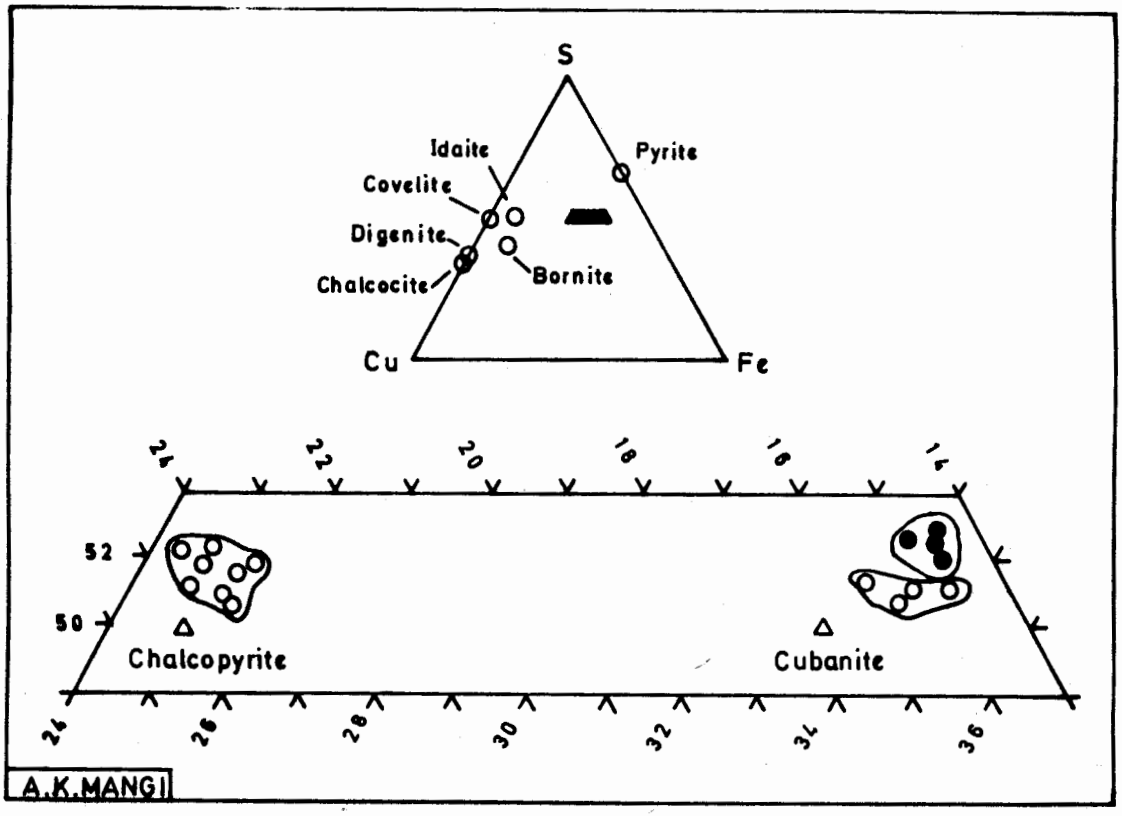

Fig. 4. Composition of cubanite from the Escanaba Trough (solid circles) compared to southern Juan de Fuca Ridge (open circles) (Koski *et al.*, 1984). Labelled triangles are stoichiometric chalcopyrite and cubanite.

The composition of barite from the barite chimney (658-R2-B) and from sample 662-1 provides confirmation that chemical zoning observed in SEM primarily reflects fluctuations in Sr content and to a lesser extent fluctuations in Ca content (Table 5). The Pb content of barite in both samples is consistently about 0.2 wt%.

DISCUSSION

The Escanaba Trough, southern Gorda Ridge, Guaymas Basin, Gulf of California and Middle Valley, Endeavor Ridge are all sediment-filled spreading ridges with polymetallic sulphides forming from the interaction between hydrothermal fluids, basalts and sediments All three sediment-covered ridges have a higher proportion of non-sulphide minerals (barite, opaline silica and talc) than at 21°N, EPR or southern Juan de Fuca Ridge which are sediment-free ridges. In terms of major mineralogy and textures, sulphide chimneys from the Escanaba Trough are most similar to chimney samples recovered from the Guaymas Basin. Despite differing sediment chemistry, both hydrothermal systems precipitated abundant pyrrhotite and barite. Sphalerite and Cu-Fe sulphides are interstitial to the boxwork pyrrhotite texture. Pyrite is less common. Both regions contain Fe-rich sphalerite when associated with pyrrhotite, but the abundance of Zn-sulphide is greater in Escanaba Trough deposits than in Guaymas Basin deposits.

Koski *et al.* (1985) calculated phase relations in the system Cu-Fe-S-O at 300°C and 20MPa (Fig. 5) to estimate the approximate sulphur and oxygen fugacities of the hydrothermal fludis. The presence of pyrrhotite signifies fluids with lower sulphur fugacity than fluids that precipitate pyrite. The fluid may have been depleted in sulphur by precipitation of pyrite in volcanic turbidites as observed by Karlin & Lyle (1989). Koski *et al.* (1985) suggest that the lower sulphidation state may also result from the removal of S_2 by reactions within the sediments such as:

$$S_2 + 2H_2O + C = CO_2 + 2H_2S$$

Figure 6 shows that pyrrhotite and barite represent disequilibrium assemblages (Koski *et al.*, 1985). The sulphur fugacity of sphalerite in equilibrium with pyrrhotite at 300°C is estimated based on its FeS content (Scott & Barnes, 1971). The FeS contents of sphalerite (30-36 mole%) from the Escanaba Trough (Table 2c) show it could have precipitated in equilibrium with pyrrhotite and chalcopyrite. Only one sample (662-1) crystallized abundant pyrite and the FeS content of associated sphalerite (15 mile%) is predictably low.

The lack of carbonate minerals in hydrothermal deposits from both Escanaba Trough and Middle Valley is in stark contrast to Guaymas

Table 2. **Electron microprobe analyses of iron sulphides.**

Analysis	Fe	Cu	Zn	Mn	Cd	S	SUM	Phase
NESCA								
	Sample: 658-R3-A							
1	59.91	0.13	0.16	0.04	nd	38.10	98.34	po
2	61.19	0.13	0.16	0.04	nd	37.99	99.51	po
3	46.29	0.13	0.14	0.30	nd	52.45	99.32	mc
4	60.03	0.13	0.16	0.04	0.21	37.98	98.55	po
NESCA		Sample: 659-3						
1	58.47	0.13	0.16	0.04	0.21	37.26	96.26	po
2	59.37	0.13	0.16	0.04	0.21	37.61	97.52	po
3	60.28	0.16	0.16	0.05	0.21	37.74	98.60	po
4	58.70	0.13	0.16	0.05	0.21	38.27	97.52	po
5	59.04	0.13	0.16	0.04	0.20	36.87	96.44	po
6	58.23	0.13	0.16	0.04	0.20	36.76	95.58	po
SESCA								
	Sample: 662-1							
1	48.75	0.22	0.21	0.04	0.16	53.21	102.59	py
2	48.31	0.22	0.21	0.04	0.16	52.53	101.47	py
3	45.86	0.22	0.21	0.04	0.16	51.00	97.49	py
4	48.35	0.22	0.21	0.04	0.16	52.27	101.25	py

po = pyrrhotite, mc = marcasite, py = pyrite.
* Each analysis represents a separate grain.

Table 3. **Electron microprobe analyses of sphalerite.**

Analysis	Fe	Cu	Zn	Mn	Cd	S	SUM	Mole% Fe
	Sample: 662-1							
1	14.86	1.71	31.17	0.32	0.22	22.78	71.06	36
2	13.10	1.47	25.09	0.39	0.22	29.57	69.84	30
3	17.39	0.46	28.83	0.04	0.22	39.09	86.04	31
4	18.37	1.10	31.92	0.04	0.22	41.03	92.69	31
	Sample: 662-1							
	7.30	0.67	43.72	0.04	0.31	29.93	81.96	15

Table 4. **Electron microprobe analyses of isocubanite from sample 658-R3-A.**

Analysis	Fe	Cu	Zn	Mn	Cd	S	SUM
1	41.14	20.59	1.41	0.04	0.22	35.58	98.99
2	41.95	20.36	1.58	0.04	0.22	35.56	99.72
3	41.89	20.08	1.69	0.05	0.22	34.94	98.87
4	41.35	19.90	1.30	0.04	0.22	35.62	98.43
iss*	42.0	22.6	–	–	–	35.1	99.7

* from Brett *et al.*, (1987).

Basin deposits and implies either carbonates dissolved at lower temperatures because of retrograde solubility (Holland & Malinin, 1979), or carbonate minerals dissolve in acidic solutions associated with active chimney formation or weathering of sulphides.

Barite has been identified in hydrothermal deposits from sediment-free spreading ridges (Corliss *et al.*, 1978, Hekinian *et al.*, 1980; Fisk & Howard, 1989), but it is observed in greatest abundance at sediment-covered spreading ridges (Koski *et al.*, 1985; Davis *et al.*, 1987). In Guaymas Basin deposits, barium in barite could precipitate with organic carbon as it falls through the water (Lyle, pers. comm., 1989). The barium in Escanaba Trough chimney fragments may be partially derived from this source, but feldspars in the terrigenous sediments are abundant (plagioclase: quartz ratio is 5:1; Karlin & Lyle, 1989) so this is also a likely source for both Ba and Sr. Sr zonation in barite could indicate fluctuations in hydrothermal fluid chemistry.

Mg-rich clays and talc in the exterior of sample 663-R2 formed when Mg-depleted hydrothermal fluids interacted with Mg-rich bottom water or pore fluid (Lonsdale *et al.*, 1980; Haymon & Kastner, 1981; Koski *et al.*, 1984, 1985). If analogous to talc described from Guaymas Basin, its formation temperature is between 270-280°C (Lonsdale *et al.*, 1980; Koski *et al.*, 1985). The formation of talc may reflect sluggish discharge of hydrothermal fluids (Koski *et al.*, 1988).

Table 5. **Electron microprobe analyses of barite. Individual crystals were analyzed twice (a and b below) to examine fluctuations in Sr and Ca.**

Sample: 658-R2-B (Barite chimney).

Analysis	Ba	Sr	Ca	Pb	S	O*	SUM
1a	60.94	1.17	0.60	0.21	12.31	24.79	100.02
b	58.82	0.78	0.88	0.21	12.67	26.64	100.00
2a	59.78	0.91	0.88	0.21	12.90	25.33	100.01
b	58.79	0.75	0.84	0.21	12.52	26.90	100.01
3a	61.03	1.19	0.42	0.21	12.34	24.82	100.01
b	59.28	1.01	0.66	0.21	12.93	25.92	100.01
4a	60.31	1.09	0.38	0.21	12.80	25.24	100.03
b	60.15	0.37	0.17	0.21	12.94	26.17	100.01
5a	55.33	1.98	0.38	0.21	12.97	29.15	100.02
b	51.97	2.38	0.44	0.21	13.29	31.71	100.00
6a	53.59	1.98	0.44	0.21	13.40	30.40	100.02
b	52.23	2.48	0.65	0.21	13.57	30.87	100.01
Sample: 662-1							
1a	56.14	0.73	0.22	0.21	12.35	28.36	100.01
b	56.12	1.01	0.27	0.21	12.54	29.86	100.01
2a	60.94	0.12	0.03	0.21	11.96	26.77	100.03
b	60.23	0.44	0.05	0.21	12.38	26.70	100.01
3a	61.55	1.06	0.30	0.21	11.46	25.44	100.02
b	60.31	1.46	0.47	0.21	12.59	24.97	100.01

*Oxygen by difference.

Cinnabar, identified in sample 658-R2-B (Table 1) may be preserved because of the lower temperatures associated with the formation of the barite chimney. Most Hg ores form at relatively low temperatures (between 100° and 200°C) and thermodynamic calculations of Varekamp and Buseck (1984) predict that cinnabar cannot coexist with pyrrhotite at temperatures between 100° and 250°C. This may account for its absence in pyrrhotite-rich chimneys.

The paragenetic sequence observed in Escanaba Trough hydrothermal deposits differs from Guaymas Basin deposits in the order of Cu-Fe sulphides versus Zn-sulphide precipitation. In contrast to Guaymas Basin, Cu-Fe sulphides precipitate earlier than Zn-sulphides in Escanaba Trough deposits. The earlier precipitation of Cu-Fe sulphides at Escanaba Trough implies temperatures of the hydrothermal fluid rose, possibly in response to sealing off of the chimneys by precipitation of anyhydrite, barite and amorphous silica (Haymon & Kastner, 1983; Tivey & Delaney, 1986) at an earlier stage of chimney growth. As hydrothermal activity wanes and finally shuts down, dissolution and oxidation of chimney deposits results in mineralogical changes that are recorded in the weathered rind of Escanaba Trough deposits.

Newly identified trace minerals provide evidence for fluid- sediment interaction. Trace minerals bismuith telluride and cassiterite are unknown in Cyprus or 21°N, EPR sulphide deposits, but are often found in island arc massive sulphide ore (Oudin *et al.*, 1981). Cassiterite, in particular, is typically associated with acidic volcanism (Oudin *et al.*, 1981) and native bismuith (identified in Escanaba

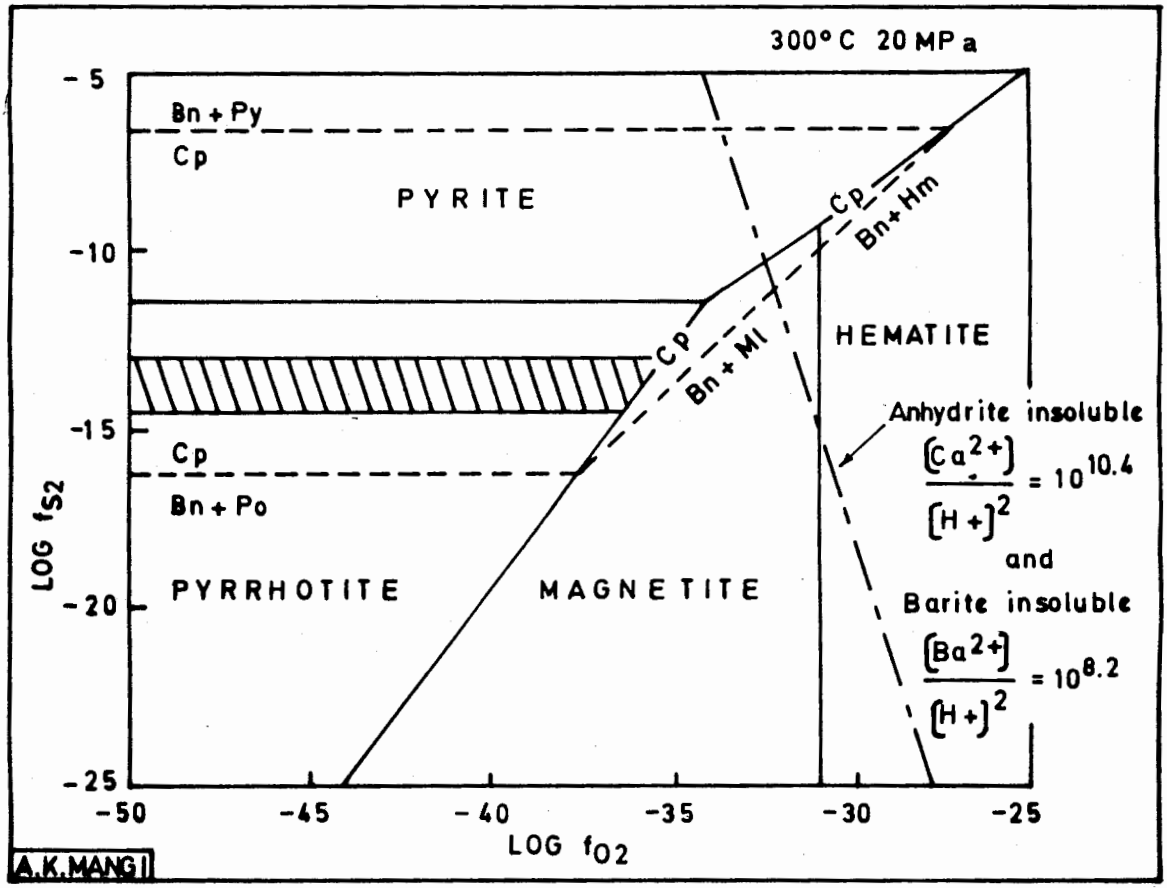

Fig. 5. Phase relations in the system Cu-Fe-S-O at 300°C and 20MPa from Koski *et al.*, 1985 with approximate fs for sphalerite with mole % FeS contents equal to those measured in Escanaba Trough sulfides (cross-hatched area). Bn = bornite, Cp = chalcopyrite, Hm = hematite, Mt = magnetite, Po = pyrrhotite, Py = pyrite.

Trough chimney samples by Koski *et al.*, 1988) is frequently associated with Pb, an indicator of sediment interaction in mid-ocean rige hydrothermal deposits. The presence of both cassiterite and bismuith telluride is strong evidence for the interaction between hydrothermal fluids and terrigenous sediments filling the Escanaba Trough.

CONCLUSIONS

(1) Sulphide chimneys from the Escanaba Trough are dominantly boxwork latices of pyrrhotite with interstitial sphalerite, Cu-Fe sulphides, barite and amorphous silica. Temperatures of formation are > 250°C based on the presence of hexagonal pyrrhotite.

(2) Observations of mineral textures and replacement mineralogy suggests the following paragenetic sequence: pyrrhotite → Cu-Fe sulphides + galena → sphalerite → barite.

(3) The observation of pyrrhotite rimmed by a Ni-Cu-Zn sulphide suggests either some mobilization of Ni by hydrothermal fluids or scavenging of Ni from seawater.

(4) Weathering of sulphide chimneys proceeds by the oxidation of pyrrhotite to marcasite and finally alteration to Fe oxyhydroxides (goethite, lepidocrocite and akaganeite) and elemental sulphur. Fe oxyhydroxides also form as precipitates from cooler FeOOH saturated solutions. These processes are similar to those observed in Guaymas Basin sulphide deposits.

(5) Arsenopyrite and newly identified trace minerals, cassiterite and bismuith telluride, are evidence for the interaction of hydrothermal fluids with terrigenous sediments filling the Escanaba Trough.

(6) Studies of hydrothermal deposits from the Escanaba Trough, Southern Gorda Ridge may prove of particular interest to researchers in Pakistan because the Murray Ridge off the coast of Pakistan may be an analogous environment with similar associated formation of massive sulphide deposits.

ACKNOWLEDGEMENTS

The U.S. Geological Survey (via Rob Zierenberg) contributed SEACLIFF dive samples for this study. Randy Koski and Rob Zierenberg of the U.S.G.S. were valued scientific resources and discussions with them contributed greatly to the interpretations in this study. Randy Koski arranged for K.J.H. to use the SEM facility at Menlo Park and Bob Oscarson is thanked for technical support. Greg Campi facilitated the use of the SCINTAG X-ray diffractometer and Mike Shaffer and University of Oregon are thanked for microprobe time. K.J.H. thanks Zulfiqar Ahmed for easing her transition to the Centre of Excellence in Mineralogy and for inviting this contribution to the Centre's journal. Jim McDougall is also thanked for his editorial comments. This research was supported by a grant from Minerals Management Service administrated by Oregon Department of Geology and Mineral Industries under Grant #63-630-8509

REFERENCES

ABBOTT, D.H., MORTON, J.L. & HOLMES, M.L. (1986) Heat flow measurements on a hydrothermally-active, slow spreading ridge: The Escanaba Trough. Geophys. Res. Lett. **13**, pp. 678-80.

ALBEE, A.L. & RAY, L. (1970) Correction factors for electron probe microanalysis of silicates, oxides, carbonates, phosphates and sulphides. Anal. Chem. **42**, pp. 1408-14.

ATWATER, T. & MUDIE, J.D. (1973) Detailed near-bottom geophysical study of the Gorda Rise. J. Geophys. Res. **78**, pp. 8665-86.

BRETT, R., EVANS, H.T. JR., GIBSON, E.K. JR., HEDENQUIST, J.W., WANDLESS, M.-V. & SOMMER, M.A. (1987) Mineralogical studies of sulphide samples and volatile concentrations of basalt glasses from the southern Juan de Fuca Ridge J. Geophys. Res. **92**, pp. 11, 373-79.

CORLISS, J.B., LYLE, M., DYMOND, J. & CRANE, K. (1978) The chemistry of hydrothermal sediment mound deposits near the Galapagos Rift. Earth Planet. Sci. Lett. **40**, pp. 12-24.

CRAIG, J.R. & SCOTT, S.D. (1974) Sulphide phase equilibria. *In:* Ribbe, P.H. (ed.) SULFIDE MINERALOGY. Min. Soc. Am. Short Course Notes **1**, pp. CSI-CS110.

DAVIS, E.E., GOODFELLOW, W.D., BORNHOLD, B.D., ADSHEAD, J., BLAISE, B., VILLINGER, H. & Le CHEMINANT, G.M. (1987) Massive sulfides in a sedimented rift valley, northern Juan de Fuca Ridge. Earth Planet. Sci. Lett. **82**, pp 49-61.

DEER, W.A., HOWIE, R.A. & ZUSSMAN, J. (1966) AN INTRODUCTION TO THE ROCK-FORMING MINERALS. J. Wiley & Sons, 528p.

FISK, M.R. & HOWARD, K.J. (1989) Mineral deposits recovered from the northern Gorda Ridge: mineralogy and chemistry. Oregon Department of Geology and Mineral Industries, Open-File Report **0-89-09**, 26p.

HAYMON, R. (1983) The growth history of hydrothermal black smoker chimneys. Nature **301**, pp. 695-8.

——— **& KASTNER, M. (1981)** Hot spring deposits on the East Pacific Rise at 21°N: preliminary description of mineralogy and genesis. Earth Planet. Sci. Lett. **53**, pp. 363-81.

HEKINIAN, R., FEVRIER, M., BISCHOFF, J.L., PICOT, P. & SHANKS, W.C. (1980) Sulfide deposits from the East Pacific Rise near 21°N. Science **207**, pp. 1433-44.

HOLLAND, H.D. & MALININ, S.D. (1979) The solubility and occurrence of non-ore minerals. *In*: GEOCHEMISTRY OF HYDROTHERMAL ORE DEPOSITS. John Wiley & Sons, New York pp. 461-508.

HOWARD, K.J. (1989) Hydrothermal vents of the Gorda Ridge, NE Pacific: Mineralogy and chemistry of sulfide chimneys, precipitates and alteration products. M.S. Thesis, Oregon State University (Unpublished).

——— **& FISK, M.R. (1986)** Hydrothermal precipitates from basalts on the Gorda Ridge and the President Jackson Seamounts. Oregon Department of Geology and Mineral Industries, Open-File Report 0-86-18.

——— **& FISK, M.R. (1988)** Hydrothermal alumina-rich clays and boehmite on the Gorda Ridge. Geochim. Cosmochim, Acta **52**, pp. 2269-79.

HUMPHRIES, S.E. & THOMPSON, G. (1978) Trace element mobility during hydrothermal alteration of oceanic basalts. Geochim. Cosmochim. Acta. **42**, pp. 127-36.

KARLIN, R. & LYLE, M. (1989) History of Holocene volcanic and hydrothermal activity in axial valley sediments on the Gorda Ridge. Mar. Geol. (in press).

KOSKI, R.A., CLAGUE, D.A. & OUDIN, E. (1984) Mineralogy and chemistry of massive sulfide deposits from the Juan de Fuca Ridge. Geol. Soc. Am. Bull. **95**, pp. 930-45.

——— **LONSDALE, P.F., SHANKS, W.C., BERNDT, M.E. & HOWE, S.S. (1985)** Mineralogy and geochemistry of a sediment-hosted hydrothermal sulfide deposit from the southern trough of Guaymas Basin, Gulf of California. J. Geophys. Res. **90**, pp. 6695-707.

——— **SHANKS, W.C. III, BOHRSON, W.A. & OSCARSON, R.L. (1988)** The composition of massive sulfide deposits from the sediment-covered floor of Escanaba Trough, Gorda Ridge: implications for depositional processes. *In:* SEA FLOOR HYDROTHERMAL MINERALIZATION. Can. Min. **26**, pp. 655-73.

KRISSEN, S.A. & SOCTT, S.D. (1982) Phase relations involving pyrrhotite below 350°C. Econ Geol. **77**, pp. 1739-54.

KVENHOLDEN, K.A., RAPP, J.B., HOSTETTLER, F., MORTON, J.L., KING, J.D. & CLAYPOOL, G.E. (1986) Petroleum associated with polymetallic sulfide on the Gorda Ridge. Science **234**, pp. 1231-4.

LONSDALE, P.F., BISCHOFF, J.L., BURNS, V.M., KASTNER, M. & SWEENEY, R.E. (1980) A high-temperature hydrothermal deposit on the seabed at a Gulf of California spreading center. Earth Planet. Sci. Lett. **49**, pp. 8-20.

MOORE, G.W. & SHARMEN, G.F. (1970) Summary of SCAN site 4: *In:* McManus, D.A. et al., (eds.) Initial Rep. DSDP **5**, U.S. Govt. Printing Office, Washington. pp. 761-73.

MORTON, J.L., HOLMES, M.L. & KOSKI, R.A. (1987) Volcanism and massive sulfide formation at a sedimented spreading center, Escanaba Trough, Gorda Ridge. Geophys. Res. Lett. **14**, pp. 769-72.

MOTTL, M.J. (1983) Hydrothermal processes at mid-ocean spreading centers: application of basalt-seawater experimental results. *In:* Rona, P.A., Bostrom, K., Laubier, L. & Smith, E.L. (eds.) HYDROTHERMAL PROCESSES AT MID-OCEAN SPREADING CENTERS, pp. 199-224.

OUDIN, E., PICOT, P. & POUIT, G. (1981) Comparison of sulfide deposits from the East Pacific Rise and Cyprus. Nature **291**, pp. 404-7.

RAMDOHR, P. (1969) THE ORE MINERALS AND THEIR INTERGROWTHS. Pergamon, Oxford.

RIDDIHOUGH, R.P. (1980) Gorda plate motions from magnetic anomaly analysis. Earth Planet. Sci. Lett. **51**, pp. 163-70.

RONA, P. (1988) Hydrothermal mineralization at oceanic ridges. *In:* Barrett, J.T. & Jambor, J.L. (eds.) SEAFLOOR HYDROTHERMAL MINERALIZATION. Can. Mineral. **26**, pp. 431-65.

SEYFRIED, W.E. JR. & JANECKY, D.R. (1985) Heavy metal and sulfur transport during subcritical and supercritical hydrothermal alteration of basalt: Influence of fluid pressure and basalt composition and crystallinity. Geochim. Cosmochim. Acta **49**, pp. 2545-60.

TIVEY, M.K. & DELANEY, J.R. (1987) Growth of large sulfide structures on the Endeavor segment of the Juan de Fuca Ridge. Earth Planet. Sci. Lett. **77**, pp. 303-17.

VALLIER-SILVER, J.N., TERA, F., KLEIN, J. & MIDDLETON, R. (1987) Beryllium 10 in hydrothermal vent processes from the East Pacific Ridges: Role of sediments in the hydrothermal processes. J. Geophys. Res. **92**, pp. 11,364-72.

VAREKAMP, J.C., & BUSECK, P.R. (1984) The speciation of mercury in hydrothermal systems with applications to ore deposition. Geochim. Cosmochim. Acta. **48**, pp. 177-185.

WILDE, P., CHASE, T.E., HOLMES, M.L., NORMARK, W.R., TONAS, J.A., McCULLOCH, D.S. & KULM, L.D. (1978) Oceanographic data off northern California-southern Oregon, 40° to 43° North including the Gorda Deep Sea Fan. LBL Publ. 251, Lawrence Berkeley Lab, Berkeley, California.

——— **CHASE, T.E., HOLMES, M.L., NORMARK, W.R., TOMAS, J.A., McCULLOCH, D.S., CARLSON, P.R., KULM, L.D. & YOUNG, J.D. (1979)** Oceanographic data off Oregon 43° to 46° North including Astoria Deep-Sea Fan. LBL Publ. 253, Lawrence Berkeley Lab, Berkeley, California.

ZIERENBERG, R.A., SHANKS, W.C.III & BISCHOFF, J.L. (1984) Massive sulfide deposits at 21°N, East Pacific Rise: Chemical composition, Stable isotopes and phase equilibria. Geol. Soc. Am. Bull. **95**, pp. 922-929.

——— **KOSKI, R.A., SHANKS, W.C.III & ROSENBAUER, R.J. (1986)** Form and composition of sediment-hosted sulfide-sulfate deposits, Escanaba Trough, southern Gorda Ridge (abs): EOS Trans. Am. Geophys. Union **67**, pp. 1282.

ACTA MINERALOGICA PAKISTANICA
VOLUME 4 (1988) pp. 45 - 64.

MINERAL CHEMISTRY OF THE SAKHAKOT–QILA OPHIOLITE, PAKISTAN: PART 3, PHYLLOSILICATES.

ZULFIQAR AHMED
Centre of Excellence in Mineralogy, University of Balochistan, G.P.O. Box 43, Quetta, Pakistan

ABSTRACT: Phyllosilicates of the Sakhakot-Qila ophiolite are products of secondary processes and include rock-forming and vein-serpentine, chlorite and clintonite. Serpentines of rock-forming and vein types appear chemically indistinct, and are rich in Mg. Structure of the asbestose chrysotile is $2M_{c1}$. Rarely, within samples, earlier serpentines may contain higher SiO_2, MgO and lower FeO, Al_2O_3, NiO, MnO than the later ones. Chlorite shows a diversity in mode of occurrence and composition. Rodingites and chromitites often contain "IIb-even" structure type chlorite with b cell dimension varying from 9.18 to 9.24 Å. Chlorite has variable Al, Fe and Mg; and a trend of Fe-enrichment and Mg-depletion is depicted from earlier towards later magmatic differentiates. Clintonite forms in rodingites by localized Al-metasomatism.

INTRODUCTION

This chemical characterization of the phyllosilicates from the Sakhakot-Qila ophiolite (abbreviated SQO) is an accompaniment to similar data for the rest of the mineral assemblage of SQO presented in three other communications (Ahmed, 1987a, 1987b, 1988). The phyllosilicates have formed by secondary processes of serpentinization, chloritization and rodingitization, which effect most of the ophiolites. The chemistry of serpentines, chlorites and clintonite from SQO is presented below supplemented by their mineralogy and occurrence.

SERPENTINE

Serpentine photographs from SQO (Figs. 1 to 3) indicate a diversity in occurrence.

Optical examination and X-ray powder patterns indicate the presence of a variety of serpentine minerals of different habits. Serpentine occurs in rock-forming and vein-forming fashions. Late veins of serpentine occur along fractures, shear zones, faults and joint planes. Many of such veins are asbestos-bearing and contain chrysotile. The ultramafic host rocks of asbestos veins frequently show relatively more intense serpentinization in narrow zones surrounding the asbestos veins. The thicknesses of such serpentinized zones often vary in proportion to the thickness of the associated chrysotile vein. Olivine in the ultramafic rocks is frequently transformed into serpentines – lizardite or chrysotile. There also exists a pervasive serpentinization essentially characterized by the pseudomorphic replacement of olivine and, less commonly, of pyroxene.

The absestos veins contain either silky white tremolite asbestos or greenish chrysotile $2M_{c1}$ structure type, which has prominent (002) reflection varying between 7.21 and 7.38 Å in samples from different localities with a mean at 7.276 Å. The b-cell edge was calculated to

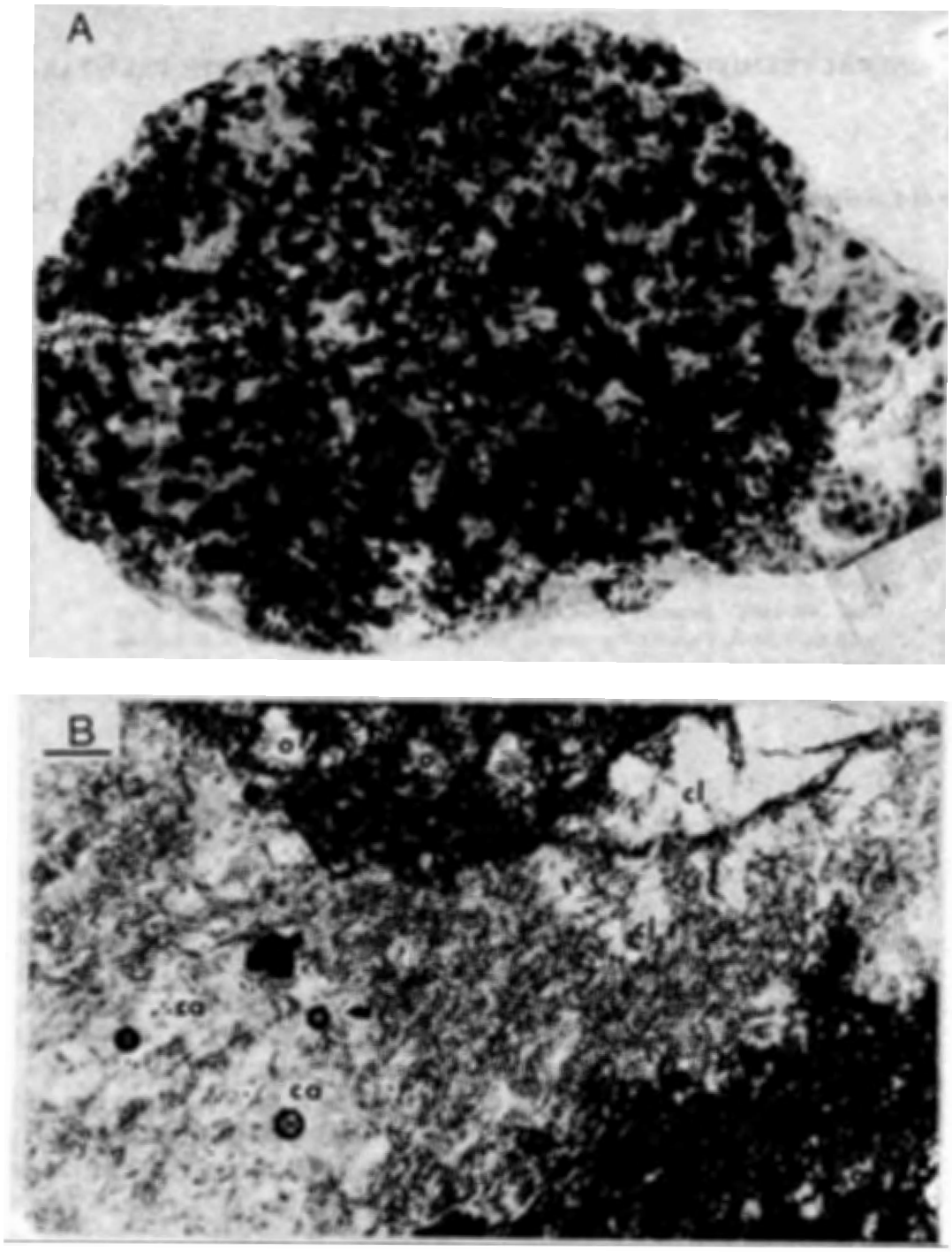

Fig. 1. (A) "Nodules" of unaltered olivine (dark grey to black) set in a matrix (light grey and white) composed of serpentine, chlorite and carbonate in the serpentinite host rock of the chrome deposit near Qila (sp. no. Z5). Black grains of fine size are chromite.

(B) Transmitted light photomicrograph, under crossed nicols, of the above sample, displaying margins of two dark olivine "nodules" in serpentine (s) and chlorite (cl) matrix which also contains carbonate (ca). The opaque specks are of heazlewoodite. Length of the scale bar is 0.2 mm. Some olivine grains are marked "o".

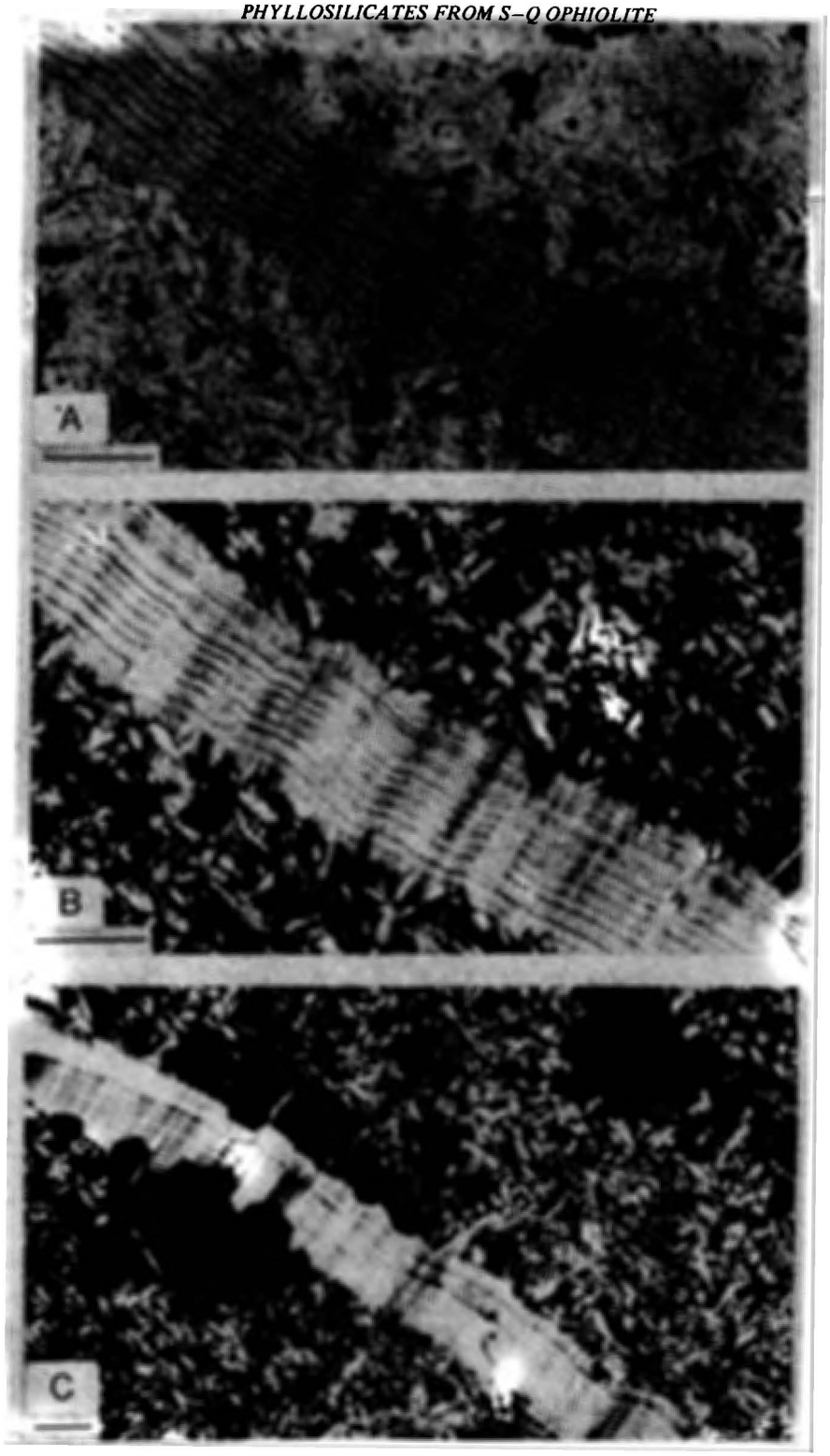

Fig. 2. (A) Transmitted light photomicrograph of serpentinite sample no. Z266 from near Zarifo Baba Ziarat showing anhedral magnetite (opaque) dispersed in serpentinite rock, cut by a younger veinlet of banded serpentine. The serpentine blades making up the rock project into the walls of banded serpentine veins.

(B) Crossed nicols photomicrograph of the above view showing interpenetrating blades composing the serpentinite; 'curtain-like' appearance of the banded serpentine vein; and optical continuity of the blades projecting from the wall inwards.

(C) Another photomicrograph from specimen Z266, showing the coarse anhedral magnetite grains (black) after chromite and changed to euhedral shapes inside the banded serpentine vein. The scale bar in each picture is 0.2 mm in length.

Fig. 3. (A) Transmitted light photomicrograph of dunite showing the most common type of serpentine alteration; as initial stage of mesh texture made of thin, faintly yellow, veinlets or 'mesh rims' carrying central partings at sites of original fractures. Sample no. Z152.

(B) Polished section of serpentine vein under reflected light, showing alternating bands of two different serpentines and euhedral magnetite (white). The sample also contained coarse awaruite, not seen in the photograph. Sample no. Z190 from GR 415-807.

vary from 9.082 to 9.275 Å with a mean at 9.216 Å.

The overlapping chemical compositions of serpentines is a well documented phenomenon and in the rock samples from SQO, the chemical distinctions, are hardly discernible.

In terms of cations per formula unit; Al substitution is up to 0.164 in the tetrahedral sheets and up to 0.173 in the octahedral sheets. Octahedral positions are mostly filled by Mg with variation range of 5.318 to 6.020. Accompanying Fe^{2+} varies from 0.090 to 0.892 cations per formula unit calculated to 14 oxygens.

Representative analyses of serpentines of various types are listed in Table 1. Analytical totals are very low; and are 0.4 to 4.0 weight percent below the expected average of 87% which is a feature of many published serpentine analyses (e.g., Cogulu & Laurent, 1984). Ideally, the major elements calculated as oxides should total 87% for chrysotile and lizardite and about 88% for an average antigorite. The lower totals of SQO serpentines may be attributable to the instability of serpentine under the electron beam as observed in some other studies (e.g., Dymek *et al.*, 1988). The results give good cationic proportions in the formulae and show that most compositions are rich in the Mg end member. MgO ranges from 31.42 to 42.55%.

SiO_2 ranges from 35.78 to 44.20 wt.%, but the values above 40 wt.% are more frequent. The formulae frequently show Si occupying all the tetrahedral sites. The serpentine compositions plotted on the MgO-FeO-SiO_2 ternary diagram (Fig. 4) also display clustering of points towards the SiO_2 end member. Al_2O_3 in serpentines is generally nil or very low, but some serpentines contain higher Al_2O_3. Serpentines in this study contain a maximum value of 2.93% Al_2O_3. Cr_2O_3 contents of serpentines are low (usually below 0.5%); however, the maximum Cr_2O_3 analyzed is 1.18%. In chromitites, the serpentine present as inclusions in chromite crystals usually is higher in Cr_2O_3 (e.g., 1% in sample Z131), than serpentines present outside the chromite crystals. Large ranges of variations in the weight percentages of various elements are obvious from Table 2. This indicates the presence of a variety of serpentines which are also discernible in Figs. 1 to 4. In thin sections of sample Z266, light brownish veins of serpentinous aggregates with banded and curtain-like appearance (Fig. 2) cut across the normal lath-like serpentines of the rock exhibiting mesh texture. The two varieties display chemical differences. The latter type is slightly richer in SiO_2 and MgO and is poorer in Al_2O_3, FeO, MnO, CaO and NiO. In sample Zc5 of a banded chromitite, the younger serpentine in a vein that cuts across the older colourless serpentines, and fills cracks in chromite grains, has relatively higher FeO, Al_2O_3, NiO and lower SiO_2 and MgO.

The microprobe analyses in Table 1 are numbered 1 through 109. The first four analyses are of serpentines that occur as inclusions in crystals of chromian spinel from the banded chromitite (Z131, Z108), disseminated ore (Z34) and harzburgite (Z105). In analysis no. 4, the analyzed serpentine inclusion makes a jacket surrounding an olivine inclusion inside a coarse crystal of chromian spinel. It has abnormally high FeO and low SiO_2 and MgO, for which the possibility of spurious counts from the chromite crystal cannot be ruled out. Al_2O_3 and Cr_2O_3 in analysis 3 are unusually high. Serpentines that occur outside the chromian spinel crystals from various textural types of chromitites are represented in analyses 5 to 40. Those from banded chromitites are given in analyses 5 to 14. Analysis 11 is of serpentine that constitutes matrix material in an area with abundant flakes of chlorite. Analyses 12 to 14 are of serpentine that is colourless in transmitted light and forms large areas of similar material. Serpentines from massive chromitites are given in analyses 15 to 18. Analyses 17 and 18 represent serpentines that make mesh-rims after olivine grains. Analysis 19 serpentine makes a mesh-rim in an area that appears to pseudomorph a large olivine crystal. Serpentine analyses from disseminated textured chromitites are given in analyses 20 to 28. Amongst these, the pseudomorphous nature after olivine is typically displayed by serpen-

Table 1. Microprobe spot analyses from serpentine grains, whose petrographic features are given in the text. – = not determined; b.d. = Below detection level

Anal. No.	1	2	3	4	5	6	7	8	9	10	11	12	13	14	15
Sp.No.	Z131	Z108	Z34	Z105	Z108	Z148	Z151	Z154	Z196	Z1	Z108	Z5	Z5	Z5	Z159
SiO_2	38.21	41.46	40.81	37.73	42.09	41.65	38.41	41.21	38.20	43.59	39.97	42.24	42.50	42.22	40.48
Al_2O_3	0.28	0.02	1.98	–	0.43	0.24	0.08	–	–	0.64	0.48	1.00	1.25	1.35	0.15
TiO_2	0.00	0.00	–	0.06	–	0.03	0.07	–	–	–	0.08	0.00	0.00	0.00	0.00
Cr_2O_3	1.01	0.33	1.18	0.35	–	0.09	–	0.16	–	0.00	0.10	0.58	0.40	0.06	0.18
FeO	5.05	2.49	2.32	7.89	3.53	6.06	3.32	2.23	2.25	2.14	2.00	1.38	1.33	1.47	3.38
MnO	0.08	0.00	0.00	0.09	–	0.11	–	–	–	–	0.05	0.01	0.04	0.14	0.00
MgO	39.72	38.39	39.64	41.23	38.63	37.12	39.97	42.55	39.77	36.79	38.88	37.82	38.31	38.53	37.44
NiO	0.48	0.22	0.05	0.32	0.47	0.55	0.39	0.47	0.29	–	0.35	0.08	0.08	0.05	0.32
CaO	0.11	0.02	0.11	0.05	–	0.10	–	0.00	–	–	0.05	0.02	0.00	0.02	b.d.
Total	84.94	82.93	86.09	87.72	85.15	85.95	82.24	86.62	80.51	83.16	81.96	83.13	83.91	83.84	81.95

Anal. No.	16	17	18	19	20	21	22	23	24	25	26	27	28	29	30
Sp.No.	Z159	Z25	Z238	Z305	Z23	Z34	Z194	Z164	Z156	Z156	Z157	Z157	Z157	Z150	Z279
SiO2	38.11	40.17	37.26	35.56	39.76	42.24	39.06	38.98	38.80	37.39	40.00	40.57	37.01	41.52	39.62
Al_2O_3	0.22	–	0.00	0.00	–	0.82	–	0.00	0.39	2.75	0.00	–	–	0.00	0.11
TiO_2	0.00	–	0.00	0.07	–	–	–	–	0.00	0.00	0.03	–	–	–	–
Cr_2O_3	0.07	0.26	0.02	0.05	–	031	0.04	0.17	0.85	0.06	0.26	0.21	0.36	0.13	0.21
FeO	9.06	4.94	3.45	10.15	3.86	2.41	2.31	4.72	2.47	3.57	9.30	5.07	3.63	2.12	3.28
MnO	0.41	–	0.12	–	0.16	0.09	–	0.02	0.04	0.05	0.14	–	–	–	–
MgO	33.83	35.38	38.12	34.60	38.42	41.23	39.12	37.62	39.84	40.76	32.48	37.75	39.39	36.40	36.59
NiO	1.11	–	0.32	1.98	0.28	0.32	0.51	0.36	0.20	0.34	0.99	0.51	0.42	–	–
CaO	b.d.	–	0.10	–	0.13	0.05	–	0.04	0.01	0.04	0.12	–	–	–	–
Total	82.81	80.75	79.39	82.41	82.61	87.47	81.04	82.30	84.96	82.24	83.29	84.11	80.81	80.17	79.81

Anal. No.	31	32	33	34	35	36	37	38	39	40	41	42	43	44	45
Sp.No.	Z279	Z8	Z8	Z9	Z146	Z179	Z121	Z198	Z198	Z214	Z266	Z266	Z266	Z132	Z342
SiO_2	40.15	41.15	38.96	39.77	40.03	38.93	39.94	39.62	35.78	36.68	44.04	44.00	43.82	40.78	42.23
Al_2O_3	0.00	–	0.00	–	0.03	0.81	–	–	–	0.20	0.00	0.03	0.08	2.80	0.88
TiO_2	–	–	–	–	0.11	–	–	–	–	–	0.00	b.d.	0.00	–	–
Cr_2O_3	0.04	0.27	0.08	–	021	0.25	0.15	–	–	0.00	–	b.d.	0.00	0.98	0.60
FeO	3.62	3.32	3.04	8.15	4.54	1.98	8.47	1.92	4.30	4.46	1.68	1.81	1.92	3.93	4.05
MnO	–	0.04	0.00	–	0.11	0.00	0.09	–	–	–	0.00	0.06	0.08	B.d.	0.12
MgO	36.04	38.23	39.26	36.71	35.38	40.63	31.42	39.40	41.93	37.41	40.52	40.64	40.01	36.40	36.94
NiO	–	0.14	0.43	0.21	1.30	0.18	0.62	0.11	0.14	0.47	0.15	0.32	0.12	–	–
CaO	–	–	0.00	–	0.06	–	0.12	–	–	0.14	0.07	0.00	0.10	0.10	b.d.
Total	79.85	83.15	81.77	84.84	81.74	82.78	80.81	81.05	82.15	79.36	86.46	86.86	86.13	84.99	84.82

Anal. No.	46	47	48	49	50	51	52	53	54	55	56	57	58	59	60
Sp.No.	Z342	Z342	Z342	Z342	Z342	Z342	Z346	Z346	Z346	Z346	Z346	Z348	Z348	Z348	Z348
SiO_2	43.59	43.88	43.52	43.48	43.49	42.66	43.28	43.71	43.29	43.83	43.97	42.20	43.27	42.38	42.96
Al_2O_3	0.53	0.46	0.00	0.59	0.39	0.21	0.62	0.71	0.74	0.35	0.54	1.23	1.06	1.17	0.38
TiO_2	0.00	0.08	0.01	0.12	0.08	0.00	0.00	0.00	0.02	0.00	0.00	0.02	0.00	0.03	0.04
Cr_2O_3	0.00	0.03	0.06	0.10	0.02	0.09	0.02	0.06	0.16	0.00	0.13	0.38	0.04	0.14	0.08
FeO	1.30	1.18	1.32	2.08	2.56	3.52	1.48	1.47	1.63	1.52	1.53	2.24	1.64	1.66	1.39
MnO	0.04	0.00	0.00	0.14	0.03	0.09	0.00	0.06	0.07	0.02	0.04	0.00	0.00	0.00	0.05
MgO	38.49	38.61	38.76	38.68	38.51	38.48	38.51	38.94	38.73	38.14	38.55	37.26	38.36	37.21	37.95
NiO	0.14	0.36	0.20	0.13	0.31	0.27	0.09	0.10	0.05	0.03	0.03	0.20	0.13	0.15	0.20
CaO	0.01	0.02	0.00	0.00	0.02	0.01	0.04	0.00	0.00	0.00	0.01	0.04	0.00	0.01	0.00
Total	84.10	84.62	83.87	85.32	85.41	85.33	84.04	85.05	84.69	83.89	84.80	83.57	84.50	82.75	83.05

Anal. No.	61	62	63	64	65	66	67	68	69	70	71	72	73	74	75
Sp.No.	Z348	Z348	Z348	Z48	Z350	Z350	Z350	Z350	Z14	Z375	Z375	Z275B	Z275B	Z275B	Z275B
SiO_2	43.30	42.86	42.35	42.81	43.94	43.65	43.32	43.47	37.57	37.15	39.94	43.00	37.65	38.03	37.82
Al_2O_3	0.71	0.63	1.03	0.65	0.72	0.40	0.48	0.54	0.02	0.11	0.18	1.50	0.00	0.10	1.12
TiO_2	0.00	0.01	0.00	0.01	0.10	0.00	0.00	0.00	0.00	0.09	0.00	0.00	0.02	0.05	0.02
Cr_2O_3	0.10	0.00	0.33	0.02	0.05	0.05	0.00	0.00	0.00	0.00	0.04	0.04	0.00	0.10	0.11
FeO	1.61	1.61	2.14	1.48	1.14	1.51	1.23	1.52	6.98	5.04	4.55	2.32	8.76	6.86	5.77
MnO	00.04	0.00	0.04	0.04	0.08	0.05	0.03	0.11	0.12	0.00	0.05	0.11	0.12	0.08	0.10
MgO	38.04	37.83	37.82	38.16	38.34	38.36	37.69	38.69	38.12	38.88	34.63	38.58	36.21	36.36	37.08
NiO	0.13	0.16	0.13	0.13	0.17	0.12	0.17	0.99	0.38	0.45	0.25	0.05	0.28	0.33	0.02
CaO	0.00	0.00	0.00	0.00	0.03	0.00	0.02	0.00	–	0.00	0.16	0.00	0.01	0.03	0.04
Total	83.93	83.10	83.84	83.30	84.57	84.19	92.94	84.62	83.19	81.72	79.70	85.60	83.05	81.94	82.09

Anal. No.	76	77	78	79	80	81	82	83	84	85	86	87	88	89	90
Sp.No.	Z274	Z274B	Z274B	Z142	Z142	Z142	Z410	Z410	Z326	Z202	Z202	Z183	Z265	Z265	Z147
SiO_2	36.27	39.31	39.90	44.60	41.71	41.59	39.10	38.55	43.99	43.91	44.04	36.18	43.71	43.95	43.91
Al_2O_3	0.00	0.00	0.71	0.34	–	–	–	–	0.00	0.63	1.04	–	0.43	0.38	0.12
TiO_2	0.00	0.04	0.11	–	–	–	–	–	0.02	0.00	0.11	–	0.07	0.05	–
Cr_2O_3	0.00	0.14	0.19	–	–	–	0.73	0.57	0.02	0.03	0.01	–	0.08	0.03	–
FeO	5.96	6.18	4.25	1.95	2.72	2.23	3.24	2.84	3.73	2.89	3.14	8.08	1.46	2.20	2.36
MnO	0.05	0.17	0.03	0.10	0.05	0.02	0.03	0.00	0.07	0.07	0.04	–	–	–	–
MgO	37.34	35.47	36.93	40.08	40.20	37.91	36.46	38.46	38.48	37.95	38.34	39.24	39.83	39.61	40.29
NiO	0.41	0.00	0.00	0.00	0.10	0.09	0.40	0.12	0.06	0.05	0.20	0.14	0.28	0.24	0.05
CaO	–	–	–	–	–	–	0.00	0.06	0.01	0.04	0.00	0.14	–	–	–
Total	80.03	81.31	82.12	87.07	84.78	81.84	79.96	81.60	86.38	85.57	86.92	83.78	85.86	86.46	86.73

Anal. No.	91	92	93	94	95	96	97	98	99	100	101	102	103	104	105	106
Sp.No.	Z264	Z264	Z274	Z274	Z264	Z264	Z264	Z264	ZA275	Z54	Z54	Z123	Z123	Z123	Z123	Z33
SiO_2	43.78	44.06	43.60	43.53	43.41	43.73	44.20	44.11	39.49	43.99	44.21	42.99	43.41	42.34	43.49	43.92
Al_2O_3	0.00	0.00	0.00	0.62	0.13	0.11	0.26	0.18	4.31	1.82	0.34	1.05	0.93	1.44	2.07	1.70
TiO_2	0.00	0.00	0.00	0.00	0.00	0.00	0.00	0.00	0.02	0.11	0.00	0.13	0.09	0.10	0.08	0.03
Cr_2O_3	0.13	0.03	0.21	0.34	0.26	0.20	0.50	0.28	1.80	0.57	0.01	0.50	0.39	0.53	0.57	0.50
FeO	2.23	1.48	1.46	1.85	1.98	1.55	1.60	1.69	1.98	2.99	2.69	3.36	3.47	3.13	3.41	2.28
MnO	0.05	0.00	0.00	0.00	0.08	0.06	0.02	0.03	0.00	0.10	0.08	–	–	–	–	0.10
MgO	39.42	40.10	38.44	39.21	38.98	39.96	39.24	39.03	35.06	36.69	37.87	37.77	37.32	37.91	38.14	36.47
NiO	0.09	0.23	0.21	0.15	0.26	0.14	0.15	0.09	0.19	0.21	0.16	0.15	0.07	0.17	0.14	0.14
CaO	–	–	–	–	–	–	–	–	0.03	0.00	0.00	b.d.	0.00	0.26	0.22	1.86
Total	85.70	85.90	83.92	85.70	85.10	85.75	85.97	85.41	82.88	86.48	85.36	85.95	85.68	85.88	88.12	87.00

Anal. No.	107	108	109	110	111	112	113	114	115	116	117	118	119	120	121	122
Sp.No.	Z33	Z188B	Z104	Z148A	Z159	Z5	Z194	ZB154	Z266	Z266	Z266	Z410	Z275B	Z375	Z202	Z347
SiO_2	43.23	42.01	42.83	40.36	41.75	39.36	41.04	40.72	40.55	40.22	39.76	38.91	41.86	35.25	42.67	43.51
Al_2O_3	1.92	2.22	0.92	0.00	0.23	2.93	0.00	0.00	2.09	2.28	2.10	–	2.40	0.00	0.55	0.68
TiO_2	0.00	0.13	0.08	0.05	0.00	0.00	–	0.02	b.d.	b.d.	0.00	–	0.03	0.18	0.00	0.07
Cr_2O_3	0.51	0.34	0.06	0.14	0.17	0.52	0.36	0.59	b.d.	b.d.	0.00	0.05	0.03	0.39	0.05	0.06
FeO	2.30	3.25	3.53	3.61	2.99	2.81	2.68	4.16	3.06	3.20	3.29	5.04	2.84	6.50	2.88	1.69
MnO	0.05	0.00	0.07	0.17	0.00	0.05	–	–	0.10	0.00	0.17	0.11	0.00	0.20	0.02	0.16
MgO	37.72	37.11	37.12	35.81	39.56	37.78	38.94	36.77	38.26	38.57	37.22	35.91	38.63	37.51	37.47	38.03
NiO	0.12	0.02	0.14	0.81	0.01	0.37	0.37	0.58	0.41	0.61	0.36	1.12	0.05	0.32	0.11	0.15
CaO	0.08	0.00	0.01	0.17	0.00	0.00	–	–	0.42	0.35	0.76	0.06	0.00	0.06	0.00	0.00
Total	85.93	85.08	84.76	81.12	84.71	83.82	83.39	82.84	84.89	85.23	83.66	81.20	85.84	80.41	83.75	84.35

tines whose analyses are numbered 21 and 22. Analysis 29 serpentine is from within the chromite nodules of porphyritic nodular ore as described by Ahmed (1982). Analyses 30 and 31 are of serpentines from within the nodules, whereas analyses 32 to 35 represent serpentines from the matrix material of chromite nodules. Such nodular texture displays tectonically deformed nodules in sample Z146 (analysis 35). Analysis 36 is of serpentine from occluded silicate ore; 37 is of serpentine from chromite-net ore, where it forms a veinlet in an olivine-rich occlusion. Serpentines from speckled chromitite are those of analysis 38 and 39. The pseudoclastic chromitite described by Ahmed & Hall (1981) contains chlorite at the immediate contacts of chromite grains but does contain outer sheaths of olivine-rich rocks. Analysis 40 represents serpentine from one such area, where it occurs in the mesh-rims around olivine.

Analyses 41 to 68 are from completely serpentinized ultramafic rocks. Analyses 41 to 43 are of lath-shaped serpentines from a serpentinite sample (Z266) and differ from analyses 115 to 117 which are from another type of serpentine from the same sample. The latter analyses represent a younger episode of serpentinization that occurs as brownish coloured, banded and curtain-like aggregates in a vein that cuts across this serpentinite. The younger serpentine has lower SiO_2 and MgO, but higher Al_2O_3, FeO, NiO and CaO. The analyses 44 and 45

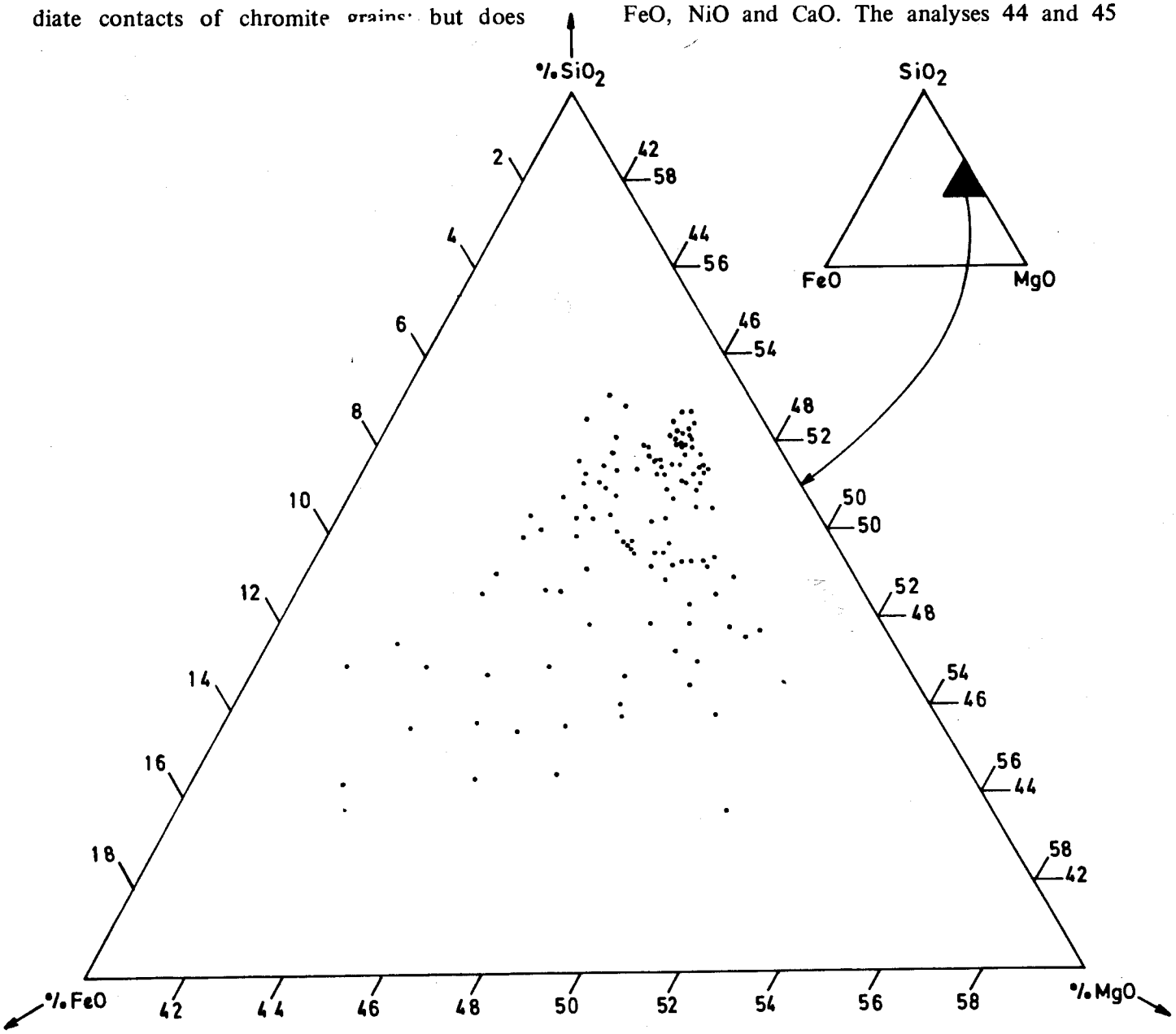

Fig.4. A plot of normalized weight percent MgO-FeO-SiO_2 in serpentines from SQO.

serpentine replaces tremolite crystals in a serpentinite. From a serpentinite sample (Z342), the common serpentine (analyses 46 to 48) resembles closely another type of serpentine (analyses 49 to 51) which occurs near opaque spots, but carries slightly higher FeO and MnO than the former type.

Analyses 52 to 68 are from serpentinite and display only slight chemical variations. Analyses 69 to 75 are of a serpentine that forms the mesh rims of olivine pseudomorphs in dunite. Serpentine of analyses 76 to 78 are from dunite at the immediate contact with massive chromitite. Analyses 79 to 83 are of long flakes of serpentine from a dunite rock that is impregnated with 15 to 20% of chromite grains. Analyses 82 and 83 are from near a "ferritchromit" grain; and the vein-forming serpentine from the same sample is given in analysis 118. Analysis 84 is from clinopyroxene-bearing harzburgite; 85 is from a wehrlite whose vein-forming serpentine appears in analysis 121. Analysis 87 is of serpentine pseudomorphing olivine of a wehrlite. Analyses 88 and 89 are from the serpentinous part of a wehrlite hand specimen. Acicular serpentine from wehrlite is shown as analysis 90, and analyses 91-98 are from a wehrlite: 91 is from the core of a chromian spinel crystal where serpentine occurs associated with magnetite; 92 and 93 are from an olivine pseudomorph; 94 to 98 from clinopyroxene pseudomorphs. Analysis 99 is of a serpentine that replaces edenite in a pyroxenite vein in chromitite. Analyses 100 to 108 are from clinopyroxenite dykes. Analysis 109 is from a serpentine after orthopyroxene lamellae that cut across an olivine grain in an orthopyroxenite dyke. Analyses 110 to 122 are of serpentine that forms later veins cutting across: chromitite (110 & 111); chromite grain in banded chromitite (112); "ferritchromit" in disseminated chromitite (113); and occluded-silicate chromitite (114); a serpentinite (115-118); dunite (118-120); and wehrlite (121-122).

CHLORITE

Chlorite occurs in all the rock types of SQO, and everywhere it is a secondary mineral derived from primary ferromagnesian minerals. Chlorite is also abundant in the surrounding metasedimentary rocks which display a thick development of the chlorite zone, low-grade, metamorphic rocks. Chlorite produced by the chemical alteration of chromite to "ferritchromit" (Ahmed & Hall, 1981) makes thin envelopes around partly to completely altered chromite grains. The "ferritchromit" in polished sections contains abundant pits filled always by chlorite. Most silicate-filled inclusions in chromite are of chlorite. A bluish grey chlorite occurs adja-

Table 2. Variation ranges (R), means ($\bar{x}$), and standard deviations (s), for 250 microprobe analyses of serpentines from SQO.

	R	$\bar{x}$	s
SiO_2	35.78 – 44.20	41.23	2.51
Al_2O_3	0.00 – 3.86	0.61	0.83
TiO_2	0.00 – 0.18	0.03	0.04
Cr_2O_3	0.00 – 1.18	0.21	0.25
V_2O_3	0.00 – 0.19	0.03	0.04
FeO	1.14 – 10.15	3.24	1.90
MnO	0.00 – 0.41	0.06	0.06
MgO	31.42 – 42.55	37.64	3.60
NiO	0.00 – 1.30	0.27	0.24
CaO	0.00 – 0.76	0.06	0.11

Table 3. Selected chlorite analyses in terms of weight percentages of oxides and atomic proportions of elements calculated to 28 Oxygens; assuming all iron as bivalent. The Oxides totals fall between 81 and 88%. Al^{iv} = 8-Si. "----" = Not determined. b.d. = below detection level. Sp.No. = Sample number, Anal. No. = Analysis number. Name = Nomenclature after Hey (1954) symbolized as 'BR', brunsvigite; 'CL', clinochlore; 'PN', penninite; 'PY', pycnochlorite; 'RI', ripidolite; 'SH', sheridanite; and 'TC', talc-chlorite.

Anal No.	1	2	3	4	5	6	7	8	9	10	11
Sp.No.	Z116	Z154	Z162	Z162	Z265	Z145	Z305	Z305	Z273	Z272	Z272
SiO_2	30.87	32.61	31.46	31.01	33.19	32.33	30.62	33.31	32.14	32.32	33.55
TiO_2	–	–	–	–	0.05	–	0.02	0.02	0.01	–	–
Al_2O_3	17.73	14.03	16.62	17.66	13.12	14.28	15.16	14.50	14.92	11.47	12.55
Cr_2O_3	0.47	1.88	1.53	1.27	2.91	2.50	3.21	0.47	1.71	1.95	0.95
TeO	0.54	0.78	1.22	1.37	3.45	1.08	1.05	1.17	1.15	1.58	1.66
MnO	–	–	–	–	–	–	–	–	0.07	–	–
MgO	32.66	35.76	32.13	31.56	33.93	32.44	32.60	34.76	33.28	35.65	36.56
NiO	0.15	0.41	–	–	0.09	–	0.00	0.00	0.14	0.14	0.16
CaO	–	–	–	–	0.02	–	–	–	0.00	–	–
Si	6.050	6.231	6.160	6.075	6.333	6.370	6.066	6.403	6.261	6.383	6.417
Al^{vi}	2.145	1.391	1.995	2.152	1.283	1.686	1.605	1.687	1.691	1.052	1.245
Fe	0.089	0.125	0.199	0.225	0.551	0.177	0.173	0.188	0.187	0.261	0.265
Mg	9.538	10.184	9.374	9.215	9.651	9.526	9.627	9.959	9.667	10.491	10.421
Name	CL	PN	CL	CL	PN	PN	CL	PN	PN	PN	PN

Anal. No.	12	13	14	15	16	17	18	19	20	21	22
Sp.No.	Z6	Z6	Z148B	Z148B	Z148B	Z148B	Z148A	Z108	Z108	Z134	Z128
SiO_2	38.21	34.18	38.61	38.41	35.49	36.03	33.89	34.44	35.38	32.77	33.05
TiO_2	–	0.00	0.02	0.07	0.00	0.08	0.03	–	–	0.00	0.06
Al_2O_3	9.97	9.22	6.18	5.90	7.98	8.07	12.27	13.29	9.99	15.33	14.75
Cr_2O_3	4.37	4.32	0.04	0.24	0.40	0.36	0.23	0.44	1.90	2.26	1.49
FeO	1.64	2.49	2.66	2.38	2.50	2.59	2.16	1.01	1.99	1.16	0.85
MnO	–	0.00	0.01	0.00	0.08	0.00	0.02	–	–	0.00	–
MgO	32.22	36.17	37.12	36.99	35.16	36.15	34.99	35.74	35.39	34.09	36.71
NiO	0.07	0.28	0.16	0.09	0.17	0.10	0.00	0.13	0.17	0.02	0.00
CaO	–	0.03	0.02	0.00	0.03	0.00	0.04	b.d.	b.d.	0.00	–
Si	7.197	6.555	7.395	7.426	7.082	7.051	6.597	6.554	6.823	6.233	6.192
Al^{vi}	1.410	0.638	0.791	0.770	0.958	0.911	1.412	1.535	1.093	1.668	1.448
Fe	0.258	0.399	0.426	0.385	0.417	0.423	0.352	0.160	0.321	0.184	0.133
Mg	9.043	10.337	10.599	10.658	10.462	10.546	10.154	10.139	10.170	9.665	10.251
Name	TC	PN	TC	TC	TC	TC	PN	PN	PN	PN	CL

Anal. No.	23	24	25	26	27	28	29	30	31	32	33	34
Sp.No.	Z128	ZB154	Z34	Z179	Z179	Z179	Z179	ZB149	ZB149	Z35	Z35	Z141
SiO_2	32.28	31.46	34.16	34.93	33.58	34.49	31.29	30.80	29.99	32.61	33.08	32.04
TiO_2	0.02	0.11	0.06	0.00	0.00	0.09	–	0.00	0.00	0.03	0.00	–
Al_2O_3	14.91	17.19	13.94	15.73	17.84	18.34	15.78	18.12	17.87	15.64	16.26	14.53
Cr_2O_3	2.90	1.88	1.35	2.08	1.63	0.75	0.51	0.21	0.21	0.04	0.33	0.24
FeO	0.76	1.41	1.08	0.72	0.63	0.63	0.76	0.97	0.97	1.00	1.09	0.88
MnO	–	0.02	0.03	–	–	–	–	0.05	0.05	0.00	0.00	–
MgO	35.70	33.56	35.84	32.89	31.63	32.98	35.07	31.69	32.38	33.34	33.88	35.98
NiO	0.12	0.06	0.07	0.00	0.00	0.10	0.00	0.07	0.07	0.01	0.06	0.22
CaO	–	0.05	0.00	0.00	0.00	0.25	–	0.08	0.08	0.00	0.02	–
Si	6.094	5.989	6.417	6.532	6.340	6.334	6.086	6.061	5.946	6.362	6.305	6.205
Al^{vi}	1.412	1.847	1.502	1.997	2.309	2.304	1.703	2.264	2.122	1.959	1.956	1.520
Fe	0.119	0.225	0.170	0.122	0.099	0.097	0.123	0.159	0.161	0.163	0.174	0.143
Mg	10.042	9.526	10.035	9.165	8.902	9.028	10.165	9.298	9.567	9.697	9.624	10.386
Name	CL	SH	PN	PN	PN	PN	CL	CL	CL	PN	PN	PN

Anal. No.	35	36	37	38	39	40	41	42	43	44	45	46
Sp.No.	Z141	Z141	Z41A	Z159	Z182	Z182	Z182	Z182	Z182	Z181	Z181	Z194
SiO_2	31.66	30.83	33.31	31.88	34.27	33.23	30.95	29.32	31.43	28.82	28.00	35.02
TiO_2	–	–	0.00	0.03	0.00	0.00	0.00	0.10	0.05	0.00	0.01	–
Al_2O_3	15.07	15.13	13.32	15.96	14.33	16.34	20.63	22.62	18.47	22.70	23.83	11.92
Cr_2O_3	0.54	0.30	2.04	1.03	0.15	0.12	0.60	0.03	0.13	0.78	0.56	1.17
FeO	0.93	0.93	1.18	0.92	1.26	1.27	1.15	1.50	1.24	1.34	1.95	1.54
MnO	–	–	0.00	0.00	0.04	0.05	0.00	0.05	0.00	0.02	0.00	–
MgO	35.91	35.12	33.03	33.95	35.33	34.95	33.28	32.20	33.81	31.60	30.82	36.12
NiO	0.37	0.00	0.17	0.00	0.02	0.07	0.00	0.14	0.13	0.20	0.11	0.09
CaO	–	–	0.62	0.00	0.04	0.00	0.00	0.00	0.00	–	–	–
Si	6.105	6.064	6.482	6.178	6.482	6.255	5.790	5.539	5.968	5.481	5.351	6.632
Al^{vi}	1.530	1.572	1.536	1.824	1.676	1.881	2.339	2.575	2.102	2.569	2.791	1.292
Fe	0.150	0.154	0.193	0.148	0.199	0.200	0.179	0.237	0.196	0.213	0.312	0.243
Mg	10.322	10.387	9.583	9.776	9.962	9.807	9.280	9.067	9.572	8.959	8.781	10.195
Name	CL	CL	PN	CL	PN	PN	CL	SH	CL	SH	SH	PN

Anal. No.	47	48	49	50	51	52	53	54	55	56	57	58
Sp. No.	Z194	Z247	Z200B	Z236	Z236	ZA228A	Z274A	Z231	Z231	Z246	Z164	Z164
SiO_2	34.28	28.92	32.97	32.16	33.38	32.42	30.06	32.08	34.46	32.29	32.19	31.22
TiO_2	–	–	–	–	–	–	0.08	–	–	–	0.05	0.02
Al_2O_3	13.37	17.93	13.23	15.63	14.48	14.30	15.03	13.65	13.58	14.27	16.86	17.41
Cr_2O_3	0.36	3.26	3.391	0.42	1.35	0.43	2.01	1.19	0.51	0.26	0.02	0.28
FeO	1.42	0.76	1.45	1.15	1.11	1.11	1.30	0.92	0.76	1.05	1.23	1.25
MnO	–	–	–	–	–	–	–	–	0.06	–	0.00	0.00
MgO	35.30	32.90	36.04	34.49	32.38	36.07	32.08	35.77	35.16	35.94	33.29	33.24
NiO	0.69	0.32	0.15	0.41	0.33	–	0.07	–	0.18	0.16	0.07	0.16
CaO	–	–	–	0.00	2.10	–	0.04	–	–	–	0.05	0.00
Si	6.530	5.650	6.374	6.203	6.417	5.247	5.091	6.247	6.573	6.249	6.213	6.058
Al^{vi}	1.532	1.779	1.388	1.757	1.698	1.494	1.681	1.380	1.627	1.504	2.047	2.038
Fe	0.226	0.123	0.234	0.186	0.178	0.178	0.220	0.149	0.121	0.170	0.198	0.203
Mg	10.023	9.578	10.384	9.917	9.277	10.360	9.689	10.381	9.996	10.366	9.576	8.615
Name	PN	CL	PN	PN	PN	PN	CL	PN	PN	PN	PN	CL

Anal. No.	59	60	61	62	63	64	65	66	67	68	69	70
Sp.No.	Z164	Z164	Z185	Z185	Z185	Z187	Z187	Z214	Z218	Z218	Z218	Z138
SiO_2	31.37	32.39	30.89	32.34	28.92	29.06	31.23	31.65	32.16	30.71	32.10	31.88
TiO_2	0.00	0.00	0.00	0.00	0.00	0.03	0.07	–	–	–	–	0.00
Al_2O_3	17.90	17.13	18.14	16.95	20.03	20.80	18.91	14.51	17.60	18.51	16.84	18.18
Cr_2O_3	0.29	0.00	0.15	0.12	0.73	1.38	0.02	1.95	0.10	1.64	0.39	0.95
FeO	1.06	1.15	1.18	1.27	1.30	1.16	1.72	1.25	0.70	0.76	0.88	1.13
MnO	0.00	0.00	0.01	0.05	0.08	0.00	0.02	–	0.03	0.00	0.00	0.00
MgO	33.43	34.31	32.84	33.67	31.40	32.35	33.96	35.42	33.81	32.99	33.96	33.54
NiO	0.11	0.07	0.04	0.16	0.15	0.11	0.03	0.14	0.04	0.00	0.10	0.00
CaO	0.07	0.00	0.02	0.06	0.01	–	–	–	–	–	–	0.00
Si	6.031	6.155	5.991	6.190	5.680	5.575	5.904	6.103	6.140	5.892	5.156	6.030
Al^{vi}	2.087	1.992	2.138	2.013	2.318	2.278	2.116	1.401	2.100	2.079	1.962	2.084
Fe	0.171	0.183	0.191	0.203	0.213	0.186	0.272	0.202	0.111	0.122	0.141	0.179
Mg	9.582	9.721	9.495	9.605	9.195	9.251	9.567	10.179	9.620	9.437	9.711	9.458
Name	CL	CL	CL	CL	CL	CL	CL	CL	CL	CL	CL	CL

Anal. No.	71	72	73	74	75	76	77	78	79	80	81	82
Sp.No.	Z138	Z138	Z138	Z277	Z277	Z300	Z300	Z300	ZC5	ZC5	ZC5	Z375
SiO_2	28.51	33.47	28.61	30.12	30.60	31.83	30.91	30.59	33.62	33.75	33.40	34.77
TiO_2	0.06	0.00	0.00	0.06	0.04	0.00	0.15	0.00	0.11	0.07	0.02	0.05
Al_2O_3	21.49	14.93	22.19	21.18	18.40	17.07	16.59	15.52	10.07	10.41	9.09	8.60
Cr_2O_3	1.60	0.40	1.36	0.35	1.59	2.15	2.76	0.06	3.24	3.23	3.70	1.91
FeO	1.26	1.06	1.20	1.32	1.70	1.36	1.38	1.05	2.49	2.52	2.62	2.14
MnO	0.00	0.00	0.00	0.00	–	–	–	0.02	0.03	0.02	0.04	0.02
MgO	30.50	34.40	31.20	32.45	32.07	35.97	34.61	32.01	34.43	34.85	34.43	35.89
NiO	0.00	0.00	0.12	0.12	0.16	0.23	0.00	0.11	0.24	0.07	0.28	0.17
CaO	0.00	0.00	0.00	0.02	0.02	–	–	–	0.00	0.00	0.00	0.04
Si	5.563	6.421	5.498	5.698	5.901	5.890	5.872	6.232	6.596	6.563	6.617	6.827
Al^{vi}	2.504	1.796	2.525	2.420	2.092	1.612	1.586	1.958	0.924	0.949	0.740	0.816
Fe	0.205	0.169	0.192	0.209	0.274	0.209	0.219	0.179	0.408	0.409	0.434	0.351
Mg	8.870	9.837	8.934	9.152	9.220	9.922	9.802	9.720	10.069	10.102	10.169	10.503
Name	SH	PN	SH	CL	CL	CL	CL	PN	PN	PN	PN	PN

Anal. No.	83	84	85	86	87	88	89	90	91	92	93	94
Sp. No.	Z410	ZA228B	Z326	ZB154	Z82	Z82	Z82	Z393	Z393	ZA222	ZA222	ZA222
SiO_2	36.55	32.45	31.68	31.45	33.27	33.22	32.45	33.17	30.60	29.87	30.85	29.50
TiO_2	0.18	0.02	0.00	0.11	–	–	–	0.01	0.06	0.01	0.00	0.38
Al_2O_3	9.12	12.88	19.47	17.19	12.57	12.92	13.93	13.23	16.52	20.34	19.64	17.69
Cr_2O_3	0.17	0.42	0.28	1.88	–	–	–	0.08	0.04	1.65	0.00	1.96
FeO	1.73	1.97	7.50	1.41	1.51	1.45	1.31	7.56	9.30	2.41	1.47	6.67
MnO	0.10	0.03	0.08	0.02	–	–	–	0.21	0.23	0.04	0.02	0.11
MgO	37.30	34.93	29.05	33.56	35.82	35.97	35.83	27.90	27.80	30.13	32.58	28.13
NiO	0.18	–	0.10	0.06	–	–	–	0.21	0.19	0.15	0.17	0.27
CaO	0.04		0.53	0.05	–	–	–	0.24	0.06	0.13	0.01	0.18
Si	6.962	6.392	5.979	5.989	6.491	6.446	6.309	6.709	6.092	5.773	5.902	5.839
Al^{vi}	1.010	1.382	2.307	1.847	1.382	1.402	1.502	1.863	1.968	2.406	2.329	1.967
Fe	0.275	0.324	1.183	0.225	0.245	0.234	0.212	1.279	1.549	0.390	0.235	1.105
Mg	10.589	10.256	8.170	9.526	10.414	10.402	10.381	8.411	8.252	8.678	9.291	8.301
Name	PN	PN	CL	CL	PN	PN	PN	PN	CL	CL	CL	CL

Anal. No.	95	96	97	98	99	100	101	102	103	104	105	106
Sp.No.	ZA222	ZA222	ZA222	ZA222	ZA222	ZA222	Z361B	Z361B	Z361B	Z361AB	Z261AB	Z361A
SiO_2	28.32	31.72	29.24	30.68	35.08	34.84	31.27	33.60	30.79	30.39	31.93	32.89
TiO_2	0.04	0.11	0.09	0.14	0.21	0.07	0.05	0.03	0.15	0.00	0.02	0.02
Al_2O_3	21.42	11.21	17.20	17.25	9.62	11.49	17.14	13.24	19.19	20.40	18.38	16.44
Cr_2O_3	0.05	0.00	0.02	0.27	0.07	0.00	0.04	0.07	0.00	0.00	0.04	0.06
FeO	4.48	1.81	2.36	3.52	1.05	3.27	5.28	3.74	6.37	7.15	5.90	4.30
MnO	0.00	0.09	0.07	0.08	0.06	0.00	0.03	0.04	0.16	0.16	0.06	0.04
MgO	29.32	34.50	30.97	31.22	35.05	29.02	30.98	34.42	30.75	29.65	31.16	32.79
NiO	0.04	0.00	0.00	0.22	0.06	0.15	0.07	0.17	0.35	0.21	0.13	0.00
CaO	0.00	0.29	0.28	0.03	0.12	0.51	0.05	0.02	0.00	0.03	0.08	0.00
Si	5.572	6.487	5.952	6.039	6.950	7.114	6.094	6.469	5.853	5.770	6.037	6.245
Al^{vi}	2.538	1.188	2.078	2.041	1.197	1.880	2.030	1.475	2.153	2.335	2.133	1.925
Fe	0.738	0.309	0.402	0.579	0.173	0.559	0.860	0.602	1.013	1.136	0.933	0.683
Mg	8.597	10.518	9.396	9.162	10.352	8.832	8.998	9.880	8.712	8.390	8.784	9.280
Name	SH	PN	CL	CL	PN	TC	CL	PN	CL	CL	CL	PN

Anal. No.	107	108	109	110	111	112	113	114	115	116	117	118
Sp.No.	Z361A	Z399	Z399	Z399	Z399	Z399	Z399	Z399	Z371B	Z371B	Z371B	Z371B
SiO_2	31.87	30.23	28.26	32.52	28.05	32.36	31.02	31.09	26.16	26.98	26.80	26.00
TiO_2	0.08	0.02	0.05	0.03	0.01	0.00	0.00	0.00	–	0.00	0.02	0.00
Al_2O_3	17.39	18.58	21.23	14.87	21.26	15.80	16.34	17.13	19.84	21.20	20.11	19.24
Cr_2O_3	0.08	0.09	0.00	0.00	0.10	0.01	0.00	0.05	0.00	0.00	0.00	0.03
FeO	4.95	4.61	8.66	3.12	7.06	2.97	4.45	4.38	24.29	23.41	26.04	16.30
MnO	0.12	0.10	0.00	0.00	0.08	0.03	0.01	0.01	0.12	0.26	0.31	0.05
MgO	30.68	30.33	27.26	32.24	27.39	32.78	30.68	30.98	16.21	17.08	15.61	20.96
NiO	0.35	0.13	0.08	0.16	0.04	0.18	0.04	0.38	0.00	0.00	0.00	0.00
CaO	0.00	–	–	–	–	–	–	–	0.12	0.06	0.09	0.18
Si	6.150	5.926	5.555	6.400	5.577	6.272	6.175	6.091	5.515	5.526	5.576	5.551
Al^{vi}	2.106	2.219	2.474	1.851	2.559	1.882	2.009	2.047	2.444	2.645	2.507	2.392
Fe	0.799	0.756	1.424	0.514	1.774	0.481	0.741	0.718	4.283	4.009	4.531	2.909
Mg	8.825	8.864	7.988	9.461	8.119	9.471	9.104	9.046	5.094	5.215	4.840	6.670
Name	CL	CL	SH	PN	SH	PN	CL	CL	RI	RI	RI	RI

Anal. No.	119	120	121	122	123	124	125	126	127	128	129
Sp.No.	Z371B	Z371B	Z233	Z233	Z233	Z394	Z394	Z394	Z368A	Z339	Z339
SiO_2	26.40	26.84	29.16	29.34	29.13	29.44	29.32	28.17	31.40	25.43	30.53
TiO_2	0.03	0.04	–	0.03	0.06	0.07	0.10	0.03	0.29	0.22	0.28
Al_2O_3	21.14	20.18	20.86	20.53	19.90	18.40	19.68	21.09	20.39	21.13	24.51
Cr_2O3	0.01	0.02	–	0.00	0.15	0.07	0.14	0.11	0.07	0.00	0.09
FeO	24.48	24.24	6.61	6.37	6.84	9.43	9.64	9.76	11.92	34.61	27.54
MnO	0.21	0.04	–	0.16	0.09	0.11	0.08	0.26	0.23	0.25	0.19
MgO	16.14	17.43	28.81	27.43	27.31	25.54	25.93	25.03	22.73	7.55	6.19
NiO	0.02	0.10	–	0.18	0.06	0.26	0.26	0.07	0.05	0.00	0.04
CaO	0.15	0.17	0.14	0.19	0.05	0.16	0.09	0.08	0.41	0.16	0.16
Si	5.471	5.527	5.678	5.789	5.798	5.974	5.829	5.649	6.103	5.512	6.135
Al^{vi}	2.633	2.423	2.464	2.563	2.469	2.373	2.440	2.634	2.775	2.909	3.940
Fe	4.243	4.173	1.076	1.050	1.139	1.600	1.603	1.637	1.937	6.272	4.629
Mg	4.985	5.348	8.360	8.067	8.104	7.723	7.684	7.480	6.586	2.439	1.853
Name	RI	RI	CL	CL	CL	CL	CL	CL	PY	RI	BR

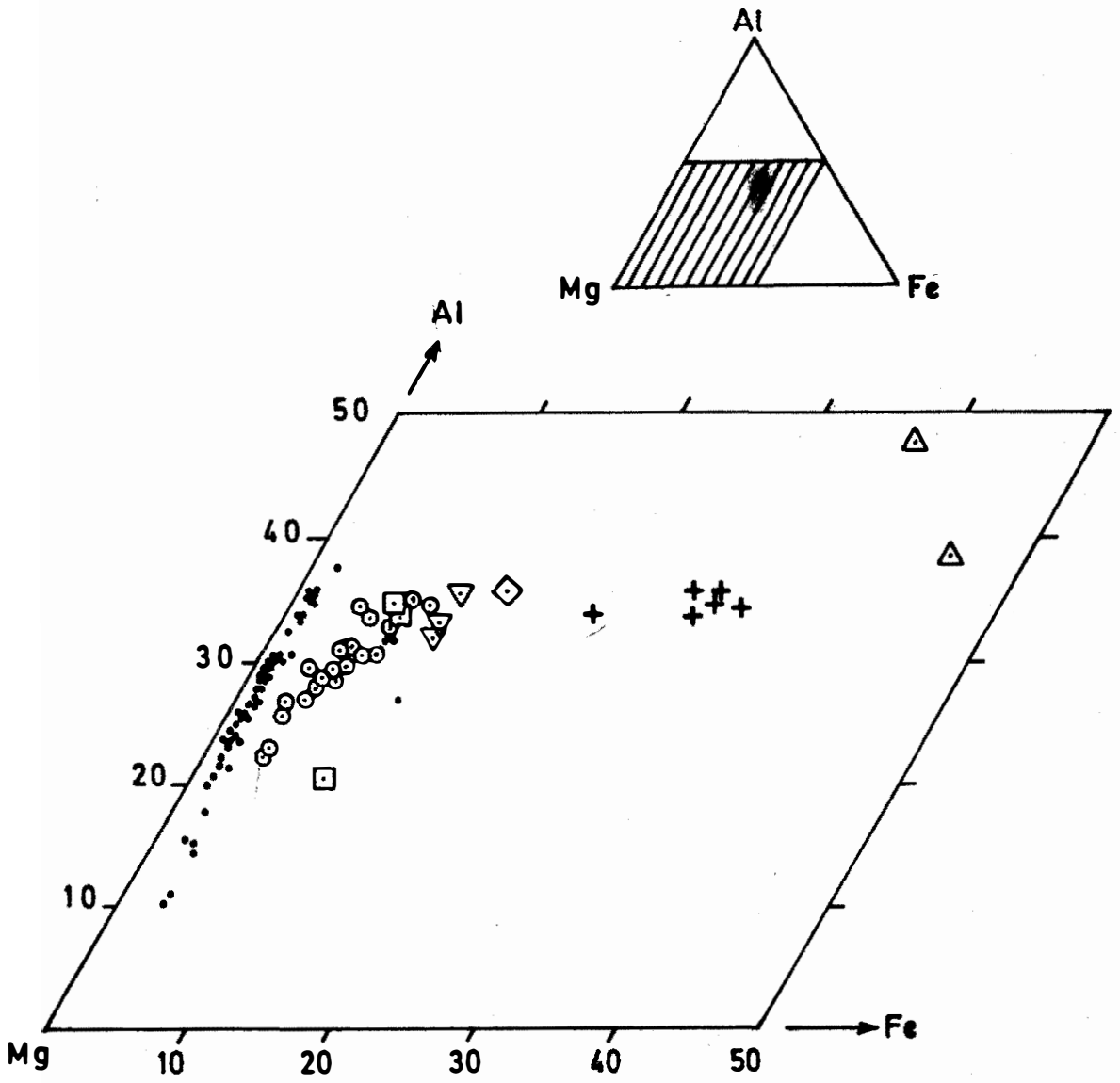

Fig.5. Chlorite analyses plotted on triangular Fe–Al–Mg diagram.

△ = Z339 Plagiogranite. ◇ = Z368A Upper Metagabbro

▽ = Z394 Middle level Metagabbro ⊡ = Z 233 Lower Meta gabbro

+ = Z 371 B Metadolerite ⊙ = Z361A, Z361B, Z222, Z399 Rodnigitic rocks

• = All rock samples except above.

cent to chromite grains, as haloes around them, and around chromite segregations especially in more aluminous chrome ores that occur towards northern parts of the ultramafic outcrops of SQO. Such chlorite is mainly the "IIb-even" structure type and shows dominant basal reflections in its powder X-ray diffraction patterns, especially the (001), (002), (003), and (004). The (002) line is most intense in such patterns. The (001) line varies between 14.04 and 14.29Å (mean = 14.17 Å). The (002) peak is the most intense and varies from 7.078 Å to 7.168 Å (mean = 7.161Å). Its '*b*' cell dimension varies from 9.18 to 9.24 Å with a mean at 9.221 Å. This chlorite has a white streak. Chlorite is also observed replacing pyroxenes, amphiboles and

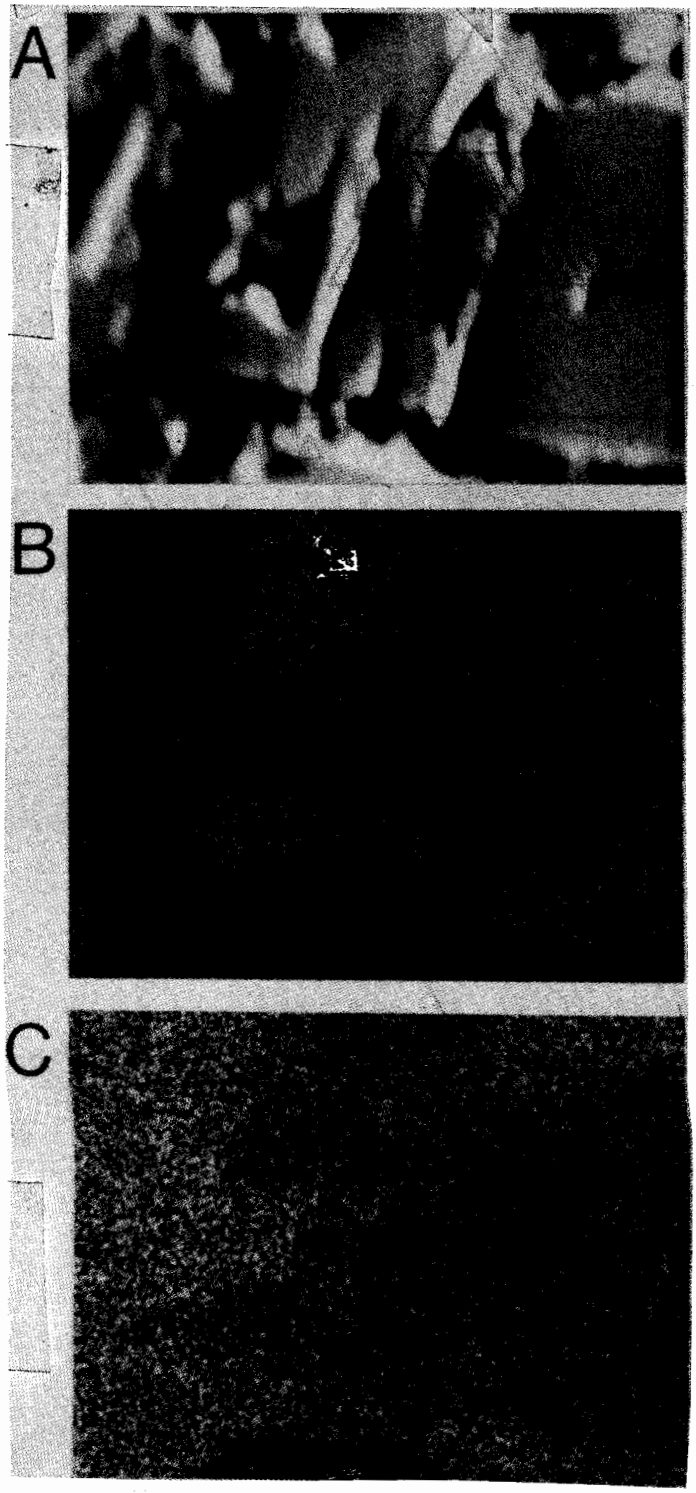

Fig.6. X-ray scanning images for a clintonite grain in the rodingite sample number ZA222. (A) Backscattered electrons image. (B) Al distribution image. (C) Mg distribution image. Clintonite is light light grey, micaceous mineral and displays higher Al count. Al-poorer, but Mg-richer and greyish mineral to its left is hydrogrossular, whereas the black matrix is chlorite, which is also Al-poorer relative to clintonite.

even serpentine. Chlorite occurs as dark greenish black walls of rodingite lenses, representing the serpentine protolith that reacted with the Al-rich rodingitizing solutions. This chlorite's X-ray diffraction pattern displays the highest intensity (002) reflection at 7.105 to 7.11 Å. Its (001), (003) and (004) reflections are also quite intense. The *'b'* cell dimension varies from 9.192 to 9.2 Å. The structure is of "IIb-even" type.

Microprobe analyses of chlorites show large, unsystematic variations of FeO, MgO and Al_2O_3 contents. TiO_2, MnO, NiO and CaO contents are quite low and alkalies negligible. The chlorites in chromitites are always of low-Fe, high-Mg type, but in mafic rocks they are slightly more Fe-enriched.

Out of 129 chlorite analyses reported in Table 3, only 4 contain CaO exceeding 0.5% (i.e., analyses nos. 37,51,85 and 100). One analysis of chlorite from plagiogranite gave the highest K_2O. Such analyses with high Na_2O, K_2O and CaO are not listed in Table 3 as they may represent submicroscopic intergrowths of chlorite with other phyllosilicates. The cationic proportions of chlorite microprobe analyses reported in Table 4 are obtained by normalization to 28 oxygens, assuming total Fe to be Fe^{2+}. A review of a large number of chlorite analyses published in the literature (Foster, 1962; Deer *et al.*, 1962; Shirozu, 1978) shows that trivalent iron typically constitutes less than 5% of the total iron. Such trivalent iron occurs mainly in the Fe-richer and Mg-poorer chlorites. Thus, in the present study, like some earlier works (e.g., Cathelineau & Nieva, 1985), consideration of all iron in the formulae to be divalent, is more appropriate than adopting certain arbitrary assumptions such as those made by McDowell & Elders (1980) who assume 10% $Fe–Fe^{3+}$, or Walshe & Solomon (1981) who balance the trivalent charge in tetrahedral and octahedral sites to reach a vacancy = 0.

It is generally known that amongst the different rock types that contain chlorite, the ultramafic rocks and rodingites contain chlorite with the least Al (Laird, 1988); with more than

3/4ths of the tetrahedral sites filled by Si. A similar behaviour is exhibited by the SQO chlorites. Al^{iv} is less than 2.0 atoms per formula unit for most of the analyses from the ultramafic rocks and it exceeds 2.0 for chlorites from less mafic and rodingitic rock samples. The total range in variation spans from 0.573 to 2.649 Al^{iv} atoms per 8 tetrahedral positions. Al substitution limits in chlorite are known to be about 0.8 to 3.6 Al atoms per 8 tetrahedral positions (Bailey, 1988). Thus, the SQO contains chlorites with lower levels of Al^{3+} in tetrahedral positions extending downwards beyond the known lower limit of 0.8 atoms per 8 tetrahedral positions. Total octahedral Al is less than the tetrahedral Al in all analyses from SQO except the last 3 analyses in Table 3 which are distinct from the rest in Fe-enrichment. The first six analyses in Table 3 are of chlorite inclusions in chromite crystals: analysis no. 1 being from massive chrome ore and analysis no. 2 from banded chromitite. Analyses nos. 3 and 4 are from a disseminated chrome ore with coarse chromite grains that are completely altered to "ferritchromit" grains with spongy cores and abundant inclusions of chlorite. Many analyses showed higher Cr_2O_3 contents for the chlorite inclusions from chromite crystals, but such analyses are not included in the present study as they may, at least partly, indicate Cr "contamination" from the host chromite crystal. However, the presence of chromian clinochlores is definitely indicated. Chlorite flakes of analysis no. 7 fill a narrow veinlet cross-cutting massive chromitite, whereas those of analysis no. 8 fill an interstitial silicate area in the same chromitite sample. Analysis no. 9 is of chlorite from a disseminated textured chromitite and analyses nos. 10 and 11 are from massive chromitite from the same locality.

Analyses nos. 12 to 24 are from chromitites of the stratigraphically middle zone, dominated by banded textures in chromitites (Ahmed, 1982). According to Hey's classification (1954), they are unoxidized chlorites and the nomenclature for each analysis is reported in Table 3. Because Mg is the dominant divalent cation, they are mostly clinochlore or penninite; but a few are different. For example, in the last differentiated magmatic rock types, ripidolite is present. A few analyses are of talc-chlorite, pycnochlorite and brunsvigite.

From the lower-level gabbro (sample Z233) towards middle-level gabbro (sample Z394) the clinochlore displays an Fe-enrichment and Mg-depletion trend, as seen in Table 3 where the Mg and Fe atoms per formula unit show a distinct change between the two samples. Among various rock types of the SQO, a distinct Fe-enrichment and Mg-depletion trend is displayed in the latest magmatic differentiates. Therefore, all the ultramafic rocks contain Mg-rich chlorites like penninite or clinochlore; but the metadolerite (sample Z371B) contains ripidolite. The uppermost gabbro (sample Z368A) contains pycnochlorite and the plagiogranitic rock (sample Z339) contains ripidolite and brusvigite.

CLINTONITE

Clintonite is widely known as a skarn mineral that forms by thermal metamorphism of Ca- and Al-rich, Si-poor, rocks, or metasomatized carbonate rocks (Guggenheim, 1984). One occurrence is known from a diorite-serpentinite contact (Stevenson & Beck, 1965). It has not been reported from rodingites so far (e.g., Coleman, 1977; Adib & Pamic, 1980). This occurrence in the SQO rocks is from rodingitic veins traversing the metasomatized ultramafic rocks and indicates strong Al activity and enrichment which is a usual feature of rodingites (Espinosa, 1980). Clintonite analyses are reported in Table 5. The characteristic high Al of clintonite is even higher in one of the analyses. The tetrahedral compositions range from $Si_{1.028}Al_{2.972}$, which very closely approaches the ideal $SiAl_3$ ratio; to $Si_{1.262}Al_{2.738}$. These Si: Al limits compare favourably to those reported for the natural clintonites from other localities by Guggenheim (1984); except that the lower limit at $Si_{1.03}Al_{2.97}$ is slightly below the $Si_{1.11}Al_{2.89}$ limit known from natural clintonites. Clintonites with such lower Si contents have been synthesized (Olesch, 1975). The abnormally high Al of clintonite in sample no. Z383 may have been due to interaction of

Table 4. Clintonite analyses, assuming all iron as Fe^{2+}

Anal No	1	2	3	4	5	6	7
Sample No	Z383	ZB222	ZB222	ZB222	ZA222	ZA222	ZA222
SiO_2	14.48	17.33	17.41	16.86	17.83	17.28	17.75
TiO_2	0.01	0.00	0.00	0.00	0.00	0.00	0.02
Al_2O_3	47.73	42.37	42.62	42.54	42.42	41.96	42.00
Cr_2O_3	0.00	0.09	0.00	0.03	0.05	0.15	0.19
FeO	2.05	1.31	1.28	1.48	1.53	1.57	1.62
MnO	0.00	0.00	0.06	0.03	0.00	0.03	0.00
MgO	16.99	19.35	19.87	19.16	19.55	19.27	19.78
NiO	0.37	0.06	0.11	0.06	0.10	0.12	0.02
CaO	13.31	12.67	12.63	12.62	13.19	12.91	12.99
Na_2O	n.d.	0.07	0.83	0.13	0.03	0.00	0.25
K_2O	n.d.	0.00	0.05	0.05	0.06	0.06	0.00
Total	94.94	93.24	94.40	92.94	94.76	93.35	94.62
Formulae to 11 oxygens:							
Si	1.028	1.243	1.236	1.216	1.262	1.243	1.260
Al^{iv}	2.972	2.757	2.764	2.704	2.738	2.757	2.740
Al^{vi}	1.022	0.827	0.803	0.913	0.801	0.800	0.773
Ti	0.001	0.000	0.000	0.000	0.000	0.000	0.001
Cr	0.000	0.005	0.000	0.002	0.003	0.008	0.011
Fe	0.122	0.079	0.076	0.089	0.091	0.095	0.096
Mn	0.000	0.000	0.004	0.002	0.000	0.002	0.000
Mg	1.798	2.070	2.103	2.061	2.063	2.066	2.092
Ni	0.021	0.004	0.006	0.004	0.006	0.007	0.001
Ca	1.013	0.974	0.961	0.975	1.000	0.995	0.988
Na	–	0.010	0.053	0.018	0.004	0.000	0.034
K	–	0.000	0.004	0.004	0.005	0.005	0.000

rodingitizing fluids with the host chromitite rock. This is because the host of other clintonites with relatively lesser Al is rodingite that cuts across not chromitite, but clinopyroxene harzburgite (Table 5, sample nos. ZA222 and ZB222). Thus the clintonite composition seems to be controlled by the bulk composition of the rock surrounding rodingitic veins.

The interlayer Ca does not display much variation. It varies only between 0.961 and 1.013 atoms per formula unit. The lower Si:Al ratio of the sample Z383 increases the net negative charge on the tetrahedral sheets which is probably compensated by a corresponding increase in net positive charge on the octahedral sheet by an increase in octahedral Al (Table 5).

Substitutions of elements outside the Ca-Mg-Al-Si cation system are only minor. This is depicted by the elemental variation ranges which show the presence of minor amounts of TiO_2 (0.00 to 0.02%), Cr_2O_3 (0.00 to 0.19%), FeO (1.28 to 2.05%), NiO (0.02 to 0.37%), MnO (0.00 to 0.06%). Na_2O (0.00 to 0.38%) and K_2O (0.00 to 0.06%). FeO is below the maximum known limit of 2.56% from natural clintonites (Olesch, 1975), and is the main octahedral substituent. CaO ranges from 12.62 to 13.31% and MgO from 16.99 to 19.87% (1.798 to 2.103 atoms per formula unit).

DISCUSSION AND CONCLUSIONS

Serpentines from the SQO display large petrographic diversity and a large variation in chemistry which may have been produced by multistage serpentinization processes. The features typical of earlier suboceanic pervasive serpentinization, as well as a later post-emplacement episode of serpentinization, are displayed, as identified also in the southern Quebec serpentinites by Cogulu & Laurent (1984).

The banded, curtain-like and ribbon textures in serpentines have been described from many localities previously (Wicks, 1984). Their formation has been attributed to physical processes such as: (a) local shearing imposed on mesh textured serpentine that recrystallized one set of mesh-rims at the expense of other mesh-rims and mesh-centres (Francis, 1956); (b) regional shearing stress that causes recrystallization (Maltman, 1978); and (c) a distinctive fracture pattern of initial olivine retained pseudomorphically by the serpentines (Wicks, 1984).

The curtain-like serpentine observed in the SQO serpentinite are of different habit (Fig. 1) and are chemically distinct from the coexisting mesh-textured serpentines (Table 1). They may have grown in a later episode of serpentinization from fluids with relatively higher Al_2O_3, FeO and lower SiO_2 and MgO.

REFERENCES

ADIB, D. & PAMIC, J. (1980) Rodingites from the south eastern parts of the Neyriz ophiolite complex in the Zagros Range, Iran. Archives des Sciences **33** (2-3), pp. 281-90.

AHMED, Z. (1982) Porphyritic nodular, nodular and orbicular chrome ores from Sakhakot- Qila complex, Pakistan, and their chemical variations. Min. Mag. **45**, pp. 167-178.

(1987a) Mineral chemistry of the Sakhakot-Qila ophiolite Pakistan: Part 1, monosilicates. Acta Mineralogica Pakistanica **3**, pp. 26-41.

---- **(1987b)** Mineral chemistry of the Sakhakot-Qila ophiolite, Pakistan: part 2, polysilicates. Acta Mineralogica Pakistanica **3**, pp. 140-58.

(1988) Mineral chemistry of the Sakhakot-Qila ophiolite, Pakistan: Part 4, disilicates, tectosilicates and non-silicates. This volume.

----, **& HALL, A. (1981)** Alteration of chromite from the Sakhakot-Qila ultramafic complex, Pakistan. Chemie der Erde **40**, pp. 209-39.

BAILEY, S.W. (1988) Chlorites: structures and crystal chemistry. *In:* Bailey, S.W. (ed) HYDROUS PHYLLOSILICATES. Min. Soc. Amer. Rev. Mineralogy **19**, pp. 347-403.

CATHELINEAU, M. & NIEVA, D. (1985) A chlorite solid solution geothermometer: The Los Azufres (Mexico) geothermal system. Contrib. Mineral. Petrol. **91**, pp. 235-44.

COGULU, E. & LAURENT, P. (1984) Mineralogical and chemical variations in chrysotile veins and peridotite host-rocks from the asbestos belt of southern Quebec. Can. Mineral **22**, pp. 173-83.

COLEMAN, R.G. (1977) OPHIOLITES–ANCIENT OCEANIC LITHOSPHERE? Springer–Verlag, Berlin. 229p.

DEER, W.A., HOWIE, R.A. & ZUSSMAN, J. (1962) ROCK–FORMING MINERALS. Vol. **3**, Sheet Silicates. Longman, London, 270p.

DYMEK, R.F., BOAK, J.L. & BROTHERS, S.C. (1988) Titanian chondrodite- and titanian clinohumite-bearing metadunite from the 3800 Ma Isua supracrustal belt, West Greenland: Chemistry, petrology, and origin. Amer. Mineral. **73**, pp. 547-68.

ESPINOSA, A. (1980) Rodingites of the Los Azules ophiolitic sequence in the Western Cordillera of the Colombian Andes. Archives des Sciences **33**, (2-3), pp. 337-50.

FRANCIS, G.H. (1956) The serpentinite mass in Glen Urquhart, Inverness-shire, Scotland. Amer. Jour. Sci. **254**, pp. 201-26.

FOSTER, M.D. (1962) Interpretation of the composition and a classification of the chlorites. U.S. Geol. Surv. Prof. Pap. **414A**, pp. 1-27.

GUGGENHEIM, S. (1984) The brittle micas. In: Bailey, S.W. (ed.) MICAS. Min. Soc. Amer., Reviews in Mineralogy **13**, pp. 61-104.

HEY, M.H. (1954) A new review of the chlorites. Mineral. Mag. **30**, pp. 277-92.

LAIRD, J. (1988) Chlorites: metamorphic petrology. *In:* Bailey, S.W. (ed.) HYDROUS PHYLLOSILICATES. Min. Soc. Amer. Rev. Mineralogy **19**, pp. 405-53.

MALTMAN, A.J. (1978) Serpentinite textures in Anglesey, North Wales, United Kingdom. Geol. Soc. Amer. Bull. **89**, pp. 972-80.

McDOWELL, S.D., & ELDERS, W.A. (1980) Authigenic layer silicate minerals in borehole Elmore 1, Salton Sea geothermal field, California. Contrib. Mineral. Petrol. **74**, pp. 293-310.

OLESCH, M. (1975) Synthesis and solid solubility of trioctahedral brittle micas in the system CaO-MgO-Al_2O_3- SiO_2- H_2O. Amer. Mineral. **60**, pp. 188-99.

SHIROZU, H. (1978) Chlorite minerals. *In:* DEVELOPMENTS IN SEDIMENTOLOGY, Vol. **26**. Elsevier, Amsterdam, pp. 243-64.

STEVENSON, R.C. & BECK, C.W. (1965) Xanthophyllite from the Tabacco Root Mountains, Montana Amer. Mineral. **50**, pp. 292-3.

WALSHE, J.L. & SOLOMON, M. (1981) An investigation into the environment of formation of the volcanic hosted Mt Lyell copper deposits using geology, mineralogy, stable isotopes and a six component chlorite solid solution model. Econ. Geol. **76**, pp. 246-84.

WICKS, F.J. (1984) Deformation histories as recorded by serpentinites. III. Fracture patterns developed prior to serpentinization. Can. Mineral. **22**, pp. 205-9.

Manuscript received on 4.3.1988
Accepted for publication on 2.5.1988

ACTA MINERALOGICA PAKISTANICA
VOLUME 4 (1988) pp. 65 - 80.

MINERAL CHEMISTRY OF THE SAKHAKOT–QILA OPHIOLITE, PAKISTAN: PART 4, DISILICATES, TECTOSILICATES AND NON-SILICATES

ZULFIQAR AHMED
Centre of Excellence in Mineralogy, University of Baluchistan, GPO Box 43, Quetta, Pakistan.

ABSTRACT: The rocks of Sakhakot-Qila ophiolite contain disilicates: clinozoisite and vesuvianite; tectosilicates: quartz and albite; and non-silicates: chromian spinel, ilmenite, corundum, perovskite, apatite, nantokite, native Cu and a nickeliferous opaque mineral assemblage comprised of awaruite, pentlandite, heazlewoodite, PGE-rich awaruite, and troilite. In clinozoisite, theoretical pistacite content increases from the lower-level towards the higher-level within the metagabbros. The accessory chromite in ultramafic rocks is more ferruginous and less magnesian than the associated oreforming chromite. Both types conform to compositions known from ophiolitic rocks, except the Liguria-type ophiolites. Rodingitizing fluids cause increased Al-activity that is reflected by the presence of corundum: the elevated Cu and Cl, concentrations in the fluid are reflected in native Cu, nantokite and chlorapatite; and reaction of rodingitizing fluids with chromite may result in some local perovskite. Serpentinizing fluids form a variety of nickeliferous opaque minerals whose composition depends upon host-rock chemistry.

INTRODUCTION

This last part of the chemical characterization of minerals of the Sakhakot-Qila ophiolite (abbreviated 'SQO') deals with the disilicate, tectosilicate, and non-silicate minerals. Minerals other than these are described in earlier parts (Ahmed, 1987a; 1987b; & 1988). Compositional variations in the chromian spinel and aluminian chromite are primary and indicate certain petrogenetic relations. Minerals described in this paper are related to the chemical activities brought about by the secondary processes of serpentinization and rodingitization.

DISILICATES

CLINOZOISITE

Clinozoisite is confined to the metagabbros, metadolerites and plagiogranite amongst the SQO rocks. Microprobe analyses of clinozoisite from these rocks are given in Table 1. The analyzed grains do not show chemical zoning such as the Fe-Al zoning generally shown by greenschist facies metamorphic epidotes. The iron content is generally low and Al is high; conforming to the absence of optically negative epidote among the analyzed grains. The theoretical pistacite end-member substitution is also reported in percents in Table 1. It ranges from 0.773 to 12.563%.

The metagabbro samples from stratigraphically different horizons are represented in Table 1: Z233 represents the lower-level, Z394 the middle-level and Z368A the upper-level metagabbro. In Table 1, within-sample variation in terms of theoretical pistacite component ranges from 1.943 to 2.675 for Z233; 0.819 to 6.804 for Z394 and 7.999 to 8.999 for Z368A. This means there is a general trend of increasing pis-

Table 1. Analyses of Clinozoisite. Total iron is given as Fe^{3+} – = not determined b.d. = below detection limit

Anal. No.	1	2	3	4	5	6	7	8	9	10	11	12	13	14	15
Sp.No.	Z233	Z233	Z233	Z233	Z233	Z394	Z394	Z394	Z394	Z394	Z394	Z368A	Z368A	Z368A	Z368A
SiO_2	39.26	38.66	38.72	39.35	39.08	39.60	39.17	39.14	38.44	38.81	38.38	39.37	39.51	38.88	38.70
TiO_2	0.03	0.00	0.00	–	–	0.07	0.00	0.00	0.09	0.00	0.05	0.19	0.04	0.12	0.10
Al_2O_3	31.93	31.15	31.52	32.19	32.73	32.54	32.79	32.37	31.66	31.61	30.16	29.78	30.44	29.90	29.50
Cr_2O_3	0.00	0.04	0.06	–	–	0.18	0.10	0.03	0.05	0.03	0.09	0.00	0.02	0.03	0.03
Fe_2O_3	1.00	1.30	1.33	1.33	1.40	0.42	0.64	0.88	1.07	1.36	3.45	4.11	4.14	4.23	4.57
MnO	0.12	0.04	0.13	–	–	0.05	0.06	0.07	0.00	0.00	0.07	0.21	0.05	0.14	0.19
MgO	0.23	0.20	0.42	0.45	0.00	0.30	0.27	0.22	0.24	0.01	0.05	0.73	0.27	0.09	0.08
NiO	0.00	0.00	0.00	–	–	0.00	0.06	0.00	0.00	0.07	0.00	0.02	0.00	0.12	0.00
CaO	25.11	25.24	24.95	26.25	26.17	25.13	25.15	24.93	24.72	24.94	24.48	24.11	24.72	24.63	24.57
Na_2O	b.d.	0.09	0.02	–	–	0.09	0.00	0.00	0.16	0.00	0.04	0.00	0.00	0.29	0.03
K_2O	b.d.	0.00	0.02	–	–	b.d.	b.d.	b.d.	0.02	b.d.	0.00	b.d.	0.00	0.00	0.00
Total	97.68	96.72	97.17	99.57	99.38	98.38	98.24	97.64	96.45	96.83	96.77	98.52	99.19	98.43	97.77
Number of cations on the basis of 12.5 (O) ignoring water.															
Si	3.002	2.995	2.983	2.965	2.949	3.000	2.975	2.990	2.980	2.997	2.988	3.011	3.002	2.989	2.995
Al^{iv}	0.000	0.005	0.017	0.035	0.051	0.000	0.025	0.010	0.020	0.003	0.012	0.000	0.000	0.011	0.005
Al^{vi}	2.877	2.844	2.845	2.823	2.860	2.905	2.910	2.904	2.872	2.874	2.755	2.684	2.726	2.698	2.685
Ti	0.002	0.000	0.000	–	–	0.004	0.000	0.000	0.005	0.000	0.003	0.011	0.002	0.007	0.006
Cr	0.000	0.002	0.004	–	–	0.011	0.006	0.002	0.003	0.002	0.005	0.000	0.001	0.002	0.002
Fe^{3+}	0.057	0.076	0.077	0.075	0.080	0.024	0.037	0.051	0.062	0.079	0.202	0.237	0.237	0.245	0.266
Mn	0.008	0.003	0.008	–	–	0.003	0.004	0.005	0.000	0.000	0.005	0.014	0.003	0.009	0.012
Mg	0.026	0.023	0.048	0.051	0.000	0.034	0.031	0.025	0.028	0.001	0.006	0.083	0.031	0.010	0.009
Ni	0.000	0.000	0.000	–	–	0.000	0.004	0.000	0.000	0.004	0.000	0.001	0.000	0.007	0.000
Ca	2.057	2.095	2.060	2.119	2.116	2.039	2.046	2.040	2.053	2.063	2.042	1.976	2.013	2.028	2.037
Na	–	0.014	0.003	–	–	0.013	0.000	0.000	0.024	0.000	0.006	0.000	0.000	0.043	0.004
K	–	0.000	0.002	–	–	b.d.	b.d.	b.d.	0.002	b.d.	0.000	b.d.	0.000	0.000	0.000
$\frac{100\ Fe^{3+}}{(Fe^{3+} + Al)}$	1.943	2.598	2.620	2.557	2.675	0.819	1.245	1.720	2.099	2.673	6.804	8.114	7.999	8.294	8.999

Anal. No.	16	17	18	19	20	21	22	23	24	25	26	27	28	29
Sp. No.	Z219	Z219	Z219	Z219	Z219	ZB182	ZB182	ZB182	ZB182	ZB182	ZB182	ZB182	Z339	Z339
SiO_2	39.46	39.19	39.27	39.34	39.67	41.44	49.46	39.29	39.30	39.23	39.56	39.00	38.79	39.01
TiO_2	0.12	0.11	0.18	0.05	0.07	0.01	0.06	0.02	0.08	0.09	0.12	0.07	0.17	0.09
Al_2O_3	33.15	32.05	32.11	32.92	31.97	31.56	31.83	31.52	31.81	31.87	31.64	31.51	28.75	29.05
Cr_2O_3	0.00	0.00	0.03	0.04	0.09	0.00	0.00	0.02	0.04	0.06	0.03	0.00	0.00	0.09
Fe_2O_3	0.41	0.47	0.72	0.84	0.91	1.60	3.01	3.19	3.41	3.45	3.49	3.49	6.14	6.54
MnO	0.02	0.09	0.02	0.01	0.05	0.08	0.00	0.00	0.15	0.00	0.09	0.09	0.14	0.15
MgO	0.40	0.00	0.10	0.27	0.59	1.64	0.08	0.10	0.30	0.09	0.14	0.00	0.05	0.44
NiO	0.02	0.00	0.00	0.03	0.00	0.07	0.00	0.05	0.00	0.14	0.03	0.05	0.01	0.08
CaO	24.81	24.20	24.20	24.73	24.09	21.54	23.51	23.52	23.84	23.65	23.38	23.83	24.09	24.22
Na_2O	0.00	0.00	0.00	0.04	0.00	0.00	0.00	0.00	0.07	0.06	0.00	0.00	b.d.	0.20
K_2O	0.00	0.00	0.00	0.00	b.d.	0.08	0.05	0.00	0.03	0.02	0.00	b.d.	b.d.	0.00
Total	98.39	96.11	96.63	98.27	97.44	98.02	98.00	97.71	99.03	98.66	98.38	98.04	98.14	99.87
Number of cations on the basis of 12.5 (O) ignoring water:														
Si	2.983	3.028	3.020	2.982	3.027	3.117	3.007	3.007	2.976	2.980	3.005	2.984	3.000	2.974
Al^{iv}	0.017	0.000	0.000	0.018	0.000	0.000	0.000	0.000	0.024	0.020	0.000	0.016	0.000	0.026
Al^{vi}	2.936	2.919	2.911	2.923	2.875	2.798	2.859	2.843	2.815	2.833	2.832	2.825	2.621	2.584
Ti	0.007	0.006	0.010	0.003	0.004	0.001	0.003	0.001	0.005	0.005	0.007	0.004	0.010	0.005
Cr	0.000	0.000	0.002	0.002	0.005	0.000	0.000	0.001	0.002	0.004	0.002	0.000	0.000	0.005
Fe^{3+}	0.023	0.027	0.042	0.048	0.052	0.091	0.173	0.184	0.194	0.197	0.200	0.201	0.357	0.357
Mn	0.001	0.006	0.001	0.001	0.003	0.005	0.000	0.000	0.010	0.000	0.006	0.006	0.009	0.010
Mg	0.045	0.000	0.012	0.031	0.067	0.184	0.009	0.011	0.034	0.010	0.016	0.000	0.006	0.050
Ni	0.001	0.000	0.000	0.002	0.000	0.004	0.000	0.003	0.000	0.009	0.002	0.003	0.001	0.005
Ca	2.009	2.004	1.994	2.008	1.969	1.736	1.920	1.928	1.934	1.925	1.903	1.953	1.996	1.978
Na	0.000	0.000	0.000	0.003	0.000	0.000	0.000	0.000	0.010	0.009	0.000	0.000	b.d.	0.030
K	0.000	0.000	0.000	0.000	b.d.	0.008	0.005	0.000	0.003	0.001	0.000	b.d.	b.d.	0.000
$100\ Fe^{3+}$ / $Fe^{3+} + Al$	0.773	0.917	1.422	1.606	1.777	3.150	5.706	6.079	6.396	6.459	6.596	6.608	11.988	12.563

tacite component from lower level to upper level metagabbro. Sample Z394 contains clinozoisites with bimodal pistacite content: one with 0.819 to 2.673% pistacite and the other with 6.804% pistacite. It may be possible that these two populations of clinozoisite are genetically different. Somewhat similar differences are found in the clinozoisite from metadolerite samples: the pistacite component in Z219 varies from 0.773 to 1.777% and in sample ZB182 it varies from 3.150 to 6.608%. The pistacite component in plagiogranite sample, Z339 varies from 11.988 to 12.563%, which is the highest for SQO rocks.

Analyses of Table 1 exhibit only minor replacement of Si by Al. The content of Si, varying from 2.949 to 3.028, does not depart significantly from the ideal 3 atoms per formula unit. The replacement of Ca by Mg and Mn is comparatively small. Other contains are present in very small amounts, the maximum values being: 0.19% for TiO_2, 0.18% for Cr_2O_3, 0.21% for MnO, 0.14% for NiO, 0.29% for Na_2O and 0.08% for K_2O; although most frequently these elements are present in much smaller, almost negligible amounts. The maximum values for these amounts correspond to 0.011 for Ti, 0.011 for Cr, 0.014 for Mn, 0.009 for Ni, 0.043 for Na, and 0.008 for K atoms per formula unit calculated on the basis of 12.5 oxygen atoms.

VESUVIANITE

The rodingitic dykes and veins of SQO, formed by Ca metasomatic activity, commonly contain vesuvianite which typically exhibits well developed crystal form. Chemical analyses from three samples are documented in Table 2. The arithmetic means, variation ranges and standard deviations are also given for different elements. The oxide weight percentages resemble those of hydrogrossular; as is their usual feature (Deer *et al.*, 1962; 1982). In two samples (nos. Z399A, ZA222), euhedral crystals of vesuvianite coexit with hydrogrossular from which it is indistinguishable on the basis of chemical analyses alone. Its presence is also noted in a rodingitized chromitite (sample

Table 2. Analyses of vesuvianite from rodingito dyke (Z399A), rodingite vein in harzburgite (ZA222), and rodingite-veined chromitite (Z235).

Anal. No.	1	2	3	4	5	6	7	8	9	10	11	12	13	(1 to 13)		
Sp.No.	Z399A	Z399A	Z399A	Z399A	Z399A	Z399A	Z399A	Z399A	Z399A	ZA222	ZA222	ZA222	Z235	Mean	Range	S.D.
SiO_2	35.92	35.84	36.13	35.80	36.02	36.19	36.91	37.28	36.94	37.21	36.23	36.27	37.19	36.46	35.80–37.28	0.54
TiO_2	0.08	0.06	0.26	0.05	0.06	0.08	0.00	0.03	0.08	0.05	0.01	0.03	0.06	0.07	0.00– 0.26	0.06
Al_2O_3	17.00	17.38	17.86	17.30	17.13	17.19	18.28	18.65	18.41	17.61	16.82	17.12	17.92	17.59	16.82–18.65	0.56
Cr_2O_3	0.02	0.00	0.03	0.05	0.15	0.03	0.00	0.12	0.02	0.00	0.02	0.05	0.08	0.04	0.00– 0.15	0.04
V_2O_3	0.00	0.05	0.01	0.00	0.00	0.00	–	–	–	–	–	–	0.04	0.01	0.00– 0.05	0.02
Fe_2O_3	2.61	2.96	2.67	3.05	2.78	3.00	1.89	1.64	2.23	2.44	2.99	2.27	1.58	2.47	1.58– 3.05	0.50
MnO	0.00	0.13	0.00	0.00	0.08	0.11	0.14	0.00	0.00	0.05	0.00	0.00	0.02	0.04	0.00– 0.14	0.05
MgO	2.22	2.01	2.07	2.51	2.51	2.52	2.44	2.83	2.65	2.83	3.03	2.55	2.64	2.52	2.01– 3.03	0.28
NiO	0.00	0.00	0.01	0.90	0.00	0.00	0.00	0.08	0.00	0.11	0.07	0.00	0.06	0.09	0.00– 0.90	0.24
CaO	36.35	36.47	36.43	35.64	36.57	36.87	36.12	36.59	36.52	36.42	35.94	35.84	36.86	36.36	35.64–36.87	0.36
Na_2O	0.03	0.00	0.14	0.00	0.00	0.00	0.30	0.00	0.00	0.00	0.23	0.00	0.00	0.05	0.00– 0.30	0.10
K_2	0.00	0.00	0.00	0.00	0.00	0.00	0.04	0.05	0.01	0.00	0.00	0.05	0.00	0.01	0.00– 0.05	0.02
Total	94.23	94.90	95.61	95.30	95.30	95.99	96.12	97.27	96.86	96.72	95.34	94.18	96.45	45.71	94.18–97.27	–

Table 3. Albite analyses. Total iron is assumed trivalent. Sp. = sample, No. Anal. = Number of analyses averaged. s = sample standard deviation.

Sp. No.	Z394	Z368A	Z339	ZB182	Z372
No. Anal.	$\bar{x}$ (5), s	(1)	$\bar{x}$ (4), s	$\bar{x}$ (8), s	$\bar{x}$ (4), s
SiO_2	66.65 (0.55)	64.85	68.36 (0.64)	67.76 (0.30)	67.15 (0.10)
Al_2O_3	19.23 (0.41)	19.37	19.62 (0.15)	19.65 (0.16)	19.83 (0.14)
Fe_2O_3	0.13 (0.09)	1.14	b.d.	0.14 (0.10)	0.44 (0.10)
MnO	0.00	0.23	b.d.	b.d.	0.00
CaO	0.30 (0.15)	0.56	0.10 (0.09)	0.13 (0.09)	0.46 (0.08)
Na_2O	12.05 (0.42)	10.31	11.12 (0.07)	12.66 (1.00)	10.98 (0.17)
K_2O	0.02 (0.02)	0.03	0.08 (0.08)	0.00	0.00
Total	98.38	96.49	99.08	100.34	98.86

Z235) where it appears as blades and laths cutting across coarser grossular grains. In many rodingite veins, vesuvianite shows an acicular habit.

TECTOSILICATES

Tectosilicates do not occur in the ultramafic rocks of SQO. From other rock–types, quartz and albite are known. Quartz is present in the middle- and upper-level metagabbros and in the plagiogranite which contains more than 90% modal quartz. Albite occurs in the metagabbros, metadolerites and plagiogranite and represents the metamorphic Na-rich phase of the primary plagioclase now disappeared. The analyses are given in Table 3. The molecular percentages of orthoclase are always below 1% and those of anorthite below 3%, the albite molecule being 97 to 100%. Ba was not determined and TiO_2, NiO, V_2O_3 and MgO are absent. The metabasites with albite are generally considered to indicate low grade metamorphism corresponding to greenschist facies.

NON-SILICATES

CHROMIAN SPINEL

The composition of segregated chromites that form mineable ore bodies in the SQO has been presented in earlier studies by Ahmed (1982; 1984) and Ahmed & Hall (1981). A few representative microprobe analyses of accessory chromite grains from various types of SQO rocks are given in Table 4, in which Fe^{2+} and Fe^{3+} are calculated assuming perfect spinel stoichiometry (Irvine, 1965; Thayer, 1964; Stevens, 1944). The analyses represent unaltered portions of grains located by carefully employing the criteria for the recognition of altered parts described in detail in an earlier communication (Ahmed & Hall, 1981). All the analyses exhibit very low Fe^{3+} contents. Amongst the spot analyses from each rock type, those with highest Al_2O_3 content only are listed in Table 4. These analyses of accessory chromian spinel differ from those of segregated chromite in each rock. Most of the serpentinites contain chromian spinel completely altered to "ferritchromit" and are not included in Table 4. Silicate inclusions in chromite crystals are common; and chromite analyses were performed away from such inclusions. All reported analyses are from crystals showing no compositional zoning or replacement effects. In each analysis, Na_2O and K_2O were found to be quantitatively either nil or below the detection level of the microprobe. An extreme Fe-rich and Mg-poor type of chromian spinel, from an Fe-websterite dyke (sample Z36), is different in composition from all the rest of the analyses.

At SQO, chromite deposits were found at 62 localities given in earlier communication (Ahmed, 1987a, Fig. 1). The ores are typically podiform as defined by Thayer (1964, 1969) and occur mainly in dunite. Stratigraphic zones

Table 4. **Analyses of rock-forming accessory chromite from harzburgite (1–4), clinopyroxene-harzburgite (5–7), dunite (8–12), dunite dyke cross-cutting massive chromitite (13), serpentinite (14, 15), clinopyroxene-dunite (16), wehrlite (17–22), orthopyroxenite dyke (23), clinopyroxenite dyke (24), websterite dyke (25) and Fe–websterite dyke (26). b.d. = below detection level "–" = not determined.**

Analysis No.	1	2	3	4	5	6	7	8	9	10	11	12
Sample No.	Z310	Z344	Z324	Z216	Z222	Z323	Z326	Z14	Z142	Z188	Z327	Z275B
SiO_2	0.00	0.70	0.20	0.07	0.19	0.27	0.00	0.37	0.00	b.d.	0.27	0.00
TiO_2	–	0.20	0.12	0.33	0.17	0.00	0.00	0.00	0.01	0.39	0.23	0.22
Al_2O_3	24.95	21.69	18.43	24.20	28.40	26.72	16.69	11.22	10.44	20.48	14.85	25.76
Cr_2O_3	43.31	45.48	50.51	41.57	38.85	40.51	49.42	55.09	59.29	43.91	52.93	38.59
V_2O_3	0.16	0.00	0.36	0.32	0.19	0.33	0.32	0.41	0.21	0.36	0.21	0.29
Fe_2O_3	3.25	2.68	1.82	3.63	3.37	3.00	3.88	2.45	2.44	5.73	4.18	5.77
FeO	14.90	14.82	17.78	16.46	15.65	16.21	18.15	21.26	17.19	18.28	16.13	17.13
MnO	0.50	0.59	0.32	0.44	0.47	0.31	0.43	0.59	0.41	0.54	0.37	0.20
MgO	13.57	12.99	11.23	12.31	13.52	13.01	10.27	7.72	10.41	10.78	12.02	12.25
NiO	–	0.16	0.08	0.00	0.19	0.11	0.08	0.08	0.12	0.27	0.07	0.16
CoO	–	0.28	–	0.01	–	–	0.07	0.00	0.34	b.d.	–	–
CaO	–	–	0.00	–	0.00	0.00	b.d.	b.d.	0.00	0.00	0.00	–
Total	100.64	99.59	100.85	99.34	101.00	100.47	99.31	99.19	100.86	100.74	101.26	100.37
Parameters and ratios of cations calculated to 32 oxygens:												
Cr/Fe	2.138	3.222	2.290	1.856	1.830	1.886	2.010	2.066	2.693	1.649	2.342	1.522
Cr/Al	2.244	2.711	3.545	2.222	1.769	1.960	3.829	6.347	7.348	2.772	4.610	1.937
100 x Mg/ $(Mg+Fe^{2+})$	61.879	60.965	52.956	57.140	60.593	58.860	50.211	39.267	51.900	51.248	57.052	56.034
100 x Cr/ $(Cr+Al+Fe^{3+})$	51.793	56.580	63.361	51.254	46.025	48.681	63.351	74.281	76.828	54.947	66.957	46.775
100 x Al/ $(Cr+Al+Fe^{3+})$	44.502	40.243	34.467	44.491	50.172	47.892	31.910	22.569	20.168	38.222	28.007	46.573
100 x Fe^{3+}/ $(Cr+Al+Fe^{3+})$	3.704	3.177	2.172	4.255	3.804	3.427	4.740	3.149	3.004	6.831	5.037	6.652
100 x Cr/ (Cr+Al)	53.786	58.437	64.768	53.532	47.844	50.409	66.503	76.697	79.207	58.975	70.508	50.108
Fe^{2+}/Mg	0.616	0.640	0.888	0.750	0.650	0.699	0.991	1.547	0.927	0.951	0.753	0.785

13	14	15	16	17	18	19	20	21	22	23	24	25	26
ZA228B	Z342	Z346	Z344	Z147	Z202	Z264	Z265	Z294A	Z347	Z104	Z123	Z30	Z36
0.12	b.d.	–	0.70	b.d.	b.d.	0.33	0.00	0.00	0.21	0.32	0.27	b.d.	b.d.
0.12	0.21	0.11	0.20	b.d.	0.10	0.16	0.19	0.21	0.12	0.14	0.38	0.22	1.65
26.70	12.46	32.21	21.69	22.13	26.72	12.06	22.91	22.48	27.28	15.93	14.45	12.88	18.54
36.86	55.38	34.60	45.48	48.33	41.23	55.38	46.89	43.62	38.75	51.27	55.02	56.29	27.92
0.00	0.26	0.30	0.00	0.00	0.22	0.30	0.33	0.21	0.27	0.33	0.24	0.00	0.40
7.61	2.96	3.83	2.68	1.35	3.40	3.10	1.69	3.44	3.70	2.58	1.05	2.83	20.02
16.71	21.37	16.39	14.82	16.53	15.92	21.24	15.36	18.80	17.54	20.38	20.09	17.76	27.03
0.42	0.33	0.33	0.59	0.34	0.46	0.15	0.66	0.29	0.28	0.60	0.29	0.50	0.31
12.70	8.31	13.55	12.99	12.45	13.24	8.61	13.11	10.77	12.23	9.07	9.57	10.60	5.53
0.17	0.10	0.15	0.16	0.00	0.07	0.00	–	0.00	0.08	0.07	0.00	b.d.	0.00
0.00	–	–	0.28	0.00	–	0.00	–	–	–	0.08	0.00	0.00	–
–	0.00	0.00	–	0.00	0.00	–	–	–	0.00	0.00	0.00	0.00	0.05
101.41	101.38	101.47	99.59	101.13	101.36	101.33	101.14	99.82	100.46	100.77	101.36	101.08	101.45
Parmeters and ratios of cations calculated to 32 oxygens:													
1.377	2.029	1.535	2.322	2.398	1.912	2.029	2.445	1.754	1.634	1.988	2.303	2.440	0.546
1.785	5.745	1.389	2.711	2.824	1.995	5.940	2.647	2.510	1.837	4.163	4.923	5.652	1.948
57.521	40.932	59.565	60.965	57.297	59.700	41.951	60.339	50.519	55.402	44.234	45.908	51.548	26.722
43.918	72.125	40.102	56.580	58.501	48.900	72.573	56.724	52.246	46.709	66.174	70.926	71.993	37.417
47.451	24.209	55.674	40.243	39.942	47.267	23.562	41.330	41.682	49.042	30.655	27.784	24.562	37.044
8.630	3.666	4.224	3.177	1.557	3.833	3.864	1.946	4.073	4.249	3.172	1.289	3.446	25.538
48.067	74.869	41.871	58.437	59.426	50.849	75.491	57.850	56.549	48.782	68.341	71.853	74.562	50.250
0.738	1.443	0.679	0.640	0.745	0.675	1.384	0.657	0.980	0.805	1.261	1.178	0.940	2.742

have been identified by distinctions in composition and texture of chromitites (Ahmed, 1984). Deposits may have slickensided contacts with barren dunite, or, may grade to more disseminated ore in a dunite matrix, or to chromitiferous dunite. Small dunite lenses may be enclosed in massive chromitites. Tabular layers of massive ore may taper to barren dunite. Relict magmatic textures in chromitites include massive, disseminated, banded, nodular, 'porphyritic nodular', orbicular, 'pseudoclastic', chromite-net and occluded-silicate textures (Ahmed, 1982; 1984; Thayer, 1969). Later cataclastic effects are also observed. Gneissic ores are rarely seen; but pull-apart fracture is common in chromitites.

Major element concentrations in chromite, in general, agree with those given for chromite ores and accessory chromite from typical ophiolite complexes. The accessory chromian spinel is more Fe-enriched than the ore-forming chromite.

The "ferritchromit" is invariably enriched in Cr, total Fe, Fe^{3+}, Fe^{2+} and Mn and impoverished in Mg and Al relative to its parent chromite grains. The change is often considerable. Different spots in each chromite grain show constant compositions for the primary chromite portions, but variable compositions within the "ferritchromit" portions, depending upon the intensity of alteration. The contacts between the two are

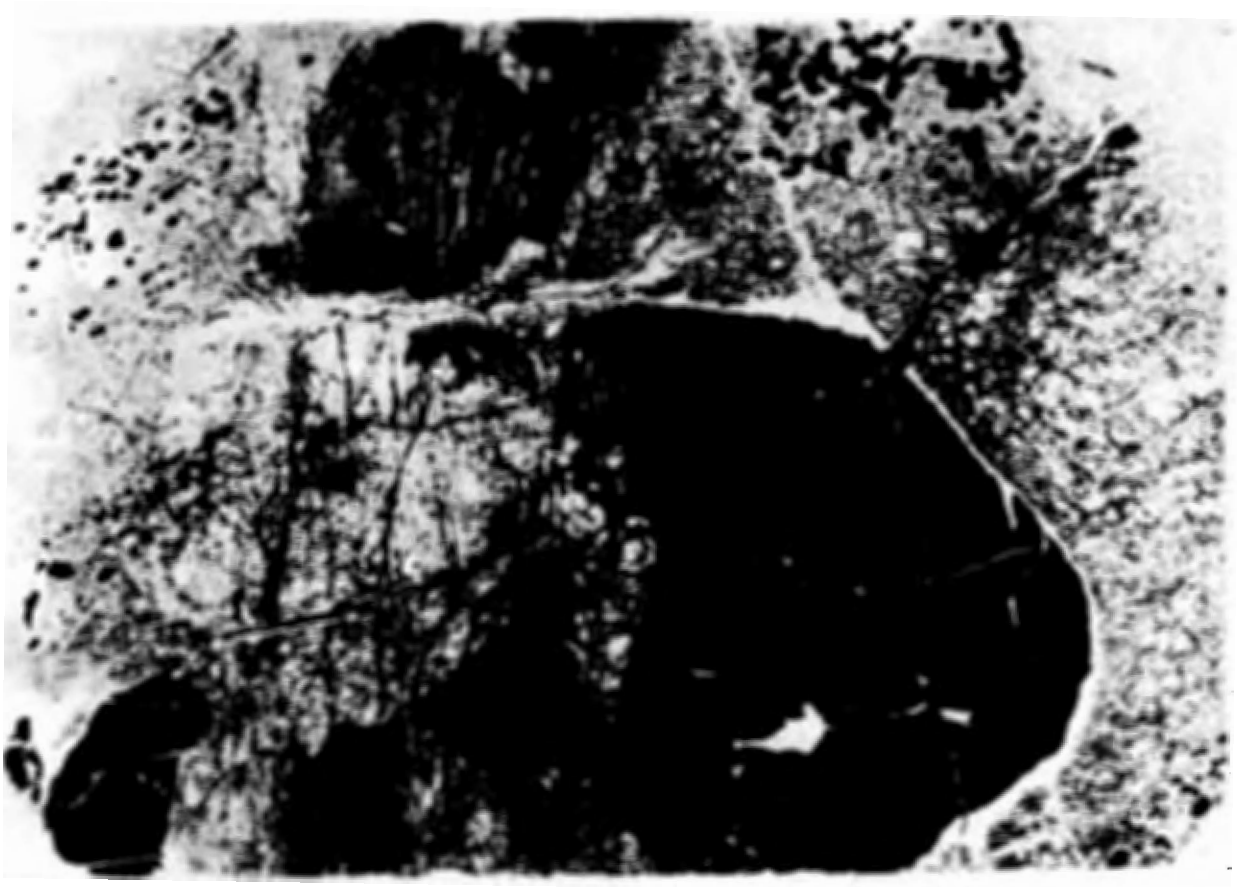

Fig. 1. Thin section photomicrograph of an orbicular chromitite from Landi Raud Mine of SMO. The rock is crosscut by a cm-scale dyke of diopsidite which has broken apart the chromite (black) nodule into two pieces. Finer chromite (also black) belongs to the orbicule rim. Dyke width is shown by a bar in upper margin which measures 1 cm. Diopside is coarse and makes well-cleaved clear crystals (central part) as well as dirty crystals (dark grey upper and lower parts of photograph).

often sharp (within ten microns distance). The homogeneous primary chromite does not show optical or chemical zoning towards "ferritchromit" areas. In cases of intense alteration, the Mg and Al of the primary chromite may be lost completely, and Cr/Al ratios may increase by 50 to 100 times. The Al released from "ferritchromit" is absrobed by the chlorite which is always associated with the "ferritchromit" as inclusions, coronas and envelopes around chromite grains and segregations. A second type of chromite alteration to "secondary chromite" is described by Ahmed & Hall (1981, Fig. 6). In a third type of alteration, chromite alters to typical magnetite as homogeneous rims on chromite.

The compositional variation of primary chromites, both segregated and accessory, from the SQO ranges as follows: Cr_2O_3, 24.3 to 64.1%; Al_2O_3, 6.5 to 42.7%; FeO (total iron), 13.7 to 22.1%; MgO, 10.6 to 18.5%; TiO_2, 0.00 to 0.45%; Cr/Fe, 1.4 to 4.5 and Cr/Al, 0.7 to 12.3. According to the classification by Stevens (1944), these chromites belong to the "aluminian chromite" and "chromian spinel" fields, and many analyses plot in the metallurgical grade. The data on SQO chromites, including that published earlier by Ahmed (1982; 1984) and Ahmed & Hall (1983), points to a strong resemblance of these chromites to other podiform chromite deposits which develop in the alpine-type peridotites of ophiolites. Various chemical parameters used to establish this resemblance are as follows:

(a) Relative constancy of total iron content, and its independence from variation in Cr_2O_3 content (Thayer, 1970).

(b) More magnesian character, with total Fe content lower than that of stratiform chromites (Thayer, 1964a, 1969; Dickey, 1975). The MgO: FeO ratio for most analyses is more than 1. Thayer (1970) gave the values of 1 to 2.3 for podiform deposits and 0.6 to 1 for stratiform deposits. Moreover, the total Fe content for SQO chromites is below 20%, which is the maximum limit for podiform class (Thayer, 1970).

(c) Relative constancy of Fe^{2+}/Mg ratio in chromites from individual deposits, compared to stratiform complexes (Dickey, 1975).

(d) An Fe_2O_3 content which is below 8%, and is different from the stratiform chromites which have 10 to 24% Fe_2O_3 (Thayer, 1970).

(e) Low TiO_2 content; in most analyses below 0.3% (Dickey & Yoder, 1972; Malpas & Strong, 1975) and lack of significant correlation between Ti and major elements (Dickey, 1975).

(f) Large range of reciprocal Cr-Al variation (Thayer, 1964, 1969, 1970; Dickey, 1975; Irvine, 1967) with Fe^{3+} staying low and roughly constant. This behaviour is unlike stratiform deposits in which the chromite compositions show a reciprocal relationship between Cr and Fe and not between Cr and Al.

(g) In grade, the chrome ores of SQO are mostly of the high-Cr, low-Fe (metallurgical) grade with a lesser fraction of high-Al (refractory) grade. The chemical analyses presented here do not show high-Fe (chemical grade) ores, except in their secondarily altered parts, which do not change the overall grade of the ore.

(h) The elemental Cr/Fe ratio that varies from 1.4 to 4.5 matches the range shown by most podiform chromite deposits.

Accessory chromite is ubiquitous in the ultramafic rocks and often constitutes 1 to 3% modally, with a maximum arbitrary limit of 10% chosen after Jackson (1961) and Thayer (1970). The accessory chromite shows a consistent Fe-enrichment and Mg-impoverishment compared to the segregated chromites and plots separately in the spinel prism (Ahmed, 1984, Fig. 5). In terms of trivalent cations, the accessory chromites of SQO show an overall Cr-Al variation similar to that found in the ore-forming chromites; and in general, at individual deposits, a higher Al_2O_3, and total Fe or

FeO, and lower Cr_2O_3 and MgO for the accessory chromites compared to the segregated chromites is displayed. The trend in pyroxenite dykes is different.

Accessory chromites display a narrow range of cation contents in harzburgites compared to the other rock types. This may be due to the residual character of the harzburgite. Cr content of chromite in harzburgite does not exceed that found in the associated dunite. The accessory chromite is more aluminous and magnesian in harzburgite than the associated cumulate dunites. This relationship is comparable to that observed in a number of alpine-type complexes such as Vourinos, Greece (Harkins *et al.*, 1980), Vavdos and Gomati, Greece, and other examples quoted from elsewhere by Christodoulou and Hirst (1985), Troodos, Cyprus (Greenbaum, 1977), Oman (Brown, 1980), the Josephine peridotite, U.S.A. (Dick, 1977) and the Canyon Mountain Complex, Oregon, U.S.A. (Himmelberg and Loney, 1980). The residual tectonite peridotites contain more aluminous and magnesian chromite than the cumulate dunite; whether the cumulate dunites overlie harzburgite (e.g., Himmelberg & Loney, 1980) or, occur within harzburgite as layers and dykes (e.g., Harkins *et al.*, 1980). In SQO, the chromite from dunite contains higher Fe^{3+} contents than the pyroxene-bearing ultramafic rocks, and resembles the trend of the Bay of Islands ophiolite, Canada (Malpas, 1978). A regular stratigraphic variation among the accessory chromite compositions is not obvious in the present set of analyses.

ILMENITE

Illmenite analyses that appear in Table 5 are either from metadolerite sample Z219 or from the rodingitized metadolerite sample Z371B. Ilmenite has high TiO_2 and FeO; and its MnO content varies from 0.28 to 0.42% in Z219 but from 1.35 to 1.38% in Z371B.

Among trace elements analyzed from ilmenite, Cr, Ni, Co, Cu, Na, K and Cl are below the detection limit of the microprobe. Ilmenite is, therefore, uncontaminated by the rodingitizing fluids that contained Cl, Cu, etc., or the primary elements from surrounding ultrabasic rocks such as Cr and Ni. Mg and Mn increase simultaneously in the ilmenite of sample Z371B. In terms of MgO and TiO_2 contents, the ilmenite resembles those known from basic igneous rocks (Haggerty, 1976, Fig. Hg-41D).

Table 5. **Ilmenite analyses.**

Anal. No.	1	2	3	4	5
Sp.No.	Z219	Z219	Z219	Z371B	Z371B
SiO_2	0.20	0.21	0.27	0.59	0.55
TiO_2	54.15	53.95	50.35	52.96	54.38
Al_2O_3	0.07	0.09	2.21	b.d.	b.d.
V_2O_3	0.07	0.17	0.31	0.40	b.d.
FeO	45.15	45.30	43.63	42.46	42.81
MnO	1.47	1.48	1.40	1.72	1.83
MgO	0.28	0.30	0.42	1.35	1.38
CaO	0.08	0.14	0.10	b.d.	b.d.
Total	101.47	101.64	98.69	99.48	100.95

CORUNDUM

Corundum, like clintonite, has not been reported from rodingites prior to this study (e.g., Coleman, 1977; Adib & Pamic, 1980) and its presence in the SQO indicates high Al activity and enrichment usually found in rodingites (e.g., Espinosa, 1980). Corundum is not chemically variable and one representative analysis is given in Table 6.

Table 6. **Analysis of corundum from rodingitic vein (sample no. ZA222) in clinopyroxene harzburgite Na_2O and K_2O are below detection level.**

SiO_2	TiO_2	Al_2O_3	Cr_2O_3	FeO	MnO	MgO	NiO	CaO	Total
b.d.	0.80	98.40	0.00	0.09	0.00	0.33	0.00	0.07	98.97

PEROVSKITE

Perovskite is normally absent in the SQO rocks; but one sample of massive chromitite, no Z41A, is cut by rodingitic grossular veins that also contained uvarovite, hydrogrossular,

Table 7. Perovskite analyses from sample no Z41A.

Anal. No.	1	2		1	2
Oxides percents by mass:			Cations to 3 oxygens:		
TiO_2	59.15	58.52	Ti	0.99	0.98
SiO_2	0.40	0.40	Si	<0.01 <	0.01
Cr_2O_3	0.40	0.50	Cr	< 0.01<	0.01
V_2O_3	0.40	0.40	V	< 0.01<	0.01
CaO	41.08	41.63	Ca	0.98	1.00
Total	101.08	101.45			

Table 8. Apatite analyses by microprobe assuming bivalent total iron. Z339=mean of four analyses from plagiogranite; Z219=mean of two analyses from moderate. – = not determined.

Sp.No.	Z339	Z219
SiO_2	0.63	0.60
Al_2O_3	0.11	0.00
FeO	0.44	0.27
MnO	0.00	0.00
MgO	0.15	0.00
CaO	56.14	52.57
Na_2O	0.02	0.00
K_2O	0.06	0.00
P_2O_5	42.11	41.10
Cl	–	4.00
Total	99.66	98.54

Table 9. Nantokite analyses from sample Z371B.

Mass percents:			Atomic percents:		
	1	2		1	2
Cu	66.10	65.78	Cu	52.00	51.95
Cl	34.06	33.95	Cl	48.00	48.05
Total	100.16	99.73			

apatite, and in addition, perovskite. Two analyses of the pervoskite are given in Table 7. Its high Cr_2O_3 content was probably derived from the host chromitite by the rodingitizing fluids. The analyses yielded values below detection level for Al_2O_3, FeO, MnO, MgO, NiO and CoO.

APATITE

Apatite has been detected from metadolerites and plagiogranite of the SQO. Chlorapatite is an abundant accessory in the metadolerite represented by sample Z219; and forms colourless, relatively undeformed grains. The chemical analyses are given in Table 8, along with an analysis of chlorine-free apatite present in the plagiogranite (sample No. Z339).

NANTOKITE AND NATIVE Cu

Native copper, often accompanied by nantokite grains, occurs in the outer zones of whitish veins of grossular crosscutting rodingitized metadolerites. These veins occur commonly as ladder veins. Grossular that surrounds the native copper grains also occurs as inclusions inside them. The mode of occurrence is illustrated by Fig. 2 which also gives the elemental X-ray scans obtained by microprobe. The occurrence indicates probable enrichment of rodingitizing waters in Cu and Cl. In the energy-dispersive spectra of nantokite as well as native copper, small amounts of As were also detected. Analyses of nantokite are given in Table 9.

NICKELIFEROUS OPAQUE MINERALS

Certain nickeliferous opaque minerals are present in accessory amounts in the ultramafic rock types of SQO. They formed during serpentinization and chromite alteration, and their microprobe analyses have appeared in earlier papers by Ahmed & Bevan (1981) and Ahmed & Hall (1982). The assemblage includes awaruite-heazlewoodite-pentlandite and rare instances of troilite, or PGE-bearing awaruites such as the iridian awaruite, and a Ru-Os–Ir–Ni–Fe alloy. The assemblage awaruite-heazlewoodite-pentlandite does not commonly occur in nature (Ashley, 1975; Eckstrand, 1975; Kanehira *et al.*, 1975), especially in Ni-sulphide ores, although it has a wide stability field in the

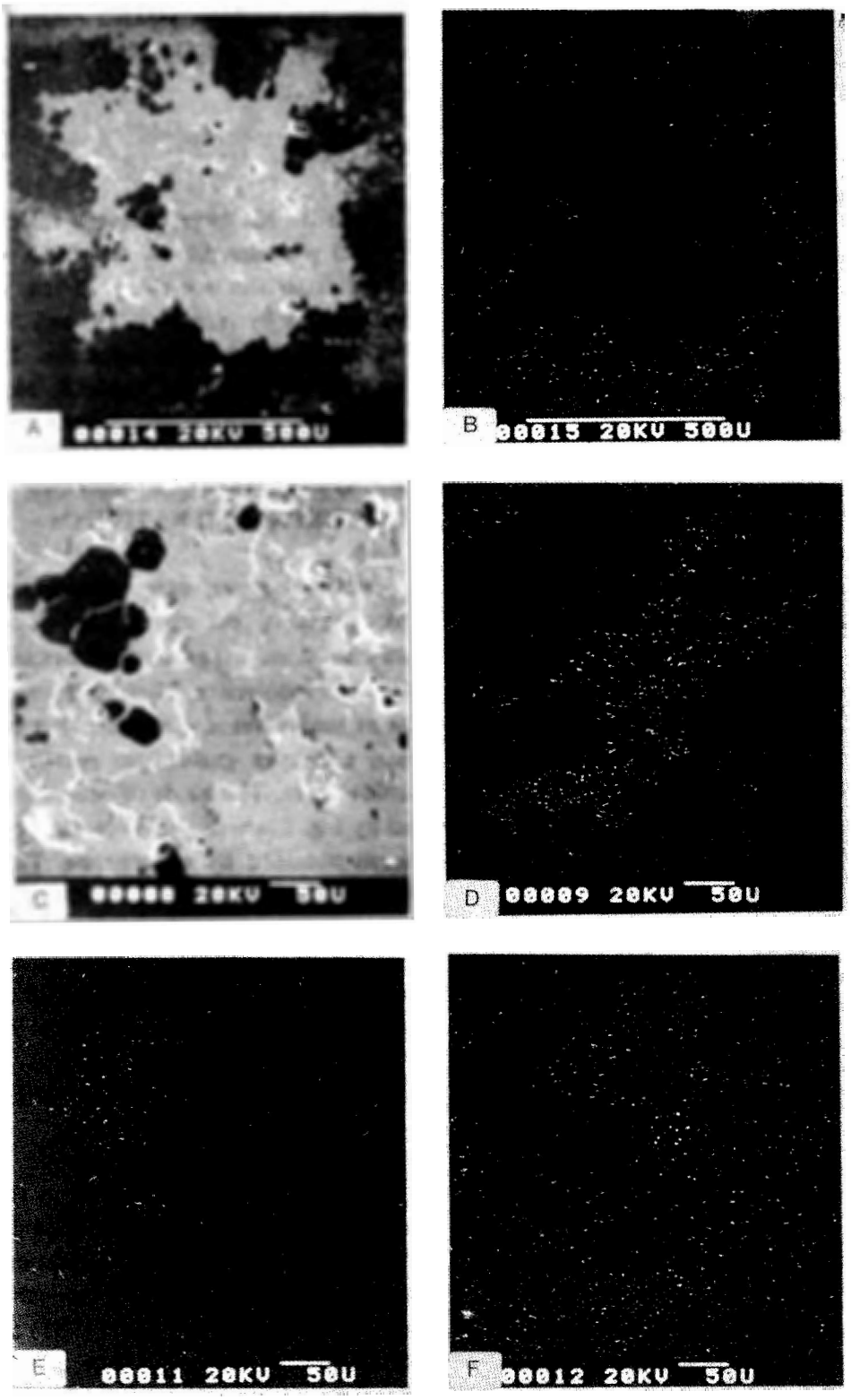

Fig. 2. (A) Backscattered electrons picture of the white grossular vein (sp.no. Z371B) that cuts across the metasomatized metadolerite (sp. no. Z371). Black area is grossular, that surrounds grey amoeboid area occupied by native Cu. Grossular also forms euhedra within native Cu (black crystals in grey area). Within native Cu, an irregular, low relief, grey area is nantokite. (B) Ca distribution image of (A), showing Ca present in grossular area, and absent from native Cu and nantokite area. (C) Backscattered electrons enlarged view of a part of (A), showing grossular crystals (black) in native Cu (grey) and the low relief nantokite (grey) (D–F) Distribution of chlorine (D), Si (E) and Cu (F) in the area shown in (C).

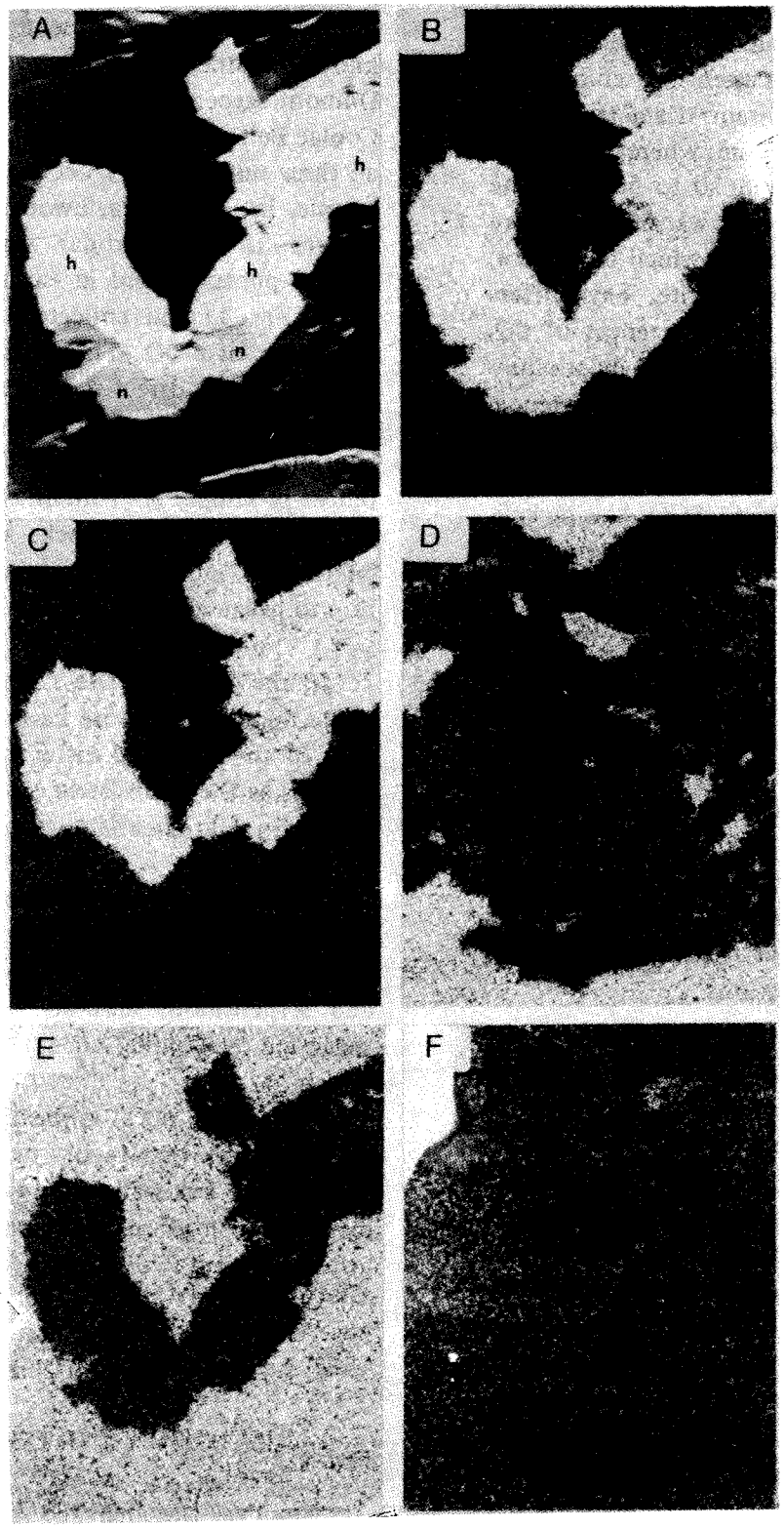

Fig. 3. Backscattered electrons image (A); and distribution pictures of Ni (B); S (C); Si (D); Mg (E); and Fe (F) for an area around a heazlewoodite grain that appears white in (A) and is labelled 'h'. An associated grain of hydrated oxide of Ni, light grey in (A) is labelled 'n'. Both the nickel minerals are surrounded by Mg -carbonate, which appears black in (A), and is seen as growing in between the two heazlewoodite grains. The serpentine area is revealed in Si-distribution picture. Width of each photograph is 150 μm.

relevant experimental systems (Harris & Nickel, 1972; Misra & Fleet, 1973). At SQO, the minerals occur as blebs, grains, specks, and fine dusty particles surrounded by secondary silicates or oxides such as serpentine, chlorite or "ferritchromit" Their grain diameters range from less than 1 μ m to 5 mm; whereas the most frequent grain size is from 10 to 50 μ m. The relatively coarser grains of awaruite are more abundant than heazlewoodite which is, in turn, more abundant than pentlandite. This differs from petrologically similar occurrences of this assemblage where pentlandite is the most abundant, e.g., New Caledonia (Guillon & Lawrence, 1973); Mt. Keith Betheno, Western Australia (Groves & Keays, 1979) and the Coolac Belt, Australia (Ashley, 1975). At SQO, the nickeliferous opaque minerals are more abundant in chromitites than in any other rock type and demonstrate a close association with the "ferritchromit" and chloritic by-products of chromite alteration. Inside the "ferritchromit" grains, heazlewoodite, and to a lesser degree pentlandite, are more common as inclusions, although awaruite also displays such a mode of occurrence. The sulphide inclusions in "ferritchromit" may form elongated grains and appear to be later fillings along internal fractures. The minerals show a strong petrographic association with "ferritchromit" locations.

Awaruite is the principal opaque mineral outside chromite grains and occurs in serpentine and coronas of chlorite that often accompany "ferritchromit" alteration. Awaruite appears to occur in large amounts in chromitites relative to the other rock types. The amount and grain size of these opaque minerals decreases sharply in adjacent silicate minerals of dunite, harzburgite or wehrlite. Composite grains made of any two of the opaque minerals are common, e.g., the pentlandite- awaruite intergrowths displayed in Ahmed & Hall (1982, Figs. 2E, 3). In other cases, such opaque minerals from discrete grains which lie side-by-side but do not interpentrate. In awaruite-pentlandite intergrowths, either awaruite rims pentlandite cores or pentlandite rims awaruite cores; or, both minerals may not display any core or rim preference. Heazlewoodite- pentlandite integrowths also occur, and sometimes close to the awaruite single-phase grains. Heazlewoodite-awaruite intergrowths are relatively rare. Three-phase intergrowths are not present, although they are known in other similar environments such as the Dumont serpentinite (Eckstrand, 1975) and the Coolac Belt (Ashley, 1975). In the SQO samples, all three minerals may occur in a single polished sample. In Fig. 3, heazlewoodite is shown to be present in the nodular serpentinite sample no. Z5 photographed in earlier paper (Ahmed, 1988, Fig. 1) and collected from the western periphery of SQO. The heazlewoodite in this sample is in direct contact with carbonate produced by the serpentinizing fluids. The serpentinized areas matrixing nodule-shaped olivine relices in sample Z5 contain chlorite, carbonate, serpentine and rare specks of a non-sulphide Ni-mineral (unidentified), and niccolite in addition to heazlewoodite.

In the Fe-websterite sample (Z36), the sulphide minerals compose more than 2 modal per cent of the rock and differ from all other rock samples as they consist of either discrete troilite grains or troilite-pentlandite integrowths.

Although the nickeliferous opaque minerals show extensive distribution at SQO, they do not enable differentiation between the chloritic and serpentinous chrome ores in the manner suggested by Golding & Bayliss (1968).

From the SQO, Ahmed & Bevan (1981) published the first report on the occurrence of awaruite in Pakistan and adjacent regions; and elaborated on its compositional variations. They also discovered two new minerals from a chromitite deposit (Ahmed, 1987a, Fig. 1, deposit no. C23). These new minerals were 'iridian awaruite' and a 'Ru-Os-Ir-Ni-Fe alloy'.

DISCUSSION AND CONCLUSIONS

Amongst the analyzed samples of clinozoisite from SQO rocks, the pistacite component is either similar to that of the epidotes of greenschist facies metabasaltic rocks (Liou *et al.*, 1977), or is lower, indicative of slightly higher metamorphic temperatures. The pistacite content of the rodingitized basic plutonic rocks

of the East Taiwan ophiolites (Ps_{8-12}) is also similar. However, at SQO, the rodingite dykes (e.g., samples Z361 & Z399) do not contain minerals of the epidote group. Therefore, the clinozoisite found in the analyzed samples may not be of metasomatic origin.

The chromitite textures display original crystal-melt relations of the cumulates and at most places, they are not obliterated by the superimposed tectonic fabric. Ceuleneer & Nicolas (1985) observed that the textures formed during magmatic accumulation of chromite are preserved only in the discordant pods; not in the concordant pods. At SQO, the banded and layered chromitites usually form concordant pods in a specific stratigraphic zone that extends east-west (Ahmed, 1984).

The bimodal Cr: Al variation in ore-forming chromites led Thayer (1970) to conclude that chromitite layers, after formation in the upper mantle, are later reemplaced as crystal mushes, that are jumbled, broken up and partly lost. The ores at SQO, do not reflect either the host rocks, or their residual or cumulate character in their Cr-Al contents. In certain aspects of chemical variations, it seems that the Cr-rich chromite crystallized at higher temperatures by fractional crystallization of tholeiitic magma, and Al-rich chromite crystallized later at lower temperatures. However, a continuous variation of temperature is not obvious. At the Heru Shah mine, labelled 'C42' by Ahmed (1987a, Fig. 1), chromites of both the high-Cr and high-Al types are present. Both occur in separate ore bodies with different attitudes and textures, that are explicable by mixing of crystal mushes from widely separated primary layers during emplacement, as suggested by Thayer (1969).

The accessory chromites of harzburgites, dunites and wehrlites at SQO possess higher Al and Fe and lower Cr and Mg contents compared to the chromite segregated in adjacent chromites. This relationship was noticed by Marakushev (1979) who related it to the earlier crystallization of accessory chromites and olivine at higher temperatures and later crystallization of chrome ore.

The rodingitizing fluids at SQO were chloride-rich, as indicated by the occurrence of nantokite and Cl-rich apatite. Chloride-rich brines are often considered to be effective agents for mass transfer; and this raises the possibility that mineralogical, chemical and other features of the rodingitized parts of the SQO are not solely due to primary magmatic processes, but instead are influenced by the effects of hydrothermal fluids or sea-water. The non-rodingitic apatite hosted by plagiogranite lacks chlorine.

The metadolerite dykes exhibit well-preserved primary igneous textures but their mineral assemblage is partly or completely replaced by low-grade metamorphic minerals and metasomatic minerals. The dykes contain younger rodingitic veins as well.

Ophiolitic residual peridotites belong to the lherzolite-type of harzburgite-type depending on the degree of depletion of residual peridotite (Ishiwatari, 1985). The ratio $100 \times Cr/(Cr+Al+Fe^{3+})$ is one of the parameters involved and varies from 20 in lherzolite-type to 80 in harzburgite-type. In the SQO accessory chromian spinel (Table 4) this ratio varies from 37.417 to 76.828 with a mean at 57.528, and standard deviation of 11.153. This composition is intermediate between the lherzolite-type (e.g., Liguria) and the harzburgite-type (e.g., Papua) with considerable overlap of the latter. Comparison with Ishiwatari's (1985) data indicates moderate (15 to 30%) degrees of partial melting of a lherzolitic source mantle may result in the clinopyroxene-bearing harzburgite of SQO.

The occurrence of nickeliferous opaque minerals, mostly in secondary veins, shows their postmagmatic formation. The awaruite compositions from SQO reported by Ahmed & Bevan (1981) show exceptionally large chemical variations and high Ni contents that exceed 73 wt%. Atomic Ni: Fe ratios range from 2.802: 1 to 6.387 : 1, with the highest frequency between 3: 1 and 4: 1. Its Cu content, covaries with Ni, and is unusually high reaching a maximum value of 5.2wt.%. The evidence presented by Ahmed & Bevan (1981) and Ahmed & Hall (1982) shows that during serpentinization,

chromite grains altered to "ferritchromit" releasing Al that altered serpentine to chlorite, and olivine grains provided Ni for awaruite formation. The PGE were concentrated as secondary native metal alloys during the same process. Sulphide formation depends upon the oxygen and sulphur fugacities during serpentinization. According to Eckstrand (1975) serpentinization generates H_2 that forms reduced assemblages characterized by awaruite-heazlewoodite, in contrast to the conventional Ni-sulphide ores which consist mainly of iron sulphides and pentlandite. Serpentinization converts at least part of silicate Ni into sulphide. The source of sulphur is uncertain. It may have come from primary magmatic intercumulus sulphides. The presence of magmatic sulphur in the mantle is shown by Andersen *et al.* (1987). Alternatively, sulphur may have come from percolating seawater as suggested by Thalhammer *et al.* (1986). Donaldson (1981) showed from Archaean dunites of Western Australia that both the formation of Ni and Fe sulphides in barren dunites and the upgradation and change of Ni sulphide ores has taken place by serpentinization accompanied by addition of S, Cl, H_2O, and CO_2. At SQO, common heazlewoodite within porous "ferritchromit" supports the transport of Ni from adjacent olivines. Ni and Fe from similar rocks are shown to display only limited mobility (e.g., Ashley, 1973; Bogolepov, 1969; Donaldson, 1981). The primary chromites and secondary "ferritchromit" at SQO are both poor in Ni. At SQO there is no evidence for the presence of coarser, disseminated, intercumulus droplets of magmatic origin such as those described by Eckstrand (1975) from the Dumont serpentinite, Canada. At SQO, the frequent coarser grain size and abundance of awaruite over heazlewoodite; and occurrence of both minerals in many samples, is supported by the phase relations in the Fe-Ni-S system (Kullerud, 1963) as well as by some natural occurrences, e.g., Trial Harbour, Tasmania (Ramdohr, 1950) and Heazlewood, Tasmania (Williams, 1960).

The exceptional Fe-enrichment of the host ultramafic rock (sample Z36) is reflected in its unique nickeliferous opaque minerals assemblage which is troilite-pentlandite.

When plotted on the $fO_2 - fS_2$ diagram for the Fe-Ni-S system, following Eckstrand (1975), the assemblage indicates a low to intermediate fO_2 and fS_2, lower than the values needed for millerite formation (Ahmed & Hall, 1982, Fig. 6). The occurrence of awaruite alone in many samples shows weak alteration of ultramafic rocks at such places and probably indicates very low fO_2 and fS_2 values at these locations. However, these were not reducing enough to produce native iron. Probably the reducing environment generated by the partial reaction: $3\ FeO + H_2O \rightarrow Fe_3O_4 + H_2$ is more readily produced near the "ferritchromit" alteration sites than in ordinary serpentinization of olivine-rich rock. This may be responsible for the more frequent occurrence of richer nickeliferous minerals in proximity to the "ferritchromit" and chlorite. Replacement of chromian spinel by chromian valeriite, produced by Cu, Ni and S from preexisting sulphides and Mg from serpentinizing olivines, during hydrothermal reactions or serpentinization is substantiated by Nickel & Hudson (1976). The "ferritchromit" grains at SQO do not show higher Ni contents than those of magmatic chromite, as the Ni was preferentially distributed amongst the awaruite-sulphides grains. The idea of Ahmed & Hall (1982) is now supported by Thalhammer *et al.*, (1986) who link the formation of sulphide minerals of the Limassol Forest ophiolite, Cyprus, to serpentinization commencing with the deposition of "ferritchromit" and magnetite around primary chromite cores.

REFERENCES

ADIB, D. & PAMIC, J. (1980) Rodingites from the southeastern parts of the Neyriz ophiolite complex in the Zagros Range, Iran. Archives des Sciences 33(2-3), pp. 281-90.

AHMED, Z. (1982) Porphyritic nodular, nodular and orbicular chrome ores from Sakhakot-Qila complex, Pakistan, and their chemical variations. Min. Mag. 45 "Deer, Howie & Zussman Volume", pp. 167-78.

———(1984) Stratigraphic and textural variations in the chromite composition of the ophiolitic Sakhakot-Qila complex, Pakistan. Econ. Geol. **79** (6), pp. 1334-59.

———(1987a) Mineral chemistry of the Sakhakot-Qila ophiolite, Pakistan: Part 1, monosilicates. Acta Mineralogica Pakistanica 3, pp. 26-41.

———(1987b) Mineral chemistry of the Sakhakot-Qila ophiolite, Pakistan: Part 2, polysilicates. Acta Mineralogica Pakistanica 3, pp. 140-58.

———(1988) Mineral chemistry of the Sakhakot-Qila ophiolite, Pakistan: Part 3, phyllosilicates. This Volume.

———, & **BEVAN, J.C. (1981)** Awaruite, iridian awaruite and a new Ru-Os-Ir-Ni-Fe alloy from the Sakhakot-Qila complex, Malakand Agency, Pakistan. Min. Mag. **44**, pp. 225-30.

———, & **HALL, A. (1981)** Alteration of chromite from the Sakhakot-Qila ultramafic complex, Pakistan. Chemie der Erde **40**, pp. 209-39.

———, & **HALL, A. (1982)** Nickeliferous opaque minerals associated with chromite alteration in the Sakhakot-Qila complex, Pakistan, and their chemical variation. Lithos **15**, pp. 39-47.

ANDERSEN, T., GRIFFIN, W.L. & O'REILLY, S.Y. (1987) Primary sulphide melt inclusions in mantle-derived megacrysts and pyroxenites. Lithos **20**, pp. 274-94.

ASHLEY, P.M. (1973) Petrogenesis of sulphide-bearing reaction zones in the Coolac ultramafic belt, New South Wales, Australia. Mineral. Deposita 8, pp. 370-8.

——— **(1975)** Opaque mineral assemblage formed during serpentinization in the Coolac ultramafic belt, New South Wales. Jour. Geol. Soc. Australia 22 (2), pp. 91-102.

BOGOLEPOV, V.G. (1969) Problem of serpentinization of ultrabasic rocks. Internat. Geol. Rev. **12**, pp. 421-32.

BROWN, M. (1980) Textural and geochemical evidence for the origin of some chromite deposits in the Oman ophiolite. *In:* Panayiotou, A. (ed.) OPHIOLITES: Proc. Internat. Ophiolite Symp., Cyprus. Geol. Surv. Cyprus, pp. 714-21.

CEULENEER, G. & NICOLAS, A. (1985) Structures in podiform chromite from the Maqsad district (Sumail ophiolite, Oman). Mineral. Deposita **20**, pp. 177-85.

CHRISTODOULOU, C. & HIRST, D.M. (1985) The chemistry of chromite from two mafic-ultramafic complexes in northern Greece. Chem. Geol. **49**, pp. 415-28.

COLEMAN, R.G. (1977) OPHIOLITES – ANCIENT OCEANIC LITHOSPHERE? Springer-Verlag, Berlin. 229 p.

DEER, W.A., HOWIE, R.A. & ZUSSMAN, J. (1962) AN INTRODUCTION TO THE ROCK FORMING MINERALS. Longman, London. 528p.

——— **(1982)** ROCK FORMING MINERALS, VOLUME 1A, ORTHOSILICATES. Longman, London. 919p.

DICK, H. (1977) Partial melting in the Josephine peridotite, the effect on mineral composition and its consequence for geobarometry and geothermometry. Amer. Jour. Sci. **277**, pp. 801-32.

DICKEY JR., J S. (1975) A hypothesis of origin for podiform chromite deposits. Geochim. Cosmochim. Acta **39**, pp. 1061-75.

———, & **YODER JR., H.S. (1972)** Partitioning of chromium and aluminium between clinopyroxene and spinel. Carnegie Inst. Wash. Yearb. **71**, pp. 384-92.

DONALDSON, M.J. (1981) Redistribution of ore elements during serpentinization and talc carbonate alteration of some Archean dunites, Western Australia. Econ. Geol. **76**, pp. 1698-713.

ECKSTRAND, O.R. (1975) The Dumont serpentinite: a model for control of nickeliferous opaque mineral assemblages by alteration reactions in ultramafic rocks. Econ. Geol. **70**, pp. 183-201.

ESPINOSA, A. (1980) Rodingites of the Los Azules ophiolitic sequence in the western Cordillera of the Colombian Andes. Archives des Sciences **33** (2-3), pp. 337-50.

GOLDING, H.G. & BAYLISS, P. (1968) Altered chrome ores from the Coolac serpentine belt, New South Wales, Australia. Amer. Mineral. **53**, pp. 162-83.

GREENBANUM, D. (1977) The chromitiferous rocks of the Troodos ophiolite complex, Cyprus. Econ. Geol. **72**, pp. 1175-94.

GROVES, D.I. & KEAYS, R.R. (1979) Mobilization of ore-forming elements during alteration of dunites, Mt. Keith-Betheno, Western Australia. Can. Mineral. **17**, pp. 373-89.

GUILLON, J.H. & LAWRENCE, L.J. (1973) The opaque minerals of the ultramafic rocks of New Caledonia. Mineral. Deposita **8**, pp. 115-26.

HAGGERTY, S.E. (1976) Opaque mineral oxides in terrestrial igneous rocks. *In:* Rumble, D. (ed.) OXIDE MINERALS. Min. Soc. Amer. Rev. Mineralogy **3**, pp. Hg101-Hg277.

HIMMELBERG, G.R. & LONEY, R.A. (1980) Petrology of ultramafic and gabbroic rocks of Canyon Mountain ophiolite, Oregon. Amer. Jour. Sci. **280-A**, pp. 232-68.

HARKINS, M.E., GREEN II, H.W. & MOORES, E.M. (1980) Multiple intrusive events documented from the Vourinos ophiolite complex, northern Greece. Amer. Jour. Sci. **280-A** "The Jackson Volume", pp. 284-95.

HARRIS, D.C. & NICKEL, E.H. (1972) Pentlandite compositions and associations in some mineral deposits. Can. Mineral. **11**, pp. 861-78.

IRVINE, T.N. (1965) Chromian spinel as a petrogenetic indicator, Part 1. Theory. Can. Jour. Earth Sci. **2**, pp. 648-72.

——— **(1967)** Chromian spinel as a petrogenetic indicator: Part 2, Petrologic implications. Can. Jour. Earth Sci. **4**, pp. 71-103.

ISHIWATARI, A. (1985) Igneous petrogenesis of the Yakuno ophiolite (Japan) in the context of the diversity of ophiolites. Contrib. Mineral. Petrol. **89**, pp. 155-67.

JACKSON, E.D. (1961) Primary textures and mineral associations in the ultramafic zone of the Stillwater complex, Montana. U.S. Geol. Surv. Prof. Pap. **358**, 106p.

——— **(1969)** Chemical variations in coexisting chromite and divine in chromitite zones of the Stillwater complex. Econ. Geol. Monagraph **4**, pp. 41-71.

KANEHIRA, K., BANNO, S. & YUI, S. (1975) Awaruite, heazlewoodite and native copper in serpentinized peridotite from the Mineoka District, southeastern Boso Peninsula. Jour. Japan Assoc. Mineralogists, Petrologists & Economic Geologists **70**, pp. 388-94.

KULLERUD, G. (1963) The Fe-Ni-S system. Carnegie Inst. Wash. Yearb. **62**, pp. 175-89.

LIOU, J.G., LAN, C-Y., SUPPE, J. & ERNST, W.G. (1977) The East Taiwan Ophiolite: its occurrence, petrology, metamorphism and tectonic setting. Min. Res. Serv. Org., Indust. Tech. Res. Inst. Taiwan, Spec. Rep. **1**, 212p.

MALPAS, J. (1978) Magma generation in the upper mantle, field evidence from ophiolite suites, and application to the generation of oceanic lithosphere. Phil. Trans. Roy. Soc. London A-**288**, pp. 527-46.

———, **& STRONG, D.F. (1975)** A comparison of chrome spinels in ophiolites and mantle diapirs of Newfoundland. Geochim. Cosmochim. Acta **39**, pp. 1045-60.

MARAKUSHEV, A.A. (1979) Some aspects of ore formation in ultramafics. Mineral. Deposita **14**, pp. 81-101.

MISRA, K.C. & FLEET, M.E. (1973) The chemical composition of synthetic and natural pentlandite assemblages. Econ. Geol. **68**, pp. 518-39.

NICKEL, E.H. & HUDSON, D.R. (1976) The replacement of chromian spinel by chromian valeriite in sulphide bearing ultramafic rocks in Western Australia. Contrib. Mineral. Petrol. **55**, pp. 265-77.

RAMDOHR, P. (1950) Über Josephinit, Awaruit, Souesit, ihre Eigenschaften, Entstehung und paragenesis. Min. Mag. **29**, pp. 374-94.

STEVENS, R.E. (1944) Composition of some chromites of the Western Hemisphere. Amer. Mineral. **29**, pp. 1-34.

THALHAMMER, O., STUMPFL, E.F. & PANAYIOUTOU, A. (1986) Postmagmatic hydrothermal origin of sulfide and arsenide mineralizations at Limassol Forest, Cyprus. Mineral. Deposita **21**, pp. 95-105.

THAYER, T.P. (1964) Principal features and origin of podiform chromite deposits, and some observations on the Guleman-Soridag District, Turkey. Econ. Geol. **59**, pp. 1497-524.

——— **(1969)** Gravity differentiation and magmatic re-emplacement of podiform chromite deposits. *In:* Wilson, H.D.B. (ed.) MAGMATIC ORE DEPOSITS. Econ. Geol. Monog. **4**, pp. 132-46.

——— **(1970)** Chromite segregations as petrogenetic indicators. Geol. Soc. S. Africa Spec. Publ. **1**, pp. 380-90.

WILLIAMS, K.L. (1960) An association of awaruite with heazlewoodite. Amer. Mineral. **45**, pp. 450-3.

Manuscript received on 4.3.1988
Accepted for publication on 2.5.1988

ACTA MINERALOGICA PAKISTANICA
VOLUME 4 (1988) pp. 81 - 86.

ELEPHAS SARAIENSIS, A NEW ELEPHANT FROM PINJOR BEDS OF GUJRAT, PUNJAB, PAKISTAN

MUHAMMAD SARWAR
Zoology Department, Punjab University, Lahore-20, Pakistan

ABSTRACT: An elephantine cranium is described from the Pinjor formation of Gujrat, Punjab. Cranial profile being simple and generalized, is differentiated clearly from the known elephantines. On the basis of cranial and dental features, it is positioned on the ancestory of the living Asiatic elephant.

INTRODUCTION

The Siwalik elephantines are known since the publication of Fauna Antiqua Sivalensis by Falconer and Cautley (1846). These authors described three species of the genus *Elephas*, i.e., *Elephas planiforns*, *E. hysudricus* and *E. namadicus*. Since that time, more species were added to the list by Sarwar (1977, 1981). These are, (1) *Elephas irshadii* described in 1977, and (2) *Elephas corrugatus* described in 1981. The present material comprises an almost complete cranium recovered from Pinjor formation of Sarai, District Gujrat. The cranial profile as well as the molar crown of the specimen under study are of generalized type and show close affinities to the living Asiatic elephant.

SYSTEMATIC ACCOUNT

Order	PROBOSCIDEA Illiger
Suborder	ELEPHANTOIDEA Osborn
Family	ELEPHANTIDAE Gray
Sub Family	ELEPHANTINAE Osborn
Genus	ELEPHAS Linnaeus

ELEPHAS SARAIENSIS new species

(Figs. 1–2)

Elephas platycephalus angustidens Osborn, 1929

Hypselephas hysudricus ref. Osborn, 1942, Fig. 1203 (Amer. Mus. 19863).

TYPE

P.U.P.C. 65/1, a damaged cranium with second and third molars of either side.

TYPE LOCALITY

Near Sardhok, district Gujrat, Punjab, Pakistan.

HORIZON

Pinjor zone of the Upper Siwaliks.

DIAGNOSIS

Cranium hypsicephalic and much compressed anteroposteriorly. Frontals flat. Nasal aperture wide transversely and narrow vertically. Tusk stalks almost parallel and subvertical. Molars sub-hypsodont. Ridge-plates moderately compressed. Enamel layer as thick as that of *E. hysudricus*. Median expansion absent in the ridge-plates. Last upper molar with 15 ridge-plates.

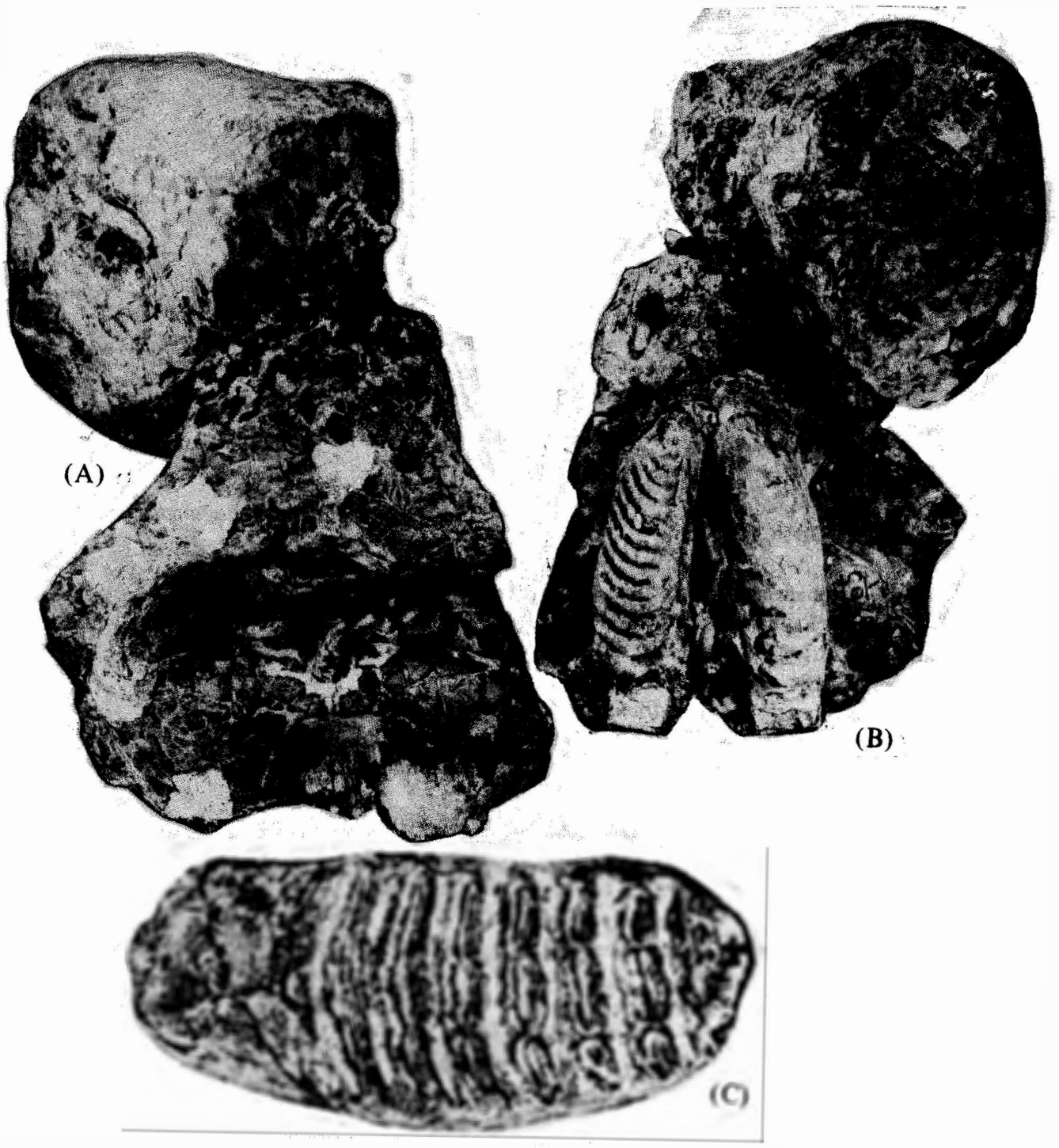

Fig. 1. Type cranuim of *Elephas saraiensis* n.sp. A, front view, x 0.18; B, posterior view, x 0.16; C, crown view, x 0.5.

DESCRIPTION

Cranium

Defenses and temporal arches are missing. Tusk-stalks, which run almost parallel, are subvertical in position. Nasal aperture is much broad transversely but compressed vertically (Table 1). Frontals, which are almost completely preserved, are quite flat. Skull top is rounded and abridged in a lateral view. A siliceous cast of cerebral hemisphere can be seen at the posterior side. The position of brain is quite helpful in determining the position of occipital condyles. The skull is much compressed anteroposteriorly and very high vertically. The parieto-occipital dome is perfectly rounded. The right orbit is of large diameter and is incompletely separated from the temporal fossa by the postorbital ridge. Lacrymal, which is a tiny bone, is separated anterodorsally from the maxilla and posteriorly from the frontal by somewhat indistinct sutures. The left temporal arch is completely missing whereas the maxillary and squamosal roots of the right arch are preserved. Palate is quite smooth and flat. It is narrow anteriorly but broad posteriorly.

Table 1. Cranial measurements (in mm) of P.U.P. 65/1

Diameter of left tusk stalk	108
Cranial height	770
Transverse width of external nares	404
Horizontal distance between right postorbital bar and median longitudinal line of fore head	288
Distance across postorbital bars (deduced from 3rd)	576
Estimated cranial width across frontoparietal constriction	260
Minimum palatal width	58
Maximum palatal width	86
Transverse width of internal nares	45

M^2

These are twelve ridge-plated, much broad (Table 2) and deeply worn teeth. Ridge-plates are bordered with moderately thick and somewhat finely plicated enamel layer. The lateral sides of the teeth are covered with a thick layer of cement. Enamel border of the ridge-plates do not show median expansion. Of the twelve ridge-plates, the anteriormost in both the teeth has worn away. The next three ridge-plates (which are most probably second, third and fourth in succession) are deeply worn to form a common dentinal shield with no sign of enamel layer. In r.M^2, the fifth, sixth and seventh ridge-plates are deeply worn but are still isolated from each other. The eighth, ninth and tenth are nearly half-worn but their conelets are still separate. The penultimate and the last ridge-plates both in right and left M^2 are damaged nearly to their crown basis. The outer half of l.M^2 is damaged but otherwise structurally it is quite identical with r.M^2

M^3

M^3 of both sides are unerupted but due to the damage of the pterygoid and maxilla, the crown of l.M^3 has become exposed, showing a total of 15 ridge-plates. The ridge-plates are quite thin, laminated and forwardly projecting. The are subhypsodont and moderately broad (Table 3).

Table 2. Measurements of M^2 of P.U.P.C. 65/1.

	r.M^2	l.M^2
Number of ridge-plates (preserved)	12	12
Length (preserved)	200	194
Crown width	88	–
Height (preserved)	70	72
Enamel thickness	3.5	3.5

Fig. 2. Type cranium of *Elephas saraiensis* n. sp.
Lateral view with reconstruction. x 0.18.

Table 3. Measurements (in mm) of 1.M^3 of P.U.P.C. 65/1.

Number of ridge-plates	15
Crown length	265
Lamellar frequency	5.7
Maximum width	90
Width/length index	34
Maximum crown height	110
Height/width index	122
Enamel thickness	3.5

REMARKS

P.U.P.C. 65/1 is evidently a new species of *Elephas* as it differs from all the known species of the genus both in structure of the teeth and the cranial profile. It cannot be referred to *E. planifrons*, the cranium of which shows very small nasal aperture and widely spaced ridge-plates (Falconer & Cautley, 1846). On the basis of flat frontals, it can be easily separated from E. hysudricus which shows deeply concave frontals (Falconer & Cautley, 1846; Osborn, 1942). The hypsicephaly of the cranium under

study distinguishes it from *Platelephas platycephalus* which shows elongated cranial profile (Osborn, 1942). The cranial profile of P.U.P.C. 65/1 resembles those of the specimens of the living Asiatic elephant figured by Deraniyagala (1955).

All the known elephants, i.e., *Elephas planifrons, E. hysudricus* and *E. namadicus* are specialised forms and none could be taken as ancestral to the living Asiatic species, *E. maximus*. However, the present cranium, P.U.P.C. 65/1 is not a specialised form and does not differ much from *E. maximus*. It rather shows very close relationship with the latter and demonstrates such characters which could be anticipated in the immediate ancestor of the living Asiatic elephant. These are:

1. Flat frontals.
2. Relatively less high cranium.
3. Subvertical position of the tusk-stalks.
4. Relatively less crown height of the molars.
5. Ridge-plate of teeth relatively less in number and also less compressed.
6. Enamel border of the ridge-plates relatively thick with tendency of fine plications.

In view of such characteristics, the cranium under discussion is regarded as a member of the line leading to the emergence of the living Asiatic elephant, i.e., *Elephas maximus*.

Osborn (1929) erected a new subspecies, *Elephas platelephas angustidens* based upon a $1.M_3$ (Amer. Mus. 19915) from Chandigarh, India. This tooth resembles very well with the M^3 of *Elephas saraiensis* sp.n. Both are subhypsodont and thin ridge-plated and do not show any remarkable difference on which they could be separated from one another. Therefore, the tooth, Amer. Mus. 19915 is here included in the new species, *Elephas saraiensis* and the subspecies, *E. platelephas angustidens* which was based upon a single tooth becomes invalid.

An upper left third molar (Amer. Mus. 19863) which was identified as *"Hypselephas hysudricus"* by Osborn (1942) is here included in *E. saraiensis* sp.n. It is because of the fact that it resembles very much with the dentition of the latter and differs greatly from *E. hysudricus* in the number of ridge-plates.

The great abundance of fossils of the genus *Elephas* together with the great abundance of stegodonts, stegolophadonts, the Asiatic endemism of the stegodonts and stegolophodonts and gradual anterioposterior cranial abbreviation from *Stegolophodon* to *Elephas* through *Stegodon* favours the stegolophodont/stegodont evolution of the elephants as has been suggested by Lull (1908), Osborn (1918, 1942), Sarwar (1979) and Sarwar and Nafees (1984) and negates the suggestion given by Thenius and Hofer (1960), Maglio and Hendey (1970), Maglio (1973) and Tassy (1983) that stegodonts had nothing to do with the emergence of elephants. *Elephas saraiensis* n.sp. was probably a Middle Pleistocene step towards the emergence of the living Asiatic elephant.

REFERENCES

DERANIYAGALA, P.E.P. (1955). Some extinct elephants, their relatives and the two living species. Ceylon National Museums Publication, pp. 1-161.

FALCONER, H. AND CAUTLEY, P.T. (1846) Fauna Antiqua Sivalensis, being the fossil zoology of the Siwalik Hills in the North of India. Pt. 1.

LULL, R.S. (1908) The evolution of the elephant. Amer. Journ. Sci. **4**, (25), pp. 169-212.

MAGLIO, V.J. (1973) Origin and evolution of the elephantidae, Trans. Amer. Phil. Soc. N.S. **63(3)**, pp. 1-149.

——— **& HENDEY, Q.B. (1970)** New evidence relating to the supposed stegolophodont ancestry of the elephantidae. S. Afr. Archaeo. Bull. **25** (3-4), pp. 85-7.

OSBORN, H.F. (1918) A long-jawed Mastodon Skeleton from South Dakota and phylogeny of the Proboscidea. (Abstract) Bull. Geol. Soc. Amer. **29**, pp. 133-7.

——— **(1929)** New Eurasiatic and American proboscideans. Amer. Mus. Nov. New York, **393**, pp. 1-23.

——— (1942) Proboscidea. A monograph on the discovery, evolution, migration and extinction of the mastodonts and the elephants of the world. Stegodontoidea, Elephantoidea. New York (American Museum Press) 2, pp. 805-1675.

SARWAR, M. (1977) Taxonomy and distribution of the Siwalik Proboscidea. Bull. Dept. Zool. Univ. Punjab, Pakistan, 10, pp. 1-172.

——— (1979) A new elephant from the Upper Siwaliks of Pakistan. Pakistan Journ. Sci. 31 (3-6), pp. 133-8.

——— (1981) A new elephant from the Upper Siwaliks of Pabbi Hills, Punjab, Pakistan. Geol. Bull. Univ. Punjab Pakistan. 16, pp. 131-8.

——— & NAFEES, G., (1984) Evolution of the Siwalik bunodont and bunolophodont Proboscidea. Kashmir Jour. Geol. 2(1), pp. 109-14.

TASSY, P. (1983) Les Elephantoidea Miocenes du plateau du Potwar, Groupe de Siwalik, Pakistan. Pt. III-Stegodontides, elephantoides indetermines. Restes postcraniens. Conclusion. Ann. de Paleont. 69(4), pp. 317-54.

THENIUS, E. AND HOFER, H. (1960) STAMMESGESCHICHTE DER SAUGETIORE. Springer Verlag, Berlin, pp. 1-322.

Manuscript received on 31.7.1988
Accepted for publication on 9.10.1988

ACTA MINERALOGICA PAKISTANICA
VOLUME 4 (1988) pp. 87 - 89.

THE FIRST BUNOLISTRIODONT SUID FROM THE SIWALIKS

MUHAMMAD SARWAR, FARAH AFTAB & MUHAMMAD AKHTAR
Department of Zoology, University of the Punjab, Lahore-20, Pakistan

ABSTRACT: A new bunolophodont suid is described from Chinji type locality. It is the first record of the genus *Bunolistriodon* from the Siwaliks.

INTRODUCTION

Siwalik listriodonts are known since 1876 when Lydekker transferred the species *Tapirus pentapotamiae* of Falconer (1868) to the genus. *Listriodon.* In 1878, Lydekker erected a new species with the name of *Listriodon theobaldi.* In 1926, Pilgrim added a third species, i.e., *Listriodon guptai.* The material of this species came from Kamlial beds of Bhagothoro, Sind. Being a bunolophodont in crown structure, it was transferred to the genus *Bunolistriodon* by Chen (1984). The present material comprises a lower molar from Chinji type locality. It is differentiated from Sindhi material of the genus in size and progressive lophodonty.

SYSTEMATIC ACCOUNT

SYSTEMATIC ACCOUNT

Order	ARTIODACTYLA Owen
Suborder	SUINA Gray
Superfamily	SUOIDEA Cope
Family	SUIDAE Gray
Subfamily	LISTRIODONTINAE Simpson
Genus	*BUNOLISTRIODON* Arambourg

BUNOLISTRIODON CHINJIENSIS new species

TYPE

P.U.P.C.* 102, a lower first molar of the right side.

TYPE LOCALITY

Chinji, District Chakwal, Punjab, Pakistan.

HORIZON

Chinjian of the Lower Siwaliks.

HYPODIGM

Type only.

DIAGNOSIS

A bunolistriodont larger than the species *Bunolistriodon guptai.* The molars are more lophodont than bunodont.

DESCRIPTION

LOWER DENTITION

FIRST MOLAR (Fig. 1)

The material under study is the first well preserved lower molar. It is much elongated. The crown has moderate height. The molar has thick cingulum both at its anterior and posterior sides and has comparatively thin

*Fossil collection stored in the Zoology Department, Punjab University, Lahore, Pakistan.

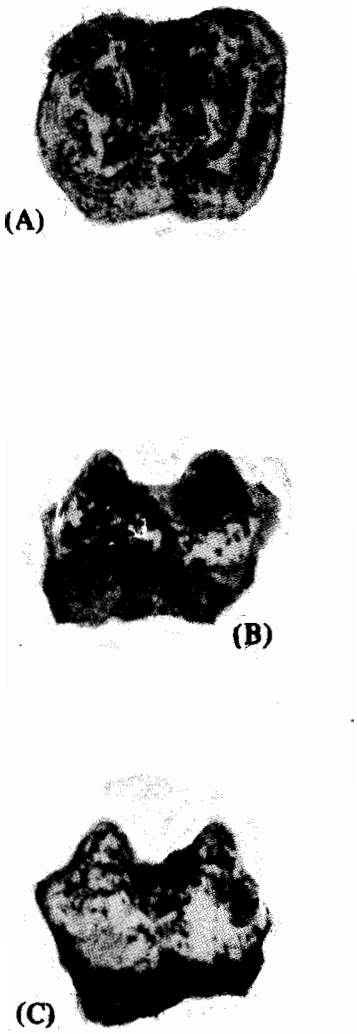

Fig. 1. Type specimen of *Bunolistriodon chinjiensis* n.sp. A, crown view; B. inner view; C. outer view. All x 2.

cingulum at its left and right sides. Metaconid is more high than its counter part, i.e., Protoconid. The two cusps meet one another transversely in the centre and form an arc-shaped structure known as protolophid. It is shallow in the centre and higher towards the extremities. In the same way another lophid, i.e., entolophid is formed by the union of entoconid and hypoconid. It is also a concavo-convex structure with higher extremities and shallower central part. Entoconid is comparatively higher than the hypoconid. Proto- and meta-conids are worn to their enamel thickness. Likewise, the ento- and hypo-conids are also worn to their enamel thickness. A deep and open cavity is formed between the two lophids, i.e., proto- and entolophids. There is no oblique ridge connecting the two lophids or blocking the valley.

Table 1. Comparative measurements (in mm) of the first lower molar P.U.P.C. 102 and *Bunolistriodon lockharti* from Ginsburg and Bulot (1987).

	P.U.P.C. 102	*Bunolistriodon lockharti*
Anteroposterior Crown length	15.5	17.2–18.3
Transverse width (anterior half)	13.2	12.7–16.2
Transverse width (posterior half)	12.8	
Width/length index	85	
Height (preserved)	7.4	
Height (reconstructed)	10.9	
Height/width index	83	

DISCUSSION

Since the molar tooth, P.U.P.C. 102 is neither truely lophodont nor truely bunodont, it is referable to the genus *Bunolistriodon*. Only one species of the genus is so far known from the Siwaliks. This is *Bunolistriodon guptai* originally named as *Listriodon guptai* by Pilgrim (1926). Very recently Chen (1984), noticing the bunolophodonty in the type material of the species transferred it to the genus *Bunolistriodon*. This transfer appears to be justified because of the fact that the molars of the species *L. guptai* figured by Pilgrim (1926)

are more bundont than lophodont, a character which makes distinction between the two genera (Arambourg, 1933).

The species under study like the type material of *Bunolistriodon guptai* exhibits a transitional structure between true bunodonty and true lophodonty. Thus, it is fair to include it in the genus *Bunolistriodon*. *B. guptai* is known by an upper last molar, two lower molars and their incisor (Pilgrim, 1926). In general contours, the type material of the species *B. guptai* and tooth under study show resemblance. However, the former appears to be much narrower transversely than the later. The transverse width of the protolophid of the last lower molars of *B. guptai* is equal to that the P.U.P.C. 102. As a matter of principle, it should have been greater if the two species are conspecific. Thus, P.U.P.C. 102 may be differentiated from *B.guptai* on specific level.

The present material differs from the relevant material of the species *Bunolistriodon lockharti* described by Ginsburg and Bulot (1987) from France in size as well as in the degree of bunodonty. The French material is comparatively larger (Table 1) and is much more bundont than the Siwalik material. Keeping in view the difference stated above, the Siwalik material is given the status of a new species. This new species is designated as *Bunolistriodon chinjiensis,* after the name of the type locality.

REFERENCES

ARAMBOURG, C. (1933) Les Mammiferes Miocenes du Turkana (Afrique Orientale). Annls. Palaeont. Paris, **22**, pp. 123-46.

CHEN, G. (1984) Suidae and Tayassuidae (Artiodactyia, Mammalia) from the Miocene of Steinhein a.A. (Germany). Palaeontographica, Stuttgart, **184**(1-4), pp. 79-83.

FALCONER, H. (1868) Note on fossil remains found in the valley of Indus, below Attock, and at Jabblpoor. Palaeontological Memoires. pp. 414-9

GINSBURG, L. & BULOT, C. (1987) Les Suiformes (Artiodactyla, Mammalia) du Miocene de Bezian (Gers). Bull. Natn. Mus. Hist. Nat. Paris, **9**(4), pp. 455-69.

LYDEKKER, R. (1876) Molar teeth and other remains of Mammals. Pal. Indica **10**(1,2).

——— **(1878)** Notices of Siwaliks Mammals. Rec. Geol. Surv. India, **11**, pp. 64-104.

PILGRIM, G.E. (1926) The Fossil Suidae of India. Pal. Indica. N.S. **8**(4), pp. 1-65.

Manuscript received on 31.7.1988
Accepted for publication on 9.10.1988

ACTA MINERALOGICA PAKISTANICA
VOLUME 4 (1988) pp. 90 - 95.

UPPER CRETACEOUS FORAMINIFERAL BIOSTRATIGRAPHY OF PAKISTAN

AFTAB AHMAD BUTT*
Institute of Geology, Punjab University, Lahore-20, Pakistan

ABSTRACT: The Upper Cretaceous succession of Pakistan covers a time interval from Cenomanian to Turonian but largely, Coniancian to Campanian and a Maastrichtian interval. Deposition of the Kawagarh Formation in northern Pakistan and correspondingly the Parh Limestone in southern Pakistan (Coniancian to Campanian in age) is the result of a major transgression along the northwestern margin of the Indian Plate, whereas the Maastrichtian interval records a major regression, marked either by the complete absence of the Maastrichtian deposits in northern Pakistan or by the development of a regional blanket of regressive facies of the shallow-water Pab Sandstone in southern Pakistan. Uninterrupted succession of argillaceous deposits, the Korara Shale, across the Cretaceous – Tertiary boudary in the Kirthar Range (Gaj River section) containing Maastrichtian and Danian planktonic foraminifera in continued sedimentary environments, is among the very few world-wide examples of a continuous section accross the boundary.

INTRODUCTION

In Pakistan, the Cretaceous succession is well developed and widely distributed. It is divided into Lower and Upper Cretaceous strata. From the view point of foraminiferal biostratigraphy, only the Upper Cretaceous sediments are significant. From this aspect the Upper Cretaceous would be split into a time span from Cenomanian to Turonian and to a large extent, from Coniancian to Campanian and a Maastrichtian interval. During this time several formational names have been established reflecting a paleogeographic setting which demonstrates either a continuity in the sedimentary environment or variation in the depositional style.

The Upper Cretaceous succession in each structural unit may be grouped as follows:

1. Northern Pakistan (Kohat-Potwar Province)
2. Northwestern Pakistan (Sulaiman Range)
3. Southern Pakistan
   - i. Quetta Region (Murree Brewery Gorge)
   - ii. Kirthar Range (Gaj River)
   - iii. Pab Range

* Included in the workshop Global Sedimentary Geology Program "Cretaceous Resources, Events and Rhythms" (September 16-22, 1988, Digne, France).

STRATIGRAPHIC SYNTHESIS

In northern Pakistan, which includes the Samana Range (Kohat and Hangu as main towns), the Kala Chitta Range (Attock, main town) and the Hazara Mountains (Abbottabad, Nathiagali, Murree, main towns), the Upper Cretaceous succession is developed as the Kawagarh Formation whose type locality is the Kawagarh Range named after the Kawa village in northern Kala Chitta Range. It is equivalent to the Kawagarh Shale of Cotter (1933).

The Kawagarh Formation is developed as a well-bedded, light grey micritic limestone or platy, argillaceous limestone reminiscent of shaly apearance (Fig. 1).

The platy appearance is typically developed in the northern Kala Chitta Range. Excellent exposures can be seen either at its type locality or behind the Chhoi Rest House on way from Attock to Basal. In this fashion, it is also present in the Hazara Mountains, for example, the spring section at Changlagali along the Murree-Nathiagali Road and near Jabri along the Lora-Maqsood Road. However, the well-bedded micritic limestone is also present along the Murree-Nathiagali Road and in other areas of the Hazara region and typically developed in the Samana Range. In the Samana Range, excellent exposure can be seen along the roadside on way to the Fort Lockhart. The Kawagarh Formation contains globotruncanid fauna (Butt, 1969; 1973; Latif, 1970) and thus its age has been determined to range from Coniacian to Campanian.

It is very interesting to note that the globotruncanids-bearing deposits of similar age and lithology are widely distributed and well-developed in the Sulaiman Range (northwestern Pakistan) and the Southern Pakistan (i.e. Murree Brewery Gorge at Quetta; Bolan Pass; Quetta-Khuzdar Road near Kalat). The formation is present as well-bedded, off-white, micritic limestone and known as the Parh limestone (type locality Parh Range, Upper reaches of the Gaj River). Nagappa (1959) illustrated *Globotruncana* from the Parh Limestone from Kalat.

In view of the plate tectonic activity and the regional distribution of micritic sediments, it can be envisaged that a major transgression happened from Coniacian to Campanian all along the northwestern margin of the Indian plate. (Butt, 1986), when the Kawagarh Formation was laid down in northern Pakistan (conventionally known as the Upper Indus Basin), and correspondingly the Parh Limestone in Southern Pakistan (conventionally called as the Lower Indus Basin).

During Campanian, however, a shallowing trend in the paleobathymetry is already observed in the Sulaiman Range, when sediments containing *Orbitoides tissoti* (typical Campanian benthic larger foraminiferal species) are developed (Marks, 1962). These constitute the upper part of the Mughalkot Formation (Fig. 2).

The Maastrichtian interval represents a major period of regression along the northwestern margin of the Indian plate. It envisages a complete "draining off" of the sea in northern Pakistan (absence of the Maastrichtian strata) and development of a regressive facies of the fossil-straved Pab Sandstone as a regional blanket in the remaining part of Pakistan except at two locations where this formation is replaced by the development of entirely different facies. These facies are either the *Orbitoides* Limestone (Gigon, 1962) of shallow water facies at Quetta (Murree Brewery Gorge section) containing *Orbitoides apiculatus* (Alleman, 1979), typical Maastrichtian benthic larger foraminiferal species; or the Maastrichtian Korara Shale developed as deep water argillaceous deposits in the Kirthar Range (Gaj River section). The Pab Sandstone is for practical purposes unfossiliferous though Vredenburg (1909) reported a Maastrichtian orbitoidal foraminifer *Lepidorbitoides minor.*

In fact the section at Gaj River is of particular interest where the Korara Shales are developed as a time transgressive unit. It represents a continuous section along the Cretaceous-Tertiary boundary both in terms of planktonic faunal content and sedimentary facies. In this way, the uninterrupted section across the Cre-

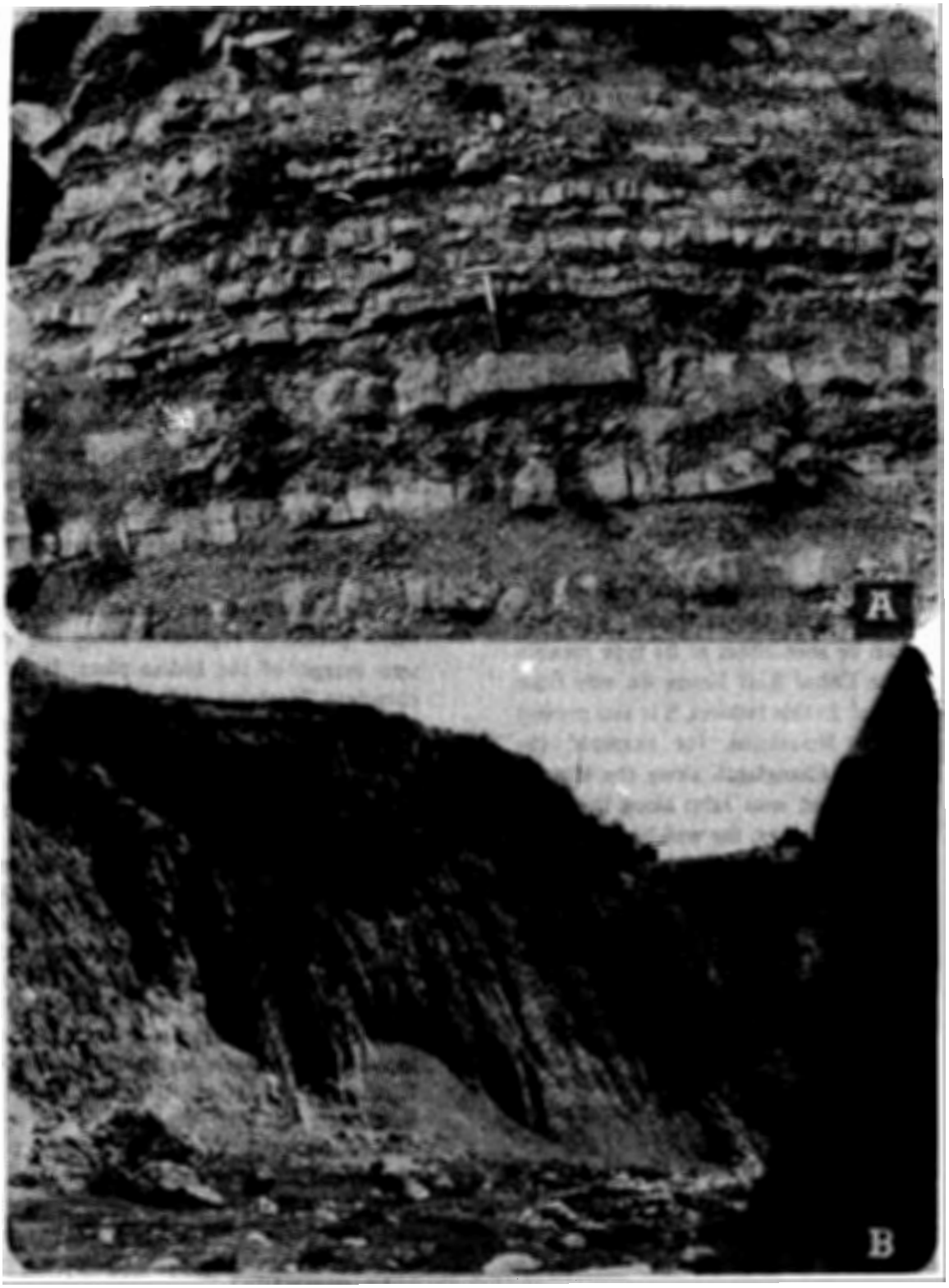

Fig. 1. (A) Thinly-bedded Kawagarh Formation, Jabri village, Lora-Maqsood road (Hazara District).

(B) Thinly-bedded (platy exposition) Kawagarh Formation behind Chhoi Rest House at confluence of tributary and main nallah, Attock-Basal road, Kala Chitta range.

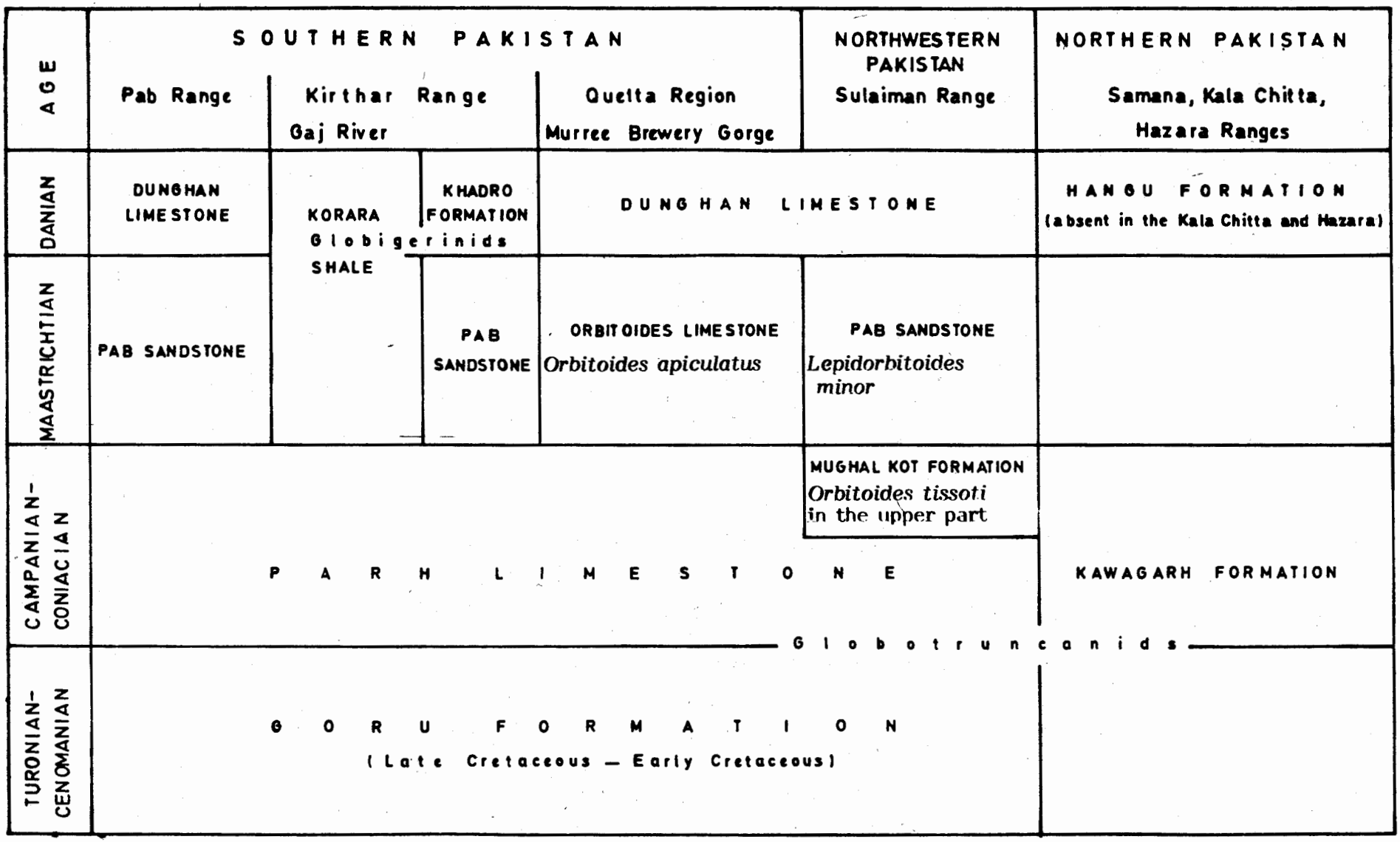

Fig. 2. Upper Cretaceous–basal Tertiary stratigraphy of Pakistan. The nomenclature is formalized by the Stratigraphic Committee of Pakistan (Fatmi, 1973; Shah, 1977) except the Korara shale and the "Orbitoides Limestone" Goru formation ranges down to lower Cretaceous (Alleman, 1979). For stratigraphy of Murree Brewery Gorge section, see Alleman (1979).

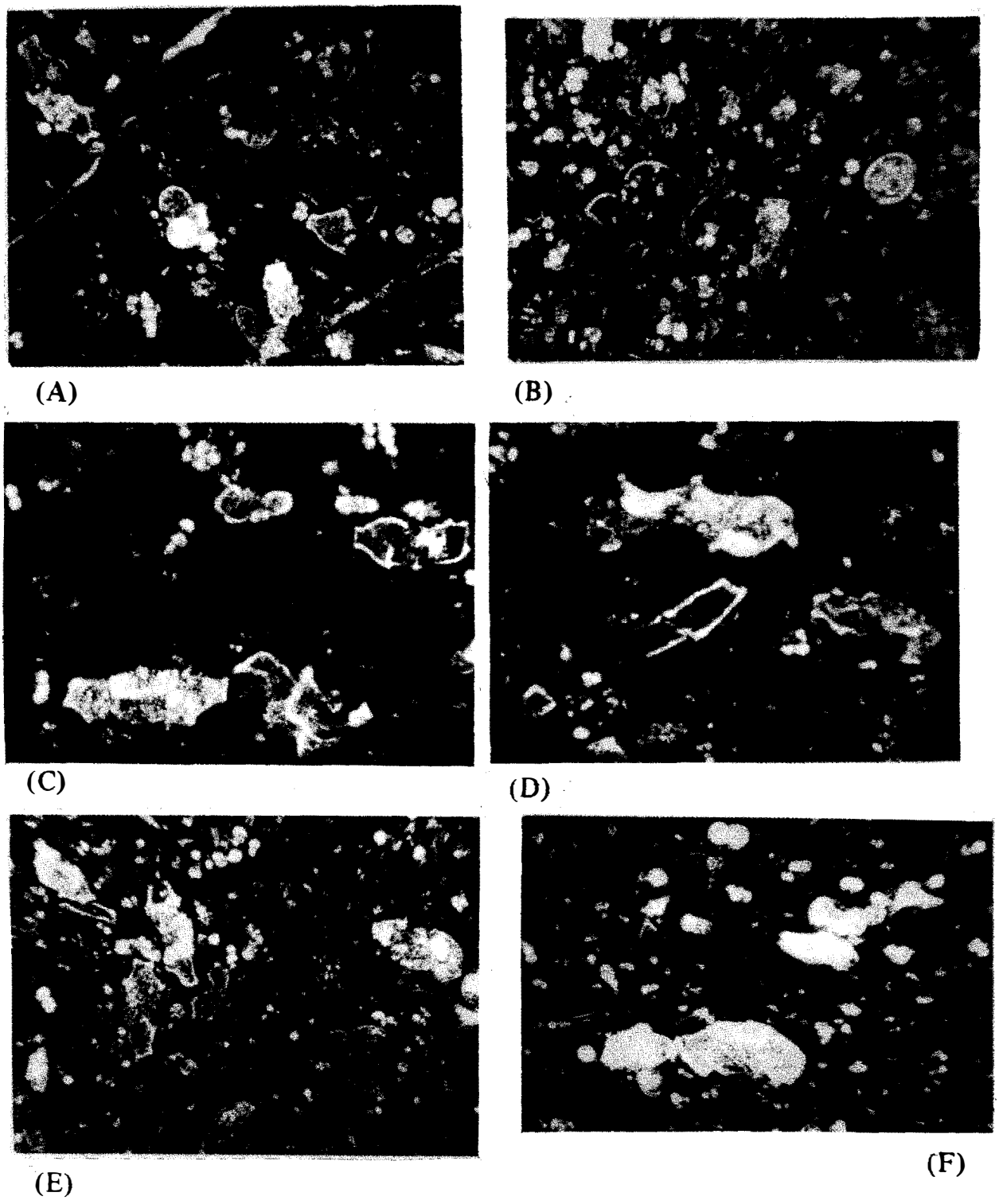

Fig. 3. Planktonic Foraminifera from the Kawagarh Formation. (A) *Heterohelix globulosa* (central part), *Globotruncana linneiana* (upper left corner), *Rugoglobigerina rugosa* (bottom right). (B) *Rugoglobigerina rugosa*. (C) *Globotruncana tricarinata* (bottom left), *Heterohelix globulosa, Rugoglobigerina rugosa* (upper side). (D) *Globotruncana arca* (right side). (E) *Globotruncana fornicata, Globotruncana linneiana* (left half). (F) *Globotruncana elevata* (bottom central), *Rugoglobigerina rugosa* (upper portion).

taceous-Tertiary boundary is among the few world-wide examples to demonstrate the continuity of depositional pattern and the planktonic faunal assemblage across the boundary. This unbroken section was first mentioned by Nagappa (1960) and later by Dorreen (1974) without giving a formal stratigraphic name. However, the name Korara Shale though formally yet to be approved by the Stratigraphic Committee of Pakistan has been used by various oil companies and also adopted by Khursheed (1972).

CONCLUSION

The Upper Cretaceous stratigraphy of Pakistan and the associated faunal content can be interpreted in the light of the concept of plate tectonic activity.

REFERENCES

ALLEMAN, F. (1979) Time of emplacement of the Zhob Valley Ophiolites and Bela Ophiolites. *In*: Farah A. & De Jong, K.A. (eds.) GEODYNAMICS OF PAKISTAN, Geol Surv. Pakistan, Quetta, pp. 215-24.

BUTT, A.A. (1969) A note on the Cretaceous – Tertiary boundary in Hazara, West Pakistan. Geol. Bull. Punjab Univ. **8**, pp. 73-8.

——— **(1973)** The Kawagarh Formation in Kala Chitta, Northern Pakistan. Proc. 24th Pakistan Science Conf. Islamabad, p.H–4.

——— **(1986)** Plate tectonics and the Upper Cretaceous biostratigraphic synthesis. Acta Mineralogica Pakistanica, **2**, pp. 60-4.

COTTER, G. De P. (1933) The geology of the part of the Attock district West of longitude 72° 45'E. Mem. Geol. Surv. India, **55**, (2), pp. 63-161.

DORREEN, J.M. (1974) The western Gaj River section, Pakistan and the Cretaceous-Tertiary boundary. Micropal. **20**, (2), pp. 178-93.

FATMI, A.N. (1973) Lithostratigraphic units of the Kohat-Potwar Province, Indus Basin, Pakistan. (Rept. Strat. Comm. Pakistan). Mem. Geol. Surv. Pakistan, Quetta, **10**, pp. 1-80.

GIGON, W.O. (1962) Upper Cretaceous stratigraphy of the Well Giandari-1 and its correlation with the Sulaiman and Kirthar Ranges, West Pakistan. Second ECAFE Petrol. Symp. Teheran, pp. 1-18.

KHURSHEED, S.H. (1972) Foraminiferal fauna of Korara Shale. Pakistan Jour. Sci. Indust. Res., **15**, (6), pp. 368-70.

LATIF, M.A. (1970) Micropaleontology of the Chanali Limestone, Upper Cretaceous of Hazara, West Pakistan. Jahrb. Geol. Bundesanst., **15**, pp. 25-62.

MARKS, P. (1962) Variation and evolution in Orbitoides of the Cretaceous of the Rakhi Nala, West Pakistan. Geol. Bull. Punjab Univ., **2**, pp. 15-30.

NAGAPPA, Y. (1959) Foraminiferal biostratigraphy of the Cretaceous-Eocene succession in the India-Pakistan-Burma region, Micropal. **5**, (1), pp. 145-92.

——— **(1960)** The Cretaceous-Tertiary boundary in the Indo-Pakistan Sub-Continent. 21st Internat. Geol. Congr. Copenhagen, **5**, pp. 41-9.

SHAH, S.M.I. (1977) Stratigraphy of Pakistan (Rept. Start. Comm. Pakistan) Mem. Geol. Surv. Pakistan, Quetta, **12**, pp. 1-138.

VREDENBURG, W. (1906) The Cretaceous Orbitoides from India. Rec. Geol. Surv. India, **36**, pp. 171-213.

Manuscript received on 4.5.1988
Accepted for publication on 12.10.1988

ACTA MINERALOGICA PAKISTANICA
VOLUME 4 (1988) pp. 96 - 101.

A METHOD FOR THE STUDY OF SILICEOUS ROCKS AS APPLIED TO ARCHEOLOGY

THIERRY AUBRY
National Centre of Excellence in Mineralogy, G.P.O. Box 43, Quetta, Pakistan, &
Institute de geologie du Quaternaire, Universite de Bordeaux I, France.

ABSTRACT: A non-destructive physical technique of characterization of the siliceous rocks is described. It should be useful in archeological studies.

INTRODUCTION

Siliceous rocks, particularly flint, have been used as raw material for the manufacture of stone tools in a majority of prehistoric sites. But this type of rock is not always available in near environment of archeological settlements. Geology can help in the archeological research on the source of this type of rock. Knowledge of displacements of material used in places far from their source permits reconstruction of territory occupied and interregional exchanges.

The siliceous rocks, particularly flint, are petrographically homogeneous which consist essentially of different forms of silica with small quantities of impurities. Thus, classical methods of study cannot always be used to differentiate amongst flints of various origins. In this study, a new physical method of characterization of flint is presented.

A wide range of rocks have been used for making prehistoric tools but tool-making requires a rock that is homogeneous, hard and dense with a conchoidal fracture to give a cutting edge.

Obsidian and siliceous sandstone have been exploited, but their occurrence is not common in different parts of the world. The most appropriate rock is flint. Flint may be variously coloured. Flint is used frequently as a synonym for chert and more specifically for nodules occurring in Cretaceous chalk. In this article, this term is used without choronological attribution.

FLINT PETROGRAPHY

Flint occurs in two principal forms: (i) as extensive bedded deposits, or (ii) as nodular segregations in limestone. The second type of occurrence was preferred by the prehistoric man because it is more homogeneous and easier to work with.

It consists of nodules of fine grained silica of the following types: quartz, chalcedony, and opal. A recent description of the varieties of these minerals is given by Hesse (1988).

FLINT SURVEY

For all the techniques presented the preliminary field work consist of a survey and range of flints in the geological formations of the environment of the prehistoric site. The sampling interval is a function of the surface occurrence of silicification in the formation. For

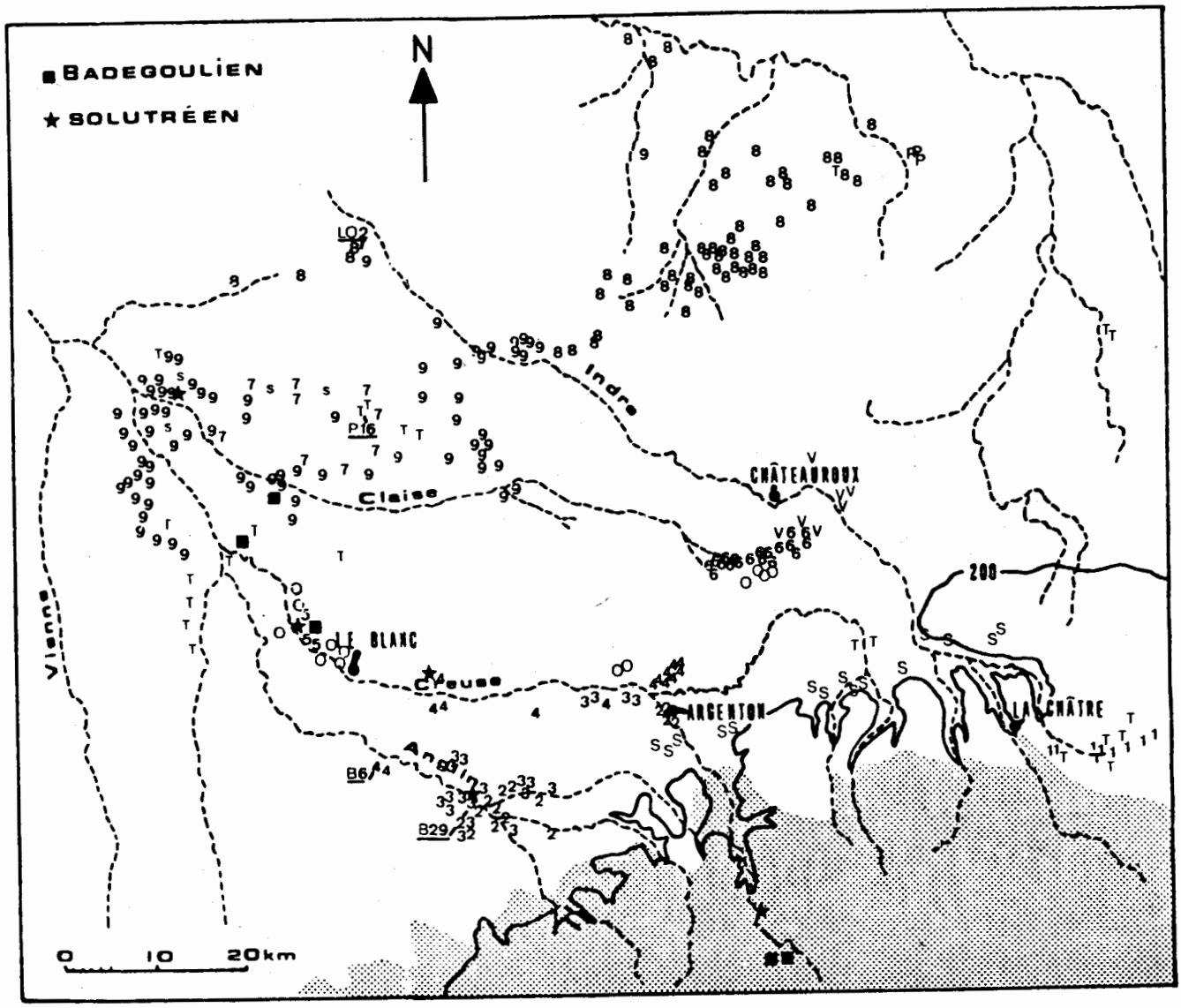

Fig.1. Distribution of flint bearing rocks in Central France. Symbols are used to represent Ludien-Stampien (T), L'infra-Eocene (S), Senonian (s), late Turonian (9), middle Turonian (7), early Turonian (8), late Cenomanian (5), late Portlandian (P), Brenne facies of Oxfordian (6), Von facies of Oxfordian (V), middle Bathonian (4), late Bajocian (3), early Bajocian (2) and early Hettangian (1).

example for a Cretaceous flint occurring over 50 km², we have chosen a sampling interval of approximately 5 km² (Fig. 1).

Removal of flint from its sites of origin by alluvial processes is the most important problem in this type of study. Such formations must also be examined and mapped.

THIN SECTION STUDY

For research on the origins of archeological raw materials, thin section techniques are often disappointing.

Observations show great uniformity of siliceous rocks and few compositional or textural variations. This method can only be used for the characterization of particular flints. For example, original ooid structures are preserved in some Jurassic nodules and are indicative of its source.

PALEONTOLOGICAL STUDY

Macrotests are rarely preserved in epigenesis, but skeletal components of the original limestone may be preserved by silicification. Chronological determination of organism is sometimes possible. Often they give an indication about sedimentation conditions.

A technique of extraction using acid attack of silica has been developed for a Cretaceous flint of the Bassin parisien (France) based on

the Dinoflagelles classification (Mauger, 1985). This destructive method only distinguishes geological attributes and does not permit a geographical determination of source.

GEOCHEMICAL METHODS

Spectrometry has been applied to distinguish the proportions of trace elements present. It is possible by this technique to relate artefacts to source areas for obsidian, which occur in a relatively fewer regions.

In the case of flint, the common rock–analytical results reveal large variations of composition in the same formation. Superficial weathering is an important factor controlling compositional variations.

The use of this destructive and expensive method is reduced and can only be applied to particular cases.

PHYSICAL METHODS OF CHARACTERIZATION

In my study of flint supply by prehistoric communities, in the centre of France, I have been confronted with a problem of characterization. Field work showed the existence of group of flint with similar petrographic origins. It was necessary to develop some new characterization methods to differentiate the origin of the rocks used for tool manufacture. Two physical properties have been measured. Density is a property of rocks that denotes the relationship between its mass and unit volume. Absorption of light is a quantitative measure of opacity.

Method of determining density:

Many methods for determining density have been proposed, the choice must be dictated by the nature and amount of material available and accuracy required (Zussman, 1977). Flint has small porosity. Its bulk density can be expressed as the weight per unit volume of the sample saturated in distillated water.

Before application to archeological material we have experimented the variation in the same formation from different sampling places, and within a nodule (Fig. 2). For Turonian flint, range of variation is low in comparison with the values obtained for the same nodule. Density can be used as a characteristic of this formation.

The method depends on immersion of the archeological and geological samples of flint in a liquid. The major source of error is due to the adherence of small air bubbles to the surface of solid which can be avoided by a preliminary saturation. A pycnometer method was used. The weight of solid is directly measured and the volume obtained by weighing the volume of liquid displaced by the solid. The measurement requires successive weighing of the empty pycnometer (W1);

- pycnometer plus sample (W 2);
- pycnometer plus sample, plus liquid (W3);
- pycnometer plus liquid (W4);
- ρt is the density of liquid at temperature, t.

- density of the sample =

$$= \rho t \left[\frac{(W2-W1)}{(W4-W1)-(W3-W2)} \right]$$

The error due to variation of pycnometer volume with temperature can be avoided with a preliminary weighing of pycnometer plus liquid as a function of temperature. By use of this technique, an accuracy of $5 \times 10^{-3} g/cm^3$ has been obtained for weight of solid greater than 5 grams.

Absorption Determination

Fig. 2 shows lower density Turonian samples overlap with maximum values of Bathonian and Ludien. Hand examination of the samples reveals that lower density Cretaceous flints correspond to opaque specimens. Thus, it has been necessary to develop another method of physical characterisation considering this property of flint, to increase the differentation. For trans-

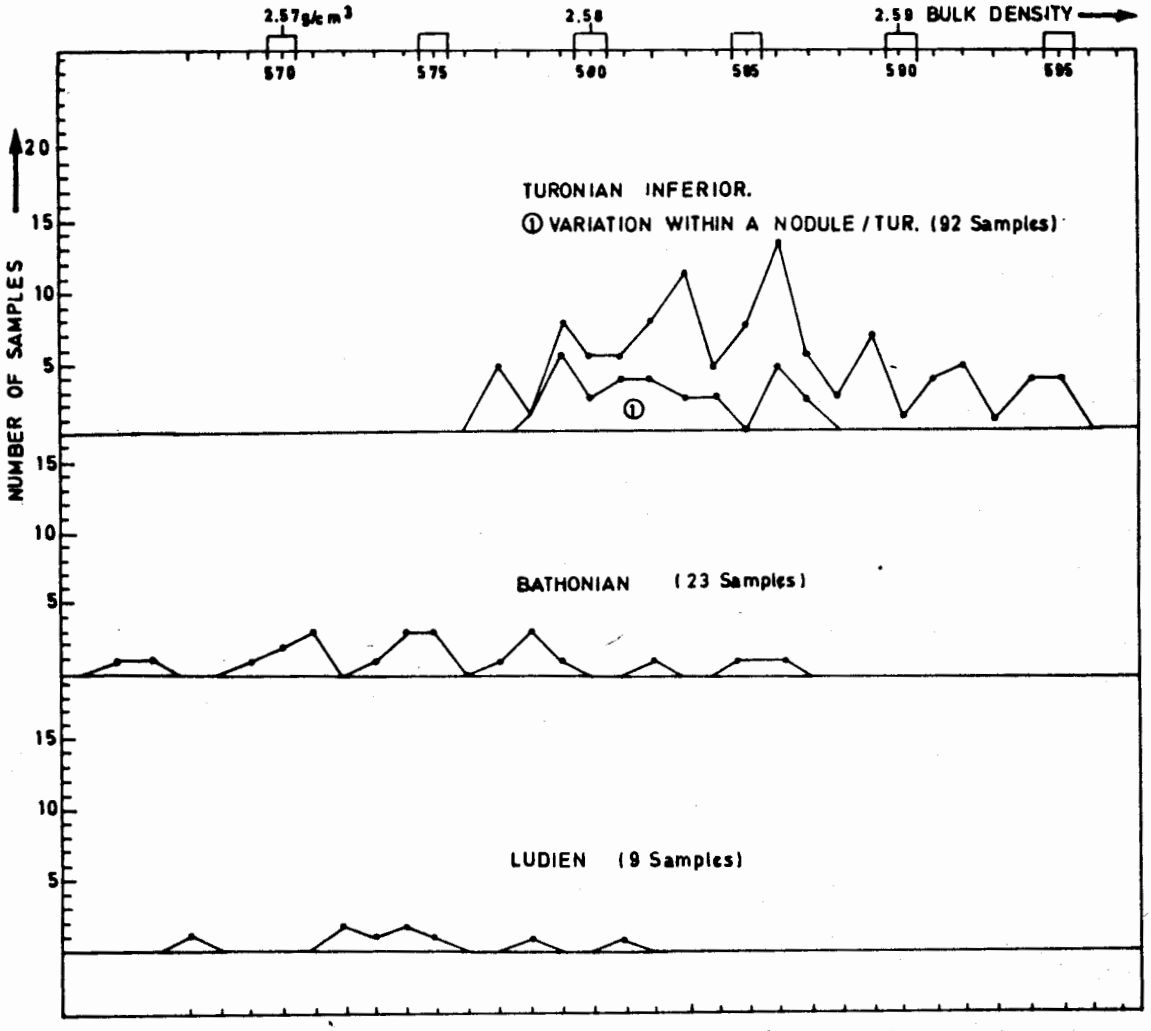

Fig. 2. Frequency histogram of the bulk density values of flint sampled from three different geological formations.

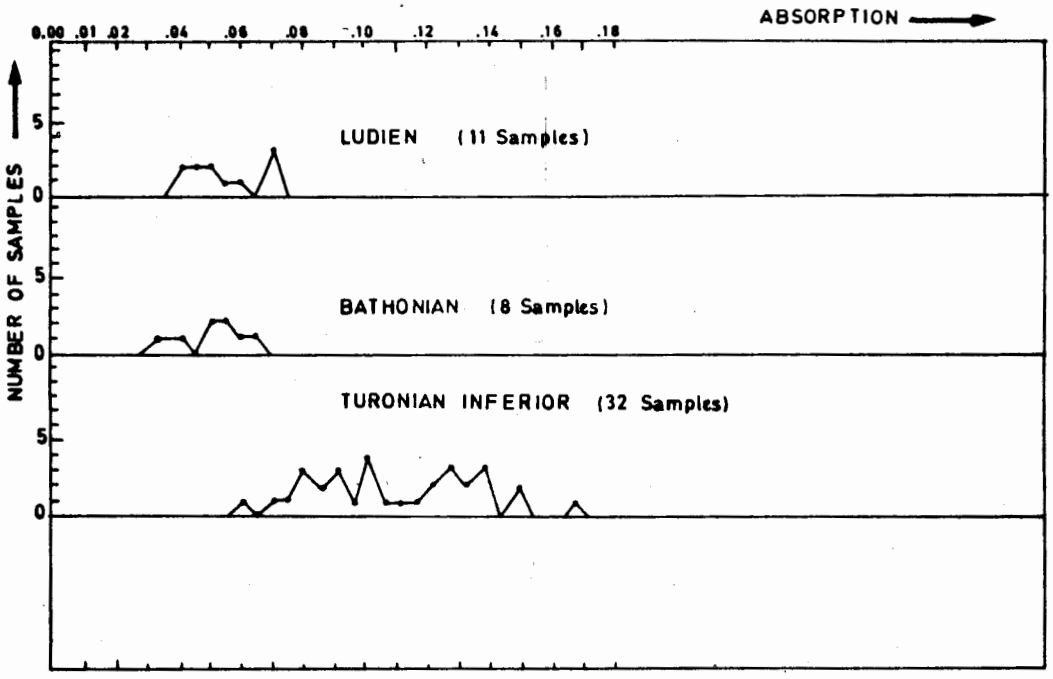

Fig. 3. Frequency histogram of absorption values of flint sampled from three geological formations.

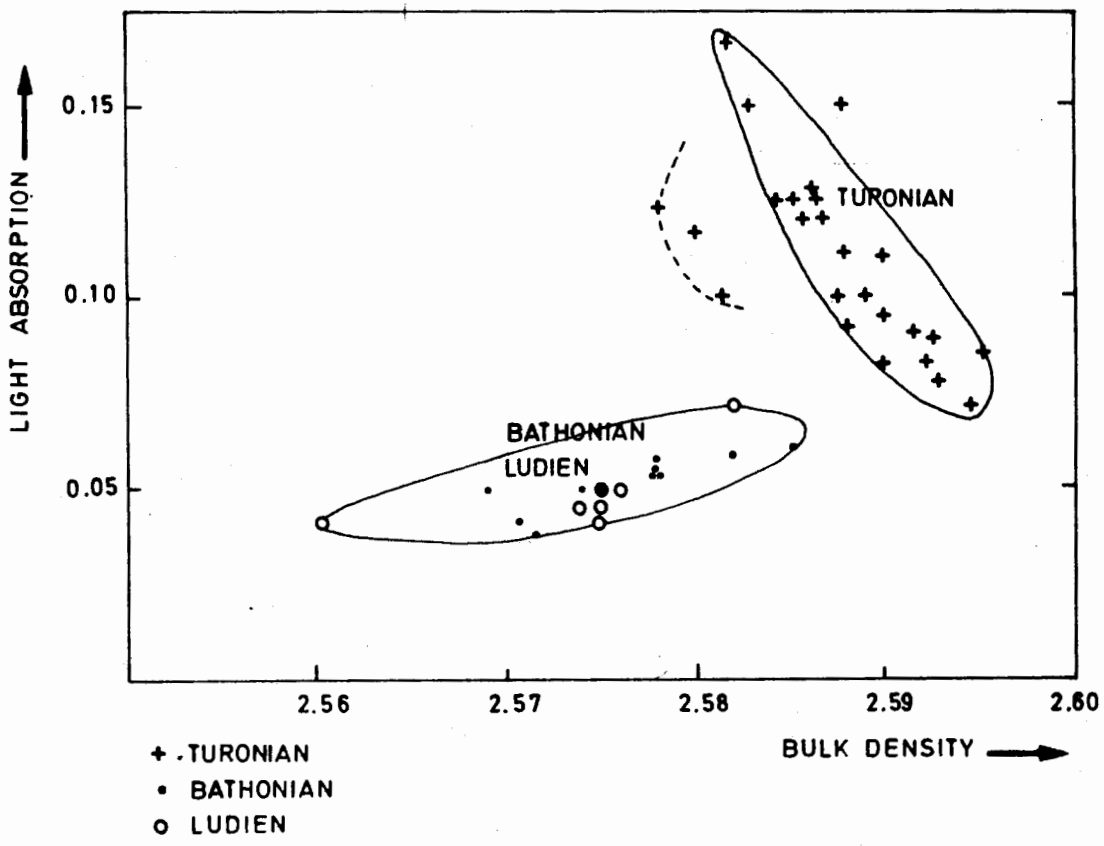

Fig. 4. Relationship between bulk density and light absorption for flint from geological samples.

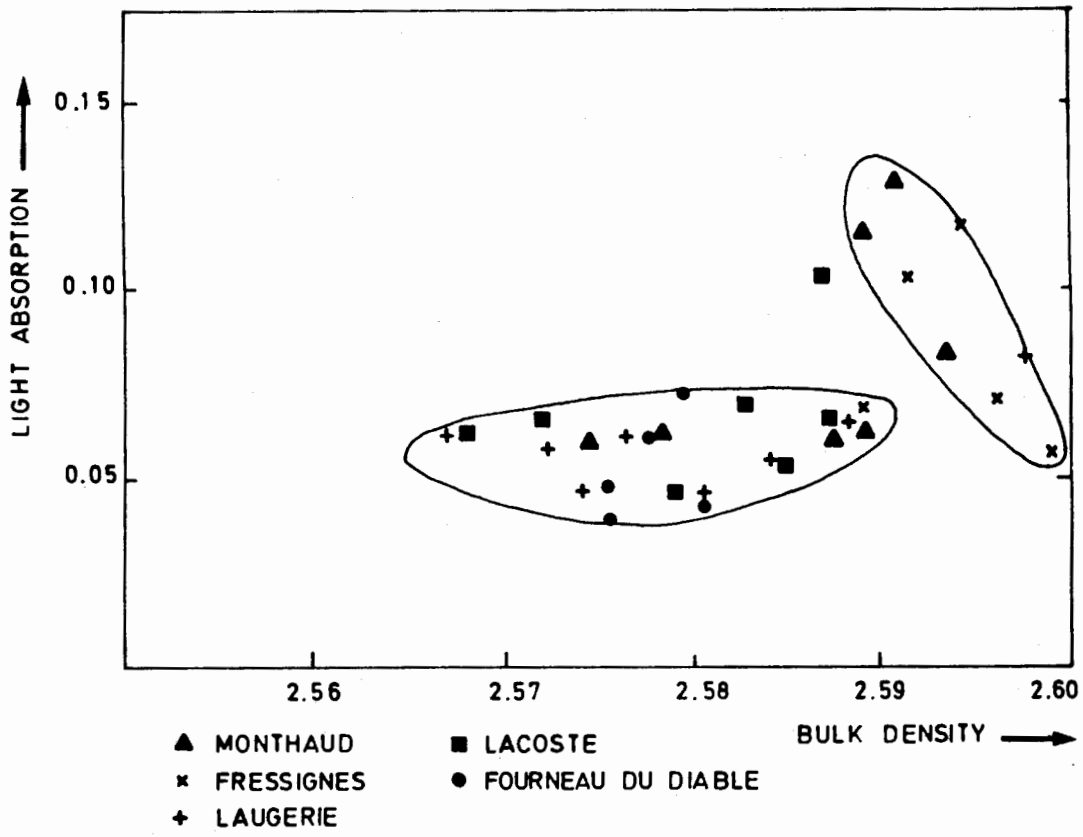

Fig. 5. Relationship between bulk density and light absorption for flint from archeological samples from 5 sites.

luscent material as flint with only a few impurities, absorption of light may be measured quantitatively by means of spectrophotometer. Continuous radiation from a tungsten lamp is passed through the sample and the percentage of radiation absorbed by the specimen may be measured and recorded as a function of sample thickness. This technique can be directly adopted to a microscope. Values obtained for the same sample used in density measurement are presented in Fig. 3. The coefficient of absorption can be expressed as:

$K = \text{Log } (Qt/Qi)$

where

Qt = transmitted light intensity
Qi = initial light intensity
t = thickness of sample.

For every sample we have measured the average absorption at different points to avoid the error due to variation in amount impurities.

Interpretation of physical methods:

Representation of the relationship between bulk density and absorption for the three geological origins and archeological samples permits some observations (Fig. 4).

Geological samples values show a direct correlation between bulk density and light absorption for Turonian flints. We suggest this relation is due to the proportion of amorphous silica, a low density and opaque material. The range of density values for Bathonian and Tertiary flints seems to result from variation of porosity.

Archeological application for few different sites permits distinction of the use of Turonian flint. Unfortunately Jurassic and Tertiary flint cannot be distinguished.

By these physical techniques we have shown (Aubry, 1987) use of Cretaceous flint far from its original source without possibility of displacement by alluvial processes. For example, Fressignes is a site of solutrean age (—18000 B.C.) 70 km from Turonian occurrences, where this type of flint has been exploited in more than 10 percent of the material.

On the other hand, we have refuted the hypothesis of displacement of this material for long distances (for La coste, Laugerie, Fourneau du diable sites) and shown that a regional resource must be found for this group of flint.

CONCLUSIONS

The existing range of geological techniques permit characterisation of flint, but may not allow determination of its source. The method proposed here consists of a non destructive physical technique of characterization. The already obtained results on the use of flint by early man, are encouraging.

REFERENCES

AUBRY, T. (in press) Problems de convergence dans l'etude de l'approvisionnement en matieres premieres siliceuses des gisements solutreens et badegouliens du centre de la France. Actes du V flint Symposium, Bordeaux, 1987.

HESSE, R. (1988) Origin of chert. Diagenesis of biogenic siliceous sediments. Geoscience Canada, **15**, (13), pp. 171-92.

MAUGER, M. (1985) Les materiaux siliceux utilises au Paleolithique superieur en ile de France. Thesis, Univ. Paris I (Unpublished), 225 p.

SCHMID, F. (1986) Flint strâtigraphy and its relationship to archeology. *In:* Sieveking, G de G. & Hart, M.B. THE SCIENTIFIC STUDY OF FLINT AND CHERT. Cambridge University Press, pp. 1-5.

SIEVEKING, G., BUSH, P., FERGUSON, J., CRADDOCK P.T., HUGHES, N.J., & COWELL, M.R. (1972) Prehistoric flint mines and their identification as sources of raw material. Archeometry, **14**, pp. 151-77.

ZUSSMAN, J. (1977) PHYSICAL METHODS IN DETERMINATIVE MINERALOGY 2nd edition. Academic Press.

Manuscript received on 15.12.1988
Accepted for publication on 31.12.1988

ACTA MINERALOGICA PAKISTANICA
VOLUME 4 (1988) pp. 102 - 112.

A PRELIMINARY STUDY OF CHERTS FROM BALOCHISTAN

THIERRY AUBRY, ZULFIQAR AHMED & MEHRAB KHAN BALOCH
Centre of Excellence in Mineralogy, University of Balochistan,
GPO Box 43, Quetta, Pakistan.

ABSTRACT: In Balochistan, sedimentary rock outcrops of lower Jurassic to Palaeocene age contain cherts with large petrographic diversity described in this study. Chert pebbles in the Oligocene–Pliocene age conglomerate resemble certain Jurassic–Cretaceous cherts. All the cherts are non-opaline and consist mainly of microquartz with some chalcedony. Some cherts contain abundant fractures caused variously by tectonism, low heat, or shrinkage attendant upon conversion of initial hydrous siliceous phases to quartz.

INTRODUCTION

Siliceous non-clastic rocks occur in many sedimentary rock formations in Balochistan. In the regional geological literature, they are named 'chert' reflecting their high silica content. However, previous studies or descriptions were not focussed on these cherts. The present study deals with cherts of diverse depositional environments and sources of silica. It presents mineralogical and petrographic data on these cherts, and comments on their petrogenetic aspects.

OCCURRENCE OF CHERT

The localities of the cherts sampled for this study are shown in Fig. 1. The stratigraphic positions of the samples are given in Table 1. The samples represent various stratigraphic levels from lower Jurassic to upper Miocene. The occurrence of this chert in various formations is described below. Photographs in Fig. 2 illustrate some of these occurrences.

1. **ZIDI FORMATION:** This formation is thickest, exceeding 928 m, in the Ferozabad area, west of Khuzdar. Fatmi *et al.* (1986) have renamed it as "Ferozabad Group" and presented its measured stratigraphic sections, paleontology and major elemental chemical variation profiles. The lithology is dominated by marine limestone with fewer shale interbeds and minor sandy rocks. According to Fatmi *et al.* (1986), the limestone in the uppermost part, at Bajocian level, contains chert or silicified rock formed by incomplete replacement along the bedding planes in grey limestone.

For study of cherts from the "Ferozabad Group", samples were collected from two localities: sample 139 from near Gunga barite mine, Gunga Valley; and sample 140 from near the ophiolitic melange contact at Katangri on the Nal-Khuzdar road. At Gunga, silicification in limestone is regarded partly as syngenetic veins, lenses and layers in limestone; and partly as epigenetic, linked to the Pb-Zn bearing hydrothermal solutions that formed jasperoid rocks described by Ahmad & Klinger (1967).

At Katangri, chert occurs as successive planar layers, pinch-and-swell layers, lenticular layers, discontinuous beds and semispherical to irregular nodules within limestone. Individual

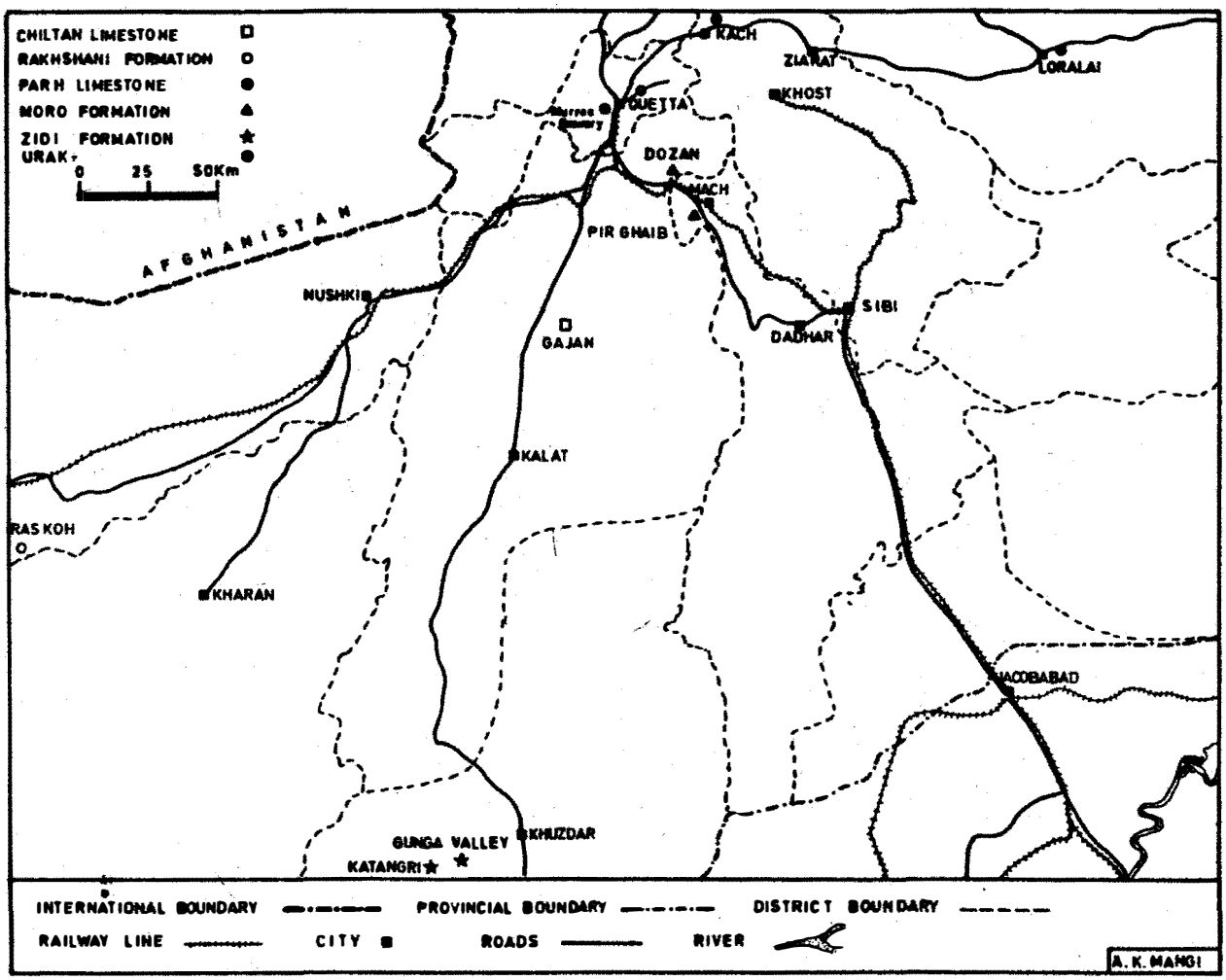

Fig.1. Location map of chert sampled for this study.

chert layers are usually 10 to 20 cm thick; and do not exceed 50 cm.

2. **CHILTAN LIMESTONE**: The Chiltan Limestone (Bajocian to Bathonian) shows a good development in Kohe Maran range, and its chert (sample No. 138) has been collected from near Gajan village. Here, about 17 chert layers are present in a section of thick-bedded limestone whose total thickness is less than 10 m (Fig. 3). The chert outlines make nodules, lenticles and irregular forms.

3. **PARH LIMESTONE**: This late Cretaceous formation with its distinctive light-coloured, lithographic to porcellaneous, hard, conchoidal-fracturing, limestone varies from 300 to 600 m in its thickness; and contains chert at many places. The limestone is a part of the "Mona Jhal Group" of Fatmi *et al.* (1986). Chert samples from the Parh Limestone were collected from the Murree Brewery Gorge near Quetta (sample No. 137); Kach town (sample No. 136): and, Loralai town (sample No. 135). The stratigraphy of the formation has been dealt by Allemann (1979) who reported the occurrence of dark chert nodules and bands in the upper Coniacian to Santonian strata which are comprised of light grey, thin- to medium-bedded, pelagic limestone which bears *Globotruncana concavata, G. elevata, G. stuartiformis* and *G. arca.*

The chert sample No. 137 is collected from a porcellaneous, white limestone with a conchoidal fracture, and discontinuous layers of nodules upto 10 cm thick. Successive layers are separated from each other by approximately 50 cm thick interbeds of limestone. Nodules of the thalassinoide burrow type occur at the upper boundary of the beds (Fig. 2).

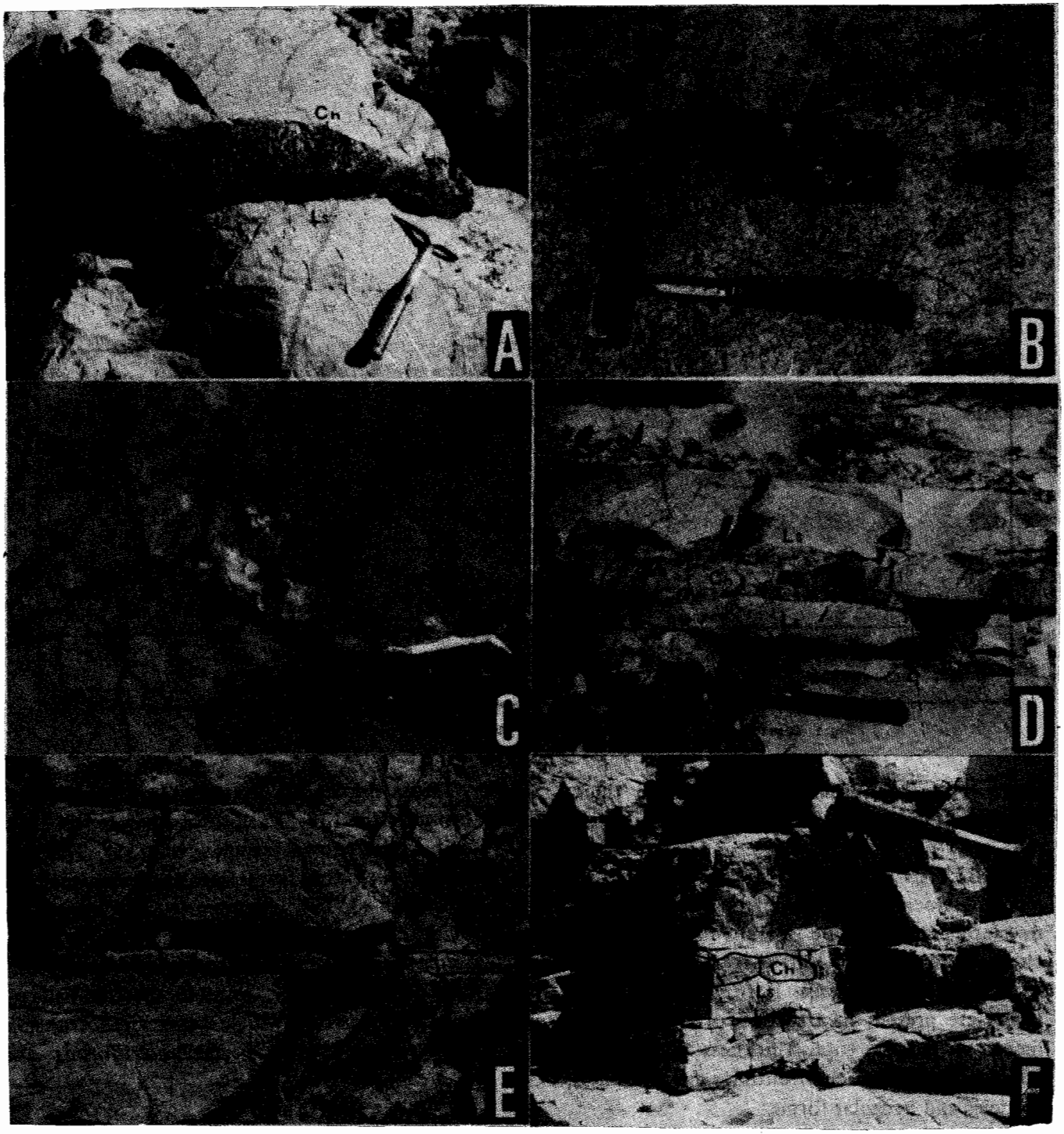

Fig. 2. Field relations of cherts from Dozan, Bolan Valley (A, B); Loralai town (C,D); and Brewery Gorge near Quetta (E,F). Ch = chert; Ls = limestone.

At Kach, chert layers and nodules occur in a fashion similar to that at the Brewery Gorge section.

The town of Loralai has several mounds made of Parh limestone which has several silicification levels (Fig. 3). Chert occurs mainly as continuous layers upto 10 cm thick (sample No. 135). When the successive siliceous layers occur closer together, they form nodules.

4. **MORO FORMATION**: From the Bolan Pass section of this formation, chert samples are collected from the hill slopes located just north of Dozan railway station (sample No. 133); and from a place 10 km SW of Mach on the Mach-Pir Ghaib road (sample No. 134). The formation is of Maastrichtian age and lithology is dominated by limestone that occurs in addition to marl, shale and sandstone.

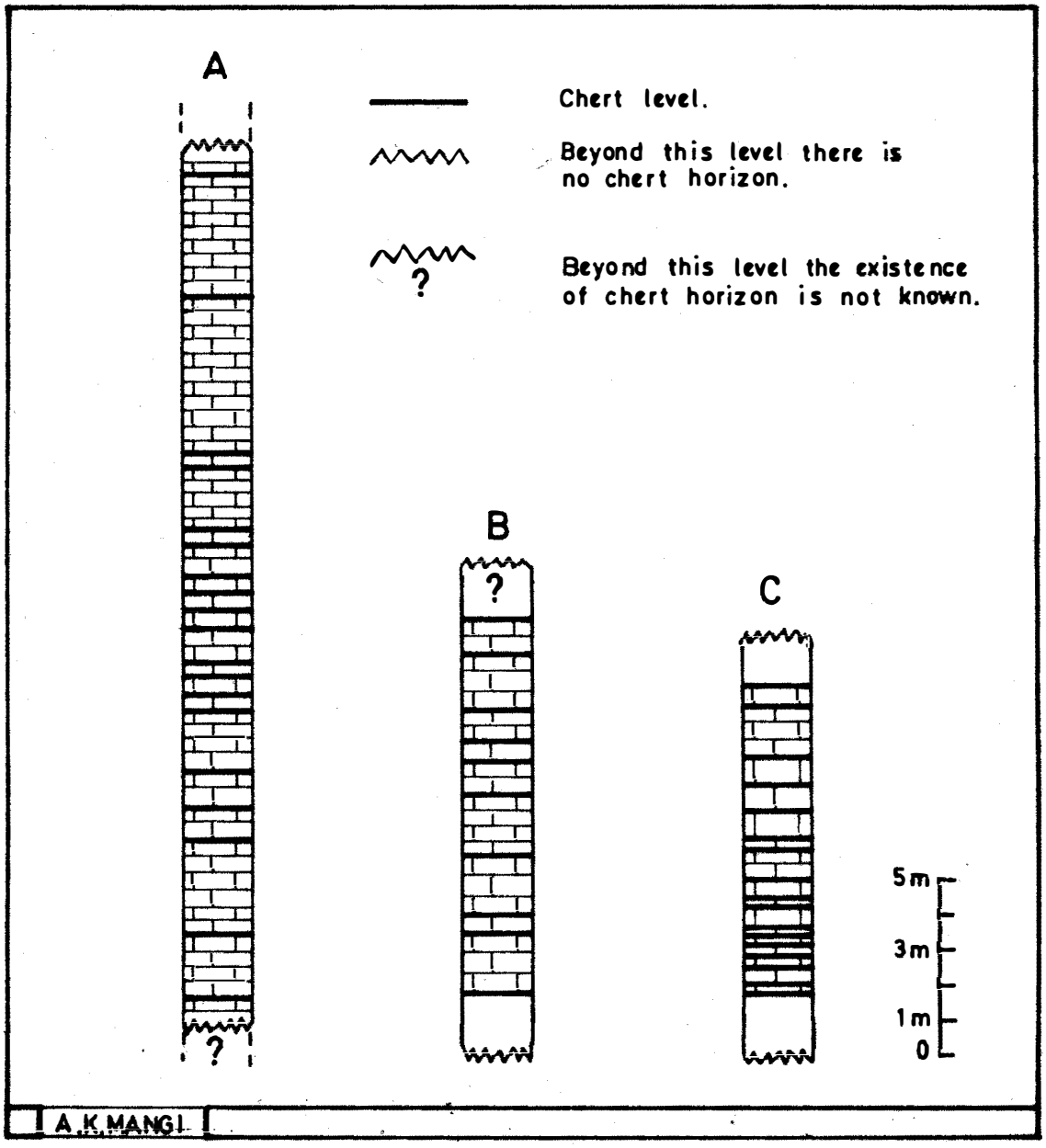

Fig. 3. Stratigraphic section (A) Part of Parh limestone exposed at Loralai town, showing chert levels. (B) Part of Moro formation exposed north of Dozan. (C) Part of Chiltan limestone exposed at Gajan.

At Dozan, chert is abundant in a dark grey limestone. It forms numerous nodular layers, veins, in a section over 20 m thick, situated north of the railway station. Chert also makes large, flat nodules of thalassinoide burrow type, sometimes more than 50 cm long. At places it consists of continuous layers, about 10 cm thick.

On Mach-Pir Ghaib road, dark grey chert is abundant and conspicuous on weathered blocks of limestone. Chert forms lenses of decimetric size and irregular nodules. Compared to the occurrence at Dozan, the chert nodules here are smaller and more irregular. The mode of occurrence does not allow the estimation of the silicification levels.

5. **RAKHSHANI FORMATION:** This Palaeocene formation consists of green to grey sandstone, shale, dark grey argillaceous limestone, conglomerate, basaltic to andesitic lava flows, tuff and conglomerate. The volcanic rocks are probably of Danian age. Chert occurs intercalated with shale, in a section exceeding 50 m in thickness. The silicification is inhomogeneous and mostly in lenticular form. The chert sample (No. 132) obtained from Banikan Kaur in the Ras Koh range was studied.

6. **URAK GROUP:** The dominant conglomerate component of the Urak Group (lower Oligocene to upper Pliocene) exposed in the Urak Valley near Quetta Cantonment contains pebbles of chert of different colours represented by sample No. 131 in this study.

PETROGRAPHY OF CHERTS AND THEIR HOST ROCKS

Chert samples are dense, hard, microcrystalline with smooth conchoidal fracture. Their colour on fresh surfaces varies considerably, and usually differs from the colour on weathered surfaces.

In general, the cherts show secondary failure by fractures. Such fractures are lacking in the sample from the Gunga Valley (sample No. 139). In some samples, e.g., No. 140, fractures are dominated by the sets perpendicular to the attitude of chert layers, and terminate at the outer boundaries of chert layers.

1. **ZIDI FORMATION:** The host rock of chert sample No. 140 is moderate yellowish brown packstone type of limestone with coarse grained calcite profusely crosscut by veins of calcite often more than 0.5 cm thick. Limestone is of pelsparite type. Allochems consist of peloids, and the cement is of sparry calcite.

The chert weathers dusky brown to greyish brown. It is very pale orange to pale yellowish brown on fresh surfaces. In some cases, it shows thin iron stringers near contact with host limestone. On joint surfaces, iron oxides are developed. The packstone structure of the host limestone is preserved in the chert layers. The chert is secondary silica that replaces the limestone of earlier deposition. The larger foraminiferal fossils in chert are well preserved. The fractures are plentiful and pervasive in chert, and abut against the contacts of host limestone rock.

The host rock of sample 139 is limestone of pale yellowish orange colour. The chert is light brown and lacks fracture.

2. **PARH LIMESTONE:** At all places sampled, the chert is hosted by biomicrite. The pelagic limestone hosting the chert at the Murree-Brewery Gorge is yellowish grey. It is biomicrite and shows a wackestone structure. It contains *Globotruncana sp., G. concavata, G. elevata* and *G. linneiana.*

The chert is medium grey to dark grey; and the nodules are traversed by several fractures perpendicular to bedding. Some samples show mottled appearance due to patchy local concentrations of dark material which may be organic. Bioclasts present in the host limestone are not preserved in the chert when highly silicified. However, they are preserved in the lesser silicified chert nodules.

Table 1. **Locations of chert samples and their host rocks.**

L. No.	Sample No.	Locality	Topographic Sheet No.	Host rock	Formation	Age
1.	131	Urak Valley, Quetta District.	34 N/3	Conglomerate	Urak Group	Upper Miocene
2.	132	Bani Kan Kaur, Ras Koh range, Kharan District.	34 D/14	Shale, marl.	Rakhshani Formation	Palaeocene.
3.	133	Dozan, Bolan Valley, Kalat District.	34 O/1	Biosparite	Moro Formation	Upper Cretaceous
4.	134	Mach-Pir Ghaib road, Bolan Valley, Kachhi District.	34 O/5	Biosparite	Moro Formation	Upper Cretaceous
5.	135	Loralai Town, Loralai District.	39 B/15	Biomicrite	Parh Limestone	Turonian to Lower Campanian
6.	136	Kach, Sibi District	34 N/7	Biomicrite	Parh Limestone	Turonian to Lower Campanian
7.	137	Murree-Brewery Gorge near Quetta City.	34 J/16	Biomicrite	Parh Limestone	Turonian to Lower Campanian
8.	138	Gajan, Koh-e Maran, Kalat District.	34 K/14	Biopelsparite	Chiltan Limestone	Jurassic
9.	139	Gunga Valley, Khuzdar District	35 I/10	Marl	Zidi Formation	Jurassic
10.	140	Katangri, Khuzdar District	35 I/6	Pelsparite	Zidi Formation	Jurassic

The pelagic Parh limestone at Kach is either a wackestone or a packstone and is biomicrite. It contains *G. concavata* and *G. linneiana* as reported by Allemann (1979). Some limestone samples contain sparite zones and stylolites with concentrations of organic material.

The chert nodules are dark reddish brown in the central parts, but have walls of pale red to greyish pink colour. The bedding is truncated by sparite vein fillings across it. Badly preserved foraminifera are found in the wall zones of chert. In the central parts of chert nodules, the foraminiferal shapes are occupied by iron oxide. Tiny, crescent-shaped cracks occur in clusters.

The Parh Limestone from Loralai is procellaneous and lithographic with conchoidal fracture, and is, at places, strongly fractured. It is very pale orange, fine to medium grained, and bears stylolites. Some samples show mudstone type texture with allochems made of foraminiferal tests and cement made of microsparite or micrite.

The chert is yellowish grey to very light grey with some pale red zones in a few samples. Fractures and veins are developed perpendicular to bedding. Their extensions into the contact rock are greatly diminished in thickness and number. Texture is of wackestone type. The

exteriors of chert nodules show high calcite content. The chert contacts with limestone are gradational over a few mm usually.

3. **MORO FORMATION:** The host rock of chert is biosparite of light olive grey colour that weathers to medium light grey but has a few mm thick greyish orange envelope at contact with chert.

The chert sample from Mach-Pir Ghaib road (No. 134) is dark grey in colour and weathers to brownish black colour. It contains sponge spicules and foraminiferal tests. Unlike sample 133, there is no dolomite present in chert from this locality. Brown iron oxide is abundant and fills the sponge spicules and cracks. In fracture style, this sample resembles sample No. 133.

The host rock of sample 133 is medium light grey biosparite and contains fossils of foraminifera, algae and molluscan fragments. The chert is medium dark grey to greyish black in colour. It contains abundant idiomorphic, often isolated, rhombohedra of dolomite, with average diameter of 0.15 mm, in the matrix composed of microquartz. There are rare microfossils such as *Orbitoides.* Chert is fine grained and profusely fractured without any dominant alignment. The chert encloses remnants from the host rock that escaped replacement by chert.

4. **CHILTAN LIMESTONE:** The host rock of sample 138 is a yellowish grey limestone that weathers to greyish orange colour. The limestone is of biopelsparite type. Grains consist of peloids cemented by sparite or microsparite. A few molluscan cast fragments are present.

The chert also has yellowish grey colour, but slightly more greyish than that of host limestone. Some chert pieces are of very light grey colour. The chert consists of coarse grained silica that preserves the packstone structure of host limestone. An iron oxide lining, about 1 mm thick, is usually present in between the chert nodules and host limestone.

5. **RAKHSHANI FORMATION:** The host rock of sample 132 is greyish shale, and it has sharp contact with the chert.

The chert has two dominant colours: greyish olive and greyish green. Some parts are dark reddish brown. The greyish green chert lacks radiolaria. The radiolaria-rich chert has greyish olive colour and contains spherical radiolaria, fewer spines and nasselarian radiolaria, all matrixed by microquartz. The initial opaline silica of radiolarian tests now has been changed to chalcedony spherulites. In some samples, sedimentary features are present resembling those of turbidite-derived cherts described by Nisbet & Price (1974). The contacts between radiolarian and non-radiolarian chert types are sharp and irregular, and at places, thin streaks of iron oxide are developed along such contacts.

6. **URAK GROUP:** The chert pebbles in the conglomerate petrographically resemble the cherts described above from the Chiltan limestone and Parh limestone; both of which occur in nearby areas, and may have provided the detritus to the conglomerate.

X–RAY DIFFRACTION CHARACTERISTICS

In every chert sample included in this study, more than one mineral constituents are present and are identifiable in the X-ray diffractogram traces. For four of the samples (nos. 132, 133, 136 and 139), and one archeological chert sample (Jalwar), the X-ray powder diffractogram peaks with respective d-values are shown in Fig. 4. This shows presence of quartz and clay minerals in sample 132; quartz, dolomite, calcite and iron oxide in sample 133; quartz, calcite, clay minerals and iron oxide in sample 136; and quartz, clay minerals, and hematite in sample 139. Feldspar is not present in most geological samples; and is present in the archeological sample of Fig. 4.

All the samples of Fig. 4 are of quartz chert which lacks other silica modifications such as cristobalite, tridymite, opal-A, opal-CT or opal-C. Presence of chalcedony is indicated, but is not discernible by the X-ray diffractograms.

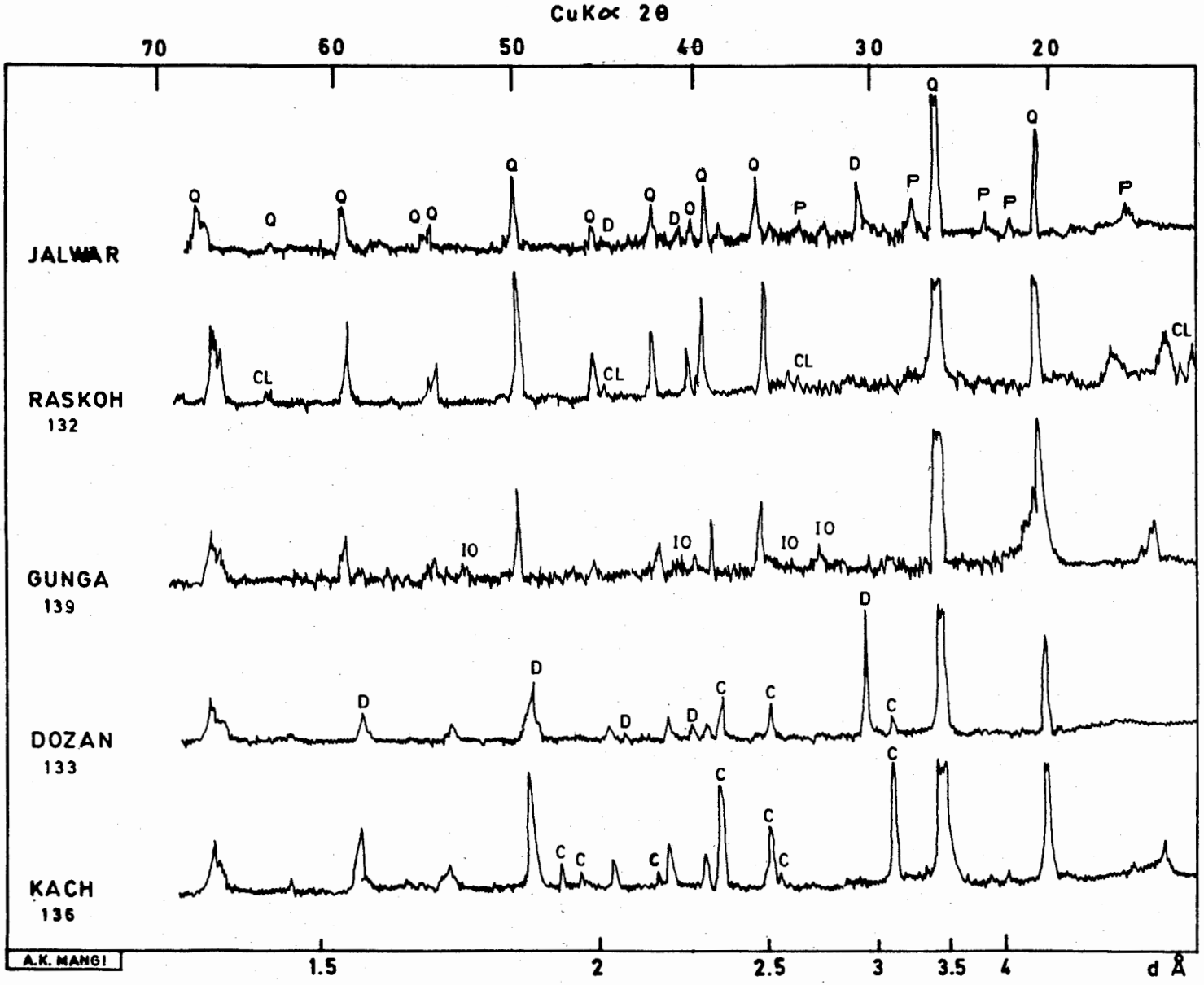

Fig. 4. X-ray diffraction traces (35 kV, 15 mA, Cu K_{α}) of five chert samples from Balochistan. The peaks identified are Q, quartz; P, plagioclase; D, dolomite; CL, clay mineral; IO, iron oxide; C, calcite. Sample nos. are given except for the sample from "Jalwar" which is an archeological sample.

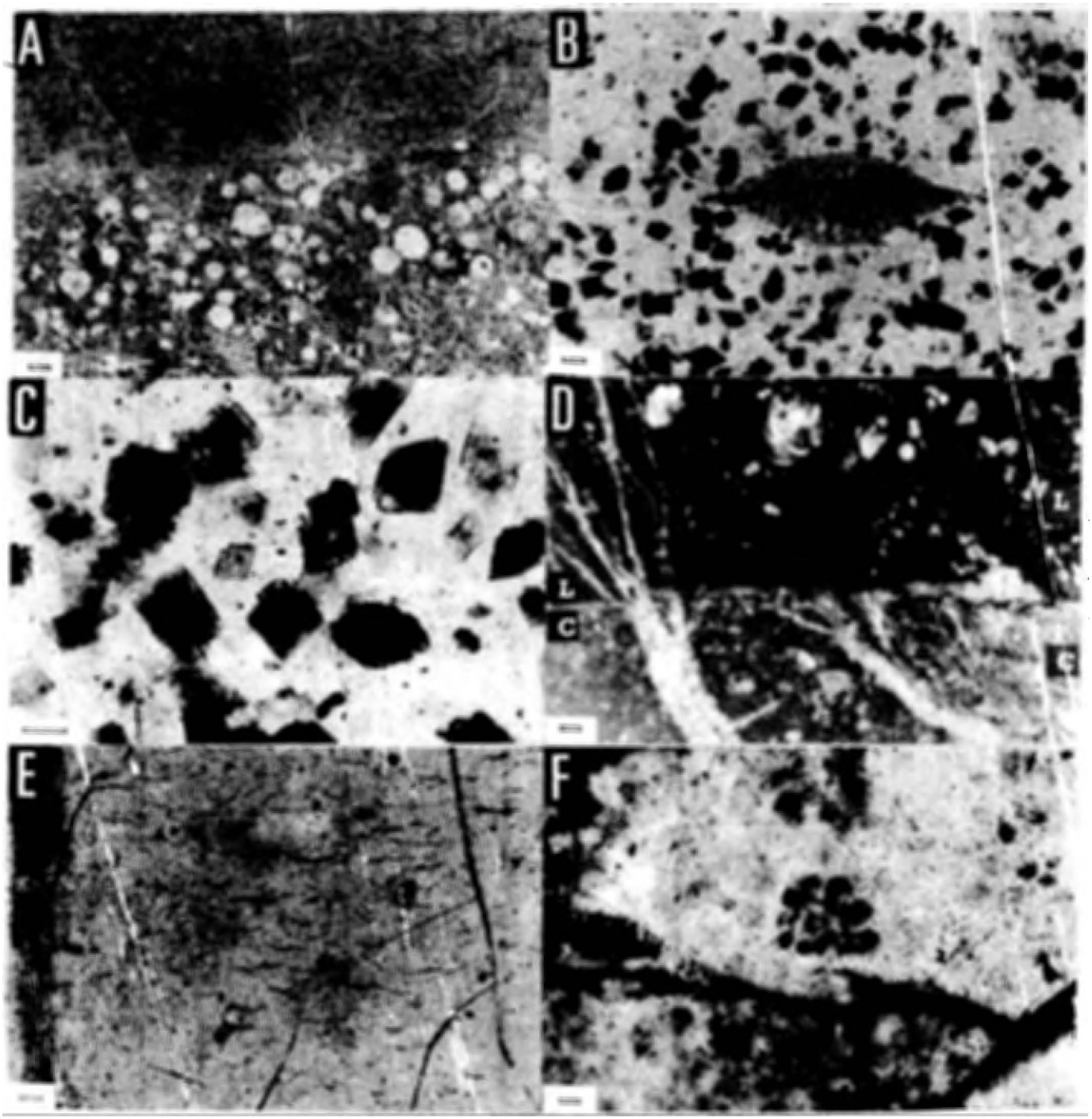

Fig. 5. Photomicrographs from chert samples taken under plane polarized light and bearing scale bars that are 0.1 mm in each case. (A) shows sharp contact between chert rich in radiolaria and that lacking radiolaria, in sample no. 132. The contact trace is irregular and gives the impression of clastic deposition of fragments of radiolarian chert in the non-radiolarian chert medium. (B) shows fossil *Orbitoides* and abundant rhombs of dolomite in sample no. 133. (C) shows dolomite rhombs set in the microquartz matrix in sample no. 133. (D) shows the contact of chert "C" with the host limestone "L", in sample no. 135. The chert fractures filled with sparry calcite diminish in abundance and width on entering the host rock. (E) shows small, crescent-shaped cracks present in clusters, in sample no. 136. (F) shows a foraminiferal test in chert, in sample no. 140.

The crystallinity index of chert samples of Fig. 3 was determined using the (212) peak at 67.74° 2θ, after Murata & Norman (1976). The index is 2.7 ± 0.1 for sample No. 132; 2.6 ± 0.1 for sample Nos. 133 and 136; and, 4.1 ± 0.1 for sample No. 139. Relatively higher crystallinity index for sample No. 139 may possibly reflect its formation from hydrothermal solutions, compared to the sedimentary origin for the other samples.

BULK DENSITY

Bulk density of three chert samples was measured by the pycnometer method as described by Muller (1977). Sample No. 132 has density of 2.668 ± 0.005, and is comparable to its constituents determined by X-ray diffraction: mainly quartz with minor clay minerals. Density of sample No. 133 was determined separately for two different parts: one gave value of 2.611 ± 0.005 and the other gave 2.631 ± 0.005. Both values indicate presence of chalcedony, as otherwise, the density should be above that of quartz (2.65). Sample No. 135 has a density of 2.565 ± 0.005; and matches its low calcite and higher chalcedony contents.

CONCLUDING REMARKS

This study reveals diversity in cherts found in various host rocks ranging in age from lower Jurassic to upper Fliocene. However, as the chert pebbles in the Urak Group conglomerate resemble, and may have been derived from, the cherts of the Mesozoic formations; the age spectrum covered by the studied samples is lower Jurassic to Paleocene. Within each formation, chert-bearing horizons were fed by dissolved silica from regions of lower relief and tropical to subtropical climates. The associated hematite stringers may also have formed similarly. Prevalence of fossils in some samples indicates their origin as biochemical accumulations. Others may have formed by silicification of carbonate rocks.

The well-preserved fauna in these cherts indicate their incorporation and diagenesis at an early stage, prior to any crushing by the overload. Preservation of fossils, e.g., sponge spicules in sample No. 134, points to minimal tectonic disturbance of the Moro formation exposed around Mach-Pir Ghaib area.

Tectonic fractures are, however, common in sample Nos. 135, 136, 137 and 138. In these, fracture sets perpendicular to chert-limestone contacts dominate and enter limestone with strongly decreased intensity. The Gunga Valley cherts display an absence of fractures that may probably be related to their genesis involving hydrothermal fluids. Neither were they initially opaline to have subsequently reduced in volume.

In the Katangri sample (No. 140), there is less likelihood of tectonism being the cause of fractures that occur confined to chert and totally terminate on reaching the limestone contact. Chert is a rock stronger than limestone, and a difference in brittleness should not result in such large difference in fracturing. These fractures appear to be shrinkage effects. Shrinkage is the likely result if the chert had formed by conversion from opal, magadiite, or other hydrous precursors. Tiny, crescent-shaped cracks in the sample from Kach (No. 136) may have been caused by low heat (circa 200°C) supplied by the minor bodies of igneous rocks in the vicinity.

In the Moro formation sample, dolomite rhombs are not present in the adjacent unsilicified limestone. Thus, the dolomite and chert may either have formed contemporaneously; or, dolomite rhombs may have formed by replacement in the chert nodules.

The bulk density and petrography of the samples from Parh limestone, show the presence of chalcedony in high proportions; and is probably related to the nature of its host rock (biomicrite) in contrast to the rest of the samples.

REFERENCES

AHMAD, M.I. & KLINGER, F.L. (1967) Barite deposits near Khuzdar, Kalat Division, West Pakistan. Rep. Geol. Surv. Pakistan, Quetta. (Unpublished).

ALLEMANN, F. (1979) Time of emplacement of the Zhob Valley ophiolites, and Bela ophiolites, Baluchistan (preliminary report). *In:* Farah, A. & De Jong, K.A. (eds.) GEODYNAMICS OF PAKISTAN. Geol. Surv. Pakistan, Quetta, pp. 215-42.

FATMI, A.N., HYDRI, I.H., ANWER, M. & MENGAL, J.M. (1986) Stratigraphy of "Zidi formation" (Ferozabad group) and "Parh group" (Mona Jhal group), Khuzdar District, Baluchistan, Pakistan. Rec. Geol. Surv. Pakistan **75**, 32p.

MULLER, L.D. (1977) Density determination. *In:* Zussman, J. (ed.) PHYSICAL METHODS IN DETERMINATIVE MINERALOGY. Academic Press, London, pp. 663-75.

MURATA, K.J. & NORMAN, M.B. (1976) An index of crystallinity for quartz. Amer. Jour. Sci. **276**, pp. 1120-30.

NISBET, E.G. & PRICE, I. (1974) Siliceous turbidites: bedded cherts as redeposited ocean-ridge derived sediments. *In:* Hsu, K.J. & Jenkyns, H.C. (eds.) PELAGIC SEDIMENTS ON LAND AND UNDER THE SEA. Internat. Assoc. Sedimentol. Spec. Publ. **1**, pp. 351-66.

Manuscript received on 15.12.1988
Accepted for publication on 31.12.1988

ACTA MINERALOGICA PAKISTANICA
VOLUME 4 (1988) pp. 113 - 133.

PLATE GEOLOGY AND RESOURCE POTENTIAL OF OFF-SHORE REGION OF PAKISTAN

ABUL FARAH[1], ROBERT D. LAWRENCE[2]
[1] National Institute of Oceanography, Karachi, Pakistan.
[2] Oregon State University, Corvallis, U.S.A.

ABSTRACT: The off-shore region of Pakistan from Rann of Kutch in the east to the Makran margin in the west has three distinct geological divisions: (1) Passive continental margin including the Indus River Delta and submarine Indus fan, (2) Murray Ridge, which probably is a leaky transform fault, and (3) Active Makran subduction zone. Understanding of the passive continental margin which began its geological history with the fragmentation of Gondwanaland about 135 m.y. ago is very important because it can help in identification of source rocks and in estimating petroleum potential. The possibility of finding both "Mesozoic" and "Cenozoic" oil reserves in this zone is good.

The Murray Ridge, identified as a north-easterly positive feature south-west of Karachi, separates the passive continental margin from the active subduction zone of Makran. Its north-eastern end may mark the triple junction between the Arabian, Eurasian and Indian plates. It may be a leaky Transform Fault like the Chaman Fracture Zone and may prove a good environment for accumulation of polymetallic sulphides.

The Makran subduction zone is a convergent ocean continent boundary where the Arabian plate perhaps dips at a shallow angle beneath the rapidly accreted thick pile of sediments of the Makran margin that hindered the development of a typical trench bathymetry. The petroleum potential of the Makran margin has not been fully evaluated. The National Institute of Oceanography has launched a long term programme of geological, geophysical and geochemical studies of the above three geological subdivisions described and discussed in this review paper.

INTRODUCTION

In the context of plate tectonics, the geology of the off-shore area of Pakistan is as uniquely interesting and intricate as that of its mountainous area stretching from the Karakoram in the north to the Makran coast in the south. The off-shore region extending from Rann of Kutch in the east, to the Makran margin in the west has three distinct geological subdivisions 1) Passive continental margin and off-shore Indus Fan Basins, 2) Murray Ridge of debated origin, and 3) Active Makran subduction margin (Fig. 1).

Geological and geophysical information on these subdivisions is limited. Most of the available data pertain to the passive continental margin and part of the upper submarine Indus Fan (Shuaib, 1982; V.N. Quadri, 1984; Farah, 1987).

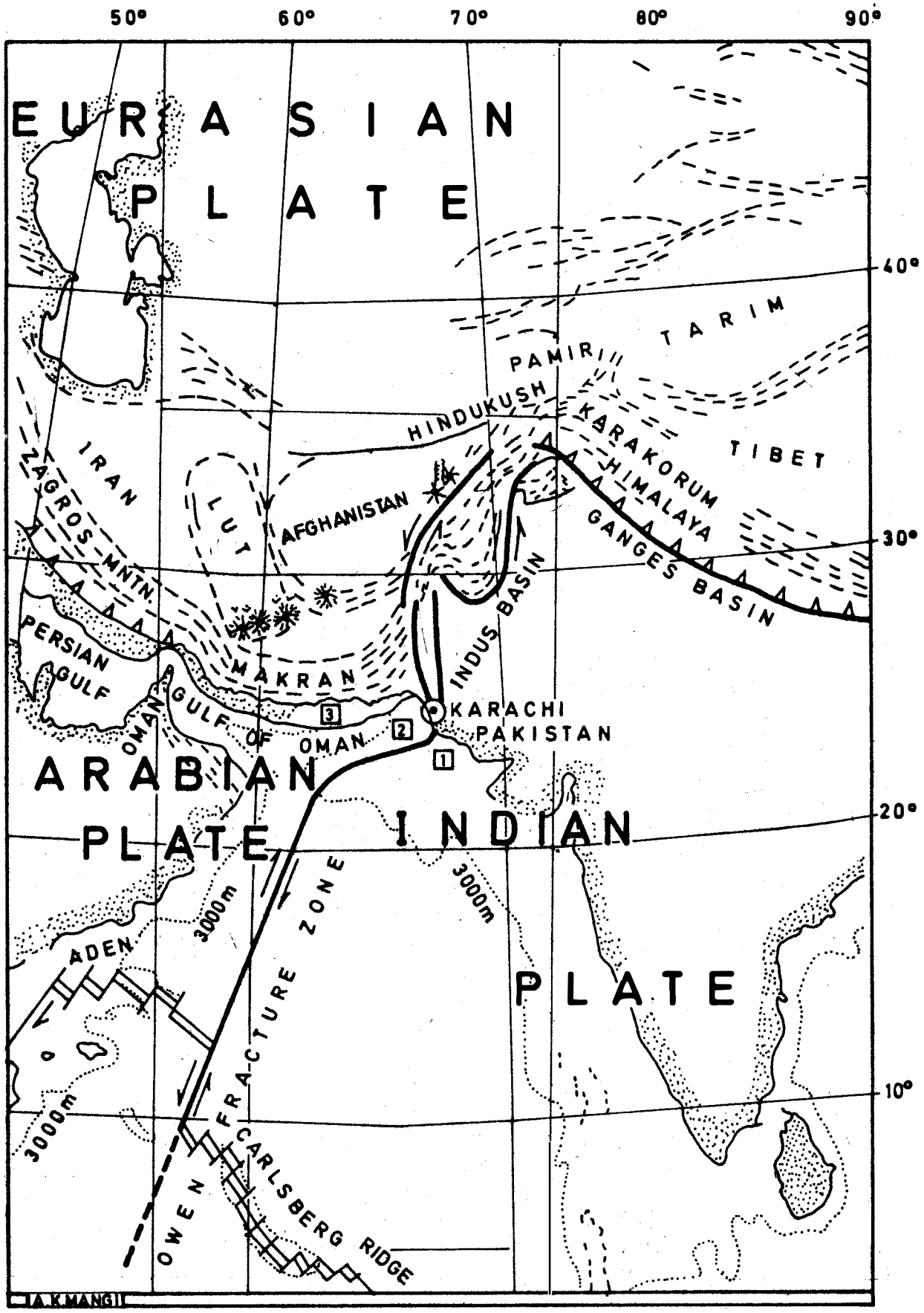

Fig.1. Plate tectonic setting of the Arabian Sea floor.
[1] Passive continental margin. [2] Murray transform domain.
[3] Makran subduction margin.

Work in the Murray Ridge zone and the Makran subduction margin is comparatively sparse. Magnetic traverses were observed in the Murray Ridge Zone and one sample (igneous rock fragments) was dredged from this area during 1961-63 H.M.S. Dalrymple Cruise (Barker, 1966). This was a reconnaissance type study. The Deep Sea Drilling Project (DSDP) of U.S. NSF, leg 23 in the Arabian Sea included two drill holes (222 and 223) which were located on the extreme southern limits of the Murray Ridge Zone (Whitmarsh, Weser & Ross, 1974). Interpretation of gravity data over the Murray Ridge has been reported by White (1979). One seismic reflection traverse oriented SE–NW away from the northern end of Murray Ridge Zone and towards Makran margin is discussed by White (1984).

The geology of the Makran coastal margin is described in some detail by Harms *et al.* (1984) and Leggett & Platt (1984). Gravity and seismic traverses in the Makran subduction zone have been described by White (1979) with information on thickness and structure of the off-shore sediments of the Makran accretionary wedge. Geological and geophysical characteristics and peculiarities of the trench-arc system of the Makran active subduction zone are discussed by Jacob & Quittmeyer (1979).

The present passive continental margin began its marine geological history with the fragmentation of Gondwanaland and separation of India from the eastern margin of Africa about 135 m.y. ago. It was the site of rifting, shearing and crustal thinning during separation followed by passive development for nearly 80 million years during India's northward flight. About 55 m.y. ago initial contact occurred between the Indian plate and the southern edge of Eurasia (Powell, 1979). Since then, the passive margin has been influenced by a vast sediment influx from the rising Himalayan and Balochistan ranges. An understanding of tectonic movement, sedimentation processes and thermal history of the continental margin is very important because it can help in identification of petroleum source rocks and reservoir rocks, in estimating their economic potential, and in delineation of near shore concentration of heavy minerals.

The Murray Ridge Zone, identified as a north-east trending positive feature south-west of Karachi, separates the passive continental margin from the active subduction margin of Makran. It appears to be a continuation of the Owen Fracture zone, extending north-east from it through the Arabian Sea and terminating near Karachi. Its north-eastern end may mark the triple junction between the Arabian, Eurasian and Indian plates. The margin of this ridge towards the Oman abyssal plain may be the site of deposition of metallic minerals.

The Makran subduction zone represents a convergent ocean-continental boundary in contrast to the continent-continent plate boundary west of the Oman line in Iran and east of the Chaman fault in northern Pakistan. Seismic reflection profiles clearly indicate that the flat lying sediments deposited on the Gulf of Oman abyssal plain are deformed into a series of fold ridges adjacent to the Makran coast (White, 1979). The Makran subduction zone is probably a rapidly accreting continental margin, a large portion of which is underlain by a mobile oceanic crust. The petroleum potential of the Makran margin, has not yet been fully evaluated.

The National Institute of Oceanography of Pakistan has launched a long term programme of geological, geophysical, and geochemical studies of the above three geological subdivisions in order to evaluate their resource potential in minerals and hydrocarbons. The mineral prospects are discussed in this paper.

PASSIVE CONTINENTAL MARGIN

The passive continental margin of Pakistan includes the continental shelf and the submarine Indus fan (Fig. 2). The shelf sedimentary sequence lies on cratonic crust and oceanic crust forms the basement of the submarine Indus Basin. The Ocean-continent crust boundary is perhaps located by the 1000m bathymetric

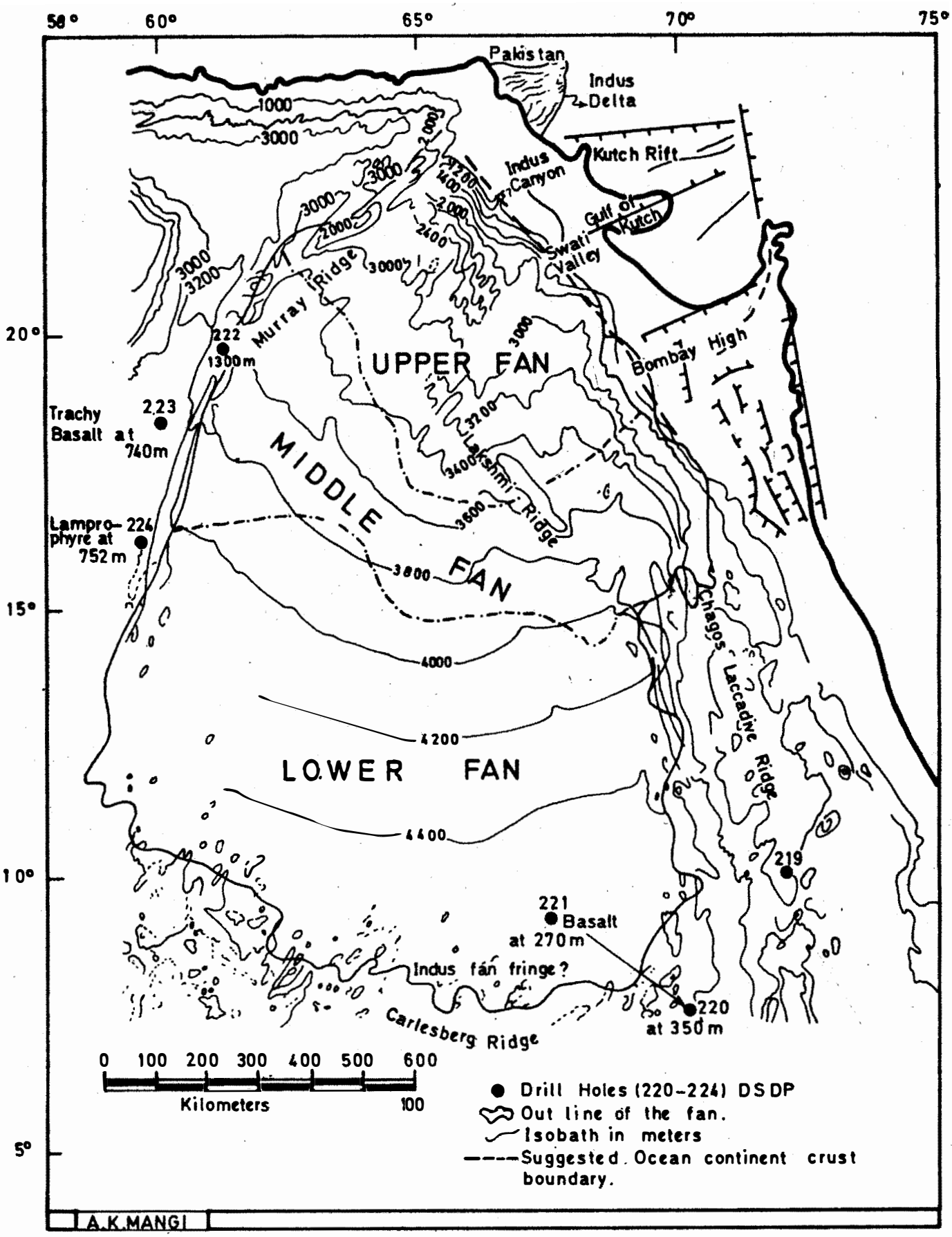

Fig. 2. The submarine Indus fan, and structures (rifting) on the western margin of India.

contour along the Pak-Indian coastline (Fig. 2). Continental structures of the western margin of the Indian craton probably terminate along a megashear which developed in the initial stages of rifting and propagated along the margin. The characteristics of the crustal transition are not known. It may be controlled by a "fundamental fault" along which rifting propagated after separation of India from Africa (Wenyou *et al.*, 1979). The continental margin is passive in the sense that besides the early rifting it has not been subjected to recent tectonic episodes such as those which characterize the collisional zone in northern Pakistan with its foreland fold and thrust belt, the left lateral shear, the transform zone, or the imbricate thrusting at the accretionary prism in the west. There is a southward sequence of the rift tectonics characterized by the younging of the structural trends and features (Biswas, 1982).

The Indus submarine fan is a major morphotectonic feature in the northern Indian Ocean and is the second largest submarine fan in the world (after the Ganges fan) covering an area of about 1.25 million km^2 (500 × Indus Delta). It extends from the Pakistan passive continental margin on the north to the Carlsberg Ridge on the south, a maximum distance of 1600 km and from the Owen-Murray Ridge Zone in the west to the Chagos-Laccadive Ridge in the east, a maximum distance of about 100 km (Fig. 2). The ridges to the west and the east restrict the lateral growth of the fan. Also, reduction in the sediment discharge of the Indus from over 600 million tons/year in 1950 to less than 100 million tons/year at present due to human activities (construction of transfer channels, barrages, embankments, dykes and dams) has markedly checked the growth of the Indus Delta and also impoverished the sediment dispersal in the offshore fan region. A temporal monitoring of the sediment dispersal pattern particularly in the upper fan will reveal the transformation of this interesting geomorphic feature under the sea.

The geological history of the submarine Indus Fan is linked with rifting and northward drift of Indian plate from Gondwana, opening of the Indian ocean, ocean floor spreading, Himalayan tectonics and the evolution of the fold-thrust belt of Kirthar and Makran ranges. On the basis of the provenance analysis of sediments recovered at DSDP sites 220-224 of leg 23 (Fig. 2) it has been suggested that the Indus River, the main source of formation of Submarine Fan came into existence after the Eocene, probably during late Oligocene (White marsh, 1974). The continuous supply of the sediments to the Arabian Sea by the Indus River through submarine canyons and a leved channel system, which has served as a conduit for deep sea sediments from Miocene to Recent time, has been mainly responsible for building up the impressively large submarine fan. We note that the submarine fan is not solely the product of the Indus River. A fairly substantial input of calcareous turbidites was provided from the continental margin in the north and the east during the Pliocene/Pleistocene epochs. Pelagic components were highly diluted by the huge terrigenous sediment contribution. Turbidity currents and tractive currents have played the leading role in the transport of terrigenous material (Whitmarsh, 1974). The overall high sedimentation rate (at times greater than 200 m/m.y. at site 222, DSDP, Fig. 2) represents a faster rate of gray facies (entirely detrital) deposition interspersed with the relatively slow green facies (nanofossil ooze and detrital) period (Jipa & Kidd, 1974).

An important and interesting question in documenting the geological history of submarine fan development is – when did sedimentation begin? There are conflicting views on this question. Coumes and Kolla (1984) are of the opinion that the total sediment thickness (2 to over 5 km) in the upper fan reflects sedimentation since rifting in late Cretaceous period or even earlier. The available geological information from off-shore bore holes and geophysical traverses in the fan region indicate a later beginning to the sedimentation processes, most probably after the collision of Indian and Eurasian plates during the Eocene epoch. Ewing *et al.* (1969) suggested a middle Miocene age for the initiation of sedimentation processes in the submarine fan. During Paleocene to Oligocene time, this area of the Indian margin was dominat-

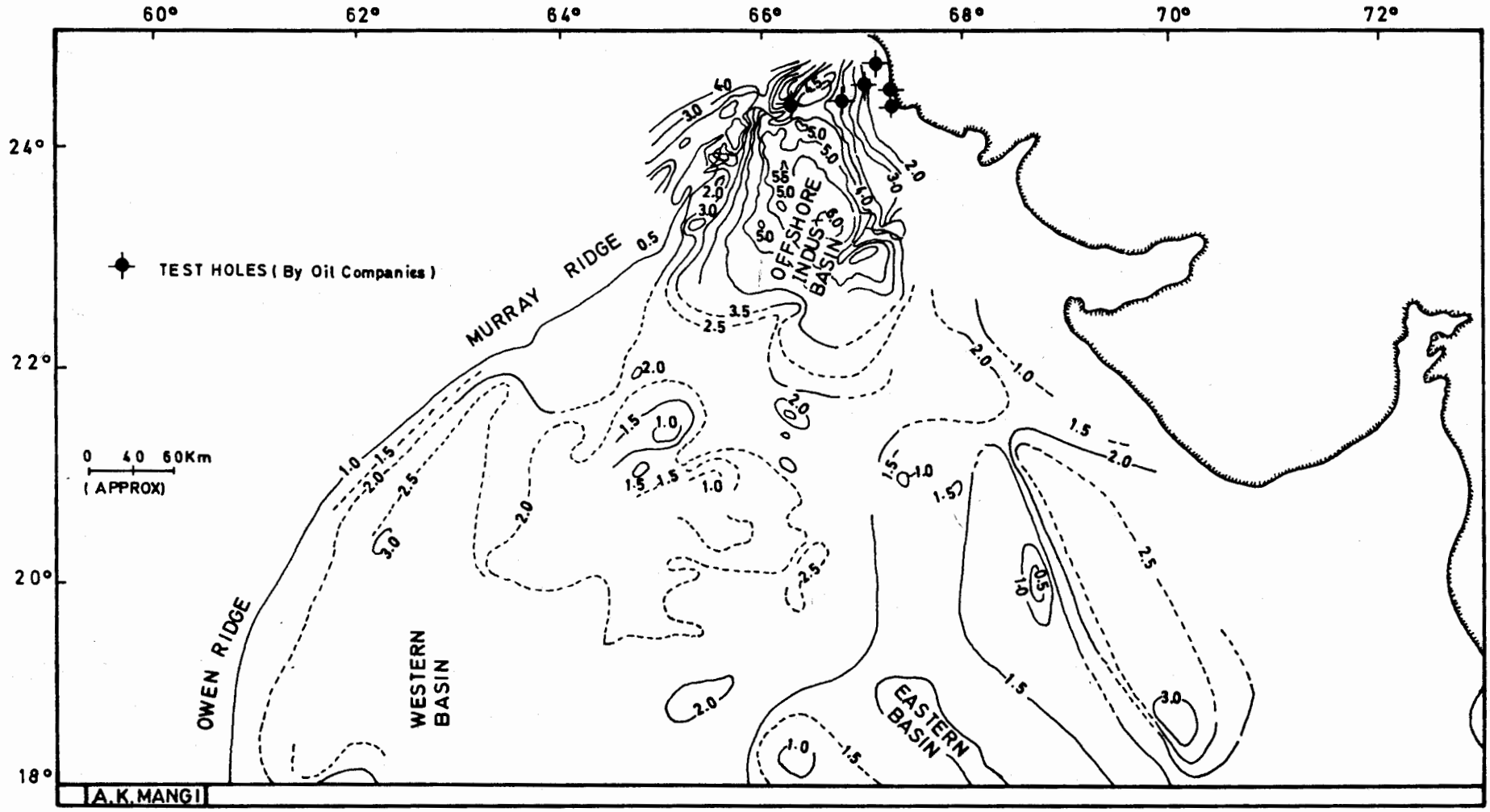

Fig.3. Sediment thickness distribution in kilometers (approximate) in Indus off-shore basins.

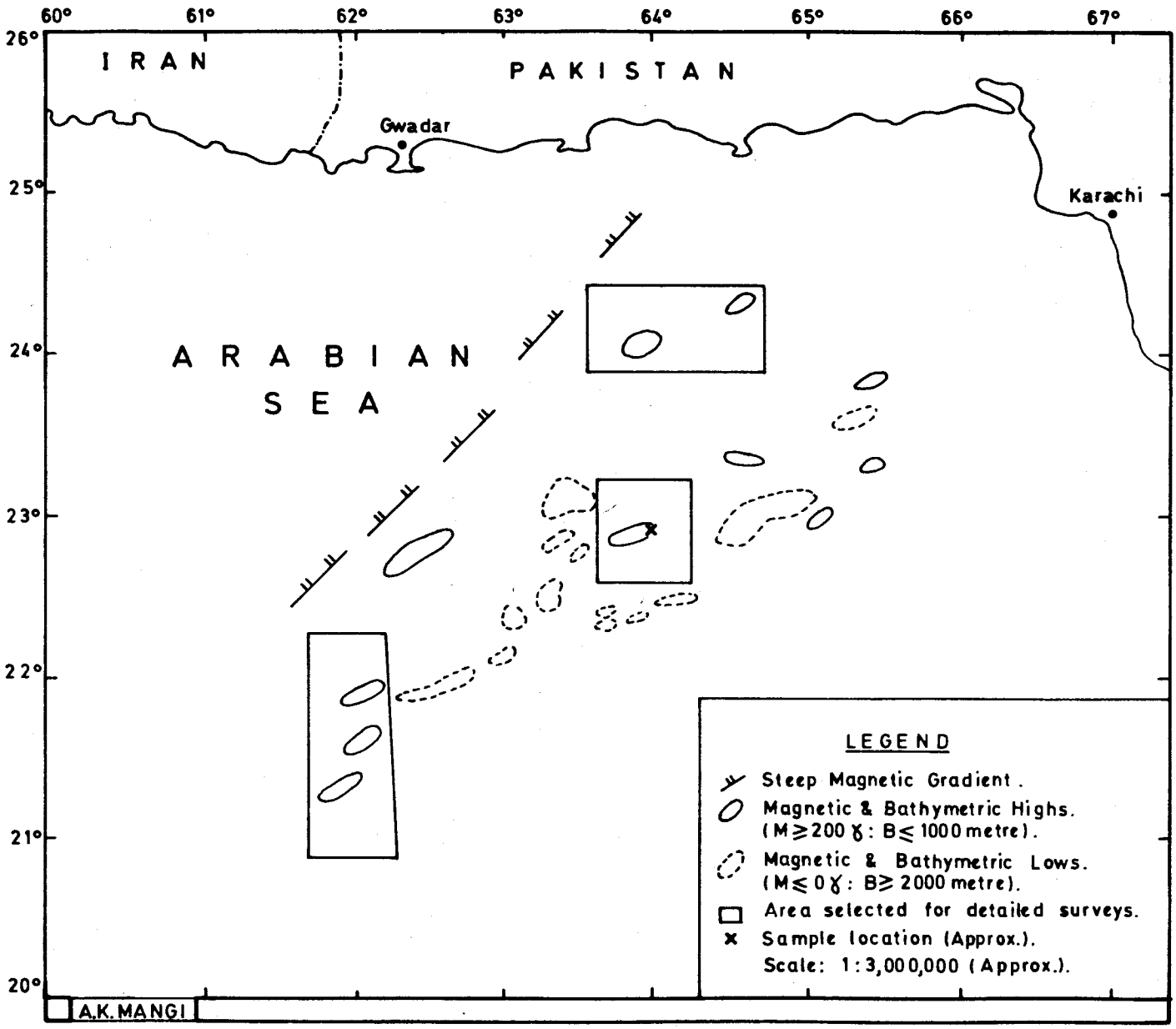

Fig. 4. Magnetic and bathymetric closures in the Murray transform fault domain.

ed by the Khojak fan (Lawrence & Khan, in press) which would be the predecessor of the Indus fan. The significant Cenozoic vertical uplift and extensional structures noted in the Makran Coastal areas (Harms *et al.*, 1984; Arthurton & Farah, 1982) and the interpreted extensional structure of off-shore Indus Basin contemporaneous with the uplift of the Himalayas support the view that the sedimentation in the submarine Indus Fan began in the early Oligocene epoch. The consensus appears to be on Oligocene age for the initiation of the sedimentation processes in the Indus submarine fan. Only a deep test hole reaching the basement in the upper fan region will provide the answer.

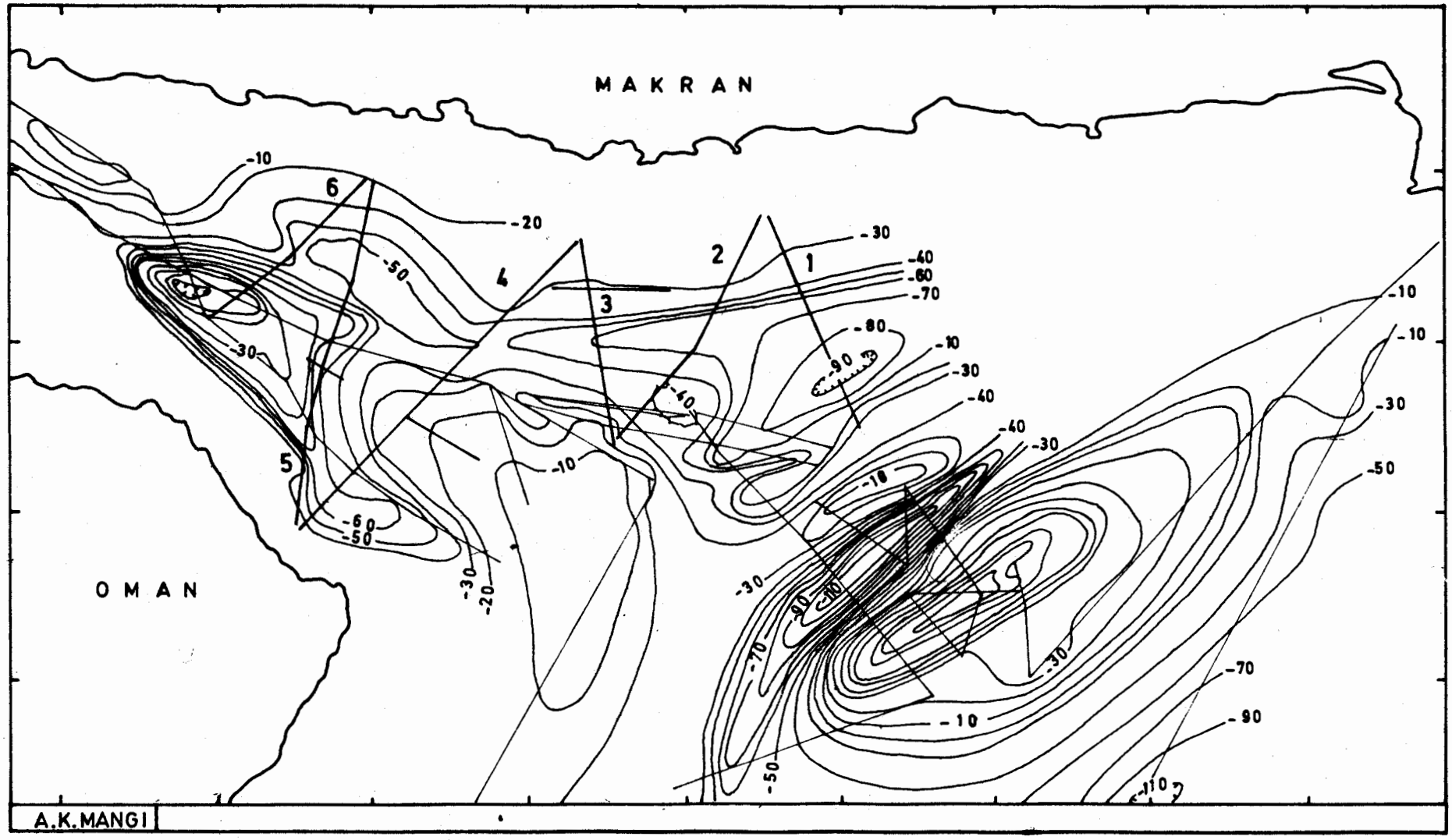

Fig. 5. Free air gravity map of the Gulf of Oman. Track control from RV METEOR (1965), and RRS SHACKLETON (1975). Shown as thin lines. Contour interval 10 milligal except in regions of high gradients over Murray Ridge, where it is 20 milligal. Free air anomalies were obtained using the 1930 International gravity formula with earth flattening of 1/297.0 and base values tied to the First Order World Gravity Network for which the gravity value at Potsdam is 981.274 gal. Seismic profiles (1–6) recorded by RRS Shackleton.

Another important question which remains unresolved relates to the delineation of ocean-continent crust boundary on the passive margin. This is a very important geological parameter in hydrocarbon exploration. The possibility of Mesozoic hydrocarbon prospects is bright in the area east of the ocean-continent crust boundary towards the platform part of the Indian plate. It is suggested here that the boundary (ocean-continental crust boundary) is approximated by the 1000 m isobath parallel to the regional trend of the coastline (Fig.2). Detailed geophysical observations (gravity and seismic) along traverses originating in the south-eastern part of the Indus Basin in the upper fan will both delineate the ocean-continent crust boundary zone and determine if it is characterized by faulting and shearing or by normal merging of slope-shelf sediments towards the eastern margin of the submarine Indus Fan. In the off-shore Indus basin and in the area occupied by the canyon leveed channel system in the upper fan there is a possible target for finding hydrocarbon prospects of the Cenozoic era.

MURRAY RIDGE

The Murray Ridge is a prominent physiographic feature on the floor of the north Arabian Sea. It consists of seamounts, scarps, and small basins in a linear pattern extending from continental slope near Karachi over 750km towards the south-west where it joins the Owen Fracture Zone and ridge – ridge transform fault (Carlsberg ridge and Gulf of Aden Ridge; Fig. 1). It has a relief of 2000 m in the middle part and as large as 3500 m on the southern part. It curves eastward near a location 22°N, 62°E, probably in response to local change in the regional stress field (Fig. 1). The main ridge of the western Indian Ocean, the Carlsberg Ridge system was discovered during the Dana Expedition of 1928-30 and was more fully outlined by the John Murray expedition. The Murray ridge was originally treated in these pre-plate tectonic studies as a branch of Carlsberg Ridge extending north through the Arabian Sea. It was regarded by some as analogous to the Rift Valley System of Africa and by some other workers it was regarded as a seaward extension of the structure of Sind (HSC, 1960).

In modern global plate tectonics model the Murray Ridge has a very uncertain role and a brief comment on it has been attempted here. Geological and geophysical (magnetic) surveys of this significant feature were carried out on the H.M.S. Dalrymple by the Geophysical Department of Imperial College, between October, 1961 and March, 1963 (Barker, 1966). A dredged sample was obtained during this expedition from a depth of about 550 m from a location (22° 45'N and 64° 10'E) in the middle of the ridge system (Fig. 4). On the basis of the bathymetric survey this location is on a feature which appears to be a seamount elongated in a northeasterly direction at a minimum depth of about 350 m. The dredged sample contains 15 angular fragments of linear dimension from 0.25 to 3 cm. The fragments were mostly tuff and variolitic or spilitic basalt with one micro-diorite and one red fine-grained (tuffaceous) sediment fragment. The magnetic susceptibility of the specimens varies from 2000 to 3 X 10–6 Cgs units indicating a maximum magnetite content of about 1%. The basalts and tuffs were weathered and altered and veined with feldspar, carbonates, and zeolites (Barker, 1966). This is suggestive of a high degree of hydrothermal alteration of the basaltic rocks and as such the Murray Ridge system may be a favourable environment for the occurrence of polymetallic sulphides. On the basis of reconnaissance bathymetric and magnetic surveys (Barker, 1966), nine features in the northeasterly rectangular area of Murray Ridge (called Murray Transform Domain in this paper) have been identified (Fig. 4). Most of these have been interpreted as seamounts. The positive magnetic anomalies are of the order of 200 to 600 gammas and show correlation with the bathymetric features. These anomalies are dipolar and the magnetic gradient and disposition of the poles indicate a very shallow source of the anomalies. These northeasterly features are bordered by a strong magnetic gradient which indicates the termination of the Murray Ridge on the western side. Free-air gravity anomalies confirm the northeasterly elongated trend of the Murray Ridge (Fig. 5, after White, 1979). The gravity anomaly map shows a positive closure on the area occupied by the scattered seamounts which are distinguish-

able on the magnetic anomaly map. The gravity closure is marked by a very high gradient on the western side as is also seen in the magnetic anomaly map. This supports the interpretation that major faults are important structures on the Murray Ridge.

Modern seismicity is prevalent in the northeastern portion of the Murray Ridge (Quittmeyer *et al.*, 1979). The level of activity has been low. The largest event had a magnitude of 6. From focal mechanism solutions of two events (April and November, 1968) right lateral strike-slip motion has been interpreted. The motion may contain extensional or rifting component (McKenzie, 1971). Similar motion has been inferred on the Owen Fracture Zone farther to the southwest. However, this interpretation is based on only one focal mechanism solution (Sykes, 1970).

The limited information and the few constraints on the known properties, both geological and geophysical, on the Murray Ridge render any comment on its origin rather speculative. Whether the Owen Fracture Zone and its continuation as the Murray Fracture Zone (1) was caused by the opening of the Gulf of Aden, or (2) is an expression of an older lineation (Tranform Fault-Primary Fault) connected with the Ornach-Nal/Chaman fault (Lawrence *et al.*, 1981) along which the Indian Plate moved northwards relative to the Afro-Arabian Plate, is unclear. Barker (1966) finds it improbable that the Murray Ridge is part of the Oman-Pakistan geosyncline since the ridge is submerged and is in isostatic equilibrium. This isostatic equilibrium is more compatible with large shear movements. He focuses on the northeasterly trend of the Murray Ridge and the similarity in the lithology of the dredged samples with the serpentinized and spilitic extrusive rocks of the Las Bela-Muslim Bagh geanticline. These rocks are now explained as obducted ophiolites (Abbas & Ahmad, 1979; Farah *et al.*, 1984). Whitmarsh (1974) in his interpretation of the apparently extrusive rocks (spilitic basalt, microdiorites, gabbro, lamprophyre) recovered at sites 223 and 224 of leg 23, Deep Sea Drilling Project of US National Science Foundation from the southwestern extremity of Murray Ridge System (Fig. 2) suggests that "if these igneous rocks are assumed to be a little older than the overlying sediments (Paleocene-Eocene) then these igneous rocks may be younger (about 10 my.) than the 90 my. old rocks in western Somali Basin. It is very likely that the extrusive rocks in the Murray Ridge are of the same age as those in the Owen Fracture Zone. Whitmarsh (1974) is of the opinion that "it is likely that this unusual petrology (for oceanic areas) is due to the proximity to a transform fault and does not represent a widespread region of anomalous rocks west of Owen Fracture Zone"

The Murray Ridge System along with the Owen Fracture Zone probably marks the trace of the present boundary between the Indian and Arabian Plates and its northeastern end marks the triple junction of Arabian, Eurasian, and Indian Plates (Jacob and Quittmeyer, 1979). The Murray Ridge System is probably in the Transform Fault domain and refers to a plate boundary undergoing strike-slip motion in the sense of a general definition of a transform fault (Kastens, 1987). Like the San Andreas fault of California, it is a transform fault but not part of a fracture zone. The motion along this fault has been oblique and the rotation of the plate motion should have influenced the stress regime in the transform domain–a term implying in a broad sense, a zone in which lithospheric properties are influenced by distributed shear. It is difficult to grasp and explain the motion history and the development of the geometry of this interpreted transform fault. However, the present information indicates that the setup in relation to Murray Ridge is (1) in the Carlsberg ridge which has Indian Ocean and Aden/Red Sea portions, (2) in the north the Makran subduction zone and Chaman transform zone, (3) the Owen fracture zone which connects the two. The Owen fracture zone accommodates differeces in the velocity of the Indian and Arabian plates with the opening of the Gulf of Aden. The Murray Ridge is a complex structure probably stemming from Owen fracture complex and influenced by the Makran subduction. We do not clearly understand the position

and role of the Murray Ridge in the setup mentioned above. Our interpretation which is certainly debatable is that the Murray Ridge is a portion of the Owen fracture which is geometrically out of line. As such, it would have transform component and a smaller component of either convergent or divergent motion (Fig 6). Divergent motion will occur when the Arabian plate moves north faster than the Indian plate. These kinematics would produce a leaky transform on which basalt and other ocean rocks would be erupted at randomly distributed locations. Such being the case the Murray Ridge has partly an oceanic ridge character in a basically transform environment. If the Indian plate moved faster convergent motion would occur producing transpression with ocean floor thrusting in which a portion of oceanic crust is thrust eastward over the oceanic floor (Fig 6) which would mean oceanic obduction. The later situation would be the one for the Murray Ridge to from as an ophiolite suite fragment related to Las Bela ophiolite (Lawrence, 1986). Clearly both of these two situations could have prevailed in Murray Ridge domain at different times historically and transpressional ridges and extensional basins were formed (Reading, 1980). It is common to observe bathymetric deeps in Transform domain. Such bathymetric deeps on a localised scale have been referred as "nodal basins" by some workers (Phillips & Fleming, 1978). In case of a Transform fault with oblique strike-slip motion, the curvature may generate alternate zones of basins and ridges within the Murray Ridge domain (Fig 7). The similarity of the lithologies of the Murray Ridge dredged sample and Las Bela ophiolite supports the suggested origin. Coleman (1981) interprets the data on the ophiolite of Oman as requiring thrusting of a hot ridge fragment over deep margin sediments in an oceanic regime. The Murray Ridge may possibly be such a thrust fragment that was never pushed farther onto the continental margin (Lawrence, 1987). If this is true it suggests that the Murray Ridge provides an ophiolite mass for study that is still on the sea floor and has never been obducted in the manner in which Las Bela ophiolites have been obducted.

It may be summarised that the Murray Ridge in all probability is in a transform domain where the lithosphere is essentially conserved, i.e. it is neither created nor is consumed. It is characterized by oblique strike-slip motion, transpressive and extensional features (ridges and basins), seismicity, varied sedimentation and magmatic activity in leaky parts of the transform fault. A model related to Carlsberg ridge-ridge transform and Makran subduction margin is to be developed for the Murray Ridge. Reading (1980) has made a very interesting remark pertinent to our case that probably the most intriguing question in global tectonics today is—whether the primary features of global tectonics are spreading centres and subduction zones, or whether they are the long-lived lineaments expressed as fundamental faults in continents and fracture zones in Oceans."

The National Institute of Oceanography in collaboration with Pakistan Navy has planned a one month cruise for the survey of Murray Ridge region on board the R/V Behr—Paima. In this cruise programme a rectangular area of 122, 500 sq. km. between latitudes 20° 30′ – 24° 25′ and 21° 30′ – 25° 22′ N; longitudes 61° 25 67° 10′ and 60° 40′ – 66° E will be covered by gravity, magnetic and seismic profiling and core samples will be obtained from selected locations. The results of this survey will enable us to resolve some of the debatable points mentioned above.

MAKRAN SUBDUCTION ZONE

This subduction margin has unusual properties. It has (i) an unusually wide trench-arc gap (ii) shallow seismicity (iii) a buried trench (iv) and a complex stress regime. These atypical features are related to peculiarities in the subduction process in this area. Extensive forearc flysch sedimentation of Eocene through Miocene epochs produced very rapid progradation of the accretionary prism which probably obscured the development of a typical topographic trench. On the basis of a ship-borne seismic survey comprising continuous seismic profiles and variable angle reflection-refraction

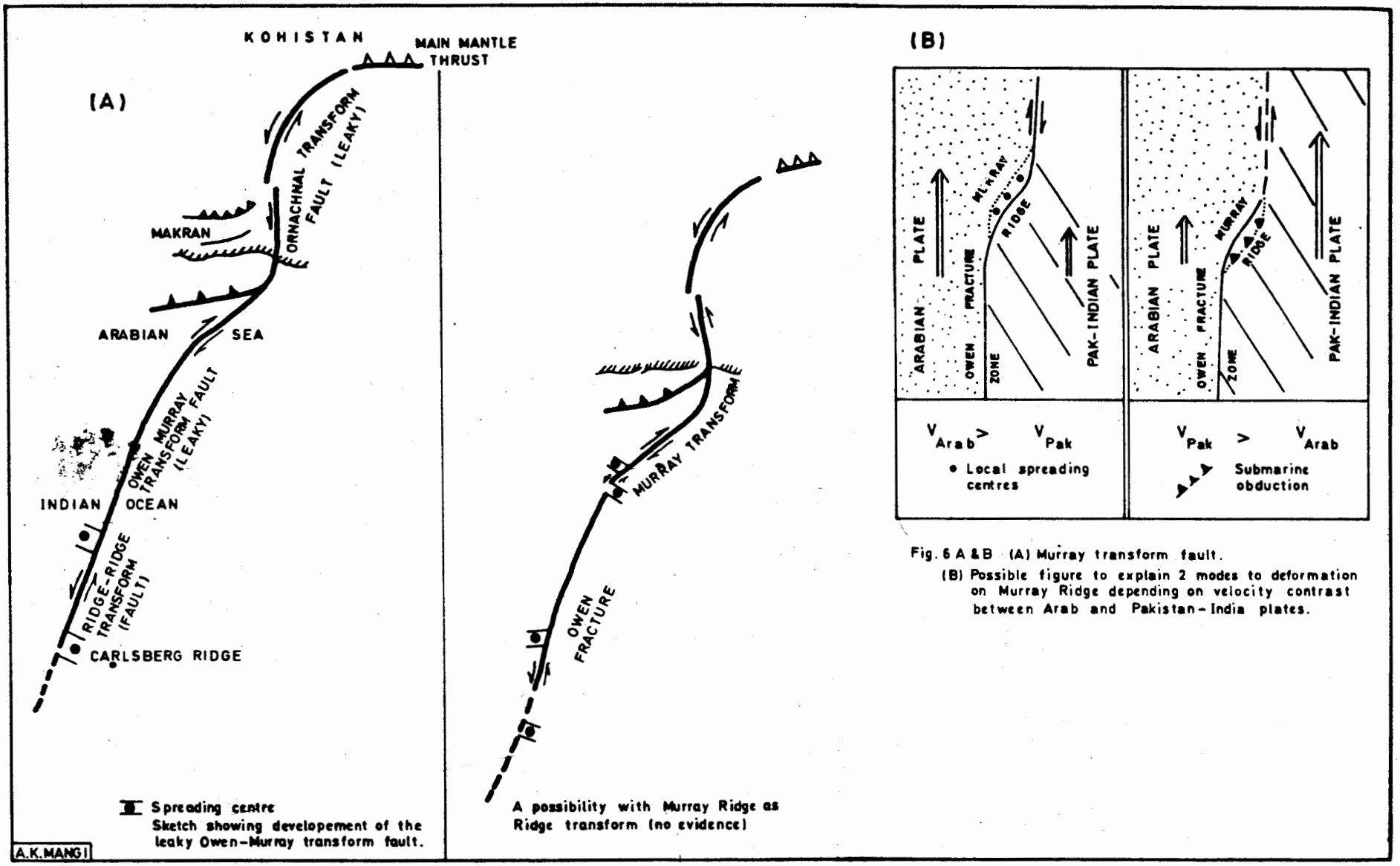

Fig. 6 A & B (A) Murray transform fault.
(B) Possible figure to explain 2 modes to deformation on Murray Ridge depending on velocity contrast between Arab and Pakistan-India plates.

profiles in the eastern part of Iranian Makran (Fig. 5), White (1979) has interpreted that only the upper 2.5 km of the 5 km thick sediment pile is initially folded (Fig. 8). The sedimentary sequence has two well defined reflection boundaries marked, A&B in Fig. (8). Sediments above "A" are flat lying while the beds below "A" down to "B" dip uniformly at a very gentle angle of about one degree towards the Makran Coast. Reflector "B" comprises an irregular series of hyperbolic echoes which mark the base of the sedimentary deposits. It dips gently beneath the continental margin and probably marks the top of the descending oceanic crust.

Jacob and Quittmeyer (1979) in their review of geophysical and geological information conclude that "oceanic portions of the Arabian plate presently subduct northward towards Eurasia with a relative motion of about 5 cm per year". Only moderate seismicity occurs in the shallow-dipping thrust zone. At subcrustal depths the dipping seismic zone has a weak and sporadic expression to depths of only 80 km, and it is not documented at greater depths. The volcanic arc is poorly developed with large spacing (100 km) between its major volcanic centres. The trenchvolcano gap measures over 500 km, more than twice the width of a typical trenchvolcano gap. In another brief review (Farah *et al.*, 1984) the features of the Iranian Makran and those of Pakistani Makran have been compared, the differences have been emphasised and the peculiarities of Pakistan subduction margin have been highlighted.

The atypically wide trench-arc gap (Makran-Chagai) is probably a result of the shallow inclination of the descending plate rather than the depth of generation of the magma as shown in Fig. 9. Strontium isotope composition (87/86) and chemical composition (K_2O/SiO_2) of the

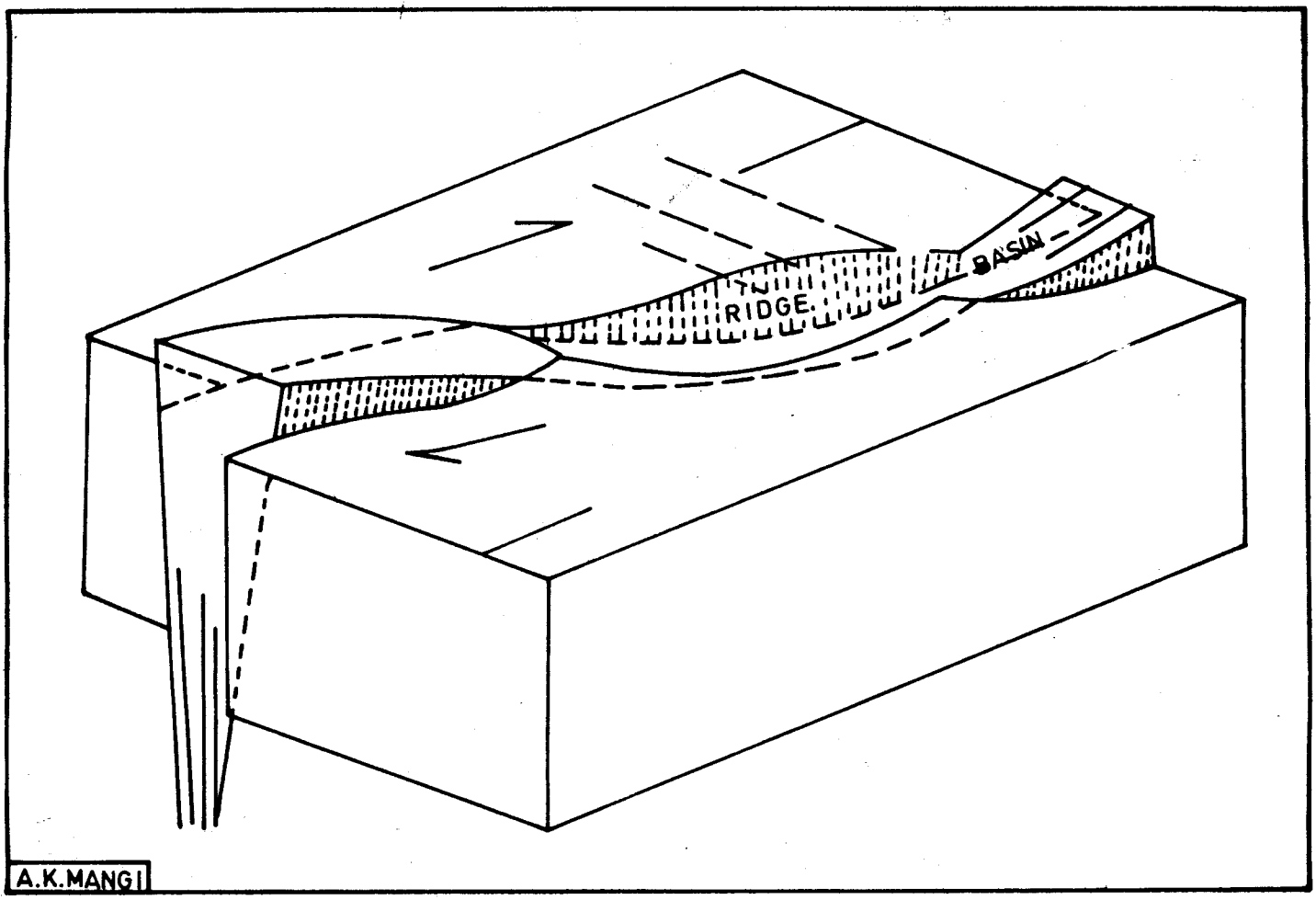

Fig. 7. Extensional subsiding basin and compressional uplifted block in a strike fault domain with oblique motion.

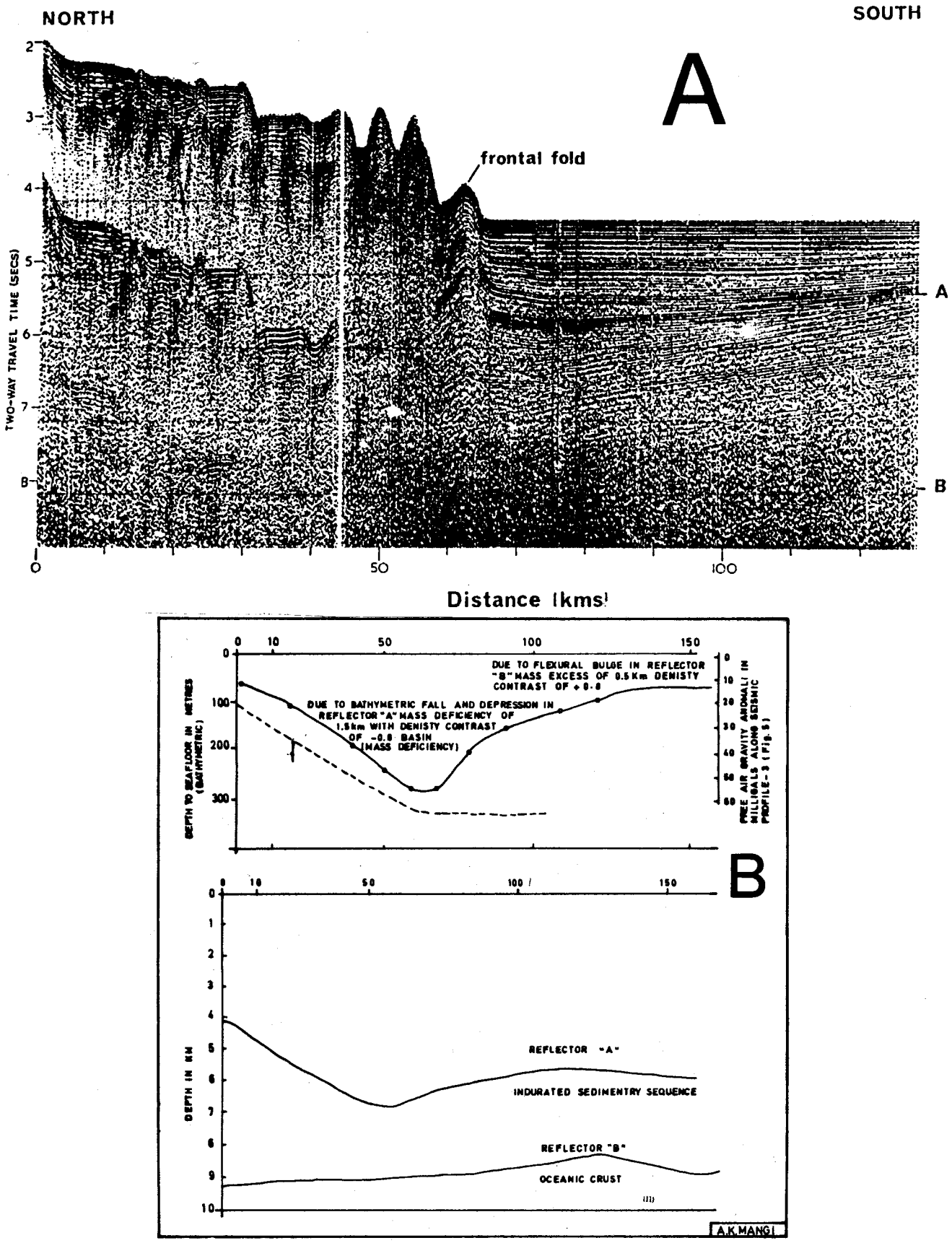

Fig. 8. (A) Continuous seismic profile along line 3 across theMakran continental margin. Notice the frontal fold 65 km, the inter-fold basins partially filled with sediment between 40 and 60 km and the ridges buried beneath secondary sediment between O to 40 km. Horizon 'A' divides the topmost flat-lying sediments from uniformaly-dipping layers below. Horizon 'B' is the deepest observable reflector, comprising numerous hyperbolae. Profiling system used a 2.6 litre (160 cubic inch) airgun fired once every 10 seconds. Linear time-variable gain and 5–80 Hz band pass filtering has been applied to the signal. Vertical exaggeration at sea floor approx. 10X. (After White, 1979).

(B) Interpreted subsurface configuration along line 3 of the continuous seismic profile (Fig. 5).

rocks across the Raskoh-Chagai arc may clarify the situation as has been done in other parts of the world (USA, Japan, Indonesia) reported in the special issue of GSA Bulletin on "Subduction of Oceanic Plates" (Gastil, 1982).

Probably the rapid sedimentation is responsible for inhibiting the development of a typical trench, for shallow inclination of the descending plate and for the shallow seismic zone. Generally it has been interpreted that in the accretionary domain, sedimentary material is added at the front of a subducting plate. However, some accretionary complex like the Nankai Trough (SW Japan) involves underplating in which case the sedimentary material is added to the base of the upper plate underneath (Leggett *et al.*, 1985). In case of the Makran subduction margin it appears that both the processes play their part. The sediments above the reflector "A" in (Fig 8) are being imbricated to the front of the accretionary wedge and those below "A" down to the reflector "B" are probably being underplated to it. If the Koh-e-Sultan volcanic arc, nearly 500 km north of the coastline, is genetically related to present day subduction, then a southward progradation of the deformational front may be postulated.

The stress pattern of this subduction margin is also complex. Active thrust tectonics in the accretionary wedge of the Makran show that compessive stress is dominant in the region, a property common to all major subduction margins (Jarrard, 1986). However, significant vertical uplift and extensional features have been noted in the coastal area. Several significant normal faults with large displacements (up to 2500m) have been noted (Harms *et al.*, 1984). The normal faults appear to continue in the off-shore region and trend approximately parallel to the coast. Such an extensional environment, with maximum horizontal extension approximately perpendicular to the trench is not unusual in active subduction margins. It is commonly associated with the oceanic crustal bulge off-shore of the trench. Such a bulge has not previously been recognized off the Makran coast, but our compilation of the off-shore gravity data (Fig. 8) is best interpreted as showing the presence of a bulge. The extensional environment near the coastal margin may be interpreted as a pull-apart above the neutral plane of the bending slab. A comprehensive description and the understanding of the dynamics of the subduction process of the Makran margin require data on several parameters and a multivariant analysis of the correlation of these parameters as has been done in case of other subduction margins (Jarrard 1986). These parameters relate to the geometry of the descending plate and its rate of convergence in relation to the upper plate. This involves a long term programme of study and the National Institute of Oceanography, Pakistan is endeavoring to develop the capabilities for conducting such studies in collaboration with Oregon State University and the Geological Survey in U.S.A.

From an appraisal of the available geological and geophysical information discussed above four properties of the Makran suduction accretion complex are clear. (1) The sedimentary material in the accretionary domain is being added at the front of the subducting plate which generally is the case and also underplating is taking place. (2) The subduction-related accretionary sediment of Makran is probably emplaced in imbricate thrust sheets in a manner similar to that observed on the inner walls of many other subduction zones, e.g., in the Barbados subduction zone. (3) Rapid sedimentation is responsible for inhibiting the development of a typical topographic trench to mark the subduction margin. (4) The gentle inclination of the descending plate has caused the unusually wide trench-arc gap and shallow dipping Benioff-Wadati seismic zone.

ECONOMIC POTENTIAL

The economic potential of the off-shore region of Pakistan in terms of non-living resources, i.e., hydrocarbons and minerals, has not been explored. The exploration effort for oil and gas is in its infancy. Only four exploratory wells have been drilled in the off-shore Indus Fan and only one on the Makran margin. Almost nothing is known about the mineral potential. In view of the location of off-shore non-living resources as shown in Fig. 10 the marine geological

environment of Pakistan's exclusive economic zone (EEZ) is favourable for the formation of these resources.

The possibility of finding oil and gas in the passive margin east of the Murray Ridge is very bright. Two environments need to be explored. East of the continent-ocean boundary one should look for Mesozoic source rocks and structural or stratigraphic traps related to rifting of the continental margin. In the off-shore Indus Basin (Fig. 2), there are possible hydrocarbon deposits in Cenozoic reservoirs of the canyon-leveed system in the submarine upper Indus fan (Fig. 2). A study of the sedimentation pattern, facies and geometry in the Canyon channel levee complex area will reveal the promising hydrocarbon facies. In a canyon leveed channel system the morphological features and sediment distribution pattern grade in three zones: degradational, transitional, and aggradational (Mechargue & Webb, 1986). The degradational pattern prevails in the inner part of the upper fan and is characterised by the presence of erosional canyon floors and walls and by the absence of levees. Seismic reflectors in such canyon complexes generally display low amplitude and discontinuous facies (LAD) suggestive of a nearly homogeneous lithology of the canyon fill. In the transitional stage, there is still an erosional base, but levees flank the channel. The internal structure of this zone is complex. The aggradational zone occupies the lower part of Canyon-channel system where the erosional process is almost and the channel complex is completely confined by its levees which are usually large and attain a vertical relief of 200-300m above the surrounding fan surface. In general, the internal seismic expression of the feature in this zone is characterised by low ampitude and continuous reflectors (LAC facies) indicating muddy deposits. With regards to the petroleum potential in the upper submarine Indus fan the most promising area would be in the transitional zone where the seismic facies of high amplitude and discontinuous distribution (HAD facies) may constitute a good reservoir of coarse clastic sediments with the overlying layers/lenses of mud producing low amplitude-discontinuous reflections (LAD facies) which may act as seal beds. As the source beds in the submarine Indus fan the indications are very encouraging although no direct evidence is available. At present a sizeable oxygen minimum zone (less than 0.5 ml per litre of O_2) extends from depths of 100-1500m along the northern margin of the Arabian Sea because of poor oceanic circulation (Demaison & Moore, 1980; Quraishee, 1984) and organic carbon is preserved in unusually high concentrations (2–10%) in the sediments in contact with this column of water. The circulation pattern within the Arabian Sea has not probably changed much since Eocene time and also a sedimentary sequence of over 6 km thick in the Indus Fan Basin should be thermally mature. Therefore, abundant and rich source beds may be present under the Indus submarine fan. It is suggested that the seismic exploration target in the submarine basin of Indus should be the delineation of high amplitude-discontinous seismic facies (HAD facies) overlain by low-amplitude discontinuous facies (LAD) at depths of 3–5 km.

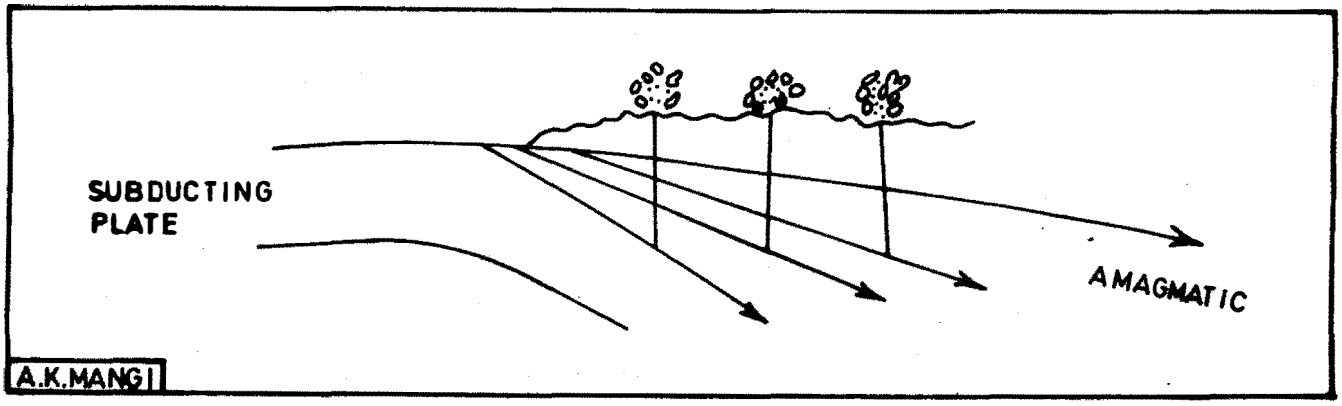

Fig.9. Different inclination angles of subducting plate.

The Makran subduction margin is a rapidly accreted margin underlain by a mobile oceanic crust, not usually considered a very favourable hydrocarbon environment. As for the existence of favourable structures Harms *et al.* (1984) made an interesting remark "certainly there is no dearth of structure". Both on-shore and off-shore such structures are known to exist. Detection of such structures at shallow depths through surface and subsurface investigations lured the oil companies to undertake almost prohibitively costly operation of test drilling in the remote region of Makran in the late fifties and early sixties. The failures daunted the daring ones. Still, the area both on-shore and off-shore is rated as high cost and high risk. The critical questions that are to be resolved relate to the evaluation of the quality of soruce rocks, degree of thermal maturity and the properties of reservoir rocks. As for the on-shore source rock quality the investigations carried out by Hydrocarbon Development Institute of Pakistan and other agencies indicate that it is "lean to adequate" with total organic carbon ranging from 0.2% to 1%. However, indications are that there may be a thickening of mudstone deposits across the slope basin off the Makran coast (White, 1984) which may have higher (2%) total organic carbon content and could prove good source rock. The possibility of good reservoir beds is strong. The sandstone beds deposited by turbidity currents in the middle Miocene are reckoned the best in terms of fine-to-medium-grain size, lack of clay matrix and proximity to the deeply buried source rocks. The main question is the thermal maturity of the source material to the stages of catagenesis-metagenesis (Hunt, 1984). The rapid deposition of the accretionary wedge and rather low temperature gradient (1 F/100 ft) measured in wells drilled on shore suggest limited chances of maturation and hydrocarbon evolution. However, the presence of active mud volcanoes with methane gas escaping may hint of greater possibilities. In view of these considerations the most promising off-shore area is south of Pasni where potential reservoirs could be researched within a few thousand feet (Harms *et al.*, 1984). The Makran's potential has not yet been fully evaluated, and no exploratory well in the Makran has yet achieved its actual exploration target.

The Murray Ridge domain as a leaky transform environment may prove a good area for occurrences of polymetallic sulphides. If the idea of an inplace ophiolitic sequence in this domain presented above is correct, there is a strong possibility of finding zinc and copper rich sulphides here. Also, manganese crusts enriched in cobalt sometimes occur as coating on hard substrates such as basalt in such regions. The seamounts surfaces with a thin cover of sediments in the Murray transform domain may prove promising places for accumulation of both manganese and cobalt. The coastal zone of shallow bathymetry west of Karachi may be dotted with small concentration of placer minerals like iron sands, rutile, zircon and monazite.

The possibility of exploiting constructional materials such as sand and gravel from the near shore belt especially along the Makran Coast is promising. Off-shore supplies of sand and gravel are now supplementing land-based sources in many countries (Canada, Denmark, France, Netherland, Nigeria, Sweden, U.K., U.S.A.). It is interesting that Japan and Great Britain obtain about 35% and 20%, respectively, of their sand and gravel requirements from off-shore. The off-shore source of constructional material will be exploited on a large scale in future.

CONCLUSIONS

The geological features and the history of their development in the off-shore region of Pakistan, are of interest and significance in the context of global plate tectonics. The three distinguishable features are: passive continental margin including the submarine Indus Fan, the Murray Ridge oblique transform zone, and the Makran subduction active margin. These are reckoned to be of economic importance as well. The passive continental margin and the subduction margin may have promising hydrocarbon potential and in the transform fault domain sizeable deposits of poly-metallic sulphides could be found. The geological and geophysical information and data of the off-shore region of

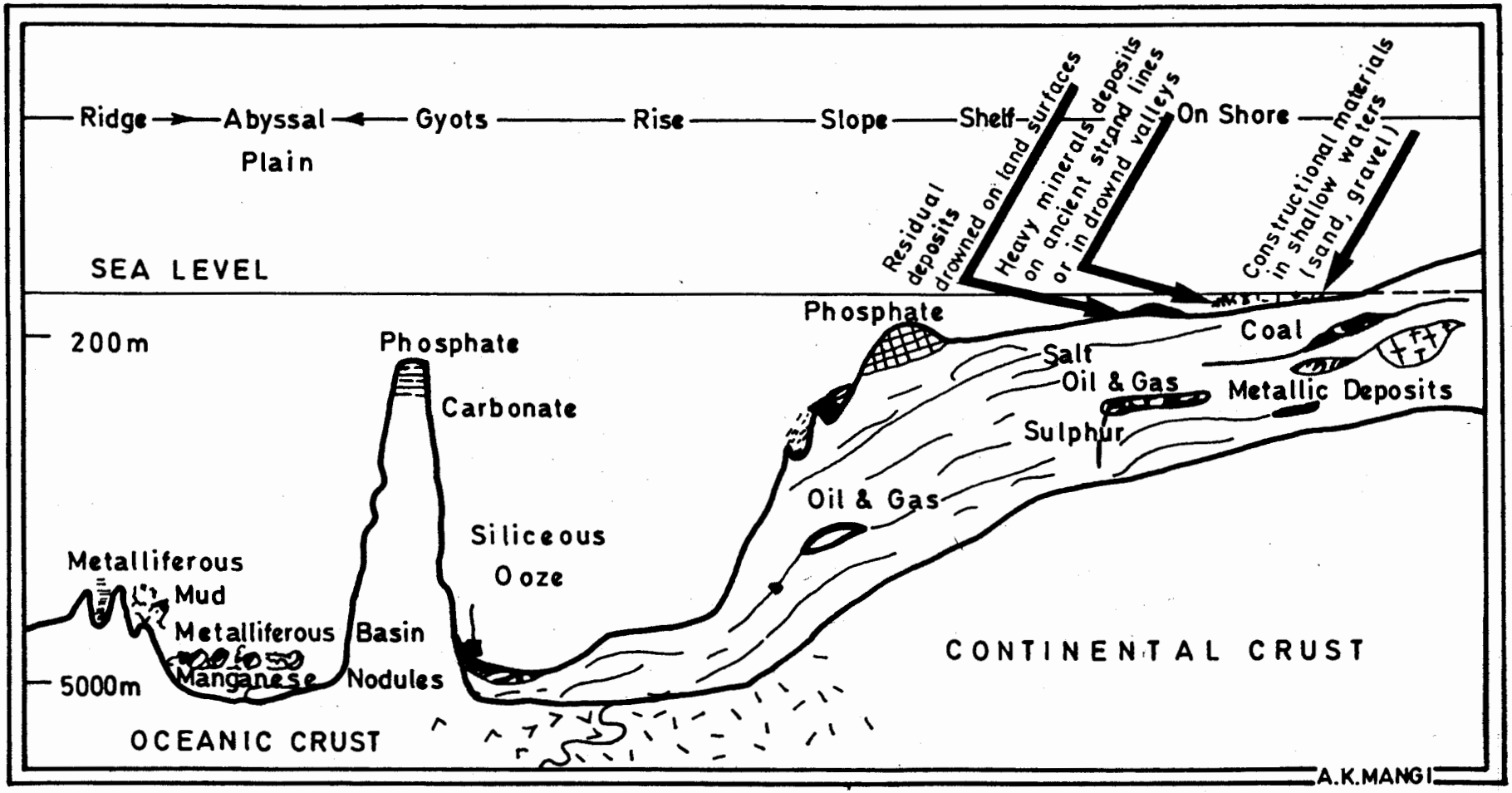

Fig.10. Schematic representation of the structure of continental margin and adjacent ocean, and the probable locations of minerals and hydrocarbon deposits. After Cook (1975).

Pakistan are sketchy and scanty. The major issues to be studied and resolved in the three geological provenances leading to a plausible evaluation of the economic potential are: (i) delineation of ocean-continent crust boundary and the tectonic history of the submarine Indus basins on the passive continental margin, (ii) geodynamics of Murray Ridge: is it a leaky transform fault marking the plate boundary (Indian & Arabian) comparable and connected to Chaman Transform boundary on land or has it a spreading ridge component (iii) determine the geometry of the Makran subduction margin and develop an acceptable model to explain the shallow seismic zone, absence of a typical trench and the presence of an unusually large arc-trench gap. The National Institute of Oceanography, Pakistan, is carrying out such studies in collaboration with Oregon State University and the Geological Survey in U.S.A.

REFERENCES

ABBAS, S.G. & AHMAD, Z. (1979) The Muslim Bagh Ophiolites. *In:* Farah, A. & De Jong, K.A. (eds) GEODYNAMICS OF PAKISTAN. Geol, Surv. Pakistan, Quetta, pp. 243-9.

ARTHURTON, R.S. & FARAH, A. (1982) The Late Cretaceons-Cenozoic history of Balochistan, Pakistan; the northern margin of the Makran subduction complex. *In:* Leggett, J.K. (ed.) TRENCH-FOREARC GEOLOGY. Spec. Pub. Geol. Soc. London, **10**, pp. 373-85.

BARKER, P.F. (1966) A Reconnaissance survey of the Murray Ridge. Phil Trans. Roy. Soc. London, **259-A**, pp. 187-97.

BISWAS, S.K. (1982) Western rift basins of India and hydrocarbon prospects. Oil & Gas Journal, Pennwenn Publishing Co. Tulsa, U.S.A. April, **19**, pp. 224-32.

COLEMAN, R.G. (1981) Tectonic setting for ophiolite obduction in OMAN. J. Geophys. Res. **86**, pp. 2497-508.

COOK, J.P. (1975) Minerals from the Oceans. *In:* RESOURCES OF THE SEA. Symposium arranged by the Roy. Soc. of Tasmania (1974).

COUMES, F. & KOLLA, V. (1984) Indus Fan: Seismic structure, channel migration and sediment thickness in the upper fan. *In:* Haq, B.U. & Milliman. J.D. (eds) MARINE GEOLOGY AND OCEANOGRAPHY OF ARABIAN SEA AND COASTAL PAKISTAN. Van Nostrand Reinhold Co. Inc. New York, pp. 101-12.

DEMAISON, G.J. & MOORE, G.T. (1988) Anoxic environments and oil source bed genesis. AAPG Bull. **64**, pp. 1179-209.

EWING, M., ETTREIM, S., TRUNCHAN, M. & EWING, J.I. (1969) Sediment distribution in the Indian Ocean. Deep Sea Res. **16**, pp. 231-48.

FARAH, A., ABBAS, S.G., DE JONG, K.A. & LAWRENCE, R.D. (1984) Evolution of the lithosphere in Pakistan. *In:* Naqvi, S.M. Gupta, H.K. & Balakrishna, S. (eds.) LITHOSPHERE: STRUCTURE, DYNAMICS & EVOLUTION. Tectonophysics **105**, pp. 207-27.

GASTIL, G. (1982) Symposium on subduction of Ocean plates: Summary. Geol. Soc. Amer. Bull. **93**, pp. 464-7.

GUIDING GROUP OF EXPERTS (1985) On the programme of Ocean science in relation to non-living resources: Concept and general strategy for the implementation of the programme. REPORT OF IOC – UN (OETB), (OSNLR), SC-85/ WS/20 UNESCO, Paris, pp. 7-11.

HARMS, J.C., CAPPEL, H.N. & FRANCIS, D.C. (1984) The Makran coast of Pakistan: Its stratigraphy and hydrocarbon potential. *In:* Haq, B.U. & Milliman, J.D. (eds) MARINE GEOLOGY & OCEANOGGRAPHY OF ARABIAN SEA & COASTAL PAKISTAN. Van Nostrand Reinhold Co, Inc. New York, pp. 3-26.

HUNT, J.M. (1984) Generation and migration of light hydrocarbons. Science, **226**, 14 Dec., pp. 1265-70.

HUNTING SURVEY CORPORATION (1960) RECONNAISSANCE GEOLOGY OF PART OF WEST PAKISTAN. Toronto, Canada, pp. 396-7.

JACOB, K.H. & QUITTMEYER, R.C. (1979) The Makran region of Pakistan and Iran: Trench-arc system with active plate subduction. *In:* Farah, A. & De Jong, K.A. GEODYNAMICS OF PAKISTAN Geol. Surv. Pakistan, Quetta, pp. 305-18.

JARRARD, R.D. (1986) Relations among subduction parameters. REVIEWS OF GEOPHYSICS, 24, No. 2 May, Amer. Geophy. Union, pp. 217-85.

KASTENS, K.A. (1987) A compendium of causes and effects of processes at transform faults and fracture zones. REVIEWS OF GEOPHYSICS 25,(7) August, pp. 1554-60.

JIPA, D. & KIDD, R.B. (1974) Sedimentation of coarse grained interbeds in the Arabian Sea and sedimentation processes in the Indus Cone. *In:* Supko, P. R. & Weser, O. E. (eds.) INITIAL REPORTS OF THE DEEP SEA DRILLING PROJECT: Joides-U.S. NSF, 23 (2), pp. 471-95.

LAWRENCE, R.D. (1987) Closure of the Neotethys Ocean in Pakistan. National Institute of Oceanography, Pakistan News Bulletin 6, (3).

——, KHAN, S.H., DE JONG, K.A., FARAH, A. & YEATS, R.S. (1981) Thrust and strikeslip fault interaction along the Chaman transform zone, Pakistan. *In:* McClay, K.A. & Price, NJ. (eds.) THRUST & NAPPE TECTONICS, Geol. Soc. London, Spec. Publ. 9, pp. 363-370.

LEGGETT, J.K. & PLATT, J.P. (1984) Structural features of the Makran fore-arc on landsat imagery. *In:* Haq, B.U. & Milliman, J.D. (eds.) MARINE GEOLOGY & OCEANOGRAPHY OF ARABIAN SEA & COASTAL PAKISTAN. Van Nostrand Reinhold Co. Inc. New York. pp. 33-43.

——, AKOI, Y.U. & TOBA, T. (1985) Transition from frontal accretion to underplating in a part of the Nankai trough accretionary complex, off Shikoku (S.W. Japan) and extensional features on the lower trench slope. MARINE & PETROLEUM GEOLOGY 2, May, Butterworth & Co. Ltd. pp. 131-41.

MACHARGUE, T.R. & KIEBB, J.E. (1986) Internal geometry, seismic facies, and petroleum potential of canyons and inner fan channels of the Indus submarine fan. AAPG BULL. 70 (2), pp. 161-80.

MCKENZIE, D.P. & SCLATER, J.D. (1971) The evolution of the Indian Ocean since the late Cretaceous. Geophs. J. Roy. Astro. Soc. 25, pp. 437-528.

PLATT, J.P. & LEGGETT, J.K. (1986) Stratal extension in thrust footwalls of Makran accretion by prism: Implications for thrust tectonics. AAPG. Bull. 70, (2), pp. 191-203.

POWELL, C. Mc A. (1979) A speculative tectonic history of Pakistan and surroundings: Some constraints from the Indian Ocean. *In:* Farah, A. & De Jong, K.A. (eds.) GEODYNAMICS OF PAKISTAN. Geol. Surv. Pakistan, Quetta, pp. 5-24.

QUADRI, V.N. (1984) Status of petroleum exploration off-shore, Pakistan. *In:* Haq, B.U. & Milliman, J.D. (eds.) MARINE GEOLOGY & OCEANOGRAPHY OF ARABIAN SEA AND COASTAL PAKISTAN. Van Nostrand Reinhold Co. Inc. New York. pp. 27-32.

QUITTMEYER, R.C., FARAH, A. & JACOB, J.K. (1979) The Seismicity of Pakistan and its relation to surface faults. *In:* Farah, A. & De Jong, K.A. (eds.) GEODYNAMICS OF PAKISTAN. Geol. Surv. Pakistan, Quetta, pp. 305-18.

QURAISHEE, G.S. (1984) Circulation in the north Arabian Sea at Murray ridge during SW monsoon *In:* Angel, M.V. (ed.) MARINE SCIENCE OF THE NORTH-WEST INDIAN OCEAN AND ADJACENT WATERS. Permagon Press, pp. 651-65.

READING, H.G. (1980) Characteristics and recognition of strike slip fault systems. *In:* Ballance, P.F. & Reading, H.C. (eds.) Sedimentation in oblique slip mobile zones. Special Publication 4, International Association of Sedimentologists, Black Well Scientific Publications, London, pp. 7-26.

SHUAIB, S.M. (1982) Geology and hydrocarbon potential of off-shore Indus basin, Pakistan. AAPG Bull. 66, pp. 940-46.

SYKES, L.R. (1970) Focal mechanism solutions for earthquakes along the world rift system. Seismol Soc. Amer. Bull. 43, pp. 1749-52.

UYEDA, S. (1977) THE NEW VIEW OF THE EARTH. W.H. Freeman & Co. U.K. pp. 157-71.

—— (1979) Subduction zones: facts, ideas and speculations. Oceanus, 22, (12), Woods Hole Oceanographic Institution U.S.A., pp. 53-62.

WENYOU, Z., HONG, Y. & JIAYON, Z. (1979) On fault blocks and plates. SCIENTIA SINICA 22, (12), Academia Sinica, Beijing. pp. 1406-29.

WHITMARSH, R.B., WESER, O.E. & ROSS, D.A. (1974) Introduction. *In:* Supko, P.R. & Weser, O.E. (eds.) INITIAL REPORTS OF THE DEEP SEA DRILLING PROJECT. Joides U.S. NSF 23 (2), pp. 5-9.

—— (1974) Some aspects of plate tectonics in the Arabian Sea. *In:* Supco, P.R. & Weser, O.E. (eds.) INITIAL REPORTS OF THE DEEP SEA DRILLING PROJECT. Joides U.S. NSF 23 (2), pp. 527-36.

WHITE, R.S. (1979) Deformation of the Makran continental margin. *In:* Farah, A. & De Jong, K.A. (eds.) GEODYNAMICS OF PAKISTAN Geol. surv. Pakistan, Quetta. pp. 295-304.

——— **(1984)** Active and passive plate boundaries around the Gulf of Oman, NW Indian Ocean. *In:* Angel, M.V. (ed.) MARINE SCIENCE OF THE NORTH- WEST INDIAN OCEAN AND ADJACENT WATERS. Pergamon Press, pp. 731-46.

Manuscript received on 10.12.1988
Accepted for publication on 31.12.1988

ACTA MINERALOGICA PAKISTANICA
VOLUME 4 (1988) pp. 134 - 144.

FACIES ANALYSIS, SEDIMENTARY STRUCTURES AND A DEPOSITIONAL MODEL FOR THE EUREKA SOUND FORMATION, ELLESMERE ISLAND, CANADIAN ARCTIC

HAMID MASOOD
Institute of Geology, Punjab University, New Campus, Lahore, Pakistan.

ABSTRACT: The Eureka Sound Formation was measured at three localities around Strathcona Fiord on Ellesmere Island. The Formation is composed of a sequence of fine sandstone, siltstone, mudstone, and coal. This study divides the Eureka Sound Formation in to different lithofacies on the basis of stratigraphic and textural relationships. Sedimentary structures were studied and interpreted. The coarsening upward cycles are because of delta progradation. On the basis of lithofacies and sedimentary structures, a deltaic model has been proposed for the Eureka Sound Formation in the Strathcona Fiord area.

INTRODUCTION

Upper Cretaceous and Lower Tertiary rocks of the Eureka Sound Formation crop out throughout the Canadian Arctic from Banks Island eastward to Ellesmere Island (Fig. 1). The formation is primarily non-marine in origin and contains unconsolidated or poorly consolidated clastic rocks with rhythmically interbedded coal, fossil wood and plant remains. The Eureka Sound Formation conformably overlies the Cenomanian to Lower Campanian Kanguk Formation in some regions and is unconformable with older formations in others (Fig. 2). Deposition of the Eureka Sound Formation occurred in seven major structurally controlled depocentres: the Banks, Remus, Eclipse, Judge Dely, Lake Hazen, West Sverdrup, and Meighan Basins (Fig. 3), (Miall, 1976). Strathcona Fiord is located in the partially fault-bounded Remus Basin located in the Eureka Sound Fold Belt (Balkwill and Bustin, 1980). The Eureka Sound Fold Belt encompasses much of eastern Axel Heiberg Island and west central Ellesmere Island.

Recent work by West *et al.* (1981) has greatly increased our understanding of the stratigraphy of the Eureka Sound Formation in central Ellesmere Island. The Eureka Sound Formation as well as temporal non-marine deposits on northern and western Greenland and Svalbard will provide an important understanding, of both the geological history of the Arctic Ocean and North Atlantic, and the climatic history of the northern hemisphere. Three stratigraphic sections in the Eureka Sound Formation were measured in the Strathcona Fiord area (Fig. 2) and are shown in detail on Fig. 4. Section I is the main focus of this study because Member III is continuously exposed. Total thickness of the section is about 3000 feet. Section 2, located to the southwest, is about 4000 feet thick. Section 3 which is 3000 feet thick, is a continuation of section 1. The top of Member I marks the transition between marine and continental conditions; this Member is about 3000 feet in thickness. The age of the Eureka Sound Formation as given by Bustin (1977) is from Late Cretaceous to Mid Eocene.

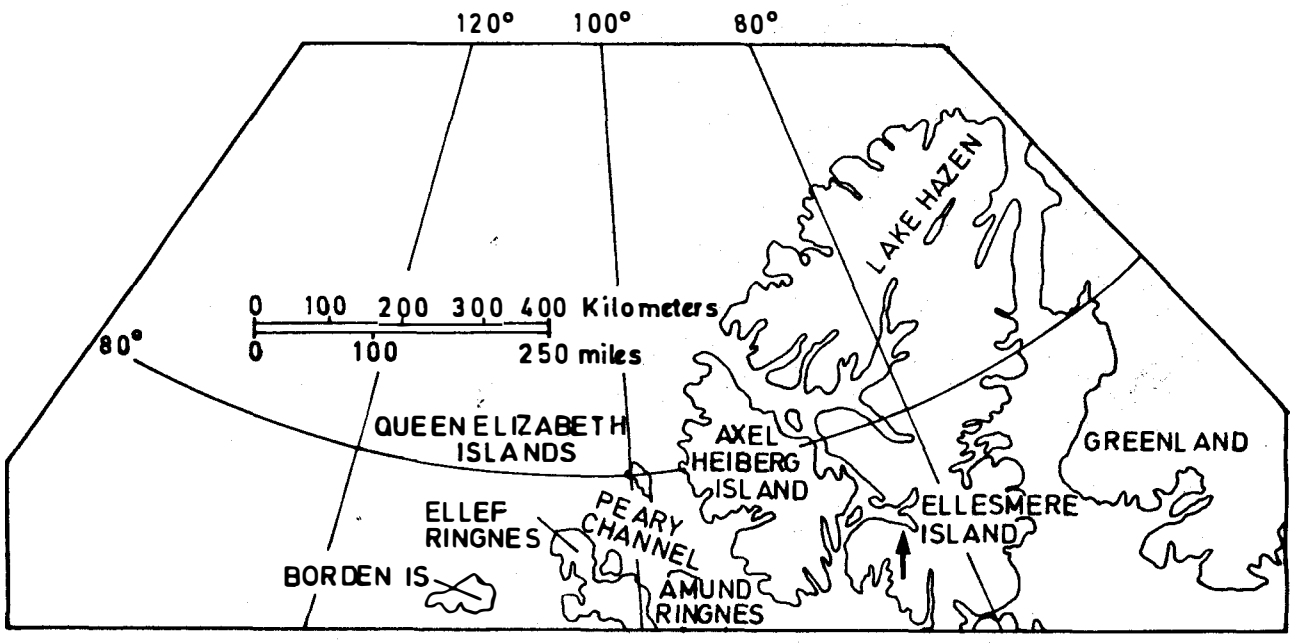

Fig. 1. Locality map: arrow points towards project area.

It conformably overlies Upper Cretaceous shale of the Kanguk Formation and unconformably overlies strata as old as Devonian.

STRATIGRAPHY

Member I

Member I consists of distinctive lenses of white to light grey, medium to coarse-grained, arkosic to quartzose, cross-bedded sandstone separated by flaggy sandstone and massive mudstone units. Coal beds are rare. In the area near the Fossil Forest River (Fig. 2), parallel-bedded siltstone and silty claystone crop out at the base of Member I.

Member II

Member II consists of predominantly white to tan sandstone with mudstone and lignite interbeds in the lower part, whereas the upper part is a repetitive sequence of somber grey, grey-green, brown, or black calcareous siltstone, fine-grained silty sandstone, scattered pebble beds, shaly mudstone, and minor lignite beds. Irostone stringers are common in the lower two-thirds of this member. Carbonized organic debris is also common throughout. The lower contact of Member II is gradational.

Member III

Member III is a sequence of light grey to tan marl, siltstone and fine-grained sandstone with upward-increasing amounts of carbonaceous matter. The light colour of this member contrasts markedly with the drab grey and brown of Member II. Member III was interpreted as marine by West *et al.* (1981), based on the presence of scaphopods, marine to brackish water bivalves, shark's teeth, and marine bony fish remains.

Member IV

Member IV is a sequence of alternating lignite, shaly mudstone, fine grained sandstone and clay. The sandstone is not well indurated and is slightly calcareous. Member IV was initially subdivided into "sand-coal" and "shale-coal" units of Miall (in West *et al.*, 1977). The lower part of the Member is characterized by alternating coals and sandstones with minor shale. Higher in the Member, coal seams are thicker and closer together and there is a greater proportion of shale interbedded with the sandstone. The sandstones are arkosic and quartzose, medium-grained, and light grey to white. Irregular sandy ironstone concretions frequently containing organic matter are common. Car-

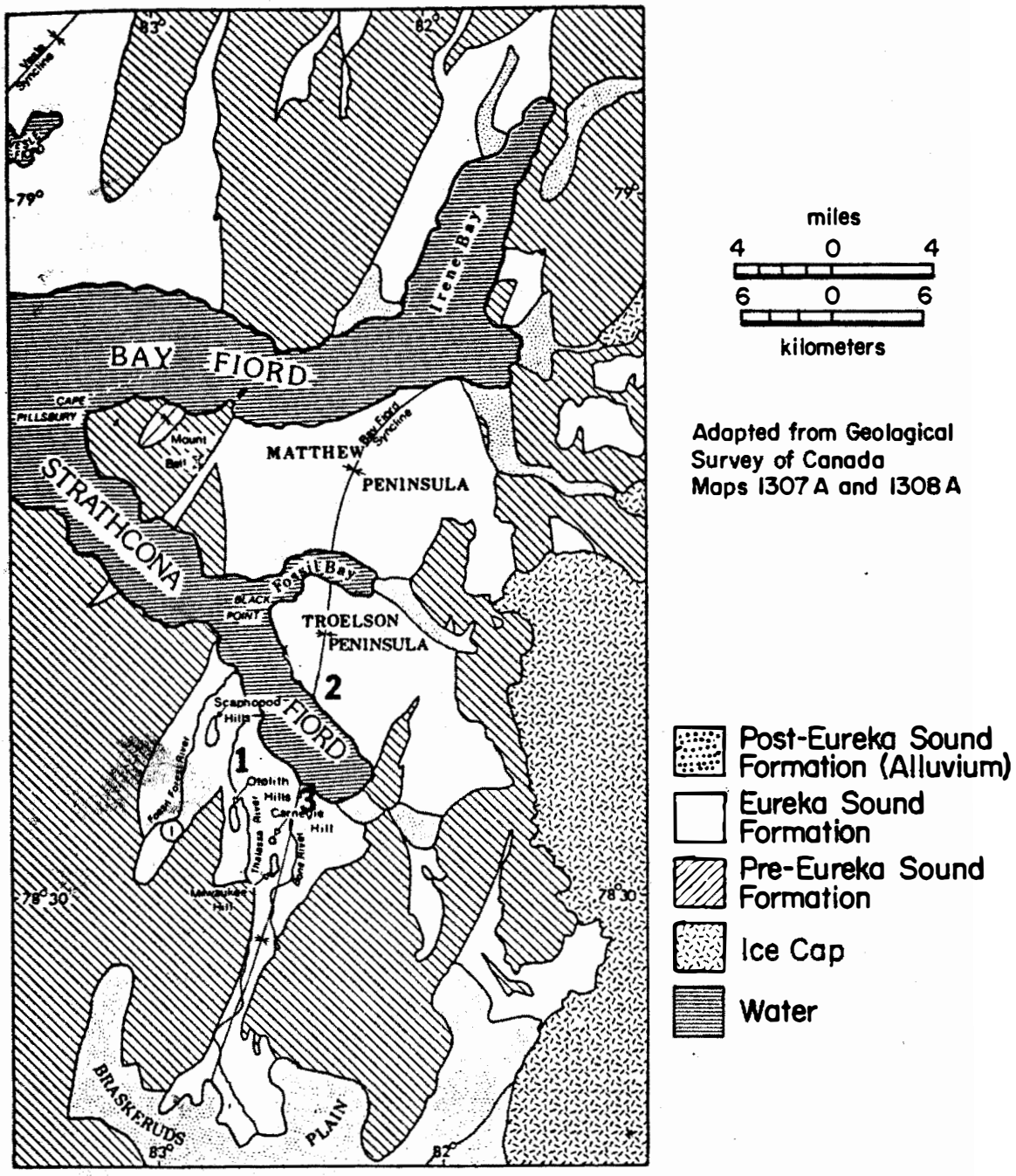

Figure 2. Geological map of the Area. (1-3 are localities of sectios measured). (From West et al. 1981)

bonized, in situ tree stumps occur at several horizons in Member IV. This Member is distinguished from Member III by its large variety of colours and by the abundance of organic matter and ironstones. All the vertebrates reported from the Eureka Sound Formation have been reported from this Member.

LITHOFACIES ANALYSIS

Lithofacies are based primarily on sedimentary and biogenic structures, and on the nature of the contacts.

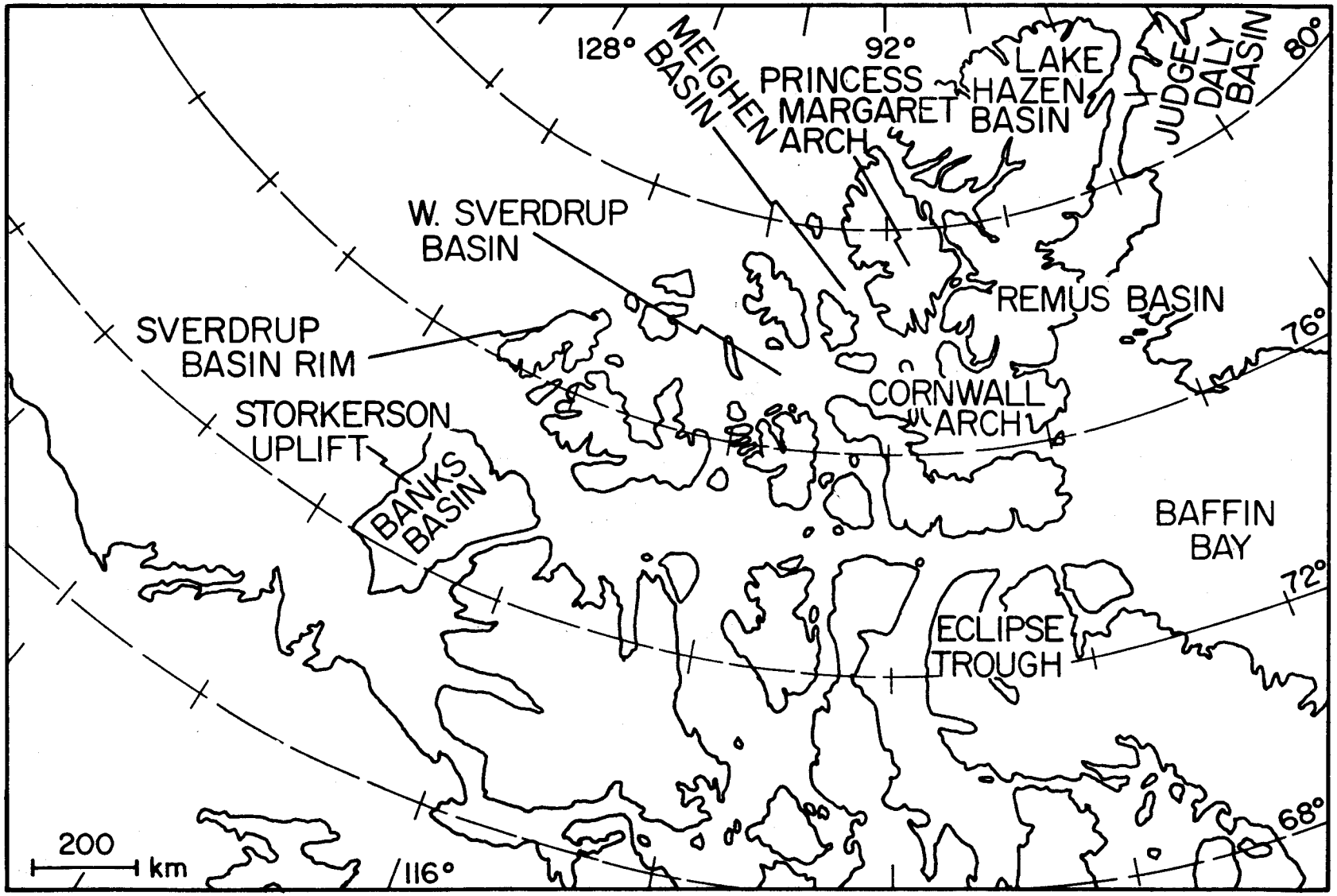

Fig.3. Location of the major depocenters of the Eureka Sound Formation.

Lithofacies 1: Mudstone

Mudstones are light to medium grey in colour and are laminated. The laminations are not continuous & are probably due to a combination of grain size difference and the presence of carbonaceous matter. These non-fissile laminae range in thickness from less than a centimetre to a few centimetres. Vertical burrows and gastropods are present in this lithofacies. The mudstone gradually grades into silstone and fine grained sandstones. An increase in fissility is directly related to the increase in the silt content and the presence of mica. The absence of the current structures and the fine grained nature of lithofacies 1 suggests that the mudstone was deposited in quiet conditions.

Lithofacies 2: Siltstone

Siltstones are interlaminated with sand and clay and occur in the upper part of section in Member III. Thickness varies from few centimetres to about a metre. The siltstones are grey to yellowish grey in colour and contain some plant and wood debris. Lamination is normally absent. The lighter colour of the siltstone indicates a lesser amount of carbonaceous matter. The sedimentary structures within this lithofacies consist of ripple marks and slump structures. The presence of both current and oscillatory ripples indicates an increase in current activity at the time of deposition. The presence of the structures like ripples, slumps and horizontal burrows suggest that siltstone was deposited under delta front to delta slope conditions.

Lithofacies 3: Finegrained Sandstone, Siltstone and Clay

Fine grained sandstones siltstones and clay are poorly indurated and contain a high percentage of carbonaceous matter. Coarser beds consist of siltstone and very fine sandstone and finer beds consist of fine grained siltstone and mudstone. All the beds vary in thickness and show parallel to very low angle cross lamination. Flaser bedding is present in this lithofacies. Some of the sandstone layers have been destroyed by biogenic activity and marine bivalves occur at a number of horizons in this lithofacies. Sandy units are interpreted as distal distributary mouth bars and the interbedded muds as prodelta deposits. The presence of occasional large scale cross-bedding suggests periods of short lived progradation of large bars or sand waves with a major distributary channel.

Lithofacies 4: Contorted Sandstones

This facies is characterized by contorted sandstones which are poorly indurated, dark grey in colour and have a silt matrix. These sandstones are highly contorted showing recumbent folds. Similar beds have been described by different authors as sedimentary slumps (King, 1967), or as movements of bottom hugging turbidity currents (Burne, 1970). Burne considered that movement of these flows ceases abruptly and subsequent dewatering results in the formation of sand volcanoes, which in places founder back into the bed to produce irregular masses of sandstones. Melvin (1986), reported similar structures from an ancient delta-fed fan and attributed contorted sandstones to be a consequence of the mobilization of beds through an initial phase of slumping along an unstable slope. The slumped units, according to Melvin, move downslope and incorporate additional sand, mud and water until the flow becomes a dense liquefied suspension of sediments. When flow ceases, the contorted appearance results from dewatering of the sediments (Burne, 1970). Boums *et al.* (1984b) have similarly postulated how slumps on the modern Mississippi fan have gradually transferred into debris flows and filled the conduits. The contorted sandstone lithofacies of the Eureka Sound Formation appears to be deposited on delta slope by gravity slides prior to compaction.

Lithofacies 5: Wavy Bedded Sandstone, Siltstone and Mudstone

This lithofacies is characterized by wavy bedded alternating mudstone, siltstone and sandstone layers. The thickness of this lithofacies varies from a few centimetres to over a metre. The sandstones are cross-laminated with burrows and plant debris. The grain size of the sandy units varies from very fine to fine grained. This lithofacies is very characteristic of strong current or wave action alternating with slack water conditions in which muds were deposited,

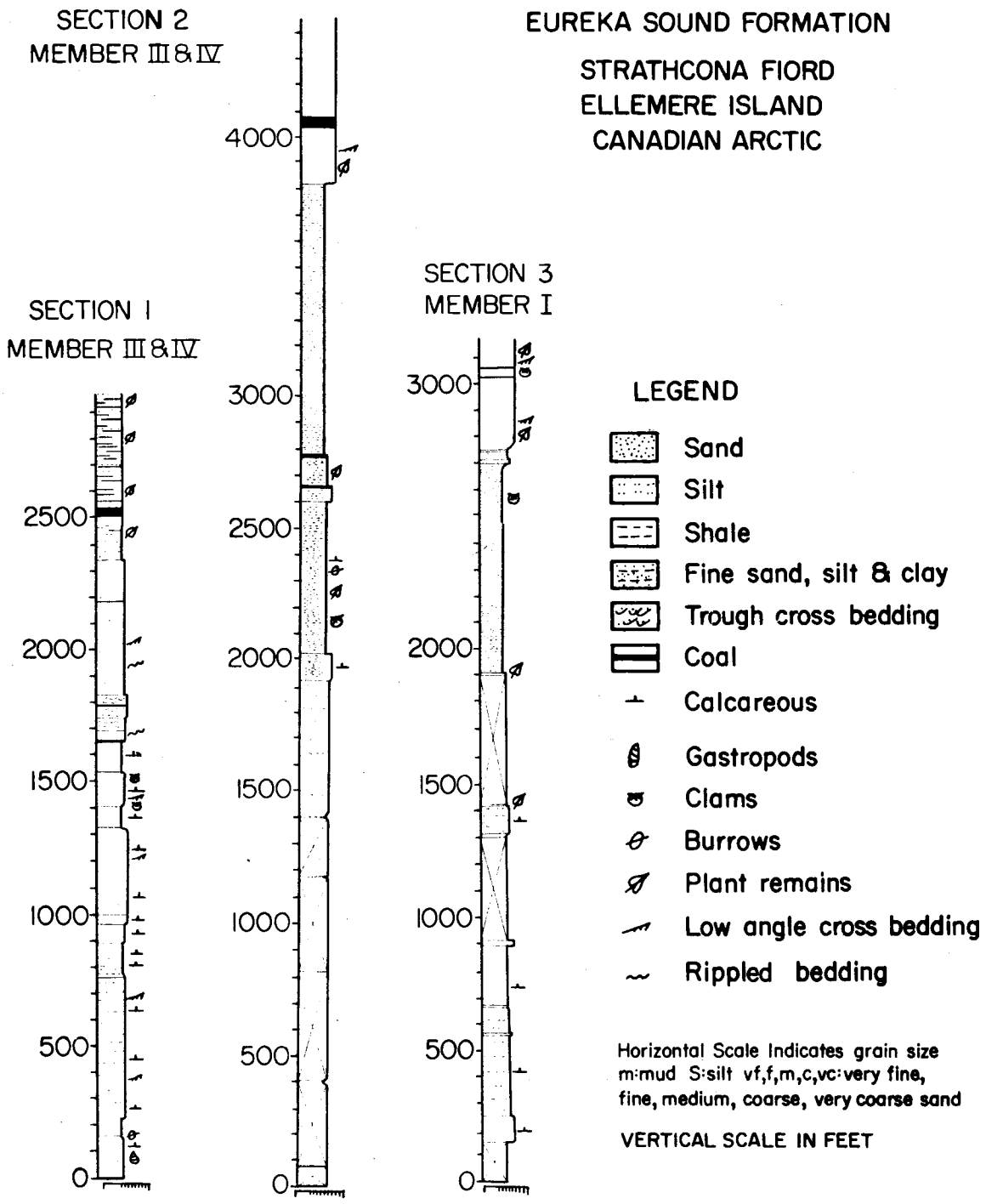

Figure.4. Stratigraphic columns of the measured sections.

resulting in the development of flaser bedding. Similar lithofacies have been described by Coleman and Gagliano (1965) from a marine delta front. Such facies characterizes the proximal part of the prodelta slope and distal mouth-bar environment.

Lithofacies 6: Cross Laminated Sandstone

Cross-laminated sandstones range in thickness froms 50 cm. to a metre. Carbonaceous matter is common in this lithofacies. The presence of current and oscillatory ripple laminations indicate frequent changes in the current or wave directions during deposition.

This lithofacies is interpreted as being the product of lower flow regime currents. (Simon *et al.*, 1965). The migration of small scale linguoid or lunate ripples produces small scale trough cross-laminations (Allen, 1963a). The variation in the shape of the cross-lamination is controlled by the hydrodynamics of the flow, the grain size and the amount of material contributed from suspended matter. This lithofacies is characteristic of distributary mouth bars.

Lithofacies 7: Small to Medium Scale Trough Cross-bedded Sandstone

This is the most common facies in Member III of the Eureka Sound Formation. The thickness of this lithofacies ranges from a fews centimetres to several metres and comprises very fine to fine grained sandstones. The foresets usually dip from 10 to 20 degrees and sometimes as much as 30 degrees. Scour and fill structures and carbonaceous matter are common.

Medium to small scale cross-bedding of this type is the product of migrating mega ripples. The migrating mega ripples are believed to indicate the upper part of the lower flow regime in the channel environments (Simon *et al.*, 1965).

Lithofacies 8: Large Scale Cross-bedded Sandstone

Large Scale Cross-bedded Sandstone attains a thickness of about 10 to 20 metres. The sandstone is fine grained and poorly lithified. Carbonaceous matter, plant and root structures are observed. This lithofacies is formed in similar conditions as lithofacies 8, but under a higher energy regime commonly found in distributary channels.

Lithofacies 9: Horizontally Bedded Sandstone

Horizontally Bedded Sandstones are common lithofacies in the Eureka Sound Formation. The sand is not very compact and has abundant carbonaceous matter and with evidence of plant rootlets and leaves. Bivalve fossils also occur within this lithofacies. Individual laminae are a few millimetres thick and the sandstone is fine grained, poorly lithified and has a high clay content.

Horizontal bedding is product of variable hydrodynamic conditions and bedloads. It can be formed by a current velocity below the critical velocity of ripple formation (Bogardi, 1965; Guy *et al.*, 1966), and can also be produced in the plane bed phase of a high flow regime (Reineck & Singh, 1973). This lithofacies is considered to represent a distributary mouth bar or distributary channel.

Lithofacies 10: Channel-form Sandstone

Channel-form Sandstone marks the beginning of Member IV and represents a change from shallow marine to completely terrestrial influence. These are products of channels and consist of fine sandstones. Small distributary channels seem to be responsible for the formation of this lithofacies.

Lithofacies 11: Coal

Coal lithofacies is distinguished by coal seams which vary in thickness from a few centimetres to several metres. Coal first appears in the uppermost part of Member III and becomes very common in Member IV. The coals are low grade and intercalated with clay, sandstone and petrified wood. The presence of the coal seams and petrified wood indicates peat forming swamps with thick vegetation. Certain horizons are characterized by in situ tree stumps.

SEDIMENTARY STRUCTURES AND INTERPRETATION

The sedimentary structures are divided into three groups: hydrodynamic, biogenic and deformational structures.

Hydrodynamic Structures

Cross-stratification is the most common hydrodynamic structure observed in the Eureka Sound Formation. Both cross-bedding and cross-lamination, distinguished on the basis of size (Allen, 1963b) are recognized.

Cross-bedding

Because the sandstones were typically poorly consolidated and weather into non-resistant slopes, three dimensional analysis of cross-bedding in the field was difficult. However,

planar and trough cross-bedding types as classified by McKee and Weir (1953) could generally be recognized. On the other hand, cross-bedding types as classified by Allen (1963b), were more difficult to recognize.

Cross-lamination

Cross-lamination is a general term for all cross-stratified sets less than 5 centimetres thick and equivalent to Allen's (1963b) small-scale cross-stratification. Mu and Nu cross-laminations were recognized in the Eureka Sound Formation.

Mu cross-lamination is formed from grouped sets each of which is underlain by a planar erosional surface. Sets are discordant with respect to this surface and are of homogeneous lithology. This type of cross-lamination is also referred to as ripple-drift cross-lamination. It occurs in fluvial, turbidity and deltaic deposits.

Nu cross-lamination consists of grouped cosets, each of which is bounded underneath by a scoop-shaped erosional surface. Such structures have also been described variously as micro-trough cross-lamination or micro cross-lamination. This type is observed in the fine sands of the Eureka Sound Formation.

Plane Bedding

Plane bedding is common in Member III as well as Member I of the Eureka Sound Formation. Plane bedding was subdivided by Harms and Fahnestock (1965) into horizontal and parallel stratification.

Horizontal Stratification

Horizontal laminations equivalent to Bouma's (1962) lower interval of parallel laminations are sand-sized horizontal and tabular sets. They extend laterally over a large distance unless truncated by younger erosion. This structure is the product of plane-bed transport in the upper flow regime (Simon *et al.*, 1965; Harms and Fehnestock, 1965). The faint internal lamination indicates that no topographic features of any prominence existed on the bed during deposition. These were found to be associated with ripples and were related to variations in depth and velocity gradients. McKee (1965) concluded that a vertical change from ripple laminae to horizontal laminae is caused by shoaling stream changing from lower to higher flow regime. Similar occurrences, probably from this sort of fluctuation in depth and flow velocity are commonly observed in the Eureka Sound Formation.

Parallel Stratification

Parallel stratification equivalent to Bouma's (1962) upper pelitic interval of parallel lamination refers to sets of horizontal laminations of siltstone and clay. In the Eureka Sound Formation, inter-lamination of very fine grained sandstone with mudstone and siltstone is common. Thickness varies from a few millimetres to about one centimetre. The finer muddy laminae often contain abundant carbonaceous material. The fine grain size indicates that deposition took place under gentle currents in which suspended sediment was settling out.

Biogenic Structures

Biogenic structures are fossils in the broadest sense of the term in that they represent some type of biotic activity. However, they occur as tracks, trails or burrows rather than preserved body parts or casts. Although long known, their study has only recently been pursued systematically. Different types of biogenic structures were observed in the Eureka Sound Formation such as vertical and horizontal burrows, and resting and crawling marks.

Rootlets and Plant Debris

Plant remains are widely distributed throughout the Eureka Sound Formation. They occur either as disseminated plant stems or as dense layers of leaves. They are particularly abundant in the upper part of Member IV. Here, plant debris is sufficiently dense to form coal seams varying in thickness from a few centimetres to several metres. Rootlets are common, particularly in the upper parts of Members III and IV.

CONCLUSIONS

Member I apparently represents a transition from the transgressive clastic wedge that marks

the beginning of Eureka Sound deposition in the area. The succeeding sandstone lenses and the massive, finer-grained beds separating them, apparently represent a zone of subaqueous channels and paralic mud flats transitional to fully terrestrial conditions.

According to West *et al.*, (1981), the lower part of Member II exhibits features consistent with a fluvial origin. The upper part has been interpreted as deposited in backwater swamp or marsh environments (Vision, 1981) or a flood plain in a humid climate where sediment was predominantly subaerially exposed.

The lower part of Member III has been interpreted by West *et al.*, (1981) to record a change from paludal sedimentation in the upper part of the Member II to fresh water lagoonal conditions. The middle part of Member III is believed to has been deposited in a lagoonal or estuarine environment which gradually changes to shallow marine. The upper part of the unit is characterized by sediments deposited in brackish water conditions.

Member IV marks the return of the fluvial conditions during deposition. Better sorted sands, less somber weathering colours, and the sandy ironstone nodules suggest a greater stream influence than those that deposited Member II.

The general pattern of lithofacies in the Strathcone Fiord Section shows that each cycle starts with a siltstone that gradually coarsens to sandstone, as well as with rapid diminution of marine fauna and an increase in plant debris. Presence of both plant material and bioturbation indicates brackish water conditions. Although bivalve fossils were found in the upper part of Member III, it is evident due to the poor preservation and the associated sedimentary structures that they were winnowed by the currents before deposition. Conditions therefore were more brackish than open marine. In addition there is evidence of gradual increase in current energy from the less influential currents of the prodelta slope to more active fluvial currents. This led to the accumulation of a sedimentary platform at or near the water surface which would favour plant colonization. Such sequences may be explained as the outgrowth of a deltaic lobe into a marine environment, giving rise to a fluvio-marine regressive cycle (Fisk, 1955; Scruton, 1960; Allen, 1963c; Gould, 1970).

It is clear that these coarsening upward cycles show a common pattern of deltaic progradation. The coarsening upward sequences occur above basal deltaic lobe sediments as distributary bay deposits. The mud and silt at the base of a cycle were supplied by overbank flooding or by longshore currents. Similar cycles were described by Coleman *et al.* (1964, 1965) and Elliot (1975). There is no evidence of tidal channels, coastal beach barrier sands or tidally influenced swamps on an accreting delta front in the Strathcona Fiord sequence. This could be explained by the continual migration of the deltaic lobe during a constructive episode. The subsequent delta destructive episode, if it occurred, was of short duration.

ACKNOWLEDGEMENTS

The author is highly indebted to Dr. W.J. Zinsmeister of Purdue University for his guidance in the field and valuable discussions later. The research was funded from his NSF grant D PP-8402858. Polar continental shelf project of Canadian Geological Survey provided logistic support and transport facilities in the field on Ellesmere Island.

REFERENCES

ALLEN, J.R.L. (1963a) Asymmetrical ripple marks and the origin of water-laid cosets of cross-strata. Liverpool Manchester Geol. Jour., **5**, pp. 182-236.

——**(1963b)** The classification of cross stratified units: with notes on their origin. Sedimentology, 2, pp. 93-114.

——**(1963c)** Sedimentation in the modern delta of the river Niger, West Africa. *In:* Van Straaten, L.M.J.U. (ed.) DELTAIC AND SHALLOW MARINE SEDIMENTATION. Elsevier, Amsterdam, pp. 26-34.

BALKWILL, R.H. & BUSTIN, R.M. (1980) Late Phanerozoic structures, Canadian Arctic Archipelago: Paleogeography, Paleoclimatology, Paleoecology, **30,** pp. 219-27.

BOGARDI, J.L. (1965) European concepts of sediment transport, J. Hydraulics Div., Am. Soc. Civil Engrs., **91**, pp. 29-54.

BUSTIN, R.M. (1977) The Eureka Sound and Beaufort Formations, Axel Heiberg and west-central Ellesmere Islands, District of Franklin, Thesis, University of Calgary, Calgary, Alberta, Canada, 208 p. (Unpublished).

BOUMA, A.H. (1962) SEDIMENTOLOGY OF SOME FLYSCH DEPOSITS. Amsterdam, Elsevier, 168p.

———, **STELTING, C.E. & COLEMAN, J.M. (1984)** Mississippi Fan: Internal structure and depositional processes. Geo-marine Letters, **3**, pp. 147-53.

BURNE, R.V. (1970), The origin and significance of sand volcanoes in the Bude Formation (Cornwall). Sedimentology **15**, pp. 211-28.

COLEMAN, J.M., & GAGLIANO, S.M. (1964) Cyclic sedimentation in the Mississippi River deltaic plain. Gulf Coast Ass. Geol. Soc. Trans. **14**, pp. 67-80.

——— **& GAGLIANO, S.M. (1965)** Sedimentary structures, Mississippi river deltaic plain. *In:* Middleton G.V. (ed.) SEDIMENTARY STRUCTURES AND THEIR HYDRODYNAMIC INTERPRETATION. Soc. Econ. Paleontol. Mineral. Spec. Publ. **12,** pp. 133-48.

ELLIOT, T. (1978) Deltas. *In*: Reading, H.G. (ed.) SEDIMENTARY ENVIRONMENTS AND FACIES. Blackwell Scientific Publication, Oxford. pp. 97-142.

FISK, H.N. (1955) Sand facies of recent Mississippi delta deposits. Proc. 4th Wld. Petrol. Congr. Sect. **1-c,** pp. 377-98.

GOULD, H.R. (1970) The Mississippi delta complex, *In*: Morgan, J.P. (ed.) DELTAIC SEDIMENTATION MODERN AND ANCIENT. Soc. Econ. Paleont. Mineral. Tulsa, Spec. Publ. **15**, pp. 3-30.

GUY, H.H., SIMON, D.B. & RICHARDSON, E.V. (1966) Sunnnary of alluvial channel data from flume experiments. U.S. Geol. Surv. Prof. Pap. **462-1**, 96 p.

HARMS, J.C. & FAHNESTOCK, R.K. (1965) Stratification, bedforms and flow phenomenon (with an example from the Rio Grande). *In:* Middleton, G.V. (ed.) PRIMARY SEDIMENTARY STRUCTURES AND THEIR HYDRODYNAMIC INTERPRETATION. Soc. Econ. Paleont. Mineral. Spec. Publ. **12,** pp. 84-115.

KING, A.F. (1967) Stratigraphy and structure of the Upper Carboniferous Bude Formation, north Cornwall. Ph.D. thesis. Univ. of Reading, U.K. (Unpublished)

McKEE, E.D., & WEIR, G.W. (1953) Terminology of stratification and cross-stratification in sedimentary rocks. Bull. Geol. Soc. Am. **64**, pp. 381-90.

————, **REYNOLD, M.A. & BAKER, C.H. (1962)** Laboratory studies on deformation in unconsolidated sediments. U.S. Geol. Surv. Prof. Paper **450-D,** pp. D155-D159.

———— **(1965),** Experimentation on ripple lamination. *In:* PRIMARY SEDIMENTARY STRUCTURES AND THEIR HYDRODYNAMIC INTERPRETATION. Soc. Econ. Paleon. Mineral., Spec. Publ. **12,** pp. 77-83.

MELVIN, J., (1986) Upper Carboniferous fine-grained turbidite sandstone from southwest England: A model for growth in an ancient delta-fed fan. Jour. Sed. Pet. **56**, pp. 19-34.

MIALL, A.D. (1976) Sedimentary structures and paleocurrents in Tertiary delta succession, Northern Banks Basin, Arctic Canada. Can. Jour. Earth Sci., **13**, pp. 1422-32.

REINECK, H.E. & SINGH, I.B. (1973) DEPOSITIONAL SEDIMENTARY ENVIRONMENTS. Springer-Verlag, Berlin, 439p.

SCRUTON, P.C. (1960) Delta building and the deltaic sequences. *In:* Shepard, F.P., Pleger, F.B. & Van Andel, T. (eds.) RECENT SEDIMENTS, NORTHWEST GULF OF MEXICO Am. Ass. Petrol. Geol., Tulsa, pp. 82-102.

SIMON, D.B., RICHARDSON, E.V. & NORDIN JR., C.F. (1965) Sedimentary structures generated by flow in alluvial channels. *In:* Middleton, G.V. (ed.) PRIMARY SEDIMENTARY STRUCTURES AND THEIR HYDRODYNAMIC INTERPRETATION. Soc. Econ. Paleont. Mineral. Spec. Publ. **12,** pp. 34-52.

STOKES, W.L. (1953) Primary sedimentary trends indicators as applied to ore findings in the Carrizo Mountains, Arizona and New Mexico: U.S. Atomic Energy Comm., RME-3043 (pt 1).

VINSON, T.E. (1981) A paleomagnetic study of the Upper Cretaceous to early Eocene Eureka Sound Formation, Strathcona Fiord, Ellesmere Island, Canada. M.Sc. Thesis University Of Wisconsin-Milwakee, 125p. (Unpublished).

WEST. R.M., DAWSON, R.M., HICKEY, L.J. & MIALL, A.D. (1981), Late Cretaceous and Paleogene sedimentary rocks, Canadian Arctic and related North Atlantic areas. *In:* Kerr, J.W. & Fergusson, A.J. (eds.) GEOLOGY OF THE NORTH ATLANTIC BORDERLANDS. Canadian Society of Petroleum Geologists, Memoir 7.

WEST, R.M., DAWSON, M.R. & HUTCHISON, J.H., (1977), Fossils from the Paleogene Eureka Sound Formation, Northwest Territories, Canada: occurrence, climatic and paleogeographic implications. *In:* West, R.M. (ed.) PALEONTOLOGY AND PLATE TECTONICS. Milwakee Public Museum Special Papers in Biology and Geology, **2**, pp. 77-93.

Manuscript received on 15.12.1988
Accepted for publication on 31.12.1988

ACTA MINERALOGICA PAKISTANICA
VOLUME 4 (1988) pp. 145 - 146.

SHORT COMMUNICATIONS

CONTACT DEMARCATION USING THE HEAVY MINERALS IN ROCKS OF THE SIWALIK AND RAWALPINDI GROUPS AT TOOT WELL-7, POTWAR REGION.

S. SADAQAT A. JAFRY
Geological Survey of Pakistan, 42/R, Block 6, PECHS, Karachi, Pakistan

The rocks of the Siwalik Group and the Rawalpindi Group are mainly sandstones, claystones and shales that are lithologically difficult to demarcate. Toot Well-7 was spudded in the Dhok Pathan Formation of the Siwalik Group; and was drilled through a depth of 4612m down to the Tredian Formation of Jurassic age. The three rock formations within the Siwalik Group, i.e., Dhok Pathan, Nagri and Chinji, may be distinguished by the criteria given below.

Table 1. **Heavy minerals in sandstones from Tool Well-7.**
Mineral Symbols are: Tur, tourmaline; Ep, epidote; Rt, rutile; Bt, biotite; Ms, Muscovite. *= weight percent of the total heavy mineral content.

Depth interval (m.)	Wt % heavy minerals	Tur %*	Ep %*	Rt %*	Bt %*	Ms %*	Unidentified % *
1590–1600	3.11	10	33	7	10	–	40
1610–1620	3.21	20	20	7	10	–	43
1620–1630	2.97	10	20	7	5	3	55
1630–1640	3.18	15	60	5	5	–	15
1700–1710	4.03	13	73	–	3	–	11
1800–1810	2.44	13	53	10	2	3	19
1900–1910	3.07	7	70	–	–	2	21
3000–3010	2.91	9	57	5	3	2	24
3070–3080	2.83	15	70	3	5	2	5
3080–3090	2.69	12	60	2	3	–	23
3090–3100	2.97	15	55	5	3	–	22
3100–3110	3.51	30	20	3	5	5	37
3110–3120	2.89	45	30	4	3	–	18
3120–3130	2.93	45	30	2	5	4	14
3160–3165	3.28	30	15	3	5	7	40
3180–3190	3.01	50	17	5	6	–	22
3190–3200	3.87	37	20	3	7	5	28
3210–3220	2.95	23	45	5	8	5	14
3220–3230	2.81	30	40	4	5	5	16
3260–3265	2.94	25	25	10	15	10	15

DHOK PATHAN FORMATION: The presence of fresh, whitish, grey to light greenish grey sandstone, with high clay content and appearance of maroon siltstone in the Dhok Pathan Formation.

NAGRI FORMATION: Greenish grey, medium hard micaceous sandstone and brown soft silty clays.

CHINJI FORMATION: Brownish clays with thin bands of sandstone.

However, the contacts between the formations belonging to the two Groups are not always demarcable at precise levels due to gradations in lithology. In the present case, their heavy mineral contents are, therefore, deployed for more precise determination of the contacts.

The samples from various depths were sieved through 80 mesh size and treated with 15% chloric acid, washed and dried. Bromoform liquid of specific gravity 2.8205 was used to separate the heavy minerals whose percentage in rock samples provided the criteria deployed to mark the contacts as mentioned below.

Contact between Chinji and Nagri Formations: Epidote is more dominant in the Chinji Formation than in the overlying Nagri Formation. At Toot Well-7, persistent dominance of epidote began at 1615m depth and decrease in tourmaline started at 1625m depth. The contact is between 1620 and 1630m depth, at 1625m.

Contact between Chinji and Kamlial Formations: Epidote is higher in the Chinji Formation than in the underlying Kamlial Formation of the Rawalpindi Group. At Toot Well-7, there is a distinct increase of tourmaline and decrease of epidote at 3105m. The contact is assumed at 3110m because the sampling interval is 10m.

Contact between Kamlial and Murree Formations: Epidote is more and tourmaline less in the Murree Formation than in the Kamlial Formation. At the well site, tourmaline shows sharp decline at 3185m; so the contact is positioned at 3190m.

The foregoing is an example of the use of heavy mineral content of sandstones and shales from flush cutting samples of the Toot Well-7 in demarcating the contacts amongst rock Formations of the Siwalik and Rawalpindi Groups.

Manuscript received on 10.4.1988
Accepted for publication on 12.10.1988

ACTA MINERALOGICA PAKISTANICA
VOLUME 4 (1988) pp. 147 - 150.

SOME GEOLOGICAL ASPECTS OF THE HAZARA ARC, NORTHERN PAKISTAN

AFTAB AHMAD BUTT
Institute of Geology, University of the Punjab, Lahore-20, Pakistan.

The Hazara arc (an arcuate NE-SW trending trough) is the northernmost extremity of the sedimentary succession along the northwestern margin of the Indian plate (Fig. 1), and is the result of continent to continent collision. The configuration of the Hazara arc shows that the Balakot to Muzaffarabad region lies in the northern tip of the Hazara arc (Fig. 2) where the following stratigraphic sequence is recognised by Ghazanfar *et al.* (1987).

Murree Formation	Miocene
Kuldana Formation Margala Hill Limestone	Eocene
Patala Formation Lockhart Limestone Hangu Formation	Paleocene
Abbottabad Formation (top member Sirban Dolomite)	Cambrian
Hazara Formation	Precambrian

Ghazanfar *et al.* (1987) established three stratigraphic provinces, namely, Hazara, Muzaffarabad and Kaghan, believing different stratigraphic setting in each region. Their stratigraphic Table (pp. 69-72), however, shows that the geology of Kaghan is undoubtedly unique, while there is no difference in the stratigraphy of Hazara and Muzaffarabad.

This finds answer by visualizing the structural configuration of the Hazara arc and the geographical locations of Balakot and Muzaffarabad. This supports the idea that the sedimentary geology of Azad Kashmir from Balakot to Muzaffarabad is an integral part of the sedimentary geology of the Hazara arc.

The geological history of the Hazara arc may be summarized as follows:–

i) Initiation of geosynclinal setting of the Hazara arc durig the Precambrian times when the Hazara Formation, having characters of turbidite deposits, was laid down.

ii) Deposition of the Abbottabad Formation, Hazara Formation and the Galdanian Formation in a narrow trough confined to the northwestern extremity of the Hazara arc. This Cambrian succession overlies the basal conglomeratic deposits (Tanakki Conglomerate) thus marking a small stratigraphical break between the Precambrian Hazara Formation and the Cambrian Abbottabad Formation.

iii) Absence of Ordovician, Silurian, Devonian, Carboniferous, Permian, and Triassic rocks recording a major time gap.

iv) Subsidence of a narrow strip of mid-portion of the Hazara arc for the deposition of Early Jurassic Datta/Shinawari stratigraphic level.

v) Major transgression during the Upper Jurassic time when a greater part of the Hazara arc represented a shallow shelf carbonate deposition (Samana Suk Limestone) evidenced by the oolitic texture, dolomitization and the presence of shallow-water benthnic macrofossils. This is then followed by the development of restricted marine trough (oxygen-deficient environments) for the deposition of the black shale facies (Chichali Formation). Pyrite concretions and fragile small-size belemnites and ammonites indicate anoxic environments.

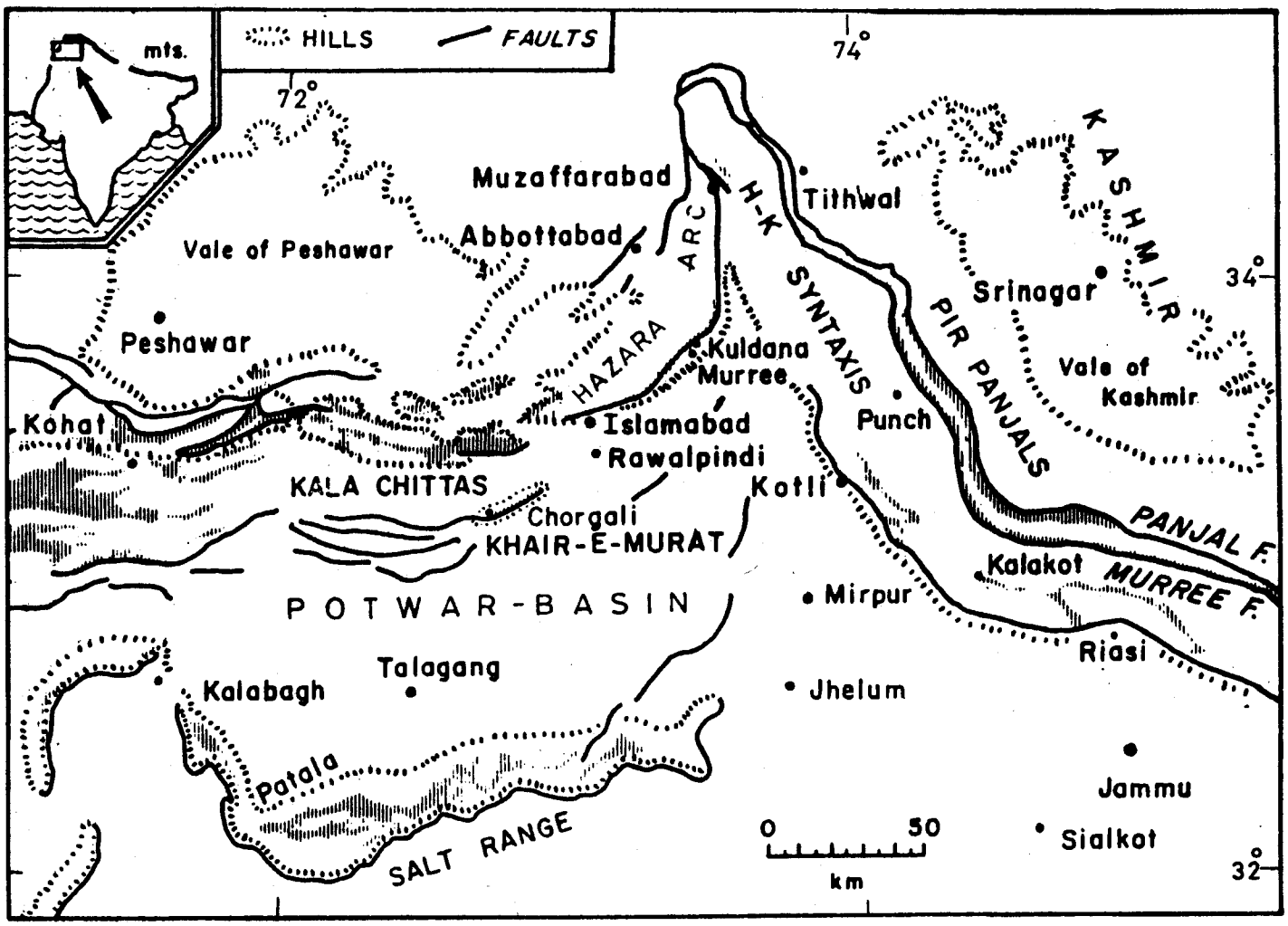

Fig. 1. The Hazara Arc – northernmost extremity of the sedimentary succession along the northwestern margin of the Indian Plate. (Map adopted from Wells & Gingerich, 1987)

vi) Return to open marine shallow shelf deposition (Lumshiwal Sandstone) during the Lower Cretaceous with glauconitic sandstone and the ammonite funa.

vii) Deepening of the Hazara arc during the Upper Cretaceous for the deposition of calcareous mud (Kawagarh Formation) in outer neritic environments evidenced by the planktonic foraminifera.

viii) Major stratigraphical break (Maastrichtian through Danian) marked by the residual lateritic deposits.

ix) Major transgression in the greater part of the Hazara arc during the Upper Paleocene, first, to establish shallow-shelf carbonate deposition of the nodular Lockhart Limestone and then, the argillaceous Patala Formation both containing shallow-water benthonic larger foraminifera.

x) Return to shallow shelf carbonate deposition during the Lower Eocene for depositing the nodular Margala Hill Limestone and flaggy limestone (Chorgali Formation) containing shallow-water benthonic larger foraminifera.

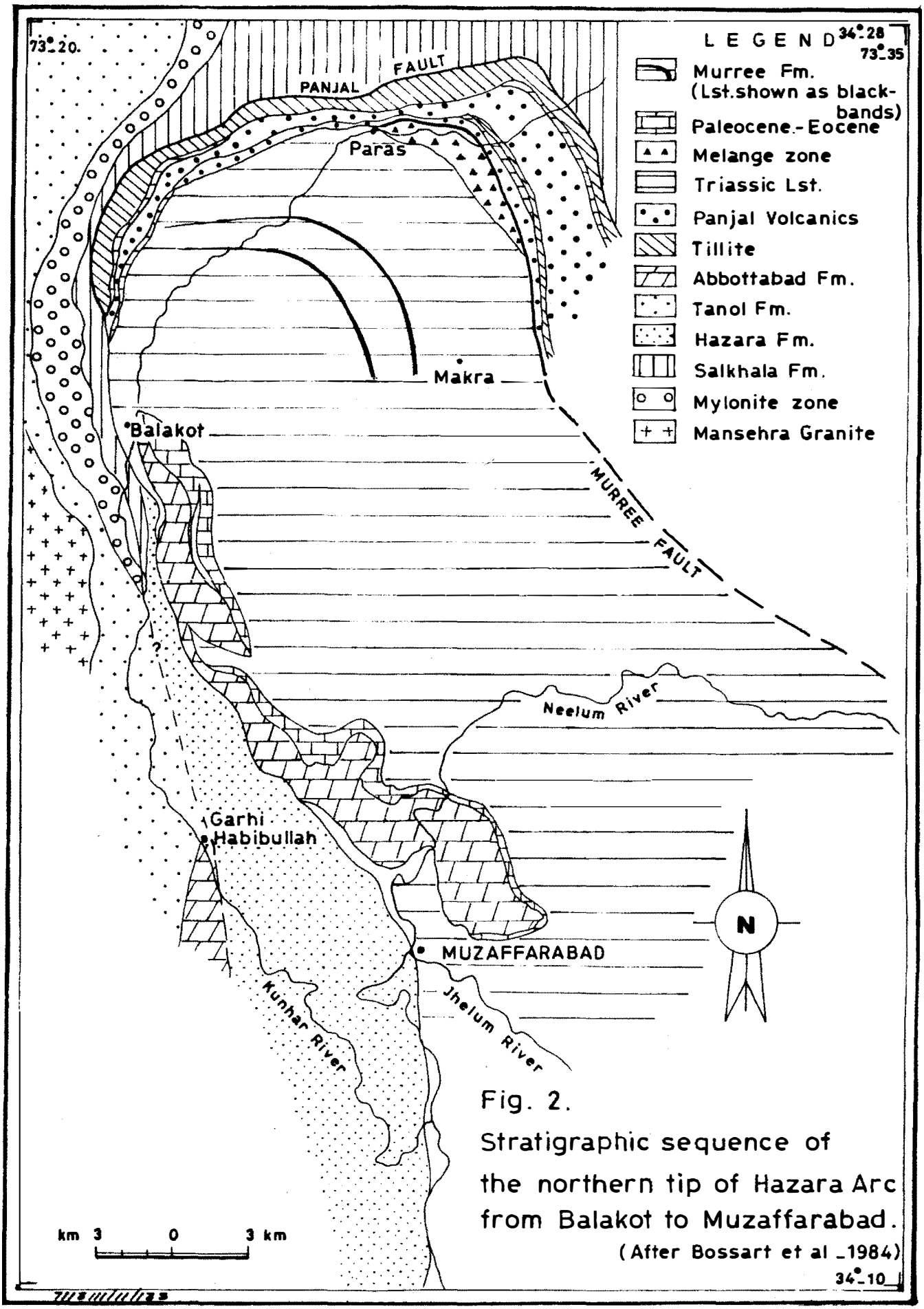

Fig. 2.
Stratigraphic sequence of the northern tip of Hazara Arc from Balakot to Muzaffarabad.
(After Bossart et al _1984)

xi) Reduction in the geographical limit and southward shift of the Hazara arc during the Middle Eocene to deposit the typical shallow-water "Red Bed Facies" (Kuldana Formation).

xii) Uplift of the entire depositional trough (Upper Eocene through Oligocene) bringing an end to the major geological events in the Hazara arc.

xiii) The Miocene time determines the major part of the Hazara arc as the main hinterland to the adjacent actively subsiding Potwar Basin, when the Murree Formation makes a southern marginal shallow shelf clastic deposits of the Hazara arc culminating into the actively subsiding Potwar Basin.

REFERENCES

BOSSART, P., DIETRICH, D., GREO, A., OTTINGER, R. & RAMSAY, J.G. (1984) A new structural interpretation of the Hazara-Kashmir Syntaxis, Southern Himalayas, Pakistan. Kashmir Jour. Geol. 2, pp. 19-36.

GHAZANFAR, M., CHAUDHRY, M.N. & LATIF, M.A. (1987) Three stratigraphic provinces at Hazara – Kashmir boundary. Kahsmir Jour. Geol. **5**, pp. 65-74.

WELLS, N.A., & GINGERICH, P.D. (1981) Paleoenvironmental interpretation of Paleogene strata near Kotli, Azad Kashmir, northeastern Pakistan. Kashmir Jour. Geol. **5**, pp. 23-41.

Manuscript received on 12.9.1988
Accepted for publication on 31.12.1988

ANNUAL REPORT OF THE CENTRE OF EXCELLENCE IN MINERALOGY, QUETTA (1988)

ACADEMIC STAFF

Date of joining C.E.M.

Professor & Director
ZULFIQAR AHMED
Ph.D. (London), P.D.M.P. (Min. Univ .Austria)
M.Sc. & B.Sc. Hons. (Punjab) 25.8.1984

Fulbright Professor
GEORGE R. McCORMICK
Ph.D. (Ohio State)

Associate Professor
MOHAMMAD MUMTAZUDDIN
M.Sc. (McGill), B.Sc. (Aligarh). 1.4.1974

Assistant Professors
MOHAMMAD MUNIR
M.Sc. (Baluchistan) 1.10.1976

JAWED AHMED
M.Sc. (Karachi) 1.4.1980

S. MAHMOOD ALI SHAH
M.S. (Dahran) 21.9.1988

Visiting Lecturer
CHRISTOPHE MIOULLET
D.E.A. (Bordeaux, France) 15.12.1986

THIERRY AUBRY
D.E.A. (Bordeaux, France) 15.12.1988

Part-time Lecturers
AFTAB AHMAD BUTT
Ph.D. (Utrecht, Hollad),
M.Sc. (Punjab)

ABDUL HAQUE
Dr. 3eme Cycle (France),
M.Sc. (Baluchistan)

GENERAL STAFF

Administrative Officer
S. SHAHABUDDIN
M.Sc. (Baluchistan) 21.5.1977

Accounts Officer
MIRZA MANZOOR AHMED
B.Com. (Karachi) 7.5.1980

Technician
KHUSHNOOD AHMED SIDDIQUI
Dipl. Assoc. Engr. (Hyderabad) 1.3.1976

Photographer
HUSSAINUDDIN 16.6.1981

Assistant Librarian
ABDUL GHAFOOR
M.L.S. (Baluchistan) 2.5.1985

Draftsman
AHMED KHAN MANGI
B.A. (Sind), Cert. Drawing 1.7.1981

Steno-typist
GHALIB SHAHEEN 17.7.1985

Assistant (Office)
LAL MOHAMMAD DURRANI 12.5.1973

Store Keeper
MUSA KHAN 20.8.1977

Senior Clerk
MOHAMMAD ANWAR 18.9.1973

Junior Clerk
GHULAM QASIM 3.10.1983

Cashier-cum-clerk
JUMA KHAN 11.6.1985

Laboratory Assistant
SHER HASSAN 22.8.1977

Rock Cutter
FARID KHAN 8.4.1985

Junior Mechanic
ABDUL QADIR 21.8.1977

Driver
ALI MOHAMMAD 17.7.1984

Loader
RAWAT KHAN 2.7.1977

Laboratory Attendants

GHULAM RASOOL	20.8.1977
MEHRAB KHAN	21.8.1977

Peons (Naib Qasid)

SIKANDAR KHAN	30.4.1976
MOHAMMAD RAFIQ	12.10.1978
ATTA MOHAMMAD	25.3.1986

Cleaner

NAZIR MASIH	1.4.1977

POSTGRADUATE STUDENTS

(SESSION 1985-87)

ABDUL WAHEED TAREEN, M.Sc. (Baluchistan)
QAISER MAHMOOD, M.Sc. (Punjab)
MEHRAB KHAN, M.Sc. (Baluchistan)
KHALID MAHMOOD, M.Sc. (Baluchistan)
MORTAZA BOSTANI, M.Sc. (Baluchistan)

(SESSION 1986-88)

DIN MUHAMMAD, M.Sc. (Baluchistan)
HAMID RAZA MIRKIANI, M.Sc. (Baluchistan)
SAADAT HUSSAIN, M.Sc. (Baluchistan)
MOHAMMAD AYUB, M.Sc. (Baluchistan)
ZIAUD DIN, M.Sc. (Baluchistan)

ACADEMIC ACTIVITIES

During 1987, geoscientific field and laboratory studies on the following M.Phil. dissertations have remained in progress:

Mortaza Bostani
Geological studies of a portion of oil-bearing strata of Potwar region, Pakistan.

Khalid Mahmood
Geology of igneous rocks and their sedimentary envelope near Nal area, Khuzdar District, Pakistan.

Mehrab Khan
Geology of ophiolitic rocks from Nal area, Khuzdar District, Pakistan.

Qaiser Mahmood
Geology of Wad-Goth Haji Shakar area, Khuzdar District, Baluchistan.

Jawed Ahmad
Clay mineralogy of the Ghazij Shale Formation of Baluchistan.

Shamim Ahmad Siddiqui
Mineralization, controls and genesis of lead-zinc-iron and barite deposits near Shekran and Gunga, Khuzdar Division, Baluchistan.

Abdul Tawab
Petrology and mineralogy of ultramafic and associated rocks near Nal, Khuzdar District, Baluchistan.

Hassan Khan Kharoti
Igneous rocks south of Khuzdar-Nal section, Baluchistan.

George R. McCormick led a week-long field mapping programme of five from the fresh applicants for M.Phil. registration. The programme focussed emphasis on mapping and sampling the volcanic rocks associated with the Parh Limestone of Cretaceous age exposed in the Zhob Valley near Zhob town. Students of M.Phil. session 1986-88 continued work on their course work and field work.

Zulfiqar Ahmed and George R. McCormick jointly carried out reconnaissance field work and sampling of the basic-ultrabasic rocks south of Zhob town, in the Zhob Valley region, the Kharan-Nal road section, in the Las Bela and Uthal areas. Zulifqar Ahmed continued his project on ophiolitic rocks that stretch in outcrop from Nal in Khuzdar District to south of Uthal. During mapping, some acidic and intermediate plutonic rocks were found occurring adjacent to the ophiolitic rocks. They were sampled for subsequent analytical work.

The mineral-analytical results on the alkaline ultramafic magmatic intrusions were submitted for publication in the Mineralogical Magazine (U.K.) in a joint paper by Zulfiqar Ahmed and George R. McCormick.

The Chairman of the Department of Geology at Iowa University, U.S.A., Professor Simkin, visited C.E.M. for about two weeks during July-August, 1988, and conducted field excursions near Quetta. He delivered a special lecture on Quaternary geology at C.E.M.

Mr. Christophe Mioullet, Visiting Lecturer from France, completed his two year's tenure at C.E.M. and left for France in December, 1988. The Embassy of France appointed Mr. Thierry Aubry to work at C.E.M. He has been

working on siliceous rocks from Balochistan and elsewhere, their geological characterization and use in archeological sites. Messrs Thierry Aubry, Zulfiqar Ahmed and Mehrab Khan Baloch have jointly pursued characterization of Balochistani cherts, part of which is published in this issue

Jawed Ahmed has continued his work on the clay minerals from Ghazij Shale Formation. More samples were included for study by the X-ray diffraction and chemical analytical techniques, to be carried out at the laboratories of Pakistan Atomic Energy Minerals Centre at Lahore.

A research paper by Zulfiqar Ahmed on the greenschist facies regional metamorphic rocks of the southern Malakand Agency was accepted for publication in the Volume 44 of the Precambrian Research (Elsevier Co., Netherlands).

The geochemistry laboratory at C.E.M. was strengthened with the addition of a new "Varian" atomic absorption spectrophotometer.

The activities at C.E.M. remained paralyzed from 17.10.1988 onwards till the end of the year, due to the closure of the University of Balochistan, due to political unrest and conflicts amongst students.

1988 PAPERS OF REGIONAL INTEREST FROM OTHER JOURNALS

(A) WITH PUBLICATION DATES OF 1988:

1. ABERS, G., BRYAN, C., ROECKER, S., & MCCAFFREY, R. Thrusting of the Hindu Kush over the southeastern Tadjik Basin, Afghanistan – evidence from 2 large earthquakes. Tectonics, Vol. 7, No. 1, pp. 41-56.

2. BAIG, M.S., LAWRENCE, R.D. & SNEE, L.W. Evidence for the late Precambrian to early Cambrian orogeny in northwest Himalaya, Pakistan. Geological Magazine, Vol. 125, No. 1, pp. 83-86.

3. BAKER, D.M., LILLIE, R.J. YEATS, R.S., JOHNSON, G.D., YOUSAF, M. & ZAMIN, A.S.H. Development of the Himalayan frontal thrust zone: Salt Range, Pakistan. Geology, Vol. 16, No. 1, pp. 3-7.

4. BERTRAND, J.M., KIENAST, J-R., & PINARDON, J.L. (1988) Structure and metamorphism of the Karakorum gneisses in the Braldu-Baltoro Valley (North Pakistan). Geodinamica Acta, Vol. 2 (3), pp. 135-150.

5. BOSSART, P., DIETRICH, D., GRECO, A., OTTIGER, R. & RAMSAY, J.G. The tectonic structure of the Hazara-Kashmir syntaxis, southern Himalayas, Pakistan. Tectonics, Vol. 7 (2), pp. 273-297.

6. BROUGHTON, R.D. & WINDLEY, B.F. The Central Himalayan Gneisses in Northern Pakistan. Journal of the Geological Society of India, Vol. 31 No. 2, pp. 185-196.

7. BURBANK, D.W. & RANYNOLDS, R.G.H. Stratigraphic keys to the timing of thrusting in terrestrial foreland basins. Applications to the northwestern Himalaya. *In:* Kleinspehn, K.L. & Paola, C. (eds.) New Perspectives in Basin Analysis. Springer-Verlag, New York, pp. 331-351.

8. BURBANK, D.W., BECK, R.A., RAYNOLDS, R.G.H., HOBBS, R. & TAHIRKHELI, R.A.K. Thrusting and gravel progradation in foreland basins: A test of post-thrusting gravel dispersal. Geology, Vol. 16, No. 12, pp. 1143-1146.

9. BUTLER, R.W.H. & PRIOR, D.J. Anatomy of a continental subduction zone – the Main Mantle Thrust in Northern Pakistan. Geologische Rundschau, Vol. 77, No. 1, pp. 239-256.

10. BUTLER, R.W.H. & PRIOR, D.J. Tectonic controls on the uplift of the Nanga Parbat Massif, Pakistan Himalayas. Nature, Vol. 333, pp. 247-250.

11. CERVENY, P.F., NAESER, N.D., ZEITLER, P.K., NAESER, C.W., & JOHNSON, N.M. History of uplift and relief of the Himalaya during the past 18 million years: evidence from fission-track ages of detrital zircons from sandstones of the Siwalik Group. *In:* Kleinspehn, K.L. & Paola, C. (eds.). New Perspectives in Basin Analysis. Springer-Verlag, New York. pp. 43-62.

12. JAN, M.Q. Geochemistry of amphibolites from the southern part of the Kohistan arc, N. Pakistan. Min. Mag. Vol. 52, pp. 147-159.

13. JAUME, S.C., & LILLIE, R.J. Mechanics of the Salt Range-Potwar Plateau, Pakistan – a fold-and-thrust belt underlain by evaporites. Tectonics, Vol. 7, No. 1, pp. 57-72.

14. JOHNSON, N.M. SHEIKH, K.A., DAWSON-SAUNDERS, E., & McRAE, L.E. The use of magnetic-reversal time lines in stratigraphic analysis; A case study in measuring variability in sedimentation rates. *In:* Kleinspehn, K.L. & Paola, C. (eds.) New Perspectives in Basin Analysis. Springer-Verlag, New York, pp. 189-200.

15. KALVODA, J. Recent orogeny of the Himalayas – a remarkable geomorphological event. Journal of Geodynamics, Vol. 9 (2-4), pp. 319-330.

16. KÖTHE, A., KHAN, A.M. & ASHRAF, M. Biostratigraphy of the Surghar Range, Salt Range, Sulaiman Range and the Kohat area, Pakistan, according to Jurassic through Palaeogene calcareous nannofossils and Paleogene Dinoflagellates. Geologisches Jahrbuch Vol. 71, pp. 3-87.

17. MALUSKI, H., MATTE, P. & BRUNEL, M. Argon 40 dating of metamorphic and plutonic events in the North and High Himalaya belts (southern Tibet, China) Tectonics, Vol. 7, pp. 299-326.

18. REX, A.J., SEARLE, M.P., TIRRUL, R., CRAWFORD, M.B., PRIOR, D.C. & BARNICOAT, A. (1988). The geochemical and tectonic evolution of the central Karakorum, N. Pakistan. *In:* Shackleton, R.M., Dewey, J.F. & Windley, B.F. (eds.) Tectonic evolution of the Himalayas and Tibet. Phil. Trans. Roy. Soc. London, Vol. A-326, pp. 229-255.

19. SHUJA, T.A. Small geothermal resources in Pakistan. Geothermics, Vol. 17, No. 2/3, Special Issue, pp. 461-464.

20. SINGH, D.D. Strain deformation in the northern Indian Ocean. Marine Geology, Vol. 79, No. 1, pp. 105-118

21. SNEE, L.W., LUND, K. & VERPLANCK, P.L. (1988). Comparison of the Salmon River suture, Idaho, with the Indus suture, northern Pakistan (Abstract). Abstracts with Programs-Geol. Soc. America, Rocky Mountain Section, 41st annual meeting, Vol. 20(6), p. 470.

22. VALSANGKAR, A.B. Morphological and interlayer geochemical studies on managanese nodules from the southwestern Carlsberg Ridge. Marine Geology, Vol. 84 (1-2), pp. 81-94.

23. WILKS, M.E. The Himalayas–a modern analogue for Archaean crustal evolution. Earth and Planetary Science Letters, Vol. 87, No. 1-2, pp. 127-136.

(B) WITH PUBLICATION DATES OF 1987:

1. DENILCHIK, W. & SHAH, S.M.I. (1987) Stratigraphy and coal resources of the Makarwal area, Trans- Indus Mountains, Mianwali District, Pakistan. U.S. Geol. Surv. Prof. Pap. 1341, 38 p.

2. DEBON, F., LE FORT, P., DAUTEL, D., SONET, J. AND ZIMMERMANN, J.L. (1987) Granites of western Karakorum and northern Kohistan (Pakistan). A composite Mid-Cretaceous to Upper Cenozoic magmatism. Lithos, Vol. 20, pp. 19-40.

3. LE FORT, P. CUNEY, M., DENIEL, C., FRANCE LANORD, C., SHEPPARD, S.M.F. & UPRETI, B.N. (1987) Crustal generation of the Himalayan leucogranites. Tectonophysics Vol. **134**, pp. 39-57.

4. SEARLE, M.P., TIRRUL, R., REX, A.J., BARMICOAT, A., PARRISH, R. & REX, D.C. (1987) Structural, metamorphic and magmatic evolution of the Central Karakorum in the Biaf-Baltoro Hushe region, N. Pakistan. (Abstract). Himalaya-Karakorum Workshop, Nancy, CRPG, p. 62.

5. SIMON, F.O., KHAN, R.A., LANDIS, E.R. & HILDEBRAND, R.T. (1987) Chemical and physical characterization of mine samples from Lakhra coalfield, South Sind, Pakistan. U.S. Geol. Surv. Open File Report 87-0662, 97 p.

INFORMATION FOR AUTHORS

ACTA MINERALOGICA PAKISTANICA publishes in English annually the results of original scientific research in the multifaceted field of mineral sciences, covering mineralogy, petrology, crystallography, geochemistry, economic geology, isotope mineralogy, petrography, petrogenesis, mineral chemistry and related disciplines. Review articles and short notes are also considered for publication.

In general, the manuscripts be organized in the following order: title; name(s) and institutional address(es) of the author(s); abstract; introduction; methods, techniques, material studied and area descriptions; results; conclusions; acknowledgements; references; tables; figure captions. The abstract should not exceed 300 words. All tables and figures should be referred in the text and numbered according to their sequence in the text. All references to publications are given in the text by author's name and year of publication; and are listed at the end of text alphabetically by author's names and chronologically per author.

Authors of the articles submitted for publication in ACTA MINERALOGICA PAKISTANICA should send two complete copies of the manuscript, typed double-spaced on one side of the paper only. Copies of tables should be in final format. As far as possible, tables and figures should be prepared for reduction to the single column size or to the page size (204mmX278mm). Use of mineral symbols by Kretz (The American Mineralogist, 1983, Volume 68, pp. 277-279) is recommended for superscripts, subscripts, equations, figures and tables. The Concise Oxford Dictionary is adopted for spelling. Underlining of text by a single line will mean printing in italics; that by a double line will mean printing in bold letters. The use of metric system and S.I. units is recommended. Bar scales should be used in all figures rather than numerical scales.

Only articles not previously published and not about to be published, wholly or in part, in either Pakistani or foreign journals, are considered for publication. Submission of an article is understood to imply that the article is original and unpublished and is not being considered for publication elsewhere. Publication is subject to the discretion of the Editor. All manuscripts are refereed before being accepted. Accepted papers become copyright of the Centre of Excellence in Mineralogy, Quetta. Authors alone are responsible for the accuracy of the contents and views expressed in their respective papers. Fifty off-prints of each published paper will be sent to authors free of charge. Additional copies may be ordered just after receiving the acceptance letter from the Editor. Manuscripts should be sent to: Acta Mineralogica Pakistanica C/O Centre of Excellence in Mineralogy, University of Baluchistan, G.P.O. Box 43, Quetta, Pakistan. Phone Nos. are (081) 41974 & 40500.

ACTA MINERALOGICA PAKISTANICA VOLUME 4, 1988

CONTENTS